DISCLAIMER

This report was prepared as an account of work sponsored by an agency of the United States Government. Neither the United States Government nor any agency thereof, nor any of their employees, makes any warranty, express or implied, or assumes any legal liability or responsibility for the accuracy, completeness, or usefulness of any information, apparatus, product, or process disclosed, or represents that its use would not infringe privately owned rights. Reference herein to any specific commercial product, process, or service by trade name, trademark, manufacturer, or otherwise does not necessarily constitute or imply its endorsement, recommendation, or favoring by the United States Government or any agency thereof. The views and opinions of authors expressed herein do not necessarily state or reflect those of the United States Government or any agency thereof. Reference herein to any social initiative (including but not limited to Diversity, Equity, and Inclusion (DEI); Community Benefits Plans (CBP); Justice 40; etc.) is made by the Author independent of any current requirement by the United States Government and does not constitute or imply endorsement, recommendation, or support by the United States Government or any agency thereof.

Sandia National Laboratories

Operated for the U.S. Department of Energy by
National Technology and Engineering Solutions of Sandia, LLC
Albuquerque, New Mexico 87185-0405
Livermore, California 94551-0969

Date: 29 May 2025

To: Michelle Gallegos, Organization 02932
Michael Hansen, Organization 02932
Kevin Schafer, Organization 02932
Philip Wang, Organization 02932

From: Neal B. Hubbard, Organization 01554

Subject: Empirical Model for Energy Required to Puncture Specimens of 7075-T651 Aluminum Bar

Executive Summary

Specimens of 7075-T651 aluminum with different thicknesses were punctured by AISI 4340 steel probes of various shapes and sizes in a series of drop-table experiments. The times when a probe contacts a specimen and when it breaks through are indicated by the acceleration of the drop-table carriage. The change in the total energy of the carriage between these times is the energy mitigated by each specimen. Only a few replications were performed with each specimen thickness, probe shape, and probe diameter, so the data sets are not amenable to classical statistical inference. Rather than calculate statistics for each combination of geometric parameters, an empirical model is derived that uniquely fits the data for each probe shape. The model predicts future observations within the range of specimen thicknesses and probe diameters that were tested. Confidence intervals based on the variance in the data account for uncertainty. The lower bounds on the mitigated energy for a few select scenarios are tabulated below.

Table 1: Results of Empirical Model for Mitigated Energy in Select Scenarios

Probe End Shape	Flat				Semi-spherical		Tri-corner	
Specimen Thickness	0.051 in		0.250 in		0.051 in	0.250 in	0.051 in	0.250 in
Probe Diameter	0.250 in	1.000 in	0.250 in	1.000 in	0.500 in	1.000 in	0.500 in	1.000 in
Median, 50%	3.9 ft-lb	24 ft-lb	58 ft-lb	356 ft-lb	10.2 ft-lb	431 ft-lb	11.1 ft-lb	487 ft-lb
Lower Bound, 1%	2.1 ft-lb	12.8 ft-lb	31 ft-lb	189 ft-lb	5.4 ft-lb	230 ft-lb	6.6 ft-lb	290 ft-lb
Lower Bound, 1E-3	1.7 ft-lb	10.2 ft-lb	25 ft-lb	151 ft-lb	4.3 ft-lb	181 ft-lb	5.4 ft-lb	237 ft-lb
Lower Bound, 1E-6	0.9 ft-lb	5.8 ft-lb	14 ft-lb	85 ft-lb	2.2 ft-lb	94 ft-lb	3.0 ft-lb	134 ft-lb
Lower Bound, 1E-9	0.6 ft-lb	3.4 ft-lb	8.2 ft-lb	50 ft-lb	1.1 ft-lb	47 ft-lb	1.6 ft-lb	70 ft-lb

Introduction

Dylan Landry performed a series of experiments on a drop table to measure the energy mitigated by 7075-T651 aluminum as projectiles passed through it (Ref. 1). Specimens were machined from bar stock that was sliced with the wire in an electrical discharge machine (EDM). Milling operations produced surface texture representative of actual components. Cracks nucleate at flaws in the material, and a normal quantity of flaws produces characteristic performance. Polished specimens would likely have mitigated more energy but would have been unrealistic for comparison to machined substrates, covers, and closures.

The disc specimens shown in Figures 1 through 3 have pockets where the thickness is reduced so that projectiles can easily penetrate them. The thick rim constrains the thin portion, giving it a fixed boundary condition around the circular perimeter. The reaction forces at the boundary pull downward and radially inward on the rim and tend to curl it such that the outer edges lift off of the table. The rim is designed to minimize this deformation.

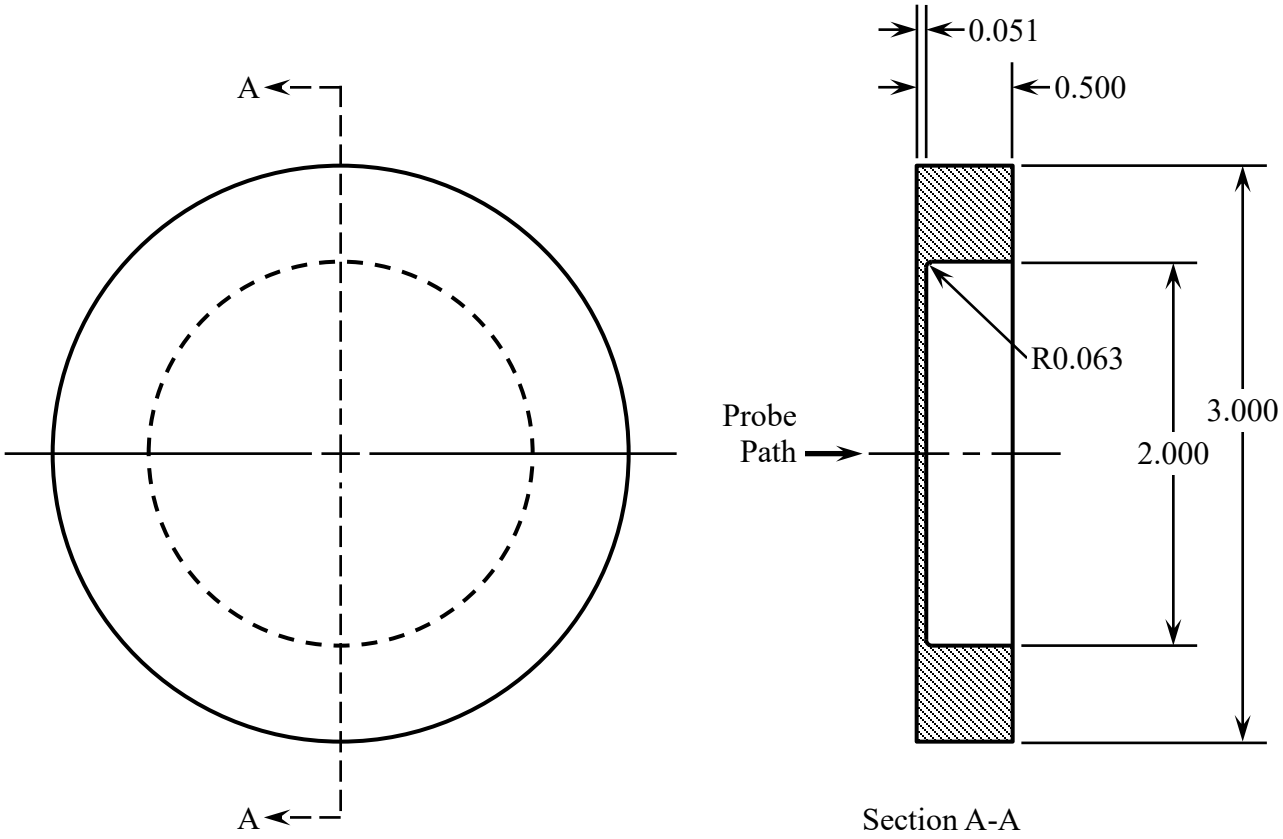

Figure 1: 7075-T651 Aluminum Disc Specimen with Thickness of 0.051 Inch

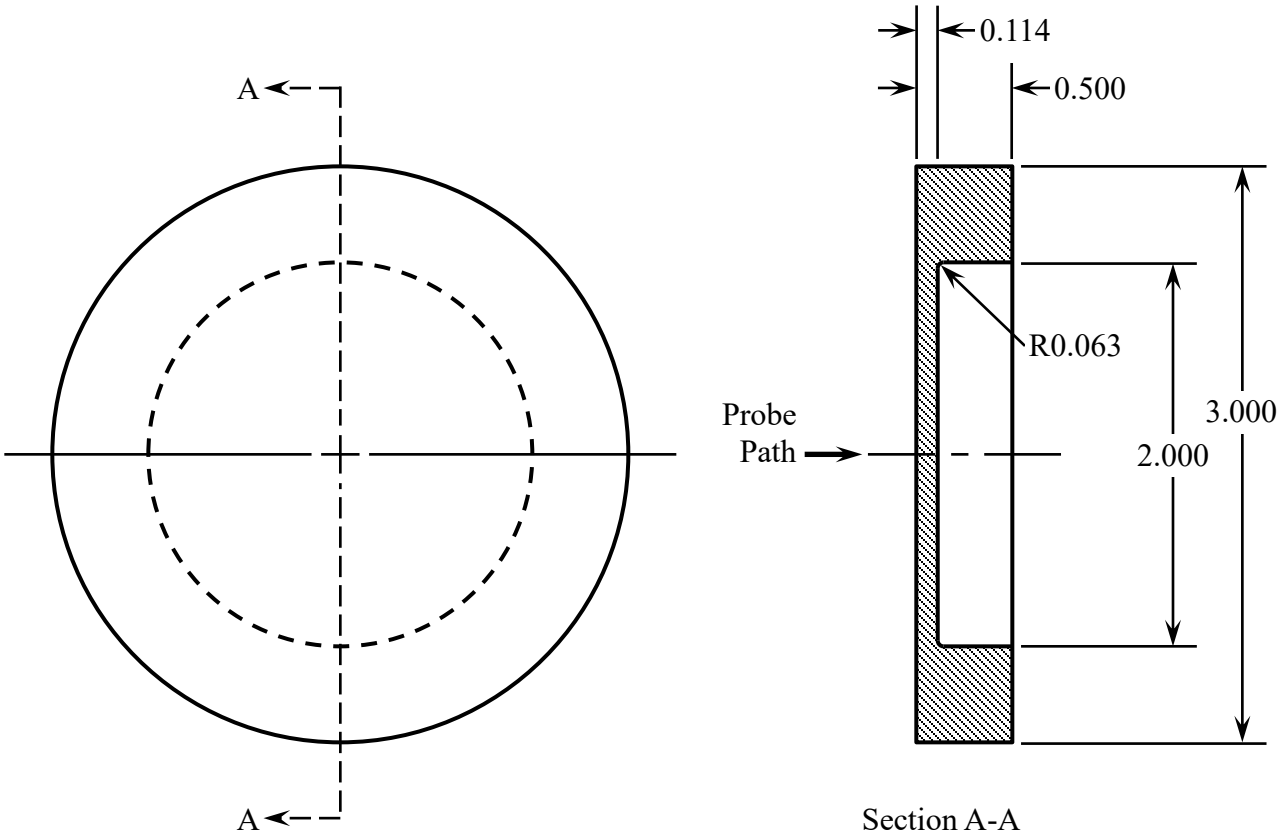

Figure 2: 7075-T651 Aluminum Disc Specimen with Thickness of 0.114 Inch

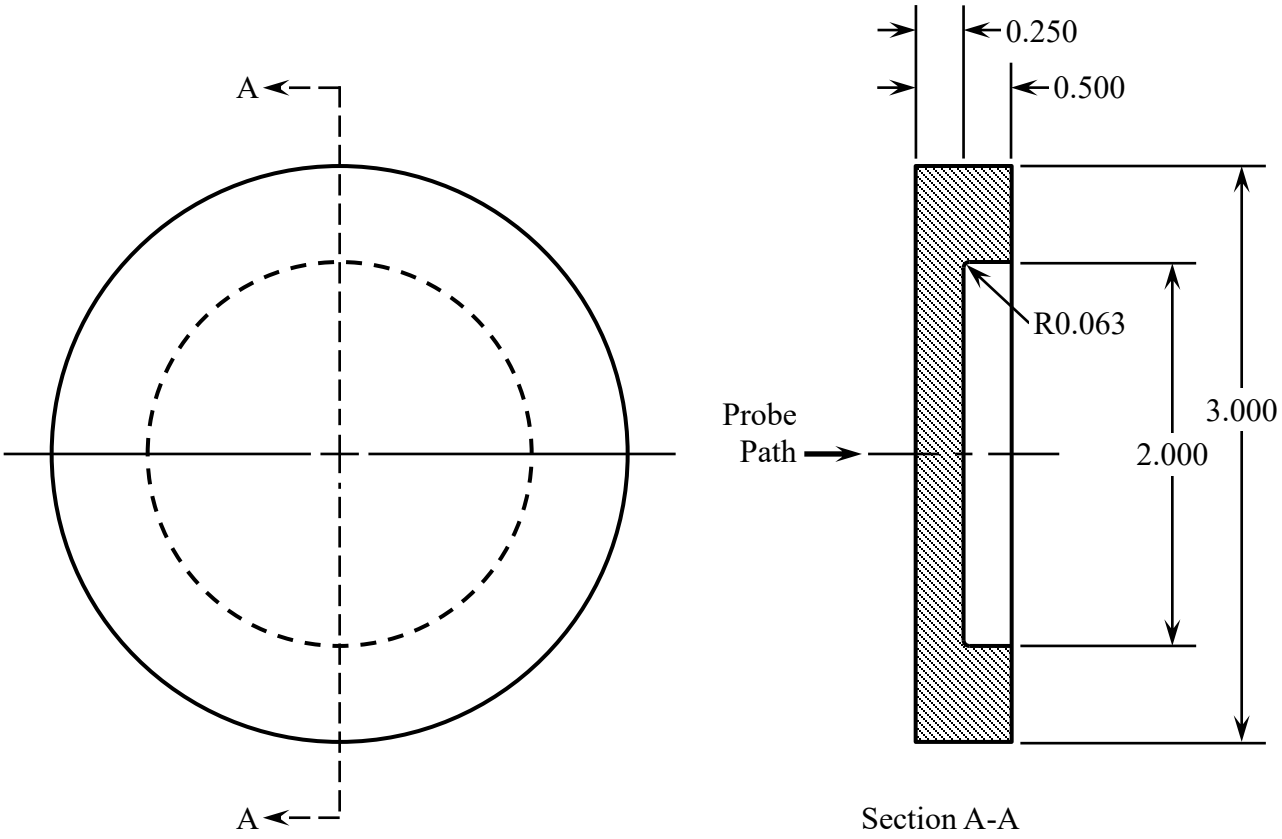

Figure 3: 7075-T651 Aluminum Disc Specimen with Thickness of 0.250 Inch

The probes are straight cylinders machined from AISI 4340 steel bars and hardened to 42–48 Rockwell C hardness (HRC). Figures 4 through 10 give the dimensions in inches. The interface between the probe and the drop table is standardized for quick probe exchanges.

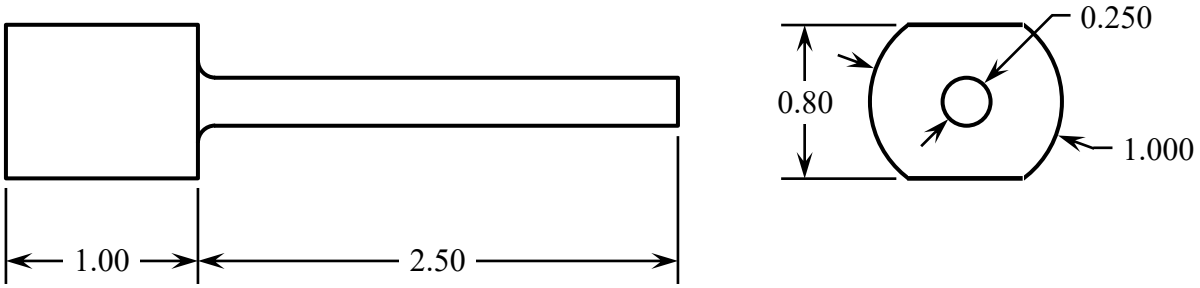

Figure 4: Cylindrical Probe with Diameter of 0.250 Inch and Flat End

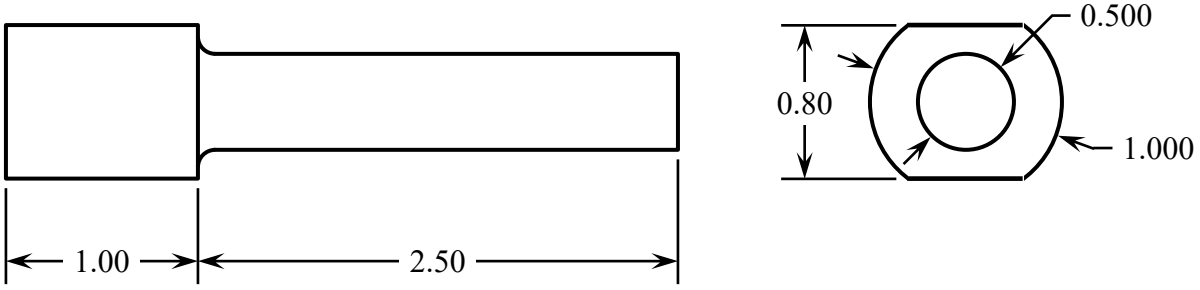

Figure 5: Cylindrical Probe with Diameter of 0.500 Inch and Flat End

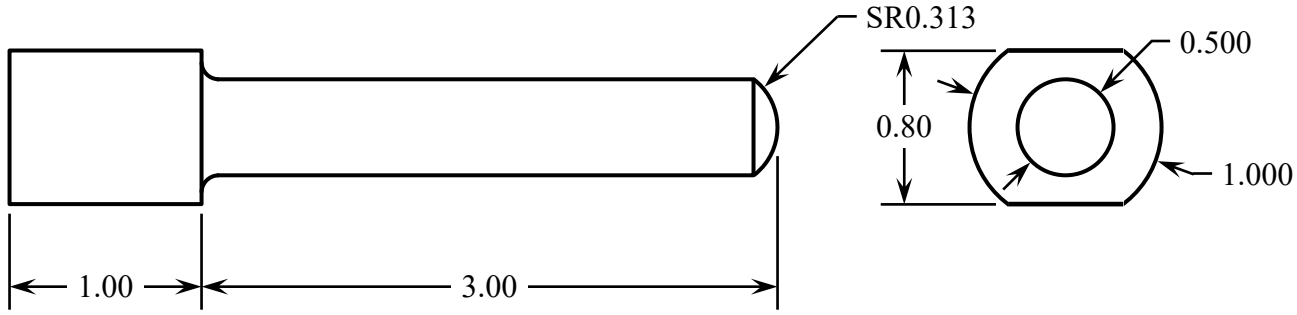

Figure 6: Cylindrical Probe with Diameter of 0.500 Inch and Semi-spherical End

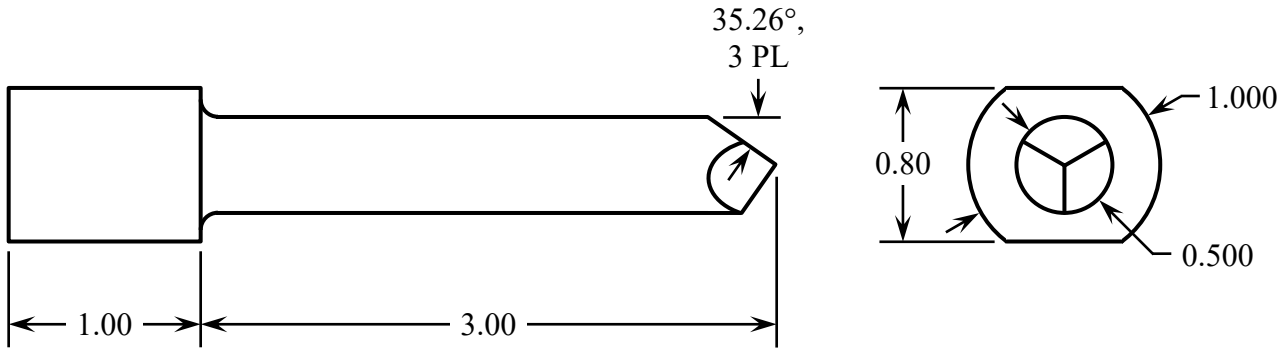

Figure 7: Cylindrical Probe with Diameter of 0.500 Inch and Tri-corner End

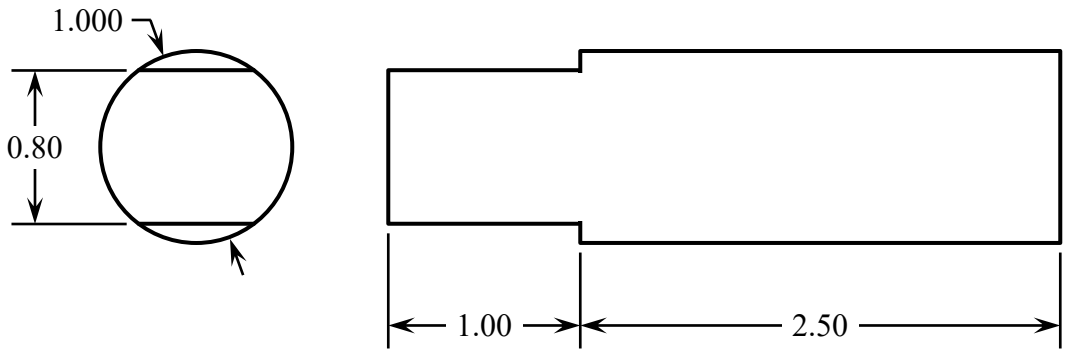

Figure 8: Cylindrical Probe with Diameter of 1.000 Inch and Flat End

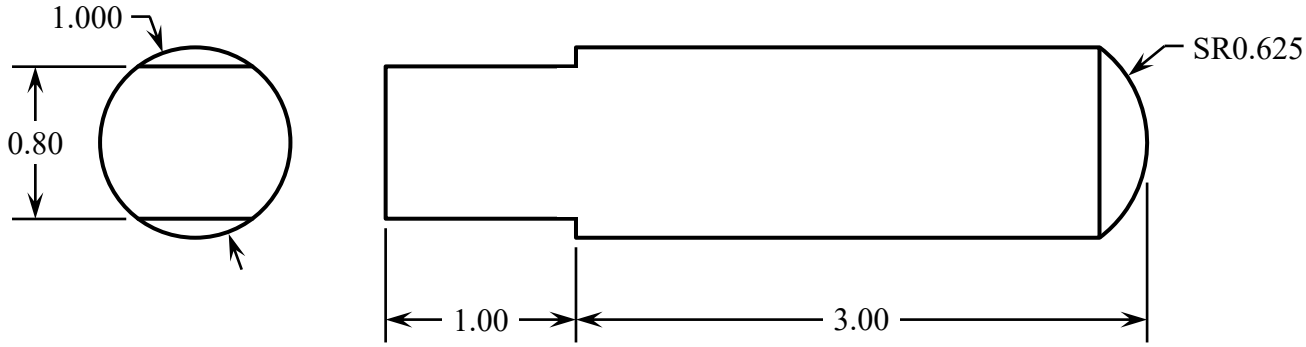

Figure 9: Cylindrical Probe with Diameter of 1.000 Inch and Semi-spherical End

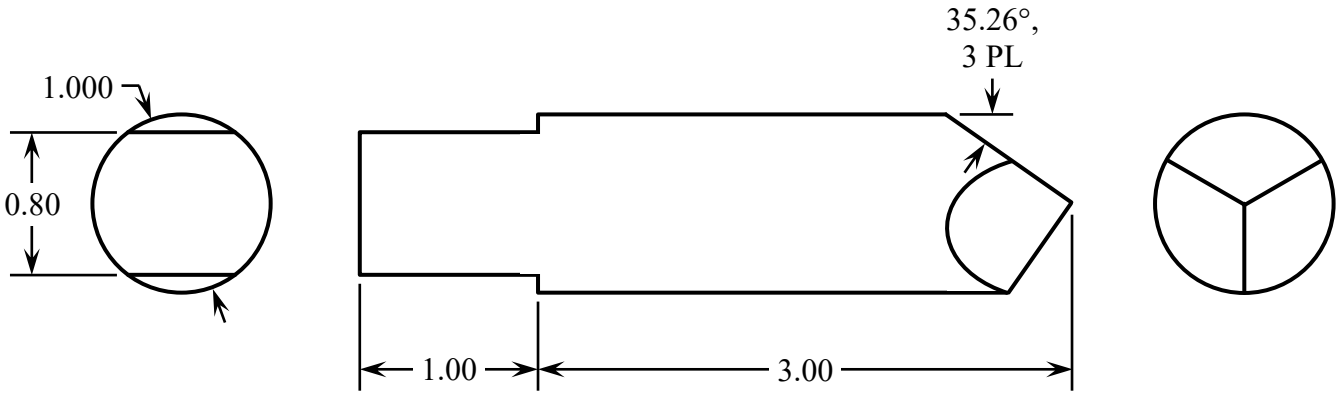

Figure 10: Cylindrical Probe with Diameter of 1.000 Inch and Tri-corner End

The drop table has a 1370 N (308 lb) carriage that guides the probes along a straight path intersecting the specimens. Fixtures constrain the specimens against being pushed by the probes and resist lateral motion (after a little clearance is removed) but allow them to lift off of the fixture and deform. Two laser interferometers measure the position of the carriage, and an accelerometer on the carriage measures the resistance to the falling mass. When the carriage is released from a planned height, the acceleration drops from 1 G to between 0.25 G and 0.96 G; friction in the guide rods prevents free-fall, and they are lubricated regularly to minimize it. Data collection begins as the probe approaches the specimen. Upon contact, an elastic wave travels through the probe to the carriage and registers an increase in the acceleration, which rises to between 2 G and 80 G as the aluminum work hardens and falls after the specimen fractures. The peak acceleration indicates the maximum force required to puncture the specimen, which depends on the thickness of the specimen and the geometry of

the probe. If friction between the specimen and the probe does not arrest the descent, the probe passes through a hole in the fixture, and the carriage settles onto felt programming rings. The data of interest are collected before the carriage either stops or contacts the rings. The drop table is shown in Figure 11 and the various probes in Figure 12.

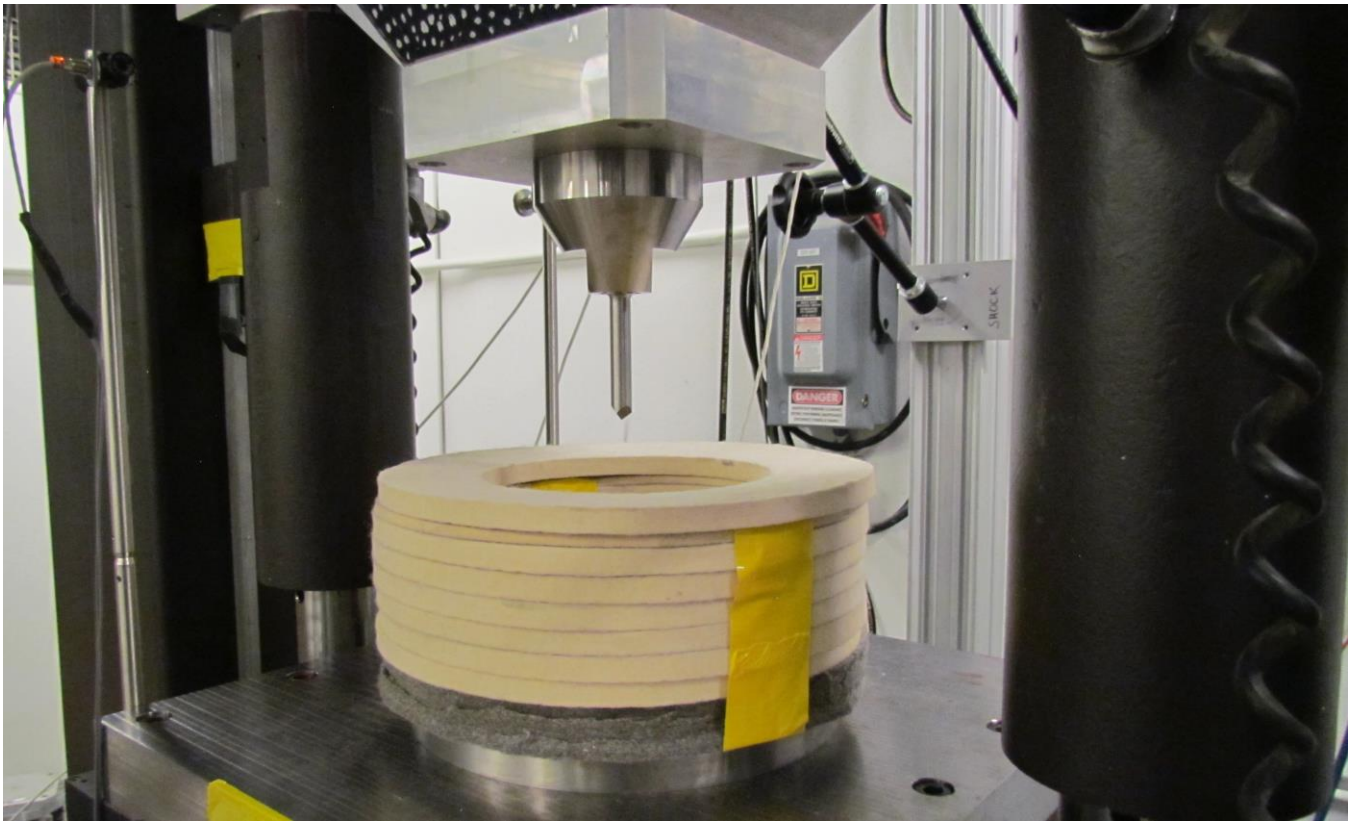

Figure 11: Drop Table Carriage Holding One-Half-Inch Tri-Corner Probe

Figure 12: Flat-End, Spherical, and Tri-corner Probes of Various Diameters

As each probe punctured a specimen, it ejected a plug or formed multiple petals, some of which broke off. Following some tests, the specimens adhered to the probe and were lifted when the carriage raised to the reset position. Significant force and energy were required to separate some of the larger probes and thicker specimens. Each combination of specimen thickness, probe diameter, and probe shape is represented in the subsequent figures. Some are viewed facing the surface that the probe impacted, others are reversed to show the damage on the surface it emerged from. The upper surface had the metallic luster of aluminum. The lower surface was painted white to reduce the glare of strong lighting required by the high-speed camera that observed the cracks forming in the specimen.

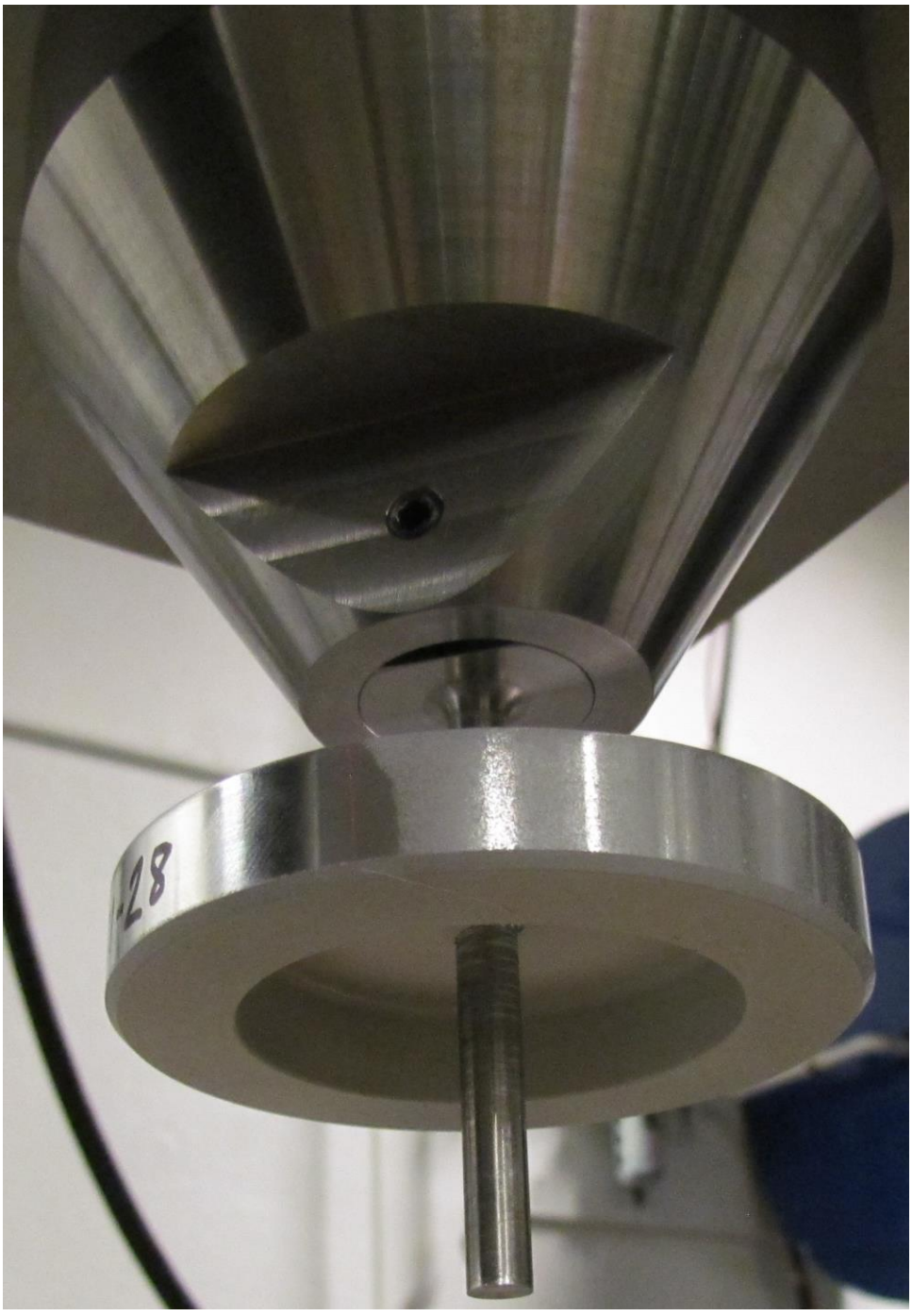

Figure 13: Specimen T051-28 Lifted by One-Quarter-Inch Flat-End Probe After Test 16

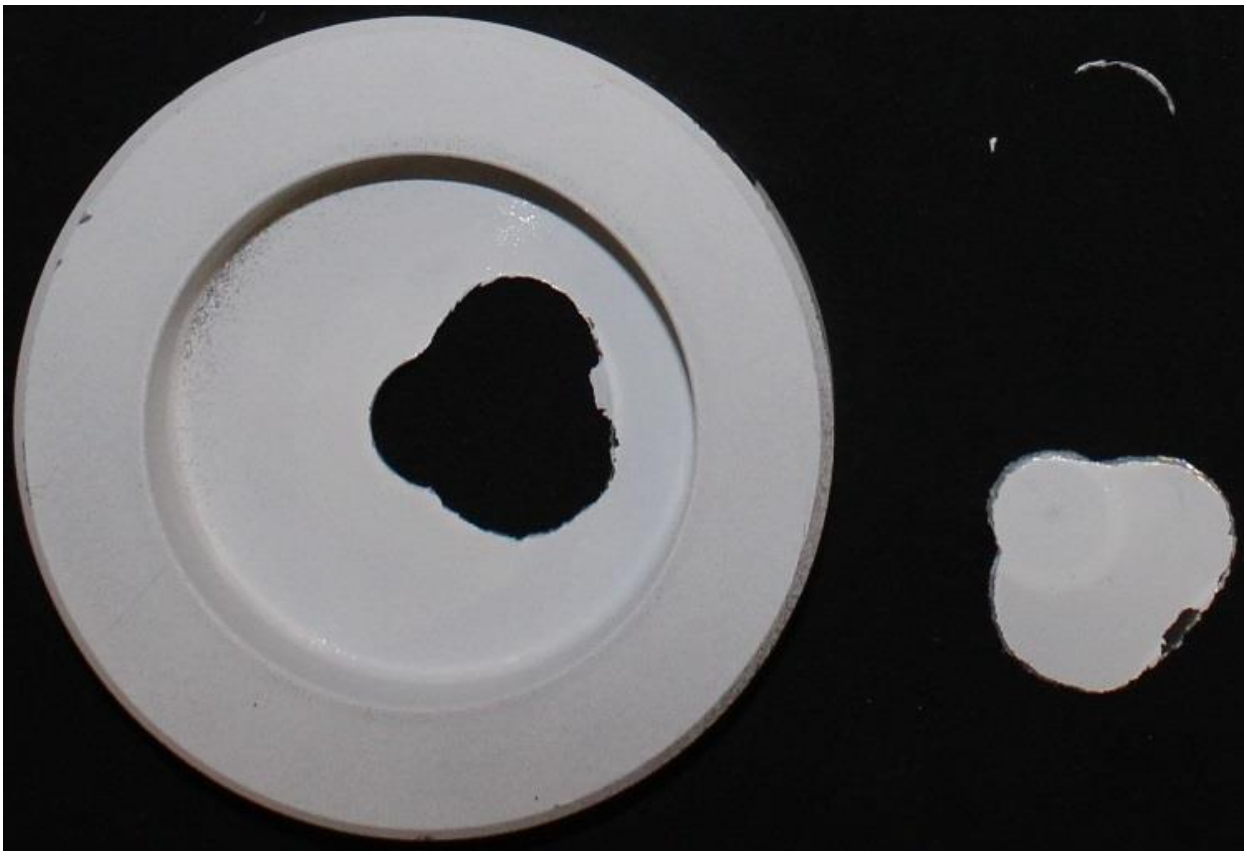

Figure 14: Specimen T051-08 After Test 29 with One-Half-Inch Flat-End Probe

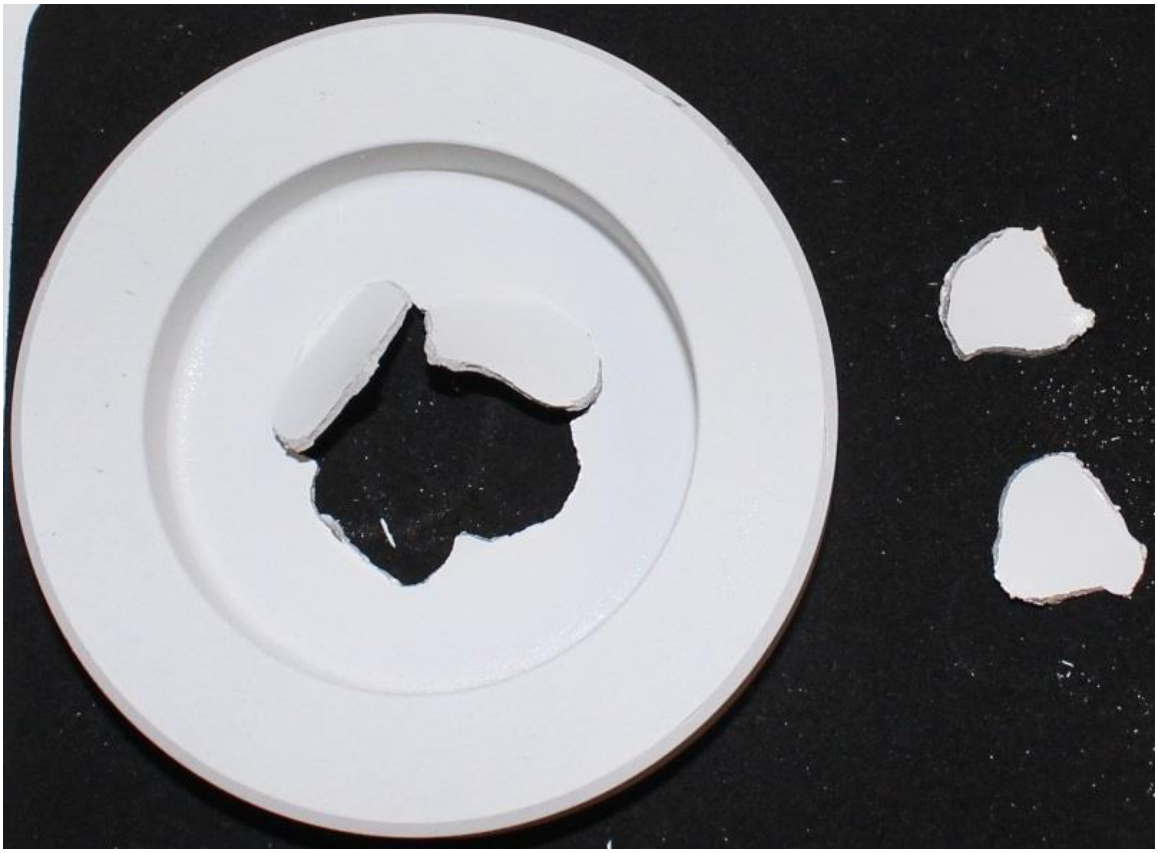

Figure 15: Specimen T051-06 After Test 61 with One-Half-Inch Spherical Probe

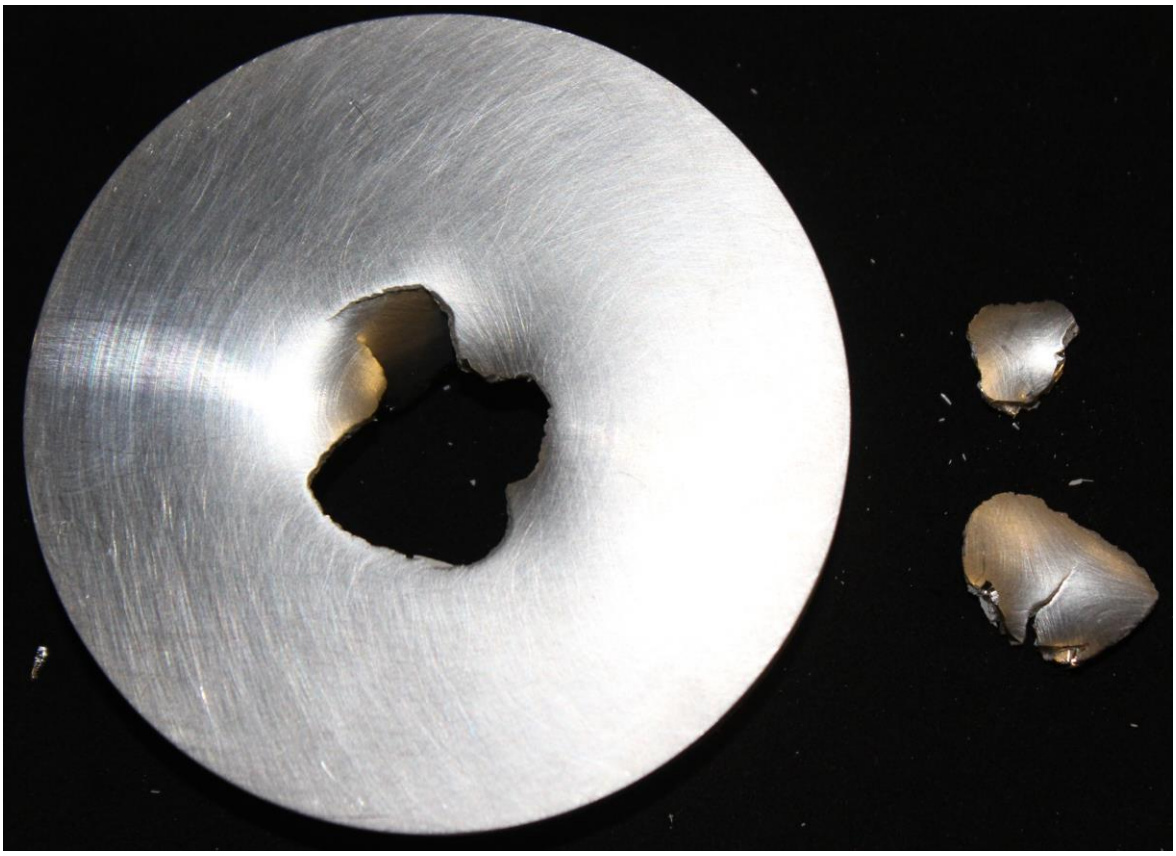

Figure 16: Specimen T051-01 After Test 103 with One-Half-Inch Tri-Corner Probe

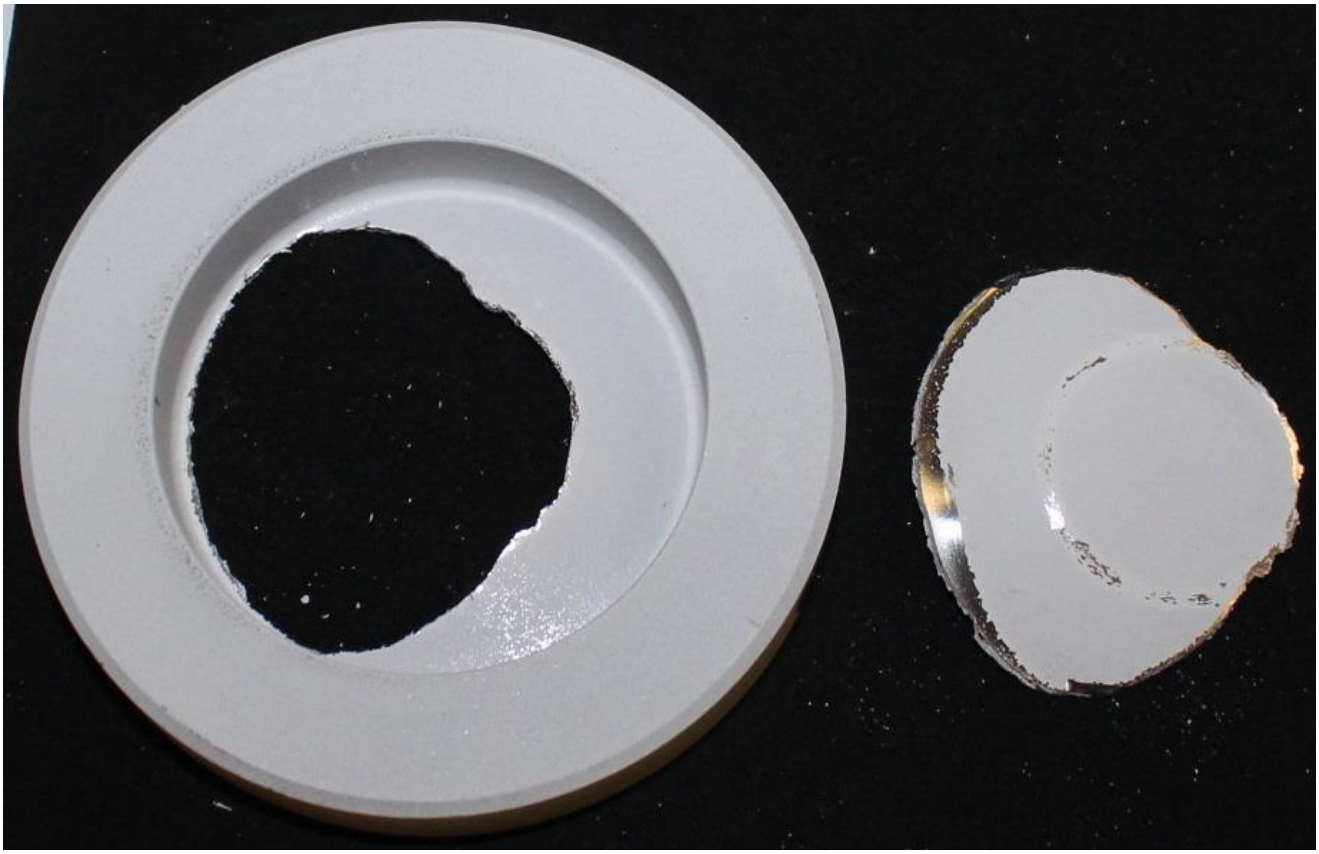

Figure 17: Specimen T051-16 After Test 46 with One-Inch Flat-End Probe

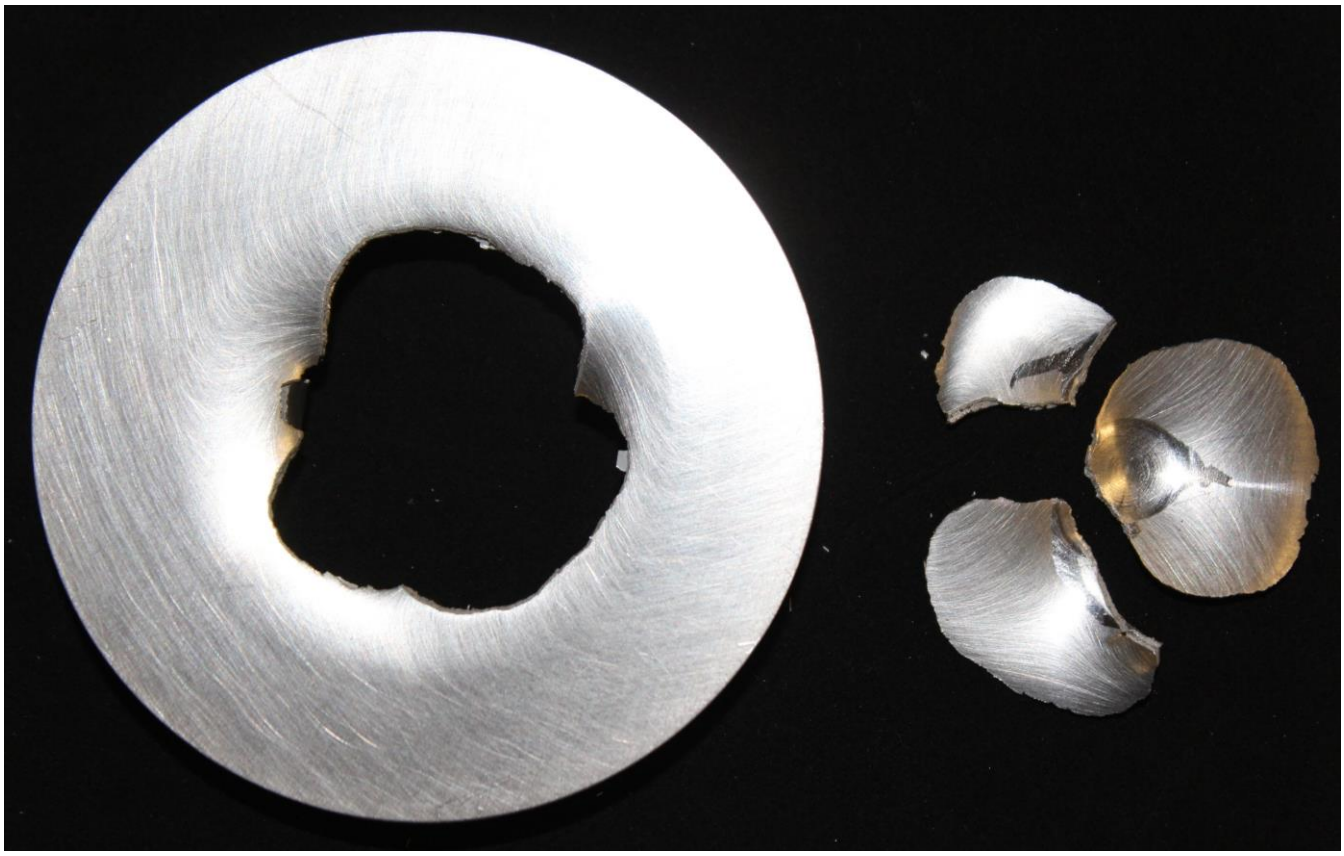

Figure 18: Specimen T051-09 After Test 76 with One-Inch Spherical Probe

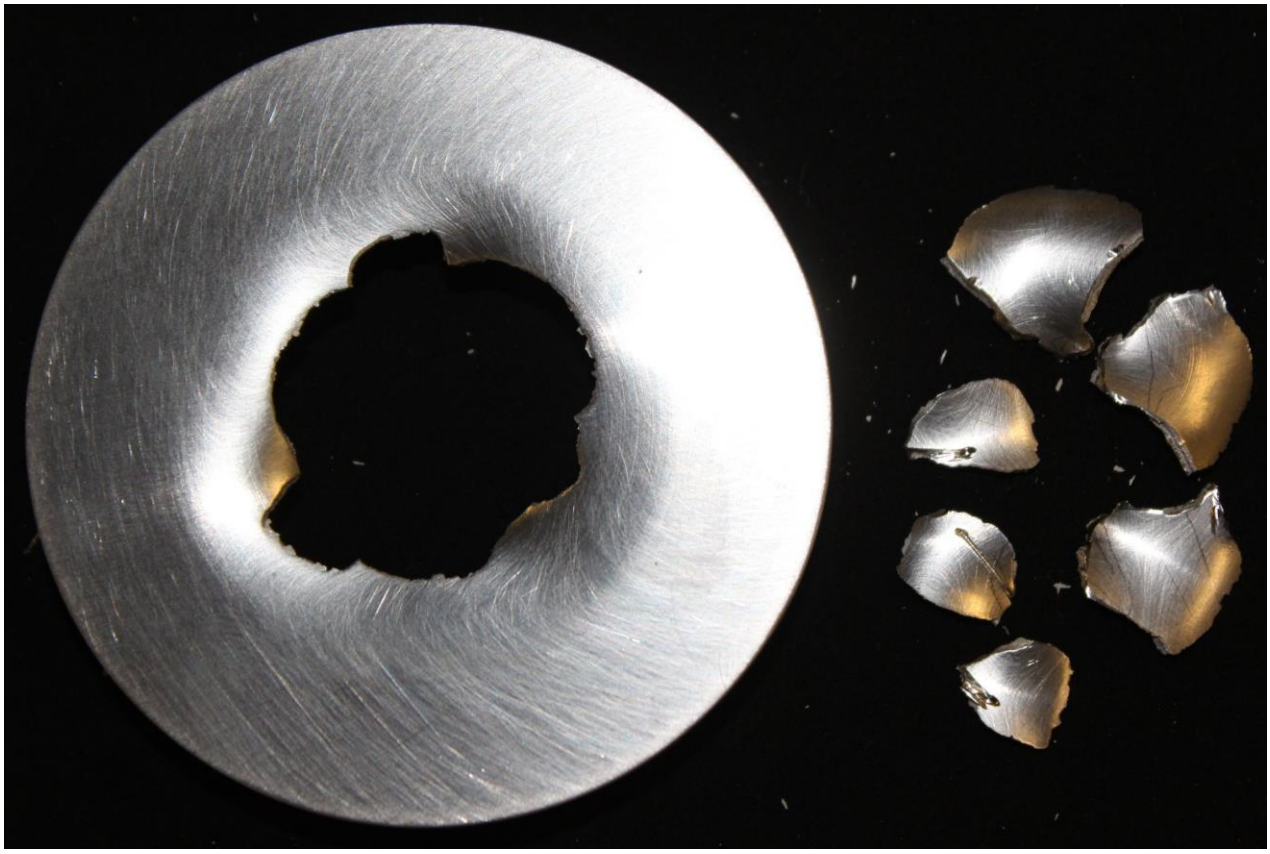

Figure 19: Specimen T051-05 After Test 105 with One-Inch Tri-Corner Probe

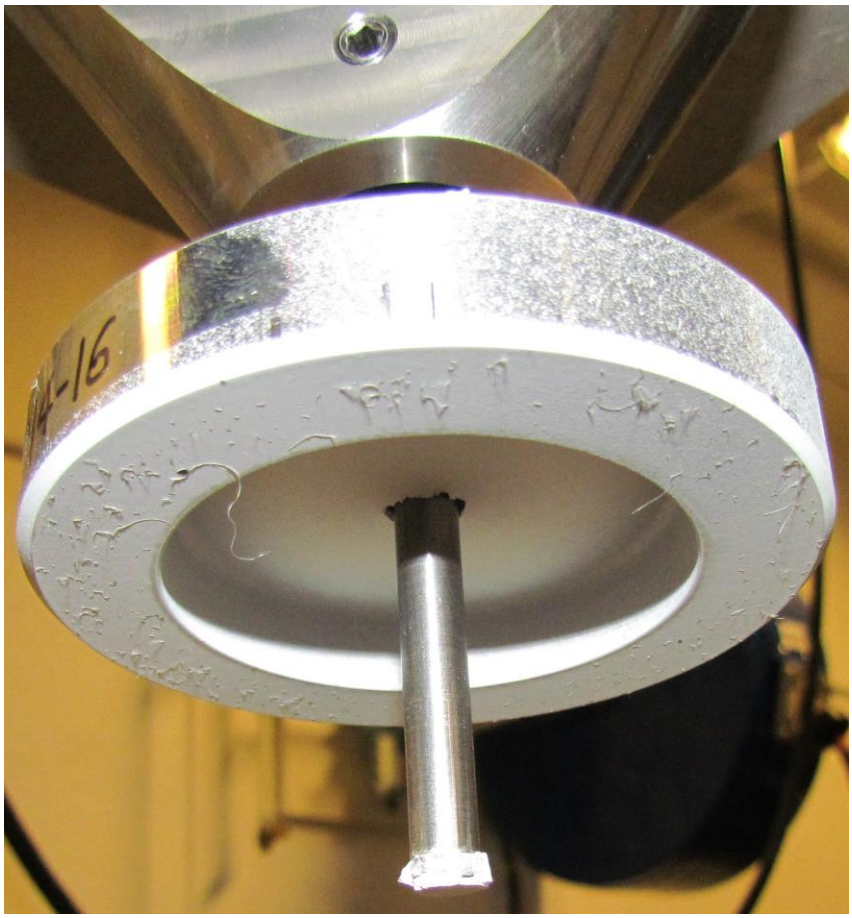

Figure 20: Plug Fused to One-Quarter-Inch Flat-End Probe In Specimen T114-16 After Test 19

Figure 21: Specimen T114-30 After Test 38 with One-Half-Inch Flat-End Probe

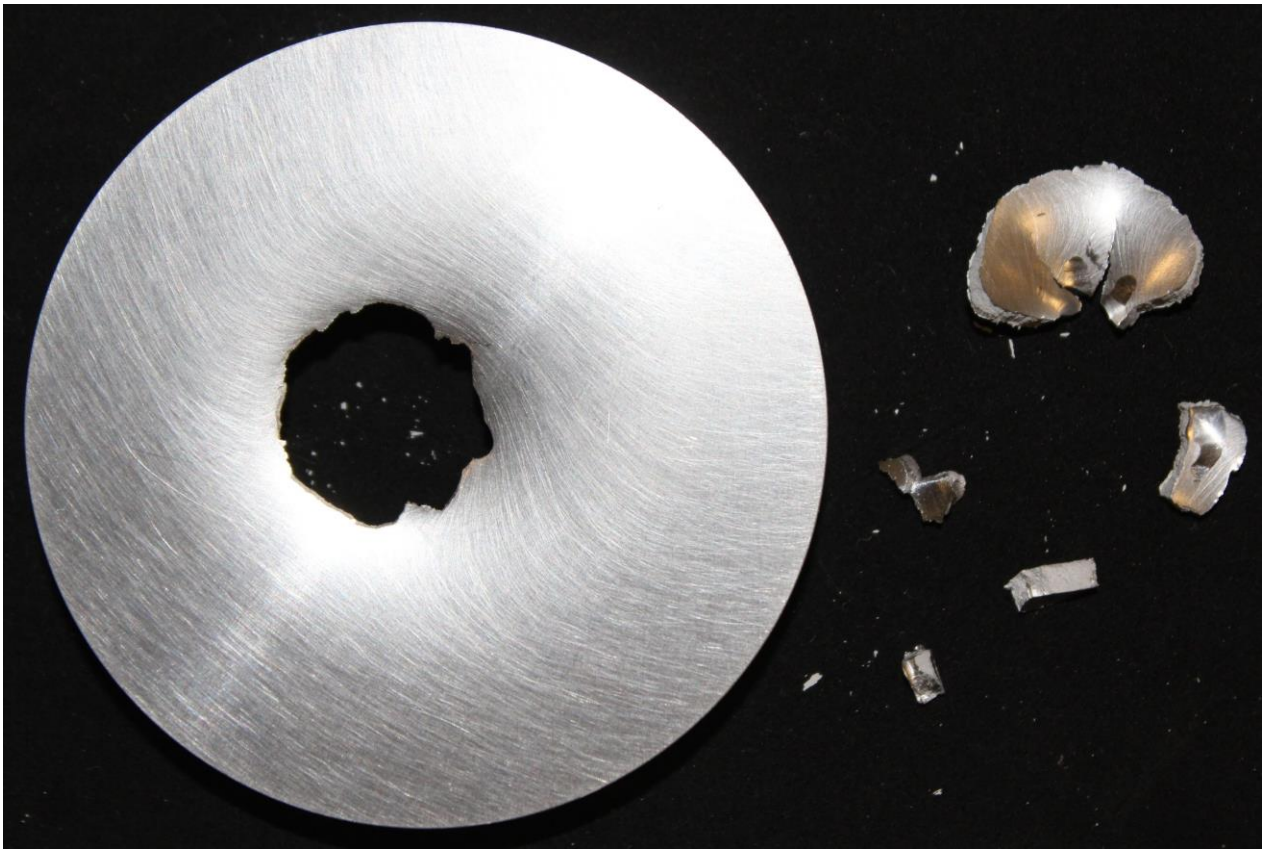

Figure 22: Specimen T114-04 After Test 66 with One-Half-Inch Spherical Probe

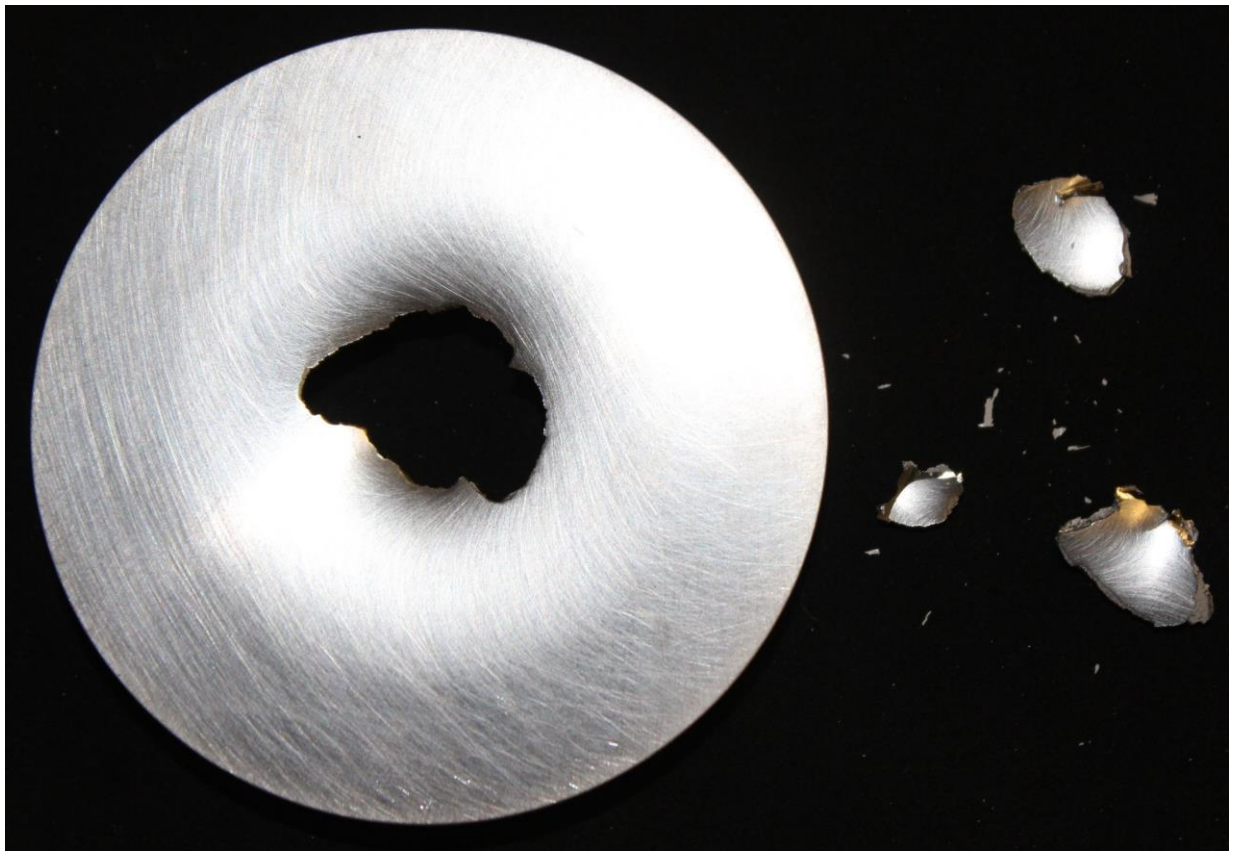

Figure 23: Specimen T114-12 After Test 93 with One-Half-Inch Tri-Corner Probe

Figure 24: One-Inch Flat-End Probe Impaled In Specimen T114-14 After Test 52

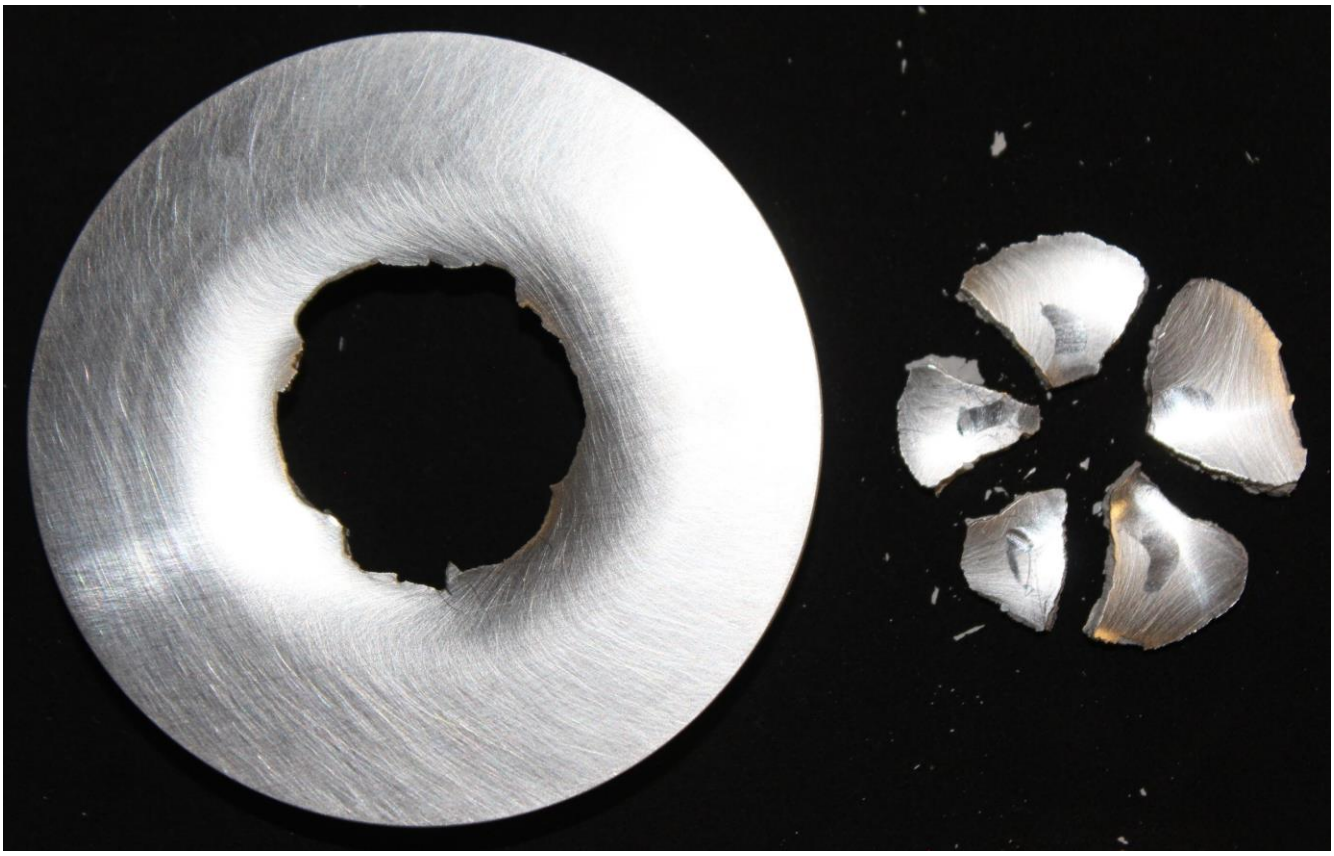

Figure 25: Specimen T114-06 After Test 81 with One-Inch Spherical Probe

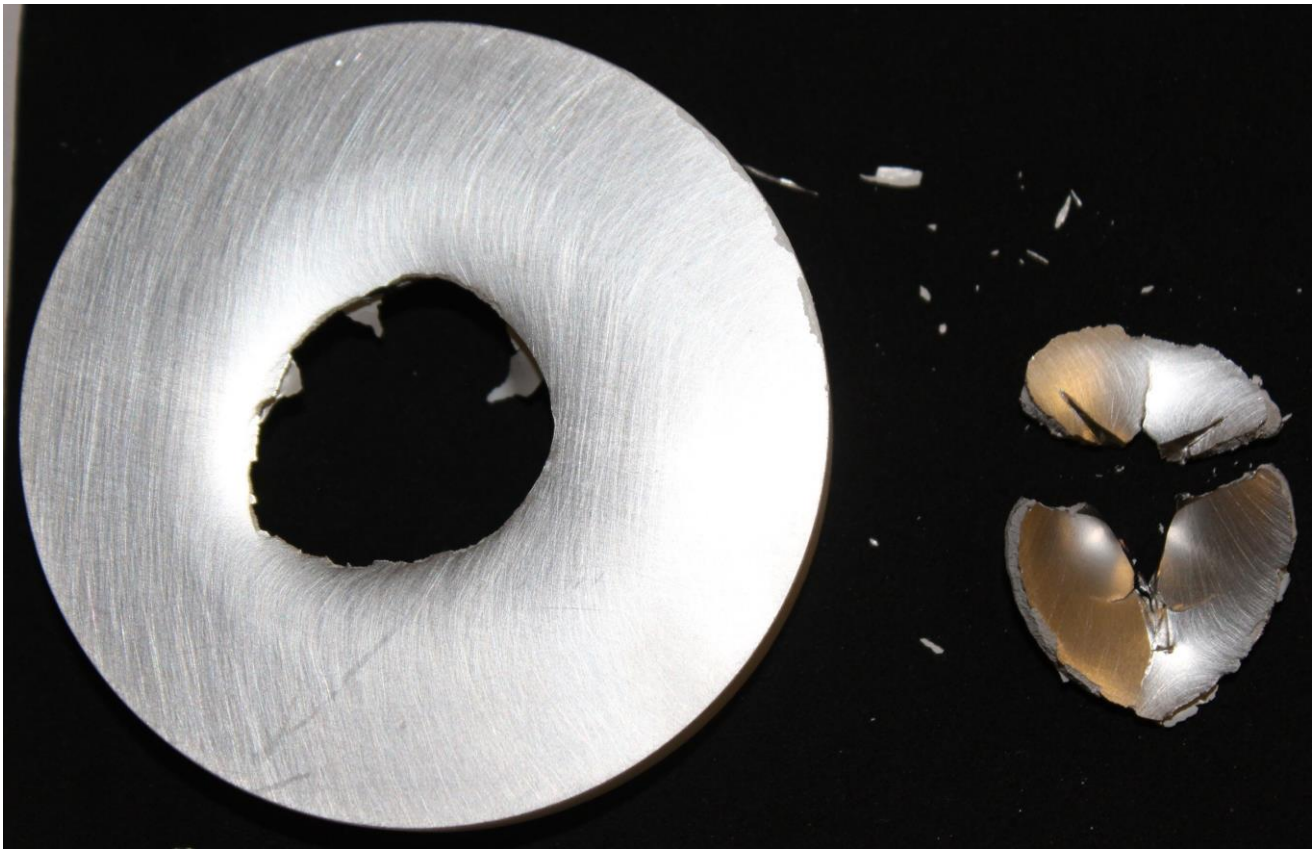

Figure 26: Specimen T114-02 After Test 109 with One-Inch Tri-Corner Probe

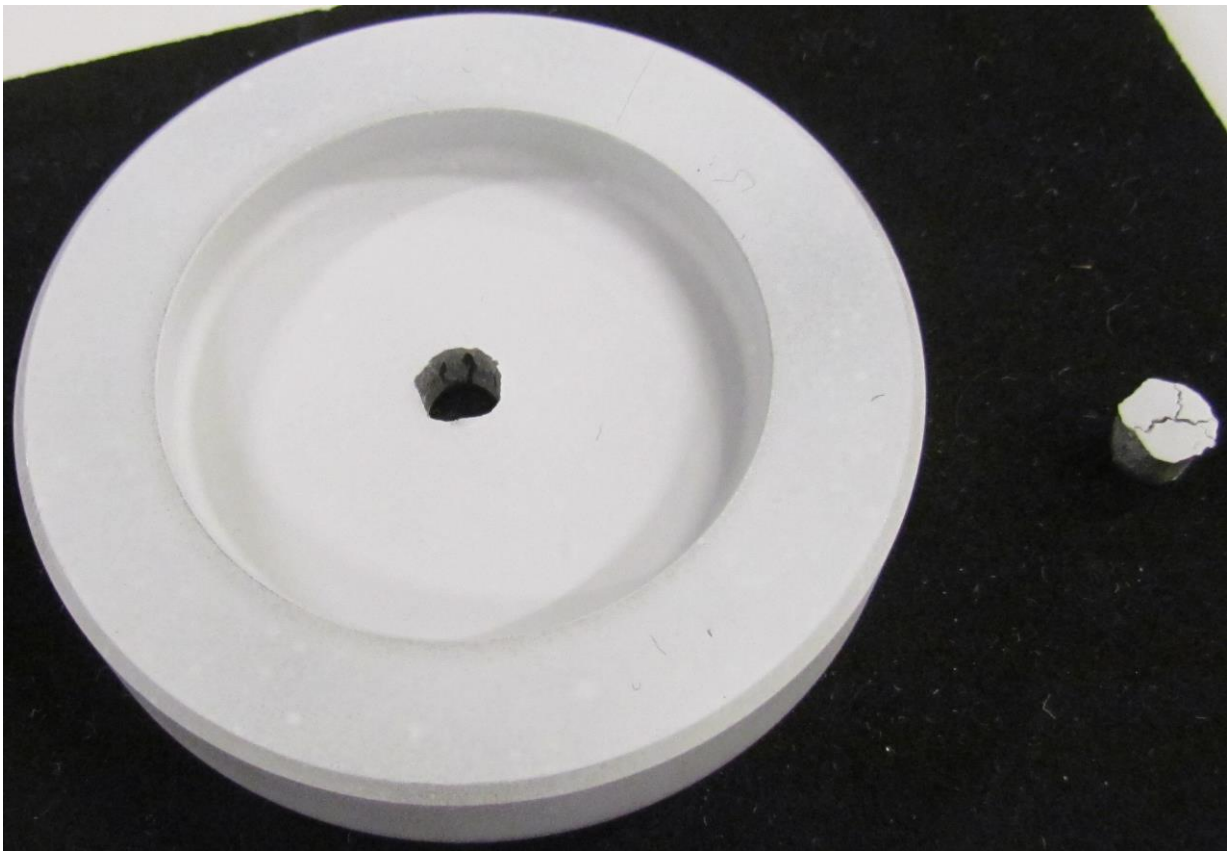

Figure 27: Specimen T250-29 After Test 27 with One-Quarter-Inch Flat-End Probe

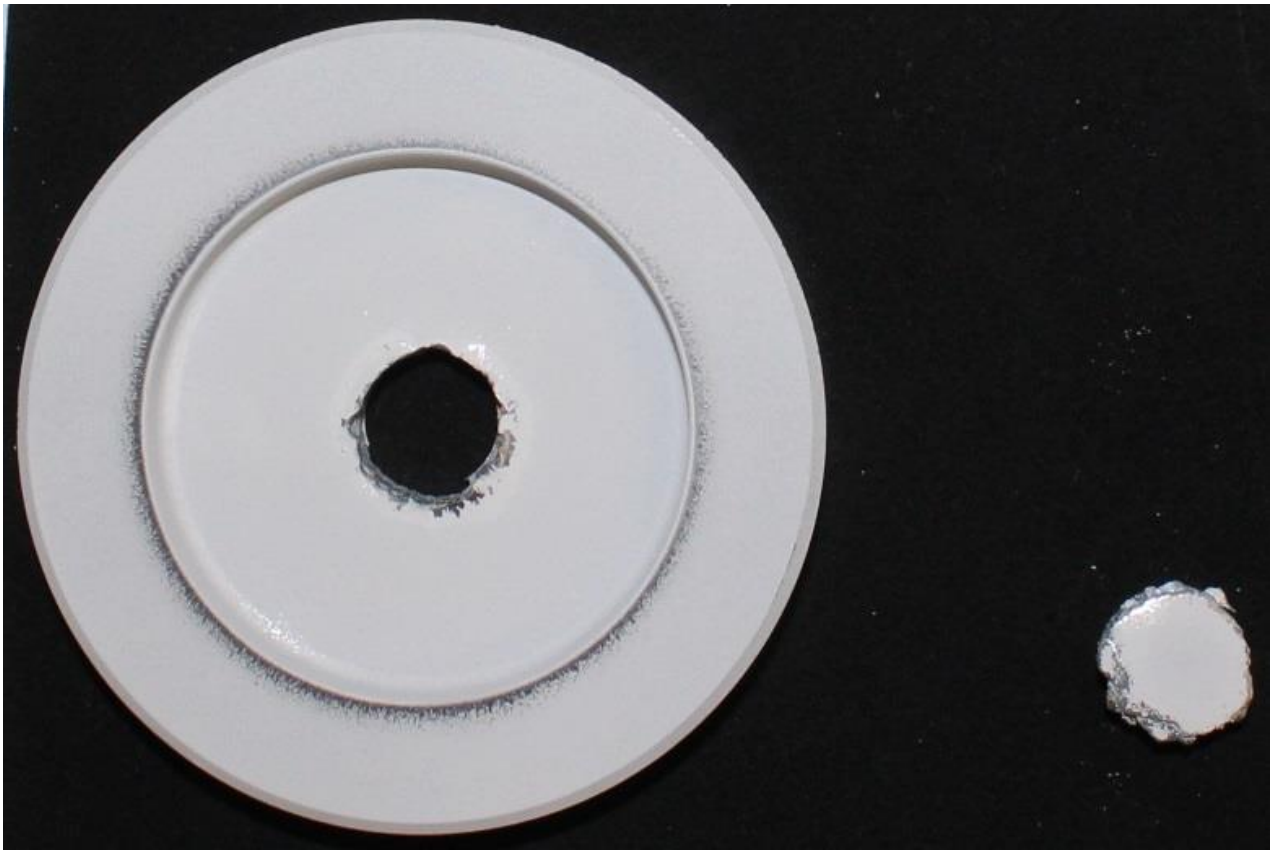

Figure 28: Specimen T250-07 After Test 39 with One-Half-Inch Flat-End Probe

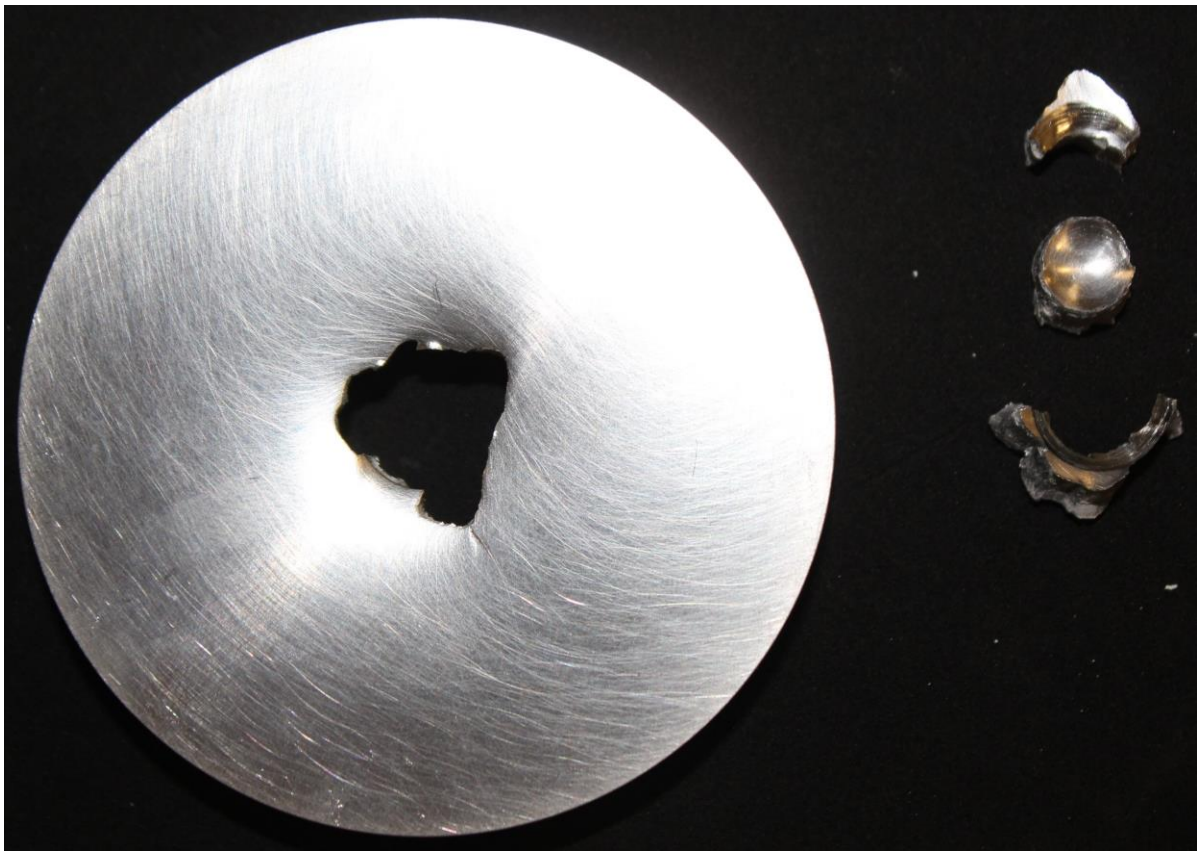

Figure 29: Specimen T250-14 After Test 72 with One-Half-Inch Spherical Probe

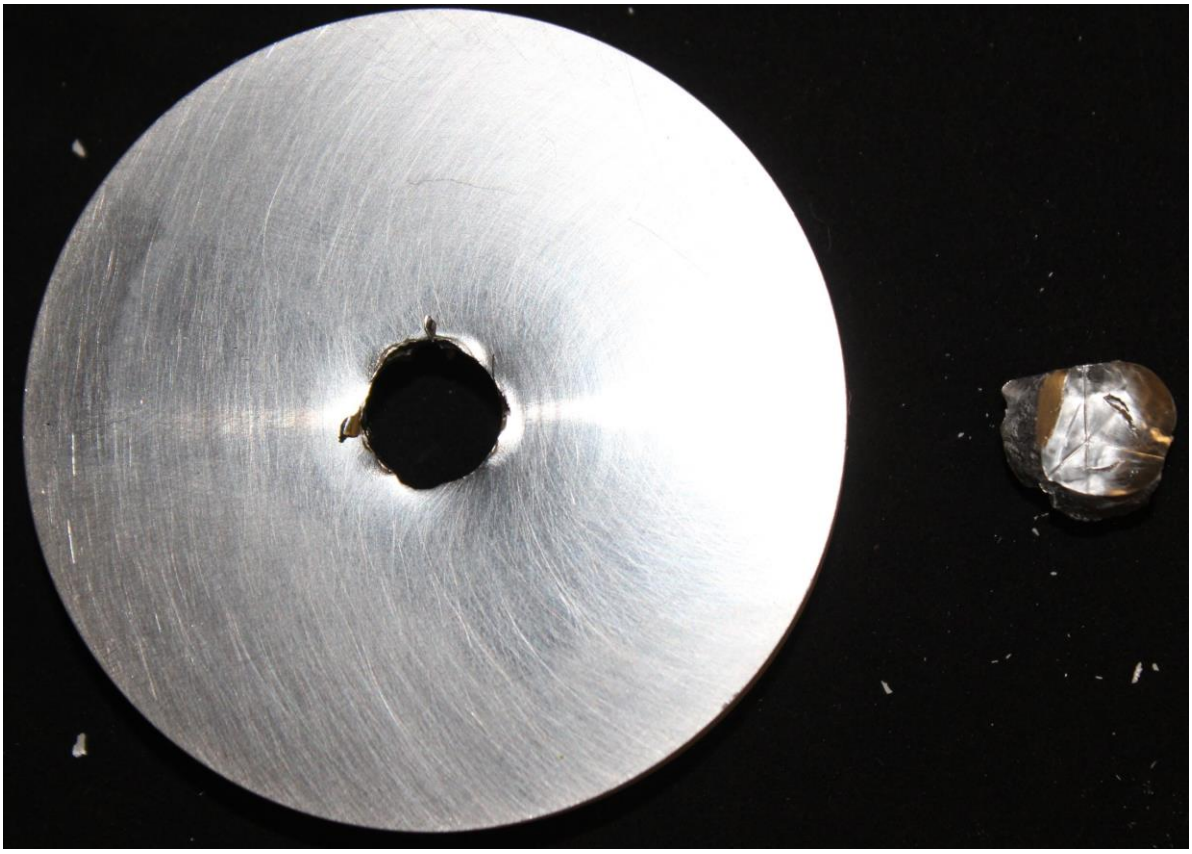

Figure 30: Specimen T250-10 After Test 99 with One-Half-Inch Tri-Corner Probe

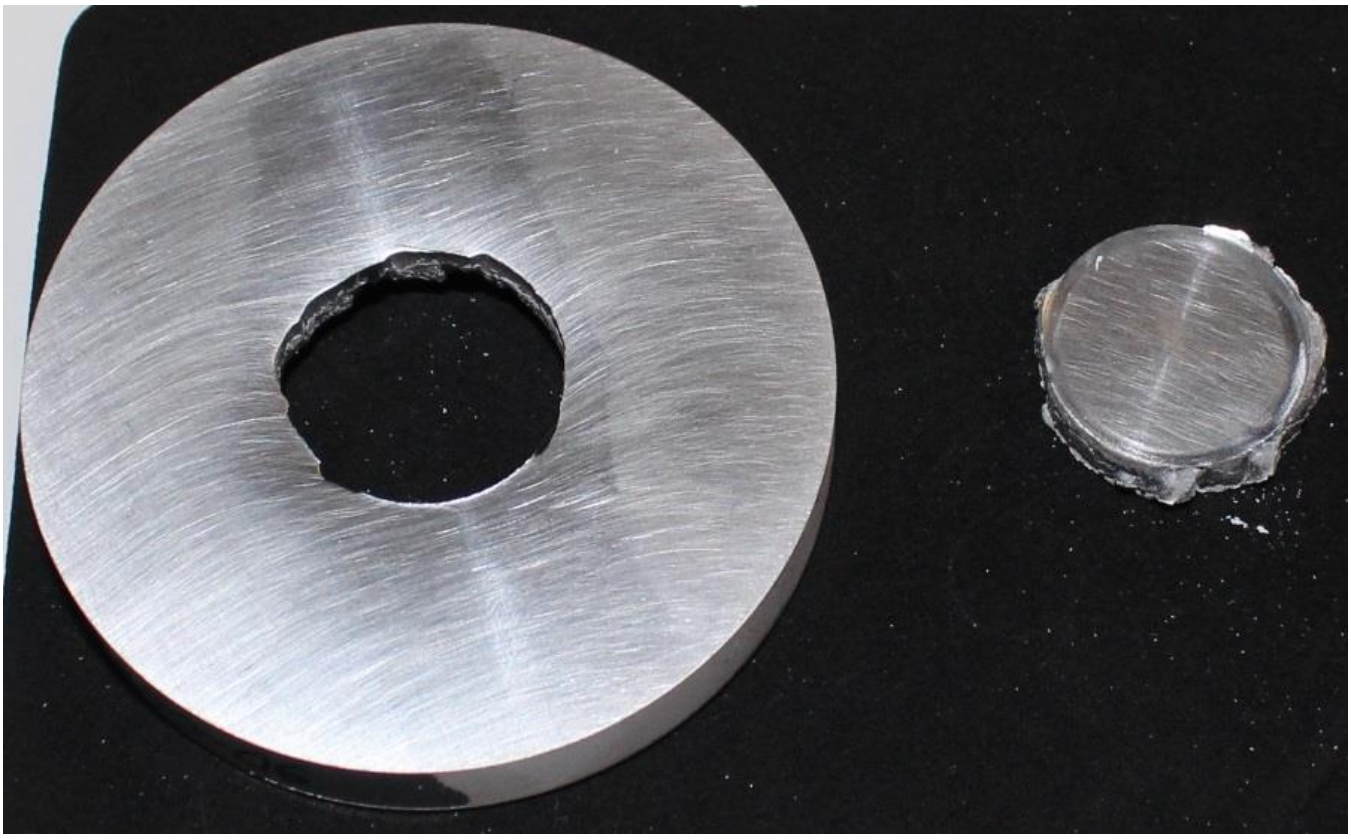

Figure 31: Specimen T250-06 After Test 55 with One-Inch Flat-End Probe

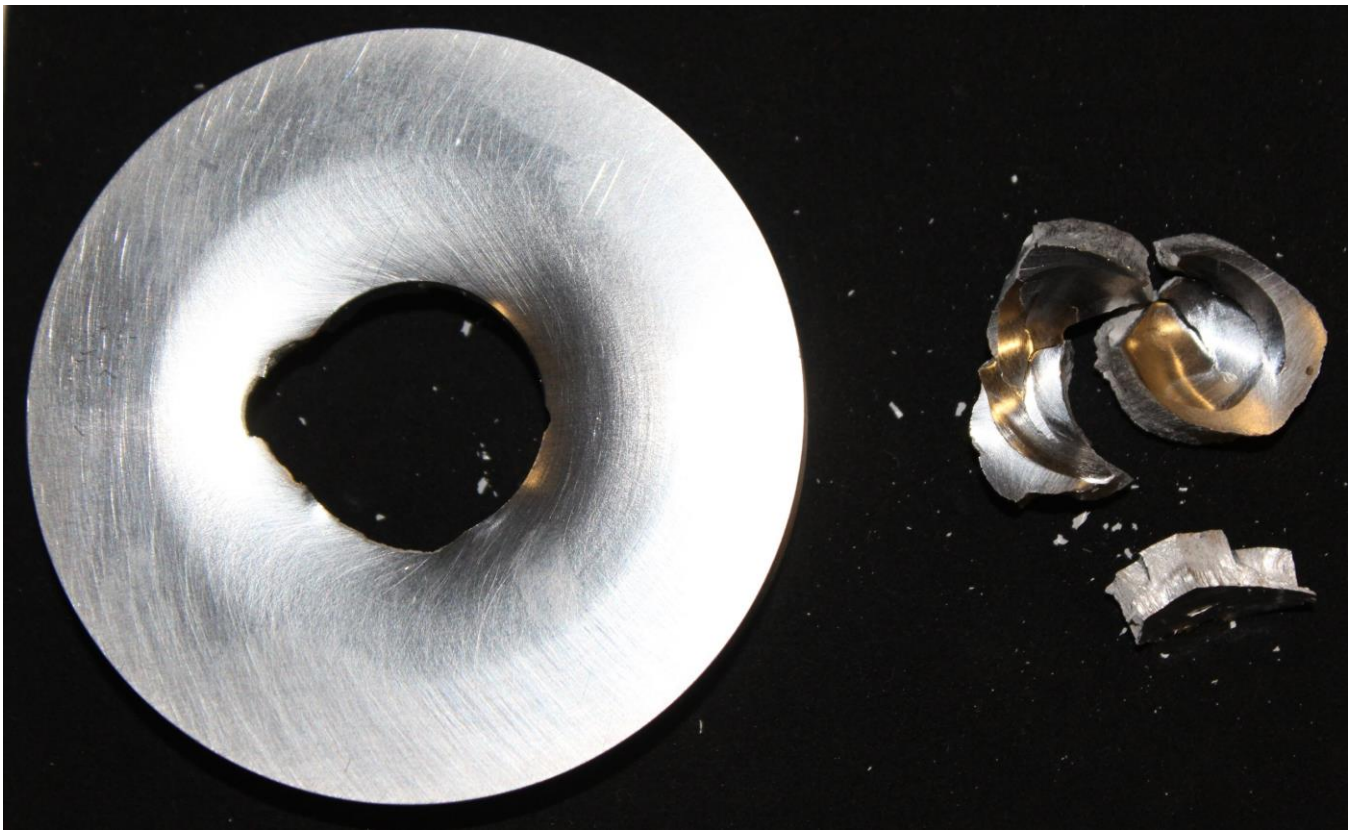

Figure 32: Specimen T250-20 After Test 89 with One-Inch Spherical Probe

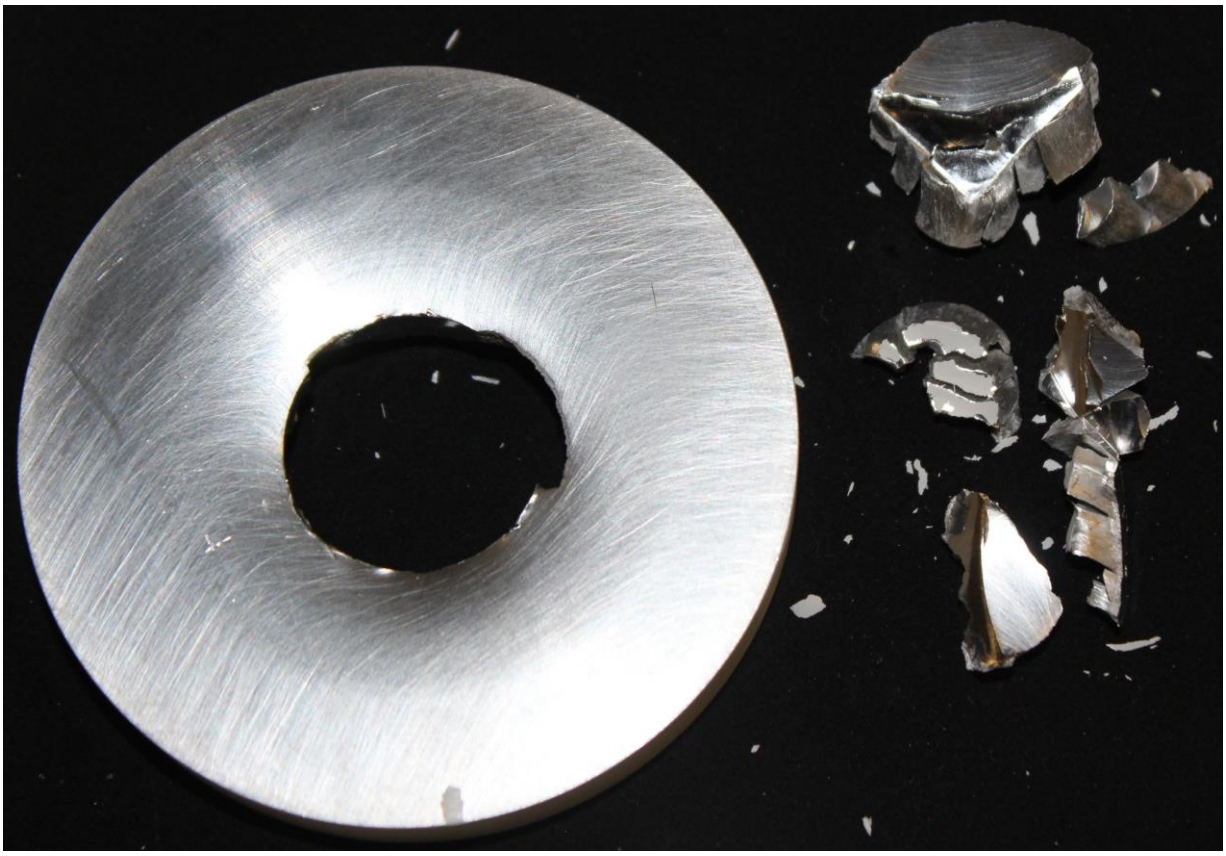

Figure 33: Specimen T250-03 After Test 114 with One-Inch Tri-Corner Probe

Data Processing Method

Most of the processing parameters are optimized for each test because of significant differences in the measured data. These values are listed in Tables 2 through 7. Although consistency in the processing parameters has been preferred, they cannot be the same for every test. Rather, a consistent approach has been taken to determine the values based on the observed data.

Table 2: Data Processing Parameters for Tests with Flat-End Probes

		Acceleration		Threshold		Time Offset		Puncture Period	
Test	Specimen	Free-Fall, a_f (G)	Peak, a_p (G)	Impact, $a_{t,i}$ (G)	Puncture, $a_{t,p}$ (G)	Impact, $\Delta t_{o,i}$ (ms)	Puncture, $\Delta t_{o,p}$ (ms)	Velocity, $\Delta t_{v,p}$ (ms)	Energy, $\Delta t_{E,p}$ (ms)
11	T051-24	0.725	2.98	0.4	0.6	0.4	0.2	1.0	5.3
12	T051-26	0.726	2.95	0.4	0.6	0.4	1.0	1.0	4.7
16	T051-28	0.715	3.00	0.5	0.6	0.7	0.6	1.0	5.4
17	T051-29	0.756	3.01	0.5	0.6	0.5	0.1	1.0	5.3
6	T051-30	0.803	2.97	0.4	0.6	0.4	0.2	1.0	5.2
5	T051-32	0.795	2.93	0.4	0.7	0.3	0.4	1.0	3.4
28	T051-03	0.432	5.28	1.0	1.2	0.5	-0.4	1.5	3.8
29	T051-08	0.387	5.87	1.0	1.2	0.3	0.3	1.6	3.2
30	T051-10	0.379	5.58	1.0	1.5	0.7	-0.1	1.4	3.8
31	T051-21	0.351	5.48	1.0	1.5	0.3	0.1	1.8	4.9
32	T051-27	0.328	5.51	1.0	1.5	0.5	-0.1	1.8	3.7

Table 2: Data Processing Parameters for Tests with Flat-End Probes, Continued

		Acceleration		Threshold		Time Offset		Puncture Period	
Test	Specimen	Free-Fall, a_f (G)	Peak, a_p (G)	Impact, $a_{t,i}$ (G)	Puncture, $a_{t,p}$ (G)	Impact, $\Delta t_{o,i}$ (ms)	Puncture, $\Delta t_{o,p}$ (ms)	Velocity, $\Delta t_{v,p}$ (ms)	Energy, $\Delta t_{E,p}$ (ms)
44	T051-14	0.778	7.65	0.8	1.0	0.8	0.0	1.0	3.2
45	T051-15	0.735	7.92	0.8	1.2	0.9	0.1	1.4	3.1
46	T051-16	0.703	7.57	0.6	1.2	1.2	0.0	1.5	3.1
48	T051-17	0.666	8.46	1.0	1.5	1.0	0.0	1.6	3.5
49	T051-20	0.621	8.24	1.0	1.5	0.2	0.2	1.3	6.6
47	T051-35	0.692	9.58	1.0	1.5	0.1	-0.1	1.7	3.4
18	T114-08	0.715	8.17	1.0	2.0	0.2	0.4	3.8	4.4
19	T114-16	0.695	8.52	0.5	1.5	0.9	0.5	3.3	5.3
20	T114-17	0.661	8.56	1.0	2.0	0.2	0.0	4.1	5.2
21	T114-23	0.631	8.82	1.0	1.5	0.2	0.1	3.4	5.7
22	T114-24	0.615	8.62	1.0	2.0	0.2	0.4	3.5	5.3
33	T114-07	0.271	13.55	1.5	3.5	0.0	0.0	3.2	5.5
35	T114-09	0.249	13.84	1.5	3.0	0.0	0.5	3.7	5.5
37	T114-27	0.678	13.03	1.0	3.0	0.6	0.3	3.4	5.4
38	T114-30	0.924	13.02	0.5	1.0	0.1	0.1	2.5	6.5
50	T114-05	0.602	24.5	2.0	4.0	0.1	0.4	5.4	5.4
51	T114-13	0.567	24.5	2.0	5.0	0.1	0.4	4.5	4.5
52	T114-14	0.525	24.9	2.0	4.0	0.1	0.1	5.0	5.9
53	T114-21	0.483	24.5	2.0	4.0	0.0	0.2	4.0	4.3
54	T114-29	0.576	24.51	2.0	5.0	0.2	0.9	3.9	4.6
23	T250-08	0.556	26.8	3.0	2.0	0.2	0.1	3.5	7.1
24	T250-16	0.560	29.8	3.0	5.0	0.2	0.3	3.7	3.7
25	T250-17	0.537	29.9	3.0	2.0	0.2	0.1	3.5	5.6
26	T250-23	0.506	28.8	3.0	2.0	0.2	0.1	3.7	7.3
27	T250-29	0.491	29.8	3.0	2.0	1.0	0.1	3.6	5.6
39	T250-07	0.823	39.8	1.0	5.0	-0.1	0.0	3.4	7.0
40	T250-09	0.881	44.5	2.0	3.0	-0.1	-0.4	3.5	7.5
41	T250-18	0.847	46.7	2.0	4.0	0.1	0.3	5.0	8.6
42	T250-24	0.822	46.6	2.0	4.0	-0.1	0.3	3.0	8.7
43	T250-30	0.788	47.3	2.0	6.0	0.0	0.5	4.5	7.5
55	T250-06	0.413	79.6	3.0	10.0	0.0	0.4	2.7	4.9
56	T250-15	0.755	68.3	4.0	8.0	0.2	0.1	5.4	7.3
57	T250-28	0.695	30.7	3.0	5.0	0.0	1.0	3.8	9.0
58	T250-34	0.675	74.3	4.0	8.0	0.2	1.0	5.2	9.0
59	T250-35	0.679	58.9	4.0	8.0	0.2	0.4	5.1	8.8

Table 3: Data Processing Parameters for Tests with Semi-spherical Probes

		Acceleration		Threshold		Time Offset		Puncture Period	
Test	Specimen	Free-Fall, a_f (G)	Peak, a_p (G)	Impact, $a_{t,i}$ (G)	Puncture, $a_{t,p}$ (G)	Impact, $\Delta t_{o,i}$ (ms)	Puncture, $\Delta t_{o,p}$ (ms)	Velocity, $\Delta t_{v,p}$ (ms)	Energy, $\Delta t_{E,p}$ (ms)
61	T051-06	0.704	2.02	0.4	0.6	0.1	0.3	1.0	5.0
62	T051-07	0.718	1.977	0.4	0.4	0.2	1.1	1.0	5.8
63	T051-11	0.714	2.03	0.4	0.4	1.0	-0.7	1.0	3.8
64	T051-13	0.654	2.25	0.5	0.5	0.1	0.5	1.0	3.5
65	T051-23	0.656	2.03	0.5	0.5	0.8	0.0	1.0	5.4
60	T051-34	0.712	1.936	0.4	0.4	0.0	0.3	1.0	4.9
76	T051-09	0.879	3.65	0.4	0.4	0.0	0.4	1.0	3.8
77	T051-12	0.802	4.24	0.5	0.5	0.2	-0.4	1.0	3.4
78	T051-18	0.757	4.92	0.5	0.5	0.0	-0.5	1.0	7.2
79	T051-19	0.728	5.43	0.6	0.6	0.5	0.6	1.0	6.6
80	T051-22	0.674	5.16	0.6	0.6	0.0	1.4	1.0	7.0
66	T114-04	0.588	8.16	1.0	1.0	0.0	0.0	3.6	7.2
67	T114-22	0.541	7.74	0.8	1.0	-0.1	0.5	4.1	7.7
68	T114-25	0.507	7.67	1.0	1.0	0.0	0.9	3.2	6.9
69	T114-33	0.452	7.67	1.0	1.0	-0.3	0.9	3.6	7.2
70	T114-35	0.442	7.89	0.8	1.0	0.0	0.6	3.7	7.2
81	T114-06	0.710	10.05	1.0	1.0	0.0	0.4	4.8	9.7
82	T114-15	0.643	10.53	1.5	1.5	0.1	0.1	3.2	5.6
83	T114-28	0.629	9.96	1.0	0.8	0.5	0.2	3.7	7.3
84	T114-31	0.606	10.24	1.0	1.5	0.2	0.4	4.8	7.9
85	T114-32	0.571	9.99	1.0	1.0	0.0	0.0	3.8	6.6
71	T250-05	0.459	37.9	2.0	5.0	-0.2	0.5	2.8	7.2
72	T250-14	0.396	39.5	3.0	8.0	-0.1	0.5	3.6	7.2
73	T250-22	0.922	32.7	2.0	6.0	-0.2	0.8	3.5	4.8
74	T250-32	0.740	36.0	3.0	4.0	0.0	0.3	3.3	5.6
75	T250-33	0.781	36.2	2.0	5.0	-0.2	0.4	3.0	6.6
87	T250-13	0.457	52.1	3.0	4.0	-0.2	0.1	5.7	7.4
89	T250-20	0.896	51.4	2.0	8.0	-0.2	0.0	4.0	5.6
90	T250-21	0.739	51.0	3.0	4.0	-0.1	0.1	5.4	5.3
91	T250-27	0.601	51.9	2.0	14.0	-0.2	0.5	3.6	7.2

Table 4: Data Processing Parameters for Tests with Tri-corner Probes

Test	Specimen	Acceleration		Threshold		Time Offset		Puncture Period	
		Free-Fall, a_f (G)	Peak, a_p (G)	Impact, $a_{t,i}$ (G)	Puncture, $a_{t,p}$ (G)	Impact, $\Delta t_{o,i}$ (ms)	Puncture, $\Delta t_{o,p}$ (ms)	Velocity, $\Delta t_{v,p}$ (ms)	Energy, $\Delta t_{E,p}$ (ms)
103	T051-01	0.744	1.781	0.3	0.4	0.2	0.6	1.0	3.8
104	T051-02	0.750	1.777	0.4	0.3	0.4	0.5	1.0	7.3
4	T051-31	0.907	1.750	0.2	0.3	-0.1	-0.4	1.0	6.0
105	T051-05	0.729	2.27	0.4	0.4	0.1	-0.8	1.0	3.6
106	T051-25	0.656	2.24	0.5	0.5	-0.1	0.9	1.0	4.2
107	T051-33	0.652	2.38	0.5	0.5	0.6	0.7	1.0	7.1
92	T114-03	0.873	6.87	0.5	1.0	-0.2	-0.1	3.7	6.8
93	T114-12	0.852	6.97	1.0	1.5	0.6	0.7	4.7	8.0
94	T114-19	0.844	6.87	0.6	1.6	0.0	0.2	3.7	6.9
95	T114-20	0.821	6.62	0.6	0.5	0.3	0.3	4.7	7.4
96	T114-34	0.814	6.95	1.0	2.0	0.3	0.5	3.3	6.0
108	T114-01	0.610	7.55	1.0	2.0	-0.2	0.4	3.5	5.5
109	T114-02	0.563	7.70	1.0	1.0	-0.1	0.3	3.8	7.6
110	T114-10	0.541	8.00	1.0	2.0	-0.1	0.2	3.0	6.8
111	T114-11	0.538	9.04	1.0	1.0	-0.2	0.6	6.5	6.8
112	T114-26	0.520	7.59	1.0	1.2	0.0	0.0	2.8	6.6
98	T250-01	0.781	30.6	2.0	5.0	-0.2	-0.2	3.1	5.9
99	T250-10	0.776	30.5	2.0	4.0	-0.2	-0.4	3.3	5.3
100	T250-19	0.764	29.5	2.0	4.0	0.0	-0.3	3.5	5.8
101	T250-25	0.719	32.3	2.0	3.0	0.1	0.5	3.5	7.2
102	T250-31	0.707	33.6	2.0	3.0	0.1	-0.7	2.8	6.9
113	T250-02	0.892	41.7	3.0	6.0	-0.2	0.8	4.6	4.6
114	T250-03	0.920	43.4	3.0	8.0	0.7	-0.6	2.0	5.5
115	T250-11	0.726	42.3	4.0	8.0	0.2	0.5	3.4	5.7
116	T250-12	0.957	40.7	3.0	8.0	-0.2	-0.1	3.3	6.7
117	T250-26	0.929	40.4	3.0	5.0	0.2	-0.3	3.4	6.3

Table 5: Reference Position for Tests with Flat-End Probes

Test	Specimen	Reference Position, p_r	
		(mm)	(in)
11	T051-24	-17.41	-0.685
12	T051-26	-17.53	-0.690
16	T051-28	-17.27	-0.680
17	T051-29	-17.17	-0.676
6	T051-30	-17.38	-0.684
5	T051-32	-17.50	-0.689
28	T051-03	-19.08	-0.751
29	T051-08	-19.10	-0.752
30	T051-10	-18.21	-0.717
31	T051-21	-18.14	-0.714
32	T051-27	-17.99	-0.708

Table 5: Reference Position for Tests with Flat-End Probes, Continued

Test	Specimen	Reference Position, p_r (mm)	(in)
44	T051-14	-18.04	-0.710
45	T051-15	-18.19	-0.716
46	T051-16	-17.76	-0.699
48	T051-17	-17.66	-0.695
49	T051-20	-17.84	-0.702
47	T051-35	-18.37	-0.723
18	T114-08	-18.50	-0.728
19	T114-16	-17.90	-0.705
20	T114-17	-18.17	-0.715
21	T114-23	-17.22	-0.678
22	T114-24	-17.96	-0.707
33	T114-07	-17.68	-0.696
35	T114-09	-18.47	-0.727
37	T114-27	-20.87	-0.822
38	T114-30	-19.39	-0.763
50	T114-05	-22.29	-0.878
51	T114-13	-20.45	-0.805
52	T114-14	-20.42	-0.804
53	T114-21	-19.79	-0.779
54	T114-29	-20.66	-0.813
23	T250-08	-17.19	-0.677
24	T250-16	-16.34	-0.643
25	T250-17	-16.20	-0.638
26	T250-23	-15.93	-0.627
27	T250-29	-16.05	-0.632
39	T250-07	-19.55	-0.770
40	T250-09	-19.89	-0.783
41	T250-18	-20.78	-0.818
42	T250-24	-19.28	-0.759
43	T250-30	-19.65	-0.774
55	T250-06	-19.52	-0.769
56	T250-15	-23.55	-0.927
57	T250-28	-23.01	-0.906
58	T250-34	-23.26	-0.916
59	T250-35	-22.48	-0.885

Table 6: Reference Position for Tests with Semi-spherical Probes

Test	Specimen	Reference Position, p_r (mm)	(in)
61	T051-06	-12.87	-0.507
62	T051-07	-12.47	-0.491
63	T051-11	-11.10	-0.437
64	T051-13	-14.26	-0.562
65	T051-23	-11.21	-0.441
60	T051-34	-14.87	-0.586
76	T051-09	-14.06	-0.554
77	T051-12	-12.66	-0.499
78	T051-18	-11.55	-0.455
79	T051-19	-12.96	-0.510
80	T051-22	-14.56	-0.573
66	T114-04	-10.66	-0.420
67	T114-22	-10.99	-0.433
68	T114-25	-13.09	-0.515
69	T114-33	-12.39	-0.488
70	T114-35	-11.23	-0.442
81	T114-06	-12.98	-0.511
82	T114-15	-11.46	-0.451
83	T114-28	-9.76	-0.384
84	T114-31	-10.61	-0.418
85	T114-32	-11.18	-0.440
71	T250-05	-8.81	-0.347
72	T250-14	-9.22	-0.363
73	T250-22	-15.95	-0.628
74	T250-32	-12.09	-0.476
75	T250-33	-11.80	-0.465
87	T250-13	-6.93	-0.273
89	T250-20	-16.36	-0.644
90	T250-21	-17.14	-0.675
91	T250-27	-16.29	-0.641

Table 7: Reference Position for Tests with Tri-corner Probes

Test	Specimen	Reference Position, p_r (mm)	(in)
103	T051-01	-17.24	-0.679
104	T051-02	-11.97	-0.471
4	T051-31	-13.57	-0.534
105	T051-05	-21.59	-0.850
106	T051-25	-21.68	-0.854
107	T051-33	-21.78	-0.857
92	T114-03	-12.63	-0.497
93	T114-12	-12.36	-0.487
94	T114-19	-14.16	-0.557
95	T114-20	-16.23	-0.639
96	T114-34	-13.55	-0.533
108	T114-01	-24.01	-0.945
109	T114-02	-23.63	-0.930
110	T114-10	-23.18	-0.913
111	T114-11	-24.64	-0.970
112	T114-26	-14.59	-0.574
98	T250-01	-14.95	-0.589
99	T250-10	-13.79	-0.543
100	T250-19	-13.95	-0.549
101	T250-25	-15.32	-0.603
102	T250-31	-12.77	-0.503
113	T250-02	-28.95	-1.140
114	T250-03	-21.74	-0.856
115	T250-11	-23.46	-0.924
116	T250-12	-22.59	-0.889
117	T250-26	-22.35	-0.880

The times when the probe contacts the specimen and penetrates it are determined from the acceleration data. Threshold accelerations are selected for identifying the impact and puncture events. Impact is considered to occur at the last time (t_i) when the acceleration is less than the impact threshold ($a_{t,i}$) prior to the peak acceleration (a_p), and the puncture is considered complete at the last time (t_p) when the acceleration is greater than the puncture threshold ($a_{t,p}$) after the peak. Figure 34 illustrates these accelerations and times. The thresholds for tests with a particular combination of input parameters are similar; however, differences in the data necessitate some variation. The figures in Appendix A show the acceleration data for each test with the thresholds for impact and complete puncture.

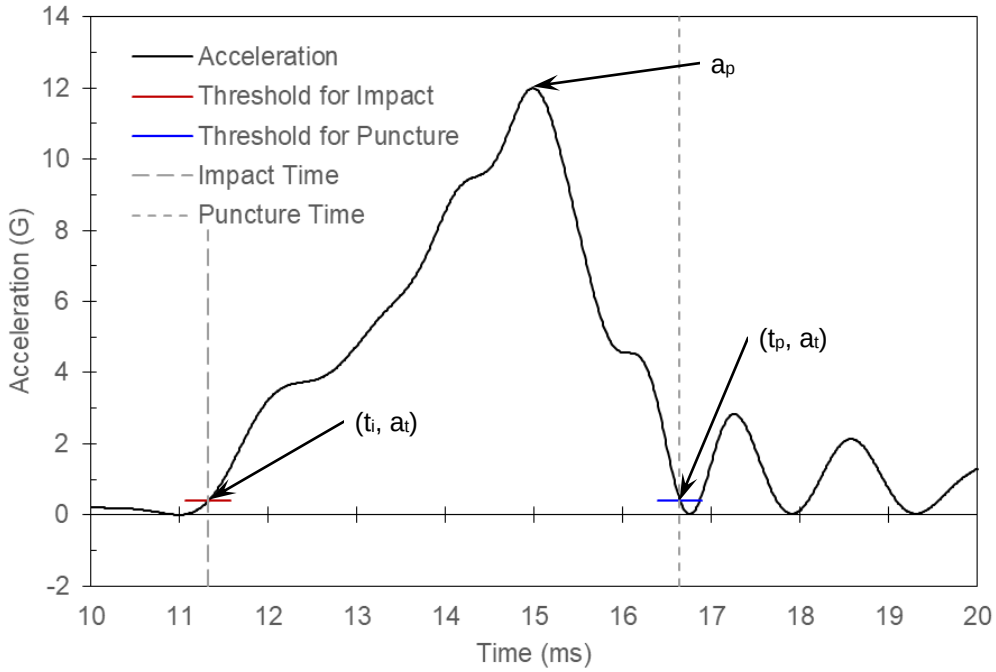

Figure 34: Representative Acceleration Curve with Impact and Puncture Times Identified

The position data from the two laser interferometers (p_L on the left and p_R on the right) are averaged and shifted with Equation 1. The reference position (p_r) is selected such that the position is zero when the puncture process is complete (t_p). The reference position also makes the potential energy (E_P, Eq. 2) positive when the probe contacts the specimen and zero when it breaks through. The mass (m) of the carriage with the attached mounting fixtures, accelerometer, and probe is 139.7 kg (9.57 slug). The free-fall acceleration of the carriage (a_f) is calibrated to correspond to a free-fall condition prior to the time of impact, accounting for friction in the guide rods, and is explained subsequently.

$$p = \frac{p_L + p_R}{2} - p_r \tag{1}$$

$$E_P = m\, a_f\, p \tag{2}$$

The average carriage position is differentiated to obtain the carriage velocity (v, Eq. 3). For each time in the data set, the velocity value (v_j) is given by Equation 4, where j is the index of the data points. The majority of the velocity values are computed with the second-order central finite difference formula; the first and last velocity values are evaluated with first-order finite difference formulas based on the available data points. The kinetic energy of the carriage and probe is defined by Equation 5 and the total energy by Equation 6.

$$v = \frac{dp}{dt} \tag{3}$$

$$v_j = \begin{cases} \dfrac{p_{j+1} - p_j}{t_{j+1} - t_j} & j = 1 \\ \dfrac{p_{j+1} - p_{j-1}}{t_{j+1} - t_{j-1}} & j = 2 \ldots n-1 \\ \dfrac{p_j - p_{j-1}}{t_j - t_{j-1}} & j = n \end{cases} \tag{4}$$

$$E_K = \frac{m\,v^2}{2} \tag{5}$$

$$E_T = E_P + E_K \tag{6}$$

The free-fall acceleration of the carriage is optimized such that a linear fit to the total energy during a certain period of time prior to the probe contacting the specimen has zero slope. This calibrates the data to a true free-fall condition prior to the time of impact. It correctly accounts for friction in the carriage guide rods and the increase in potential energy as the carriage falls through the specimen. The total energy is always averaged over a time period of 20 ms ($\Delta t_{E,i}$), but the end of the period is offset relative to the impact time (t_i), and the offset ($\Delta t_{o,i}$) differs between tests. During this period, several complete cycles of oscillation are observed in the total energy. The average of the total energy in this period is taken as the total energy before impact ($E_{T,i}$). The total energy after complete puncture ($E_{T,p}$) is the average value in a period of time beginning within 1.5 ms ($\Delta t_{o,p}$) of the puncture time (t_p) and lasting about 6 ms ($\Delta t_{E,p}$). Tables 2 through 4 have the actual values of the puncture time offset and period for each test. The total energy mitigated by the specimen is

$$E_M = E_{T,i} - E_{T,p} \tag{7}$$

Figure 35 illustrates the time periods over which the total energy is averaged and the difference between the averages. The figures in Appendix B plot the total energy as a function of time and bracket the time periods that are averaged before impact and after complete puncture.

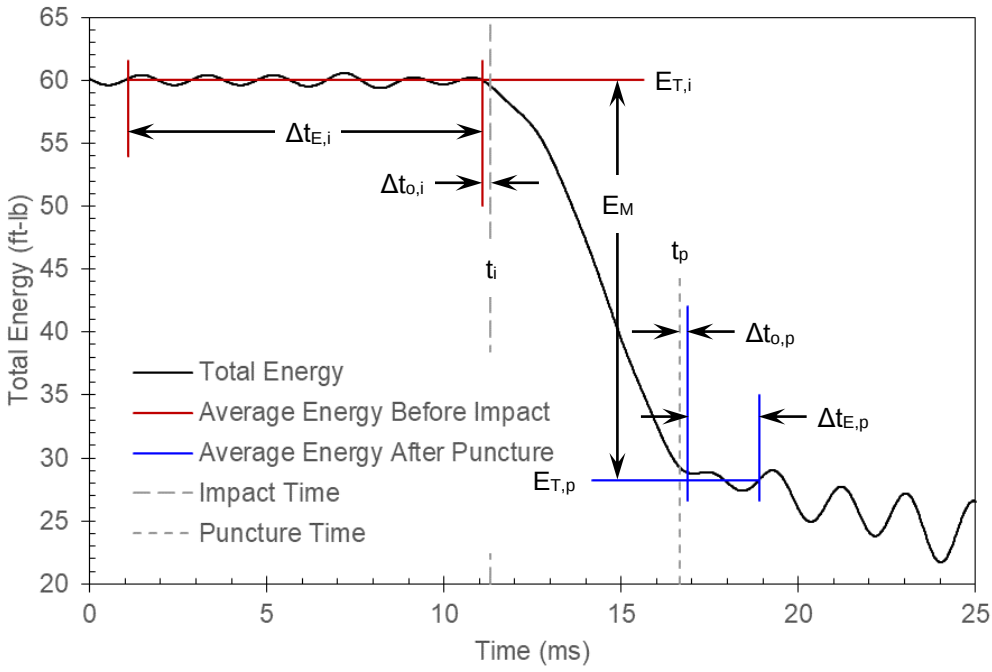

Figure 35: Representative Total Energy Curve and Time Periods for Averaging

The carriage velocity before impact (v_i) is found by averaging the velocity values over a time period of 1 ms ($\Delta t_{v,i}$) that ends at the offset impact time ($t_i - \Delta t_{o,i}$). The velocity after complete puncture (v_p) is the average value over a variable time period ($\Delta t_{v,p}$) that starts at the offset puncture time ($t_p + \Delta t_{o,p}$). The impact time period is constant, but the puncture time period and offsets are unique to each test (Tables 2–4). Figure 36 illustrates the time periods

and offsets. Appendix C has plots of the velocity data for each test and the time periods in which it is averaged.

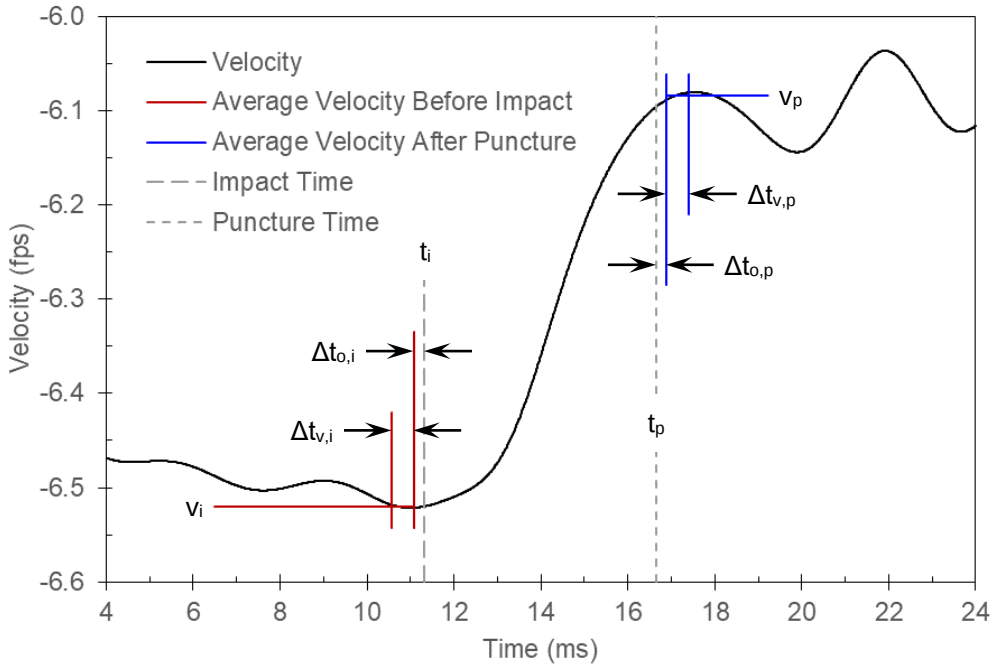

Figure 36: Representative Velocity Curve and Time Periods for Averaging

Tables 8 through 10 correlate the test and specimen numbers with the measured thickness of each specimen at the gauge section and the nominal diameter of the probe. The maximum deviation between the measured thickness (the average of several measurements) and the nominal thickness is 2.4%. The distance traveled by the probe during the puncture process is the difference in the positions at the impact and puncture times (t_i, t_p). The results of the distance, velocity, and energy calculations are provided in Tables 11 through 16.

Table 8: Measurements of Disc Specimens Made from 7075-T651 Bar and Nominal Diameters of Flat-End Probes

Test	Specimen	Probe Design	Thickness (mm)	Thickness (in)	Probe Diameter (mm)	Probe Diameter (in)
11	T051-24	F0250	1.307	0.0515	6.35	0.250
12	T051-26	F0250	1.287	0.0507	6.35	0.250
16	T051-28	F0250	1.293	0.0509	6.35	0.250
17	T051-29	F0250	1.297	0.0511	6.35	0.250
6	T051-30	F0250	1.309	0.0516	6.35	0.250
5	T051-32	F0250	1.307	0.0515	6.35	0.250
28	T051-03	F0500	1.295	0.0510	12.70	0.500
29	T051-08	F0500	1.303	0.0513	12.70	0.500
30	T051-10	F0500	1.294	0.0510	12.70	0.500
31	T051-21	F0500	1.290	0.0508	12.70	0.500
32	T051-27	F0500	1.303	0.0513	12.70	0.500
44	T051-14	F1000	1.306	0.0514	25.40	1.000
45	T051-15	F1000	1.292	0.0509	25.40	1.000
46	T051-16	F1000	1.279	0.0504	25.40	1.000

Table 8: Measurements of Disc Specimens Made from 7075-T651 Bar and Flat-End Probes, Continued

Test	Specimen	Probe Design	Thickness (mm)	Thickness (in)	Probe Diameter (mm)	Probe Diameter (in)
48	T051-17	F1000	1.265	0.0498	25.40	1.000
49	T051-20	F1000	1.280	0.0504	25.40	1.000
47	T051-35	F1000	1.308	0.0515	25.40	1.000
18	T114-08	F0250	2.868	0.1129	6.35	0.250
19	T114-16	F0250	2.869	0.1130	6.35	0.250
20	T114-17	F0250	2.869	0.1130	6.35	0.250
21	T114-23	F0250	2.869	0.1130	6.35	0.250
22	T114-24	F0250	2.870	0.1130	6.35	0.250
33	T114-07	F0500	2.865	0.1128	12.70	0.500
35	T114-09	F0500	2.878	0.1133	12.70	0.500
37	T114-27	F0500	2.873	0.1131	12.70	0.500
38	T114-30	F0500	2.871	0.1131	12.70	0.500
50	T114-05	F1000	2.866	0.1129	25.40	1.000
51	T114-13	F1000	2.877	0.1133	25.40	1.000
52	T114-14	F1000	2.842	0.1119	25.40	1.000
53	T114-21	F1000	2.870	0.1130	25.40	1.000
54	T114-29	F1000	2.863	0.1127	25.40	1.000
23	T250-08	F0250	6.332	0.2493	6.35	0.250
24	T250-16	F0250	6.335	0.2494	6.35	0.250
25	T250-17	F0250	6.339	0.2496	6.35	0.250
26	T250-23	F0250	6.327	0.2491	6.35	0.250
27	T250-29	F0250	6.337	0.2495	6.35	0.250
39	T250-07	F0500	6.331	0.2493	12.70	0.500
40	T250-09	F0500	6.331	0.2493	12.70	0.500
41	T250-18	F0500	6.328	0.2492	12.70	0.500
42	T250-24	F0500	6.326	0.2491	12.70	0.500
43	T250-30	F0500	6.328	0.2492	12.70	0.500
55	T250-06	F1000	6.333	0.2494	25.40	1.000
56	T250-15	F1000	6.331	0.2493	25.40	1.000
57	T250-28	F1000	6.337	0.2495	25.40	1.000
58	T250-34	F1000	6.330	0.2492	25.40	1.000
59	T250-35	F1000	6.325	0.2490	25.40	1.000

Table 9: Measurements of Disc Specimens Made from 7075-T651 Bar and Nominal Diameters of Semi-spherical Probes

Test	Specimen	Probe Design	Thickness (mm)	Thickness (in)	Probe Diameter (mm)	Probe Diameter (in)
61	T051-06	S0500	1.280	0.0504	12.70	0.500
62	T051-07	S0500	1.289	0.0508	12.70	0.500
63	T051-11	S0500	1.299	0.0512	12.70	0.500
64	T051-13	S0500	1.308	0.0515	12.70	0.500
65	T051-23	S0500	1.295	0.0510	12.70	0.500
60	T051-34	S0500	1.306	0.0514	12.70	0.500
76	T051-09	S1000	1.298	0.0511	25.40	1.000
77	T051-12	S1000	1.285	0.0506	25.40	1.000
78	T051-18	S1000	1.297	0.0511	25.40	1.000
79	T051-19	S1000	1.298	0.0511	25.40	1.000
80	T051-22	S1000	1.289	0.0508	25.40	1.000
66	T114-04	S0500	2.866	0.1129	12.70	0.500
67	T114-22	S0500	2.871	0.1131	12.70	0.500
68	T114-25	S0500	2.870	0.1130	12.70	0.500
69	T114-33	S0500	2.863	0.1127	12.70	0.500
70	T114-35	S0500	2.870	0.1130	12.70	0.500
81	T114-06	S1000	2.861	0.1127	25.40	1.000
82	T114-15	S1000	2.868	0.1129	25.40	1.000
83	T114-28	S1000	2.873	0.1131	25.40	1.000
84	T114-31	S1000	2.870	0.1130	25.40	1.000
85	T114-32	S1000	2.877	0.1133	25.40	1.000
71	T250-05	S0500	6.336	0.2495	12.70	0.500
72	T250-14	S0500	6.340	0.2496	12.70	0.500
73	T250-22	S0500	6.340	0.2496	12.70	0.500
74	T250-32	S0500	6.330	0.2492	12.70	0.500
75	T250-33	S0500	6.331	0.2493	12.70	0.500
87	T250-13	S1000	6.331	0.2493	25.40	1.000
89	T250-20	S1000	6.332	0.2493	25.40	1.000
90	T250-21	S1000	6.331	0.2493	25.40	1.000
91	T250-27	S1000	6.331	0.2493	25.40	1.000

Table 10: Measurements of Disc Specimens Made from 7075-T651 Bar and Nominal Diameters of Tri-corner Probes

Test	Specimen	Probe Design	Thickness (mm)	Thickness (in)	Probe Diameter (mm)	Probe Diameter (in)
103	T051-01	C0500	1.292	0.0509	12.70	0.500
104	T051-02	C0500	1.299	0.0512	12.70	0.500
4	T051-31	C0500	1.313	0.0517	12.70	0.500
105	T051-05	C1000	1.293	0.0509	25.40	1.000
106	T051-25	C1000	1.302	0.0513	25.40	1.000
107	T051-33	C1000	1.309	0.0516	25.40	1.000
92	T114-03	C0500	2.869	0.1130	12.70	0.500
93	T114-12	C0500	2.868	0.1129	12.70	0.500
94	T114-19	C0500	2.871	0.1131	12.70	0.500
95	T114-20	C0500	2.856	0.1125	12.70	0.500
96	T114-34	C0500	2.868	0.1129	12.70	0.500
108	T114-01	C1000	2.856	0.1125	25.40	1.000
109	T114-02	C1000	2.863	0.1127	25.40	1.000
110	T114-10	C1000	2.871	0.1131	25.40	1.000
111	T114-11	C1000	2.866	0.1129	25.40	1.000
112	T114-26	C1000	2.855	0.1124	25.40	1.000
98	T250-01	C0500	6.335	0.2494	12.70	0.500
99	T250-10	C0500	6.342	0.2497	12.70	0.500
100	T250-19	C0500	6.339	0.2496	12.70	0.500
101	T250-25	C0500	6.335	0.2494	12.70	0.500
102	T250-31	C0500	6.342	0.2497	12.70	0.500
113	T250-02	C1000	6.330	0.2492	25.40	1.000
114	T250-03	C1000	6.333	0.2494	25.40	1.000
115	T250-11	C1000	6.341	0.2497	25.40	1.000
116	T250-12	C1000	6.337	0.2495	25.40	1.000
117	T250-26	C1000	6.330	0.2492	25.40	1.000

Table 11: Results of Puncture Experiments with Flat-End Probes on Disc Specimens Made from 7075-T651 Bar

Test	Specimen	Probe Design	Distance Traveled (mm)	Distance Traveled (in)	Impact Velocity, v_i (m/s)	Impact Velocity, v_i (fps)	Puncture Velocity, v_p (m/s)	Puncture Velocity, v_p (fps)
11	T051-24	F0250	5.01	0.197	0.85	2.78	0.82	2.70
12	T051-26	F0250	4.79	0.189	0.59	1.94	0.56	1.85
16	T051-28	F0250	4.64	0.182	0.55	1.82	0.52	1.70
17	T051-29	F0250	4.46	0.176	0.66	2.16	0.63	2.05
6	T051-30	F0250	5.09	0.200	0.88	2.87	0.85	2.80
5	T051-32	F0250	5.08	0.200	0.87	2.85	0.85	2.78
28	T051-03	F0500	6.71	0.264	0.94	3.10	0.84	2.77
29	T051-08	F0500	6.28	0.247	0.66	2.16	0.49	1.60
30	T051-10	F0500	5.59	0.220	0.67	2.19	0.52	1.71
31	T051-21	F0500	5.28	0.208	0.67	2.18	0.52	1.70
32	T051-27	F0500	5.29	0.208	0.65	2.13	0.50	1.62

Table 11: Results of Puncture Experiments with Flat-End Probes on Disc Specimens Made from 7075-T651 Bar, Continued

Test	Specimen	Probe Design	Distance Traveled (mm)	Distance Traveled (in)	Impact Velocity, v_i (m/s)	Impact Velocity, v_i (fps)	Puncture Velocity, v_p (m/s)	Puncture Velocity, v_p (fps)
44	T051-14	F1000	7.34	0.289	1.69	5.55	1.61	5.27
45	T051-15	F1000	7.18	0.283	1.40	4.60	1.30	4.26
46	T051-16	F1000	6.78	0.267	1.15	3.78	1.04	3.42
48	T051-17	F1000	6.23	0.245	1.13	3.70	1.00	3.27
49	T051-20	F1000	5.55	0.218	1.10	3.59	0.94	3.10
47	T051-35	F1000	5.70	0.224	0.87	2.84	0.66	2.15
18	T114-08	F0250	6.26	0.247	0.99	3.26	0.82	2.70
19	T114-16	F0250	6.96	0.274	0.83	2.73	0.63	2.07
20	T114-17	F0250	5.73	0.226	0.81	2.67	0.54	1.78
21	T114-23	F0250	4.80	0.189	0.81	2.65	0.61	2.00
22	T114-24	F0250	5.54	0.218	0.82	2.70	0.56	1.82
33	T114-07	F0500	6.25	0.246	0.98	3.23	0.41	1.36
35	T114-09	F0500	6.02	0.237	0.94	3.08	0.37	1.21
37	T114-27	F0500	10.06	0.396	1.60	5.24	1.31	4.31
38	T114-30	F0500	9.28	0.365	1.92	6.30	1.74	5.70
50	T114-05	F1000	10.98	0.432	1.82	5.98	1.34	4.40
51	T114-13	F1000	8.82	0.347	1.57	5.14	0.99	3.25
52	T114-14	F1000	8.74	0.344	1.53	5.01	0.97	3.19
53	T114-21	F1000	7.92	0.312	1.48	4.84	0.90	2.96
54	T114-29	F1000	9.25	0.364	1.60	5.26	1.05	3.43
23	T250-08	F0250	5.22	0.206	1.26	4.12	0.90	2.96
24	T250-16	F0250	4.14	0.163	1.03	3.39	0.37	1.20
25	T250-17	F0250	3.99	0.157	1.01	3.31	0.35	1.14
26	T250-23	F0250	3.68	0.145	0.98	3.23	0.19	0.62
27	T250-29	F0250	4.55	0.179	0.97	3.19	0.33	1.08
39	T250-07	F0500	8.57	0.337	2.19	7.17	1.66	5.43
40	T250-09	F0500	8.30	0.327	1.80	5.91	1.07	3.51
41	T250-18	F0500	9.52	0.375	1.78	5.83	1.01	3.30
42	T250-24	F0500	7.59	0.299	1.71	5.62	0.89	2.92
43	T250-30	F0500	8.07	0.318	1.69	5.53	0.74	2.42
55	T250-06	F1000	8.87	0.349	2.35	7.71	0.78	2.56
56	T250-15	F1000	14.27	0.562	3.00	9.85	2.04	6.69
57	T250-28	F1000	12.90	0.508	2.67	8.75	1.46	4.79
58	T250-34	F1000	13.39	0.527	2.62	8.60	1.34	4.39
59	T250-35	F1000	12.61	0.496	2.59	8.51	1.15	3.77

Table 12: Results of Puncture Experiments with Semi-spherical Probes on Disc Specimens Made from 7075-T651 Bar

Test	Specimen	Probe Design	Distance Traveled (mm)	Distance Traveled (in)	Impact Velocity (m/s)	Impact Velocity (fps)	Puncture Velocity (m/s)	Puncture Velocity (fps)
61	T051-06	S0500	13.02	0.513	0.99	3.25	0.93	3.05
62	T051-07	S0500	12.49	0.492	0.81	2.66	0.77	2.54
63	T051-11	S0500	11.79	0.464	0.78	2.57	0.73	2.39
64	T051-13	S0500	14.13	0.556	0.77	2.54	0.67	2.21
65	T051-23	S0500	11.63	0.458	0.77	2.51	0.70	2.29
60	T051-34	S0500	15.43	0.608	1.41	4.62	1.38	4.54
76	T051-09	S1000	14.43	0.568	2.08	6.84	2.04	6.69
77	T051-12	S1000	12.93	0.509	1.71	5.62	1.66	5.43
78	T051-18	S1000	11.56	0.455	1.47	4.82	1.39	4.55
79	T051-19	S1000	13.10	0.516	1.05	3.46	0.93	3.05
80	T051-22	S1000	14.50	0.571	0.84	2.75	0.67	2.19
66	T114-04	S0500	11.43	0.450	1.57	5.16	1.32	4.33
67	T114-22	S0500	11.49	0.452	1.26	4.14	0.89	2.93
68	T114-25	S0500	13.59	0.535	1.23	4.04	0.76	2.48
69	T114-33	S0500	12.50	0.492	1.21	3.97	0.68	2.24
70	T114-35	S0500	11.81	0.465	1.18	3.86	0.71	2.34
81	T114-06	S1000	14.90	0.587	1.94	6.38	1.65	5.43
82	T114-15	S1000	12.00	0.473	1.56	5.10	1.12	3.69
83	T114-28	S1000	11.75	0.463	1.33	4.37	0.86	2.81
84	T114-31	S1000	12.17	0.479	1.30	4.25	0.69	2.28
85	T114-32	S1000	11.53	0.454	1.28	4.18	0.66	2.17
71	T250-05	S0500	9.79	0.385	2.06	6.76	0.95	3.10
72	T250-14	S0500	10.26	0.404	2.10	6.88	0.80	2.64
73	T250-22	S0500	17.48	0.688	2.91	9.56	2.28	7.50
74	T250-32	S0500	14.09	0.555	2.88	9.46	2.23	7.31
75	T250-33	S0500	13.35	0.525	2.86	9.38	2.19	7.17
87	T250-13	S1000	8.17	0.321	2.61	8.57	-0.48	-1.57
89	T250-20	S1000	18.73	0.737	3.66	12.02	2.24	7.34
90	T250-21	S1000	19.57	0.771	3.51	11.52	2.25	7.40
91	T250-27	S1000	18.36	0.723	3.33	10.94	1.33	4.36

Table 13: Results of Puncture Experiments with Tri-corner Probes on Disc Specimens Made from 7075-T651 Bar

Test	Specimen	Probe Design	Distance Traveled (mm)	Distance Traveled (in)	Impact Velocity, v_i (m/s)	Impact Velocity, v_i (fps)	Puncture Velocity, v_p (m/s)	Puncture Velocity, v_p (fps)
103	T051-01	C0500	17.23	0.678	0.81	2.65	0.77	2.52
104	T051-02	C0500	11.92	0.469	0.81	2.66	0.78	2.55
4	T051-31	C0500	14.04	0.553	1.47	4.83	1.45	4.77
105	T051-05	C1000	21.61	0.851	1.13	3.72	1.03	3.37
106	T051-25	C1000	21.17	0.833	0.94	3.08	0.83	2.72
107	T051-33	C1000	21.95	0.864	0.95	3.11	0.82	2.68
92	T114-03	C0500	12.58	0.495	1.11	3.65	0.74	2.44
93	T114-12	C0500	12.85	0.506	1.09	3.57	0.62	2.02
94	T114-19	C0500	14.16	0.557	1.07	3.50	0.49	1.61
95	T114-20	C0500	16.75	0.659	1.05	3.46	0.59	1.94
96	T114-34	C0500	13.63	0.537	1.06	3.47	0.39	1.29
108	T114-01	C1000	24.23	0.954	1.90	6.22	1.41	4.63
109	T114-02	C1000	23.92	0.942	1.83	6.00	1.50	4.92
110	T114-10	C1000	23.41	0.922	1.76	5.76	1.33	4.37
111	T114-11	C1000	24.52	0.965	1.58	5.20	1.03	3.38
112	T114-26	C1000	14.76	0.581	1.56	5.13	1.18	3.87
98	T250-01	C0500	15.68	0.617	3.00	9.85	2.12	6.96
99	T250-10	C0500	14.34	0.564	2.78	9.11	1.97	6.45
100	T250-19	C0500	14.81	0.583	2.62	8.60	1.67	5.48
101	T250-25	C0500	16.33	0.643	2.54	8.34	1.57	5.15
102	T250-31	C0500	13.84	0.545	2.49	8.16	1.54	5.04
113	T250-02	C1000	30.06	1.183	3.94	12.92	2.47	8.11
114	T250-03	C1000	23.33	0.918	3.74	12.27	2.01	6.61
115	T250-11	C1000	25.41	1.000	3.47	11.38	1.46	4.78
116	T250-12	C1000	23.78	0.936	4.02	13.20	2.59	8.48
117	T250-26	C1000	24.91	0.981	3.73	12.23	2.23	7.33

Table 14: Total Energy in Puncture Experiments with Flat-End Probes on Disc Specimens Made from 7075-T651 Bar

Test	Specimen	Probe Design	Total Energy Before Impact, $E_{T,i}$ (J)	Total Energy Before Impact, $E_{T,i}$ (ft-lb)	After Puncture, $E_{T,p}$ (J)	After Puncture, $E_{T,p}$ (ft-lb)	Mitigated Energy, E_M (J)	Mitigated Energy, E_M (ft-lb)
11	T051-24	F0250	55.0	40.6	47.1	34.8	7.9	5.8
12	T051-26	F0250	29.1	21.5	22.2	16.4	6.9	5.1
16	T051-28	F0250	25.9	19.1	18.7	13.8	7.2	5.3
17	T051-29	F0250	34.9	25.8	27.2	20.1	7.7	5.7
6	T051-30	F0250	59.4	43.8	50.8	37.5	8.6	6.3
5	T051-32	F0250	58.6	43.2	49.9	36.8	8.6	6.4
28	T051-03	F0500	66.6	49.1	49.6	36.6	17.0	12.5
29	T051-08	F0500	33.8	24.9	16.4	12.1	17.4	12.8
30	T051-10	F0500	34.1	25.1	18.8	13.9	15.3	11.3

Table 14: Total Energy in Puncture Experiments with Flat-End Probes on Disc Specimens Made from 7075-T651 Bar, Continued

Test	Specimen	Probe Design	Total Energy Before Impact, $E_{T,i}$ (J)	(ft-lb)	After Puncture, $E_{T,p}$ (J)	(ft-lb)	Mitigated Energy, E_M (J)	(ft-lb)
31	T051-21	F0500	33.5	24.7	18.4	13.6	15.1	11.2
32	T051-27	F0500	31.8	23.4	16.9	12.4	14.9	11.0
44	T051-14	F1000	207.8	153.2	179.8	132.6	28.0	20.6
45	T051-15	F1000	144.8	106.8	117.3	86.5	27.5	20.3
46	T051-16	F1000	99.3	73.2	75.8	55.9	23.5	17.3
48	T051-17	F1000	94.3	69.6	69.2	51.0	25.2	18.6
49	T051-20	F1000	88.7	65.4	63.0	46.5	25.7	18.9
47	T051-35	F1000	58.2	42.9	29.8	22.0	28.4	20.9
18	T114-08	F0250	75.4	55.6	47.4	35.0	28.0	20.6
19	T114-16	F0250	55.0	40.6	27.6	20.4	27.4	20.2
20	T114-17	F0250	51.6	38.1	20.3	15.0	31.3	23.1
21	T114-23	F0250	49.8	36.7	26.1	19.3	23.7	17.5
22	T114-24	F0250	52.1	38.4	20.9	15.5	31.2	23.0
33	T114-07	F0500	70.3	51.8	10.9	8.0	59.4	43.8
35	T114-09	F0500	64.0	47.2	9.0	6.7	55.0	40.6
37	T114-27	F0500	187.3	138.2	118.3	87.2	69.1	50.9
38	T114-30	F0500	269.8	199.0	210.6	155.3	59.2	43.7
50	T114-05	F1000	240.9	177.7	125.6	92.6	115.3	85.1
51	T114-13	F1000	178.2	131.5	68.4	50.5	109.8	81.0
52	T114-14	F1000	169.6	125.1	65.8	48.5	103.8	76.5
53	T114-21	F1000	157.5	116.2	56.5	41.7	101.1	74.5
54	T114-29	F1000	186.8	137.8	75.4	55.6	111.4	82.1
23	T250-08	F0250	114.1	84.2	58.1	42.8	56.1	41.3
24	T250-16	F0250	77.7	57.3	9.5	7.0	68.2	50.3
25	T250-17	F0250	74.4	54.8	8.4	6.2	66.0	48.7
26	T250-23	F0250	70.6	52.1	3.0	2.2	67.6	49.9
27	T250-29	F0250	68.9	50.8	8.2	6.1	60.6	44.7
39	T250-07	F0500	343.6	253.4	193.4	142.6	150.2	110.8
40	T250-09	F0500	237.1	174.8	80.8	59.6	156.3	115.2
41	T250-18	F0500	231.8	171.0	70.9	52.3	160.9	118.7
42	T250-24	F0500	213.9	157.8	56.4	41.6	157.5	116.2
43	T250-30	F0500	208.0	153.4	38.7	28.6	169.3	124.9
55	T250-06	F1000	391	288	45	33	346	255
56	T250-15	F1000	643	474	293	216	350	258
57	T250-28	F1000	508	375	148	109	360	266
58	T250-34	F1000	491	362	122	90	370	273
59	T250-35	F1000	481	355	89	66	392	289

Table 15: Total Energy in Puncture Experiments with Semi-spherical Probes on Disc Specimens Made from 7075-T651 Bar

Test	Specimen	Probe Design	Total Energy Before Impact, $E_{T,i}$ (J)	(ft-lb)	After Puncture, $E_{T,p}$ (J)	(ft-lb)	Mitigated Energy, E_M (J)	(ft-lb)
61	T051-06	S0500	81.1	59.8	60.2	44.4	20.9	15.4
62	T051-07	S0500	57.9	42.7	41.8	30.8	16.0	11.8
63	T051-11	S0500	54.2	39.9	36.9	27.2	17.3	12.8
64	T051-13	S0500	54.1	39.9	31.5	23.3	22.6	16.7
65	T051-23	S0500	51.3	37.9	33.7	24.9	17.6	13.0
60	T051-34	S0500	153.5	113.2	133.0	98.1	20.5	15.1
76	T051-09	S1000	320.4	236.3	290.6	214.3	29.8	22.0
77	T051-12	S1000	219.0	161.6	191.0	140.8	28.1	20.7
78	T051-18	S1000	162.0	119.5	133.9	98.8	28.1	20.8
79	T051-19	S1000	90.4	66.7	60.1	44.3	30.3	22.3
80	T051-22	S1000	62.5	46.1	31.0	22.9	31.5	23.2
66	T114-04	S0500	182.1	134.3	121.3	89.5	60.8	44.9
67	T114-22	S0500	119.6	88.2	55.8	41.2	63.8	47.0
68	T114-25	S0500	115.5	85.2	39.8	29.4	75.6	55.8
69	T114-33	S0500	109.9	81.1	32.4	23.9	77.5	57.2
70	T114-35	S0500	103.5	76.3	35.2	26.0	68.3	50.4
81	T114-06	S1000	277.0	204.3	192.2	141.7	84.8	62.6
82	T114-15	S1000	179.3	132.2	89.0	65.7	90.2	66.6
83	T114-28	S1000	133.6	98.5	51.3	37.8	82.3	60.7
84	T114-31	S1000	127.2	93.8	33.9	25.0	93.3	68.8
85	T114-32	S1000	122.3	90.2	30.6	22.6	91.7	67.6
71	T250-05	S0500	303.2	223.6	64.6	47.6	238.6	176.0
72	T250-14	S0500	312.6	230.6	44.9	33.1	267.7	197.5
73	T250-22	S0500	615.9	454.3	357.8	263.9	258.1	190.3
74	T250-32	S0500	595.3	439.1	352.0	259.6	243.4	179.5
75	T250-33	S0500	585.0	431.5	334.4	246.6	250.6	184.8
87	T250-13	S1000	481	355	16	12	465	343
89	T250-20	S1000	960	708	343	253	617	455
90	T250-21	S1000	880	649	355	262	525	387
91	T250-27	S1000	789	582	98	72	691	510

Table 16: Total Energy in Puncture Experiments with Tri-corner Probes on Disc Specimens Made from 7075-T651 Bar

Test	Specimen	Probe Design	Total Energy Before Impact, $E_{T,i}$ (J)	(ft-lb)	After Puncture, $E_{T,p}$ (J)	(ft-lb)	Mitigated Energy, E_M (J)	(ft-lb)
103	T051-01	C0500	62.8	46.3	41.2	30.4	21.6	15.9
104	T051-02	C0500	57.9	42.7	42.0	31.0	15.9	11.7
4	T051-31	C0500	168.4	124.2	146.8	108.3	21.6	15.9
105	T051-05	C1000	110.8	81.7	73.4	54.1	37.4	27.6
106	T051-25	C1000	80.5	59.4	47.6	35.1	32.9	24.3
107	T051-33	C1000	81.9	60.4	46.3	34.1	35.6	26.2
92	T114-03	C0500	101.5	74.9	37.7	27.8	63.8	47.1
93	T114-12	C0500	97.8	72.2	26.2	19.3	71.7	52.9
94	T114-19	C0500	95.9	70.8	15.5	11.5	80.4	59.3
95	T114-20	C0500	96.4	71.1	23.9	17.7	72.5	53.5
96	T114-34	C0500	93.1	68.7	9.9	7.3	83.2	61.4
108	T114-01	C1000	270.9	199.8	137.4	101.3	133.5	98.5
109	T114-02	C1000	251.0	185.1	156.0	115.0	95.0	70.1
110	T114-10	C1000	232.2	171.3	119.7	88.3	112.5	83.0
111	T114-11	C1000	192.6	142.0	74.2	54.7	118.4	87.3
112	T114-26	C1000	180.4	133.0	98.0	72.3	82.4	60.8
98	T250-01	C0500	646	476	312	230	334	246
99	T250-10	C0500	553	408	274	202	279	206
100	T250-19	C0500	494	364	196	145	298	220
101	T250-25	C0500	465	343	174	128	291	215
102	T250-31	C0500	444	327	170	125	274	202
113	T250-02	C1000	1120	826	427	315	693	511
114	T250-03	C1000	1005	741	266	196	739	545
115	T250-11	C1000	864	638	141	104	723	534
116	T250-12	C1000	1160	856	451	332	710	524
117	T250-26	C1000	1000	738	339	250	662	488

Stress-Strain Relations in Uniaxial Tension

Figure 37 shows a cube of material with each dimension equal to unity and the engineering stresses that act on it (Ref. 2, p. 53, Fig. 2.15; Ref. 3, p. 94, Fig. 3–1a). Forces act on all six surfaces of this unit volume; these are resolved into components directed normal to the surfaces and tangential to them. The engineering stress produced by each component is the force divided by the surface area; this is true for both normal stresses, denoted $\sigma_{i,j}$, and shear stresses, denoted $\tau_{i,j}$ (Ref. 2, p. 30, Eq. 2.2; Ref. 3, p. 102, Eq. 3–14, 3–15). The indices i and j take on the values x, y, and z to indicate the normal vector of the surface that the stress acts on and the direction of the stress, in either order. The stresses on opposite surfaces of the volume differ slightly because the state of stress varies spatially.

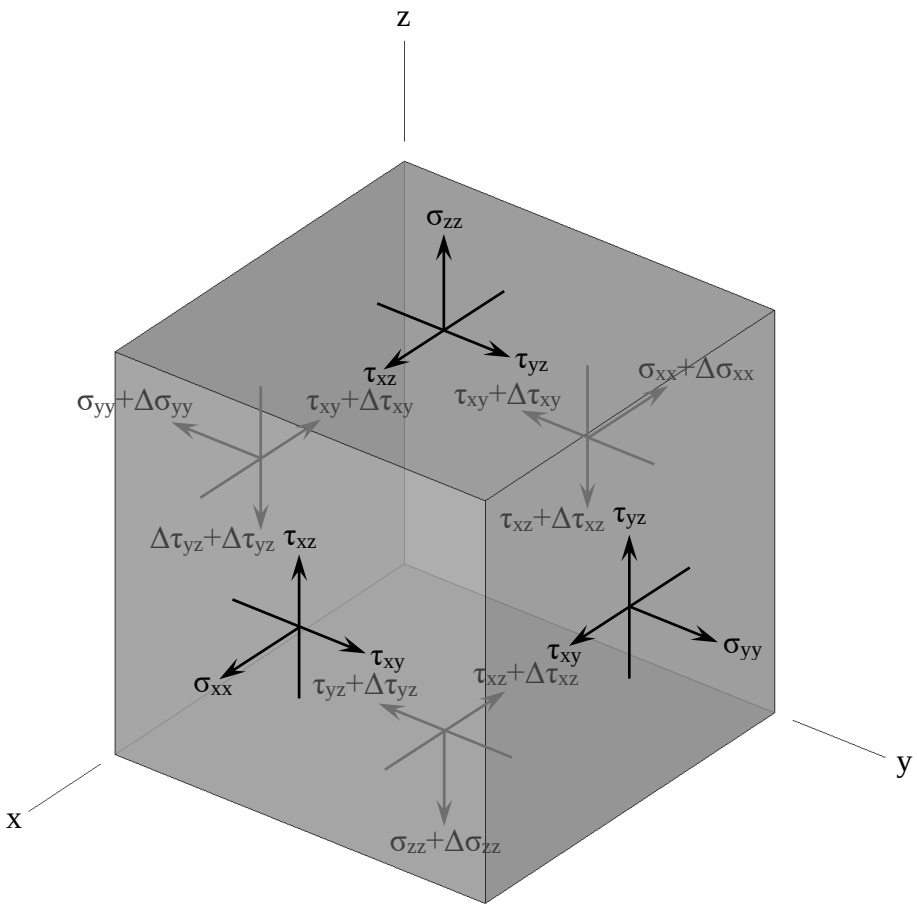

Figure 37: Components of Stress Acting on a Unit Volume

The unit volume deforms elastically and plastically in response to the state of stress. For deformations in which a surface moves in the direction normal to it (Fig. 38a), the engineering strain, labeled $\varepsilon_{i,j}$, is the ratio of the deformation to the dimension of the volume measured normal to the surface. For deformation of a surface in the direction of a vector that lies on the surface (Fig. 38b), the engineering shear strain, denoted $\gamma_{i,j}$, is the change in angle of the adjacent surfaces relative to the surface normal.

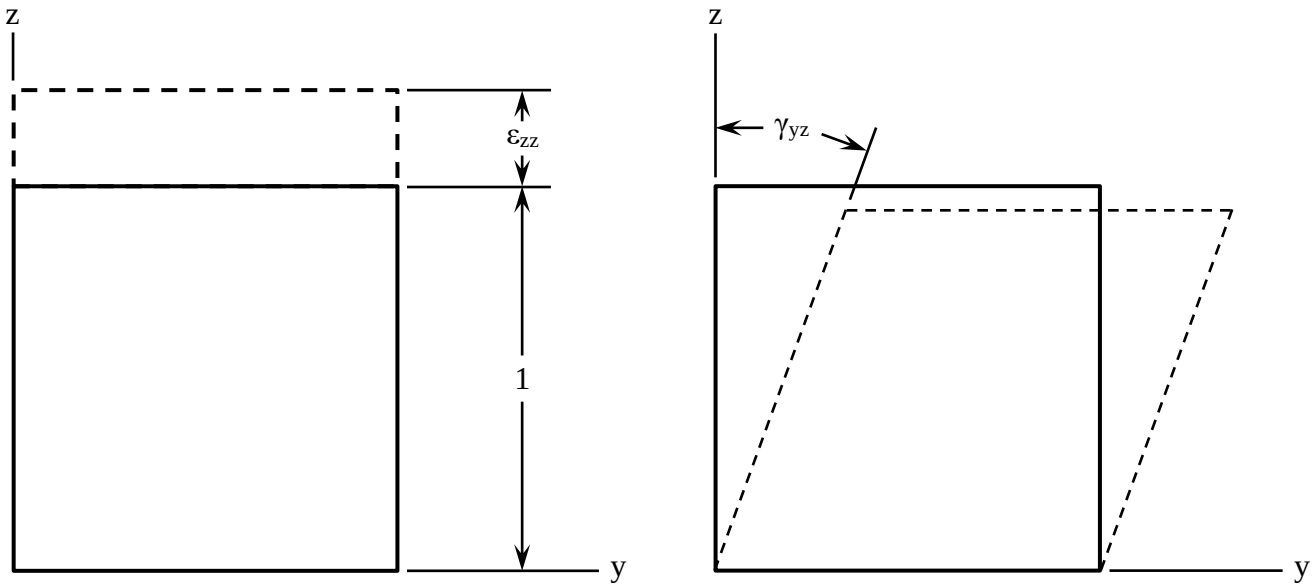

(a) Engineering Normal Strain in z Direction (b) Engineering Shear Strain in yz Plane

Figure 38: Two Types of Strain in Unit Volume

The simplest state of stress has zeros for all of the values except one axial stress. This represents pure uniaxial tension. In a real specimen under uniaxial loading, the internal stress state is more complex, having non-zero values for other components, particularly near boundaries and geometry changes, including reductions of cross-sectional area caused by strain localization. The objective of tension tests is to produce a state of stress that is as close as possible to pure uniaxial tension at the location where fracture initiates. The specimens are designed to fracture in the middle of the gauge section, where the stress is most uniform, by gradually reducing the cross-sectional area toward that location. The stress state approaches uniformity due to the length of the gauge section and Saint-Venant's principle (Ref. 2, p. 240). The state of stress and strain produced by uniaxial tension in the z coordinate direction is given in Table 17 (Ref. 2, p. 97, Eq. a & e; Ref. 3, p. 104, Table 3–1).

Table 17: State of Stress and Strain Corresponding to Tension in z Direction

Stress Component	Value	Strain Component	Value
σ_{xx}	0	ε_{xx}	$-\nu\varepsilon$
σ_{yy}	0	ε_{yy}	$-\nu\varepsilon$
σ_{zz}	σ	ε_{zz}	ε
τ_{xy}	0	γ_{xy}	0
τ_{xz}	0	γ_{xz}	0
τ_{yz}	0	γ_{yz}	0

The relationship between engineering stress and strain is initially elastic, with a constant of proportionality equal to the elastic modulus (E), and then becomes plastic as the material yields and the strain increases beyond the proportional value (Fig. 39a). Most materials harden during plastic deformation, so the stress increases beyond the yield point. As plastic strain accumulates, voids nucleate in the material and coalesce, reducing the engineering stress. When the voids become large enough, a crack propagates through the cross section and the material fractures.

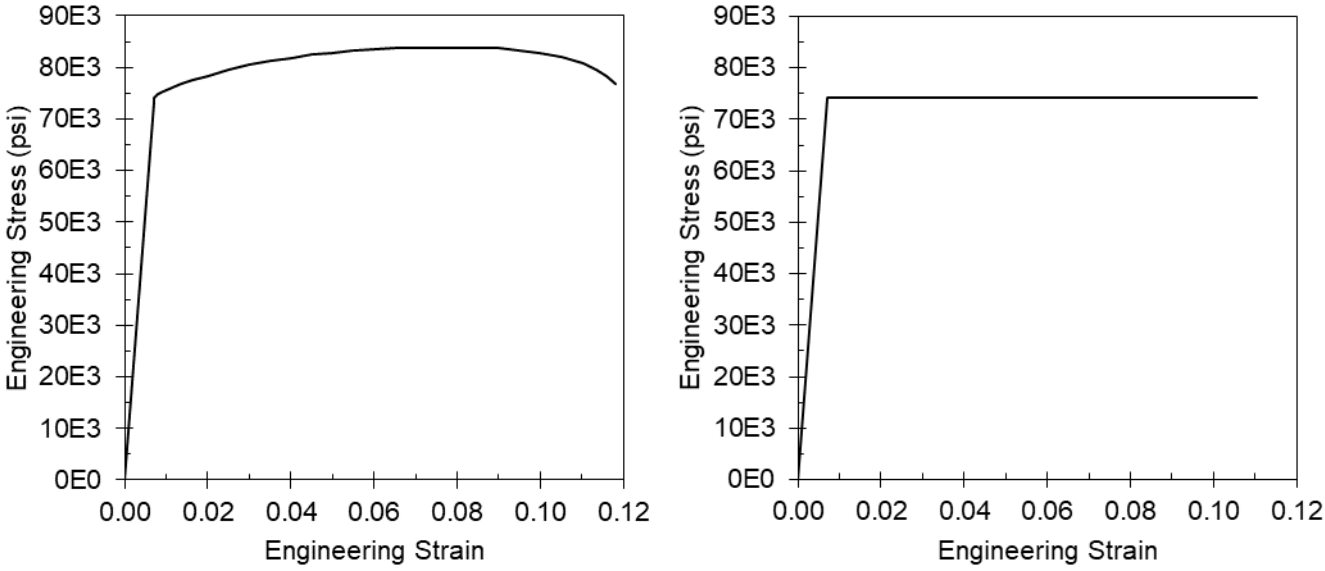

(a) Typical (Ref. 4, p. 3-659, Fig. 3.7.10.1.6(o))

(b) Perfectly Plastic

Figure 39: Examples of Engineering Stress-Strain Relations

The ultimate values of the engineering stress and strain are the maximum values over the range from the unloaded state until the specimen fractures. These values are often cited as test results. The ultimate engineering stress (σ_u) is also referred to as the ultimate tensile strength (UTS or F_{tu}). The ultimate engineering strain (ε_u) is cited in some sources as the elongation and is often expressed as a percentage, although strain is a dimensionless quantity. Given the stress-strain relation, $\sigma(\varepsilon)$, and the ultimate strain, ε_u, the strain energy in the unit volume when it fractures is

$$E_u = \int_0^{\varepsilon_u} \sigma \, d\varepsilon \tag{8}$$

The resulting energy per unit volume has units of force/length^2 but may be multiplied by the volume (1) to obtain the energy with units of force×length. Under the assumption of perfect plasticity (Fig. 39b), the yield and ultimate strengths are equal, the material yields when the strain is $\frac{\sigma_y}{E}$, and the strain energy in a unit volume of material when it fractures in tension is

$$E_u = E_e + E_p = \frac{\sigma_y}{2}\left(\frac{\sigma_y}{E}\right) + \sigma_y\left(\varepsilon_u - \frac{\sigma_y}{E}\right) = \sigma_y\left(\varepsilon_u - \frac{\sigma_y}{2E}\right) \quad (9)$$

This equation is dominated by the plastic strain energy (E_p) because the plastic strain at fracture $\left(\varepsilon_u - \frac{\sigma_y}{E}\right)$ is much greater than the elastic strain at yield $\left(\frac{\sigma_y}{E}\right)$.

The ultimate engineering stress and strain were measured from uniaxial tension specimens (Fig. 40) of the same stock material as the disc specimens (Fig. 1–3). The axes of the specimens aligned with the transverse grain direction in the bar stock. Tests were performed at an average quasi-static rate of 9.86E-3/s and ambient temperature (77°F, 25°C). The average ultimate stress is 78.8E3 psi (543 MPa) and the average ultimate strain is 118.5E-3.

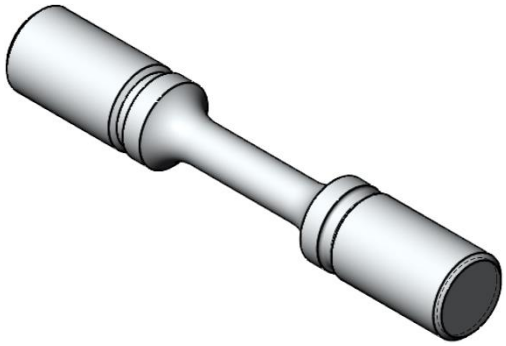

Figure 40: 7075-T651 Aluminum Uniaxial Tension Specimen with Diameter of 0.250 Inch

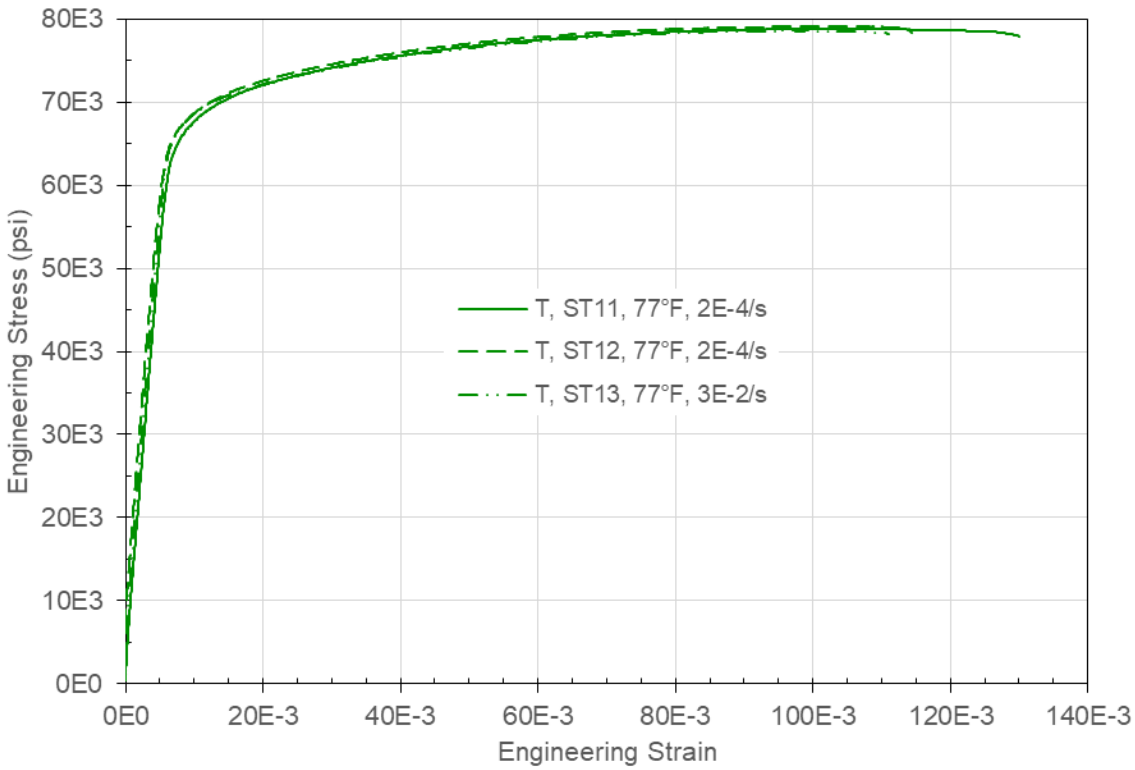

Figure 41: Engineering Stress-Strain Relations for 7075-T651 Bar in Transverse Grain Direction

Empirical Model for Energy Mitigated During Puncture Event

The sample size for each combination of geometric parameters (3–6) is too small to apply classical statistical inference techniques with reasonable confidence in the results. However, the empirical model for puncture energy provided by Reference 5 calculates the lower bounds of confidence intervals based on the entire collection of data for each probe shape.

Reference 5 suggests that the total energy required for a cylindrical probe with a flat end to puncture a metal sheet or plate is a function of the ultimate tensile strength, engineering strain at fracture, specimen thickness, and probe diameter. The product of the ultimate engineering stress and strain is a simple estimate for the area under the stress-strain relation. Assuming perfect plasticity ($\sigma_u = \sigma_y$), this product ($\sigma_u \varepsilon_u$) is the dominant term in Equation 9 and approximates the strain energy in a unit volume of the material when it ruptures in tension. This same product is the area of a rectangle that envelops the actual stress-strain relation, so it exceeds the area underneath, but it is correlated to experimental data.

In order for the probe to penetrate the specimen, the material in some volume must fracture. In puncture experiments with the thickest disc specimens, the flat-end probes are observed to eject circular plugs (Fig. 27, 28, and 31). Figure 42 illustrates a hypothetical estimate for the volume of the fractured material between the probe diameter (d) and an additional radial width (w), in which the plastic strain is concentrated, and extending through the specimen thickness (t); the volume evaluates to $\pi t(dw + w^2)$. However, the state of stress in this volume is much more complex than uniaxial tension, and additional material surrounding this volume has strain energy due to biaxial tension, bending, and shear.

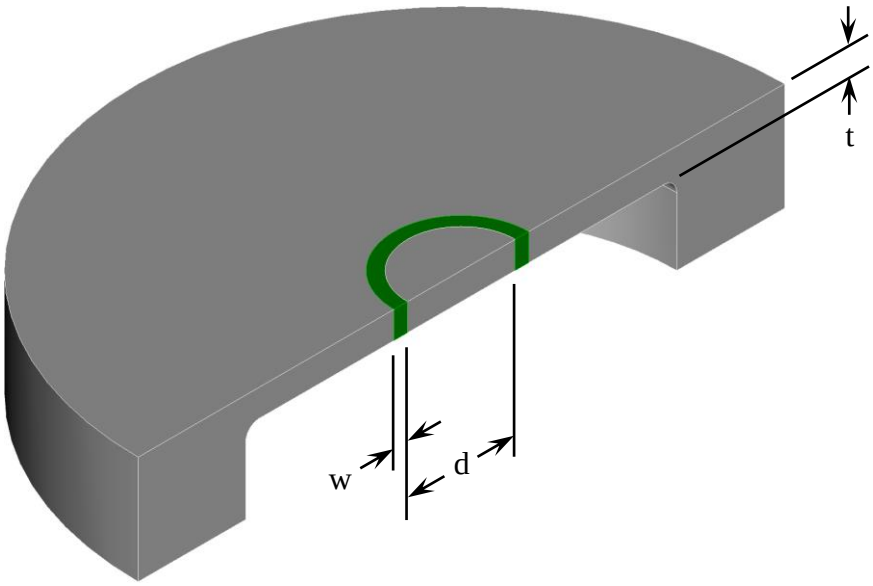

Figure 42: Half of Volume of Disc Specimen that Ruptures as Probe Penetrates

The objective is to calculate the energy expended by the probe as it penetrates the specimen. One way to obtain the energy (with units of force×length) is to multiply the product of the ultimate engineering stress and strain (which has units of stress, force/length^2) by the volume of material that ruptures (with units of length^3). The volume is hypothesized to be a combination of the specimen thickness and probe diameter, but the balance between these two parameters is determined empirically rather than by postulating the shape of the fractured volume. The other dimensions of the specimen are neglected because fracture is assumed to be a local phenomenon. This simple approach minimizes the number of input

parameters and neglects the complex state of stress and strain within the specimen. It also avoids the uncertainty in the volume of material that ruptures when cracks propagate along more complicated paths than circles, particularly with probes having other shapes besides a flat end.

Reference 5 proposes an empirical fit equation that calculates a lower bound for the energy measured in multiple puncture tests with specimens of different alloys and thicknesses and probes of different diameters but the same shape (Ref. 5, p. 2, Eq. 3 and 4):

$$E = K \sigma_u \varepsilon_u t^3 \left(\frac{d}{t}\right)^c \tag{10}$$

where E is the total energy mitigated by the specimen as the probe punctures it, σ_u is the ultimate engineering stress (tensile strength), ε_u is the ultimate engineering strain (elongation), t is the specimen thickness, and d is the probe diameter. The dimensionless coefficient (K) is derived statistically such that the equation calculates a lower bound at a specified confidence level. The exponent (c) is fit to the data; it specifies how much influence the probe diameter has on the energy. Dimensional analysis requires that the total exponent on all of the parameters with length units be +3. The effective exponent on the thickness is 3−c, which balances the equation to yield the correct dimensions for energy. If the diameter of the pocket were included in the equation, it would add a parameter and another calibrated exponent; the simplicity of the equation is considered more beneficial than including a term to account for the general deformation of the specimen.

Equation 10 expresses the mitigated energy as a function of both the specimen thickness and the probe diameter. It can be plotted in three dimensions, but multiple surfaces that serve as lower bounds with different confidence levels are difficult to visualize. Optimization of the parameters to fit the equation to the data is facilitated by normalizing the inputs and output such that there is only one input and the function can be plotted in two dimensions. The mitigated energy is normalized by the strain energy of the unit volume at fracture and the cube of the thickness to create a non-dimensional parameter (Ref. 5, p. 2, Eq. 4),

$$E_n = \frac{E}{\sigma_u \varepsilon_u t^3} \tag{11}$$

The diameter-to-thickness ratio (also non-dimensional) is defined as

$$M = \frac{d}{t} \tag{12}$$

Substituting Equations 11 and 12 into Equation 10 yields the exponential function (Ref. 5, p. 2, Eq. 3)

$$E_n = K M^c \tag{13}$$

Whereas Equation 10 directly depends on two parameters (d, t) of the experimental scenario, Equation 13 has only one input (M, Eq. 12) that differs between tests. The result of Equation 10 compares to the actual energy (E) from the tests, but Equation 13 is compared to the normalized energy (E_n, Eq. 11). Simple two-dimensional plots compare the results of Equations 11 and 13 for any values of the coefficient (K) and exponent (c), which are optimized such that the model best fits the data. The exponential equation (Eq. 13) is written in the form of a linear equation (Ref. 6, p. 2, Eq. 1) by taking common logarithms of both sides (Ref. 5, p. 2, Eq. 5):

$$\log E_n = \log K + c \log M \tag{14}$$

Let n be the number of data points, j = 1…n the index of the data, d_j the diameter data, t_j the thickness data, M_j the measured diameter-to-thickness ratios (Eq. 12), and E_j the mitigated energy data. The normalized energy that results from Equation 11 when it is evaluated with the experimental data is denoted $E_{n,d,j}$. When Equation 13 is evaluated with the parameters of the linear fit and the diameter-to-thickness ratios (M_j), the result is designated $E_{n,f,j}$. A line is fit to the common logarithms of the normalized energy and diameter-to-thickness ratio such that the sum of the squares of the residuals, $\sum_{j=1}^{n}\left(\log E_{n,d,j} - \log E_{n,f,j}\right)^2$, is minimized. The parameters are defined by Equations 15 and 16 (Ref. 7, p. 135, Eq. 4.37; Ref. 8, p. 353, Eq. 5.4; Ref. 9, p. 502). Specific parameter values for each of the three probe shapes are listed in Table 18 with the correlation coefficient, which is defined subsequently. The data and fit lines are plotted in Figures 43 through 45.

$$\log K = \frac{\sum_{j=1}^{n}\left(\log M_j\right)\sum_{j=1}^{n}\left(\log M_j \log E_{n,d,j}\right) - \sum_{j=1}^{n}\left(\log M_j\right)^2 \sum_{j=1}^{n}\left(\log E_{n,d,j}\right)}{\left[\sum_{j=1}^{n}\left(\log M_j\right)\right]^2 - n\sum_{j=1}^{n}\left(\log M_j\right)^2} \tag{15}$$

$$c = \frac{\sum_{j=1}^{n}\left(\log M_j\right)\sum_{j=1}^{n}\left(\log E_{n,d,j}\right) - n\sum_{j=1}^{n}\left(\log M_j \log E_{n,d,j}\right)}{\left[\sum_{j=1}^{n}\left(\log M_j\right)\right]^2 - n\sum_{j=1}^{n}\left(\log M_j\right)^2} \tag{16}$$

Table 18: Optimal Parameters of Linear Equation for Empirical Model

Probe End Geometry	Coefficient, K	Exponent, c	Correlation Coefficient, R^2
Flat	4.784	1.3060	0.952
Partial Sphere with 50% Larger Radius than Probe	7.234	1.1458	0.919
Three Orthogonal Planes Meeting at Corner	8.707	1.1012	0.934

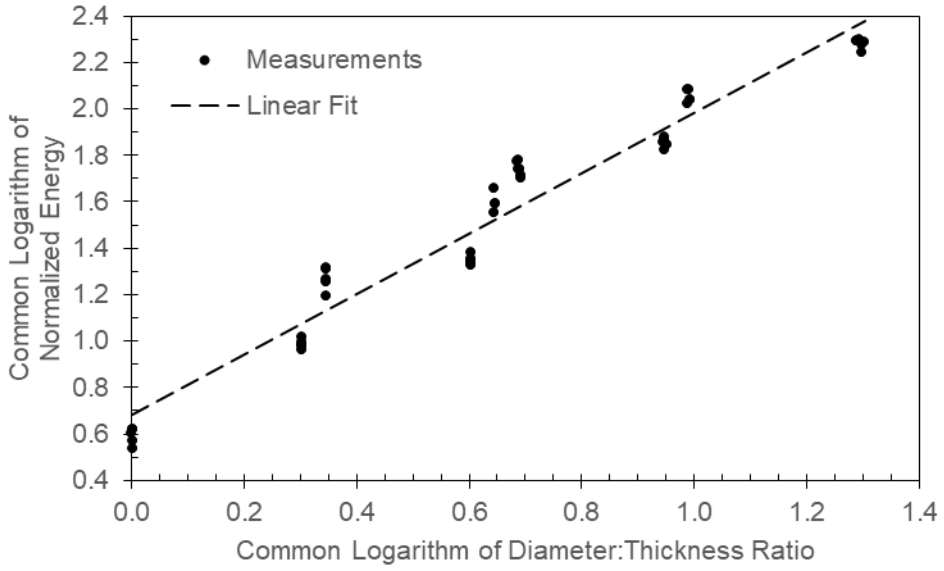

Figure 43: Linear Fit to Logarithms of Normalized Energy and Diameter-to-Thickness Ratio for Tests with Flat-End Probes

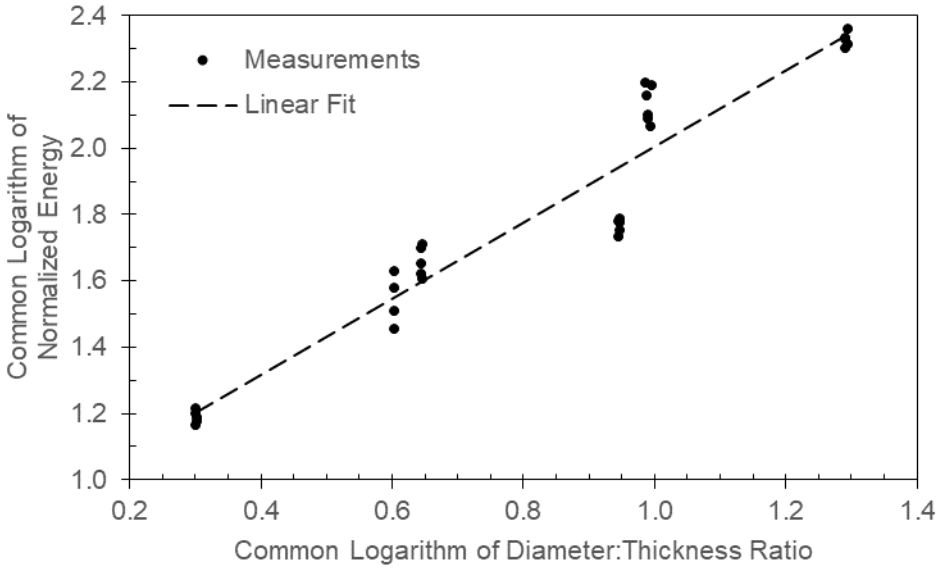

Figure 44: Linear Fit to Logarithms of Normalized Energy and Diameter-to-Thickness Ratio for Tests with Semi-spherical Probes

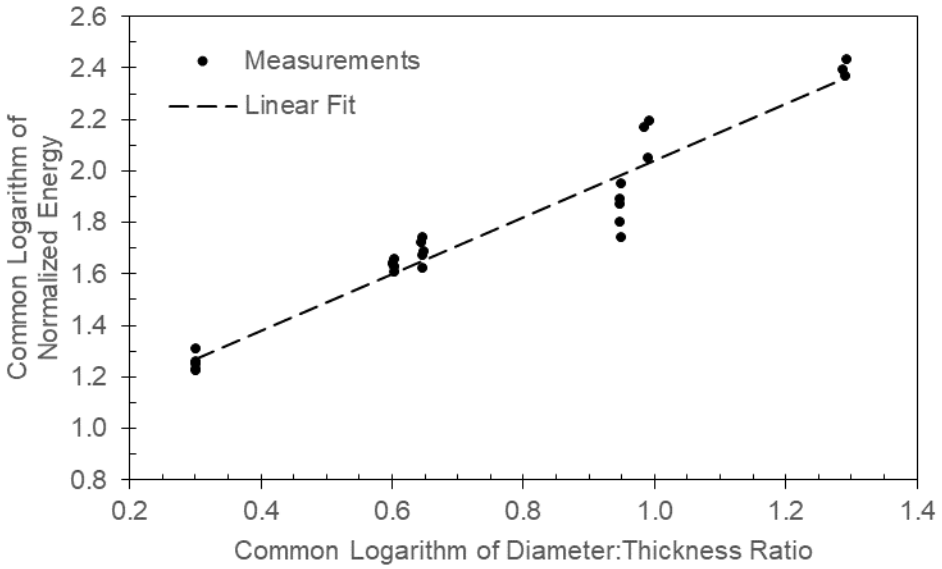

Figure 45: Linear Fit to Logarithms of Normalized Energy and Diameter-to-Thickness Ratio for Tests with Tri-corner Probes

The mean of the common logarithms of the normalized energy data is (Ref. 7, p. 121, Eq. 4.14a; Ref. 9, p. 264, Eq. 8.2.1)

$$E_{l,n,d} = \frac{1}{n}\sum_{j=1}^{n} \log E_{n,d,j} \tag{17}$$

and the variance is (Ref. 7, pp. 121, 136, Eq. 4.14b; Ref. 9, p. 266, Eq. 8.2.7)

$$S_E^2 = \frac{1}{n-1}\sum_{j=1}^{n} \left(\log E_{n,d,j} - E_{l,n,d}\right)^2 \tag{18}$$

The degrees of freedom (ν) are the number of data points less the number of coefficients in the polynomial fit (Ref. 7, p. 134):

$$\nu = n - 2 \tag{19}$$

The standard error of the linear fit compares the model to the data in terms of the logarithms of the normalized energy values (Ref. 7, p. 133, Eq. 4.34; Ref. 9, p. 502):

$$S_F = \sqrt{\frac{1}{\nu}\sum_{j=1}^{n}\left(\log E_{n,d,j} - \log E_{n,f,j}\right)^2} \tag{20}$$

The correlation coefficient is (Ref. 7, p. 135, Eq. 4.38; Ref. 8, p. 332; Ref. 9, p. 178, Eq. 5.3.1)

$$R^2 = 1 - \frac{S_F^2}{S_E^2} = 1 - \frac{(n-1)\sum_{j=1}^{n}\left(\log E_{n,d,j} - \log E_{n,f,j}\right)^2}{(n-2)\sum_{j=1}^{n}\left(\log E_{n,d,j} - E_{l,n,d}\right)^2} \tag{21}$$

Values of the correlation coefficient are listed in Table 18 for each of the probe shapes.

The Student's t distribution predicts the coefficients (K) at different confidence values based on the number of degrees of freedom. If the sample size were infinite, the normal distribution would define the coefficient at any confidence value (C). The Student's t distribution accounts for additional uncertainty with finite samples and converges to the normal distribution as the degrees of freedom approach infinity. For the 46 samples punctured by flat-end probes (44 DoF) and 95% confidence, the difference between the one-tailed bounds is 2.2%; with the 30 samples punctured by semi-spherical probes (28 DoF), the difference is 3.4%; for the 26 samples punctured by tri-corner probes (24 DoF), the difference is 4.0%.

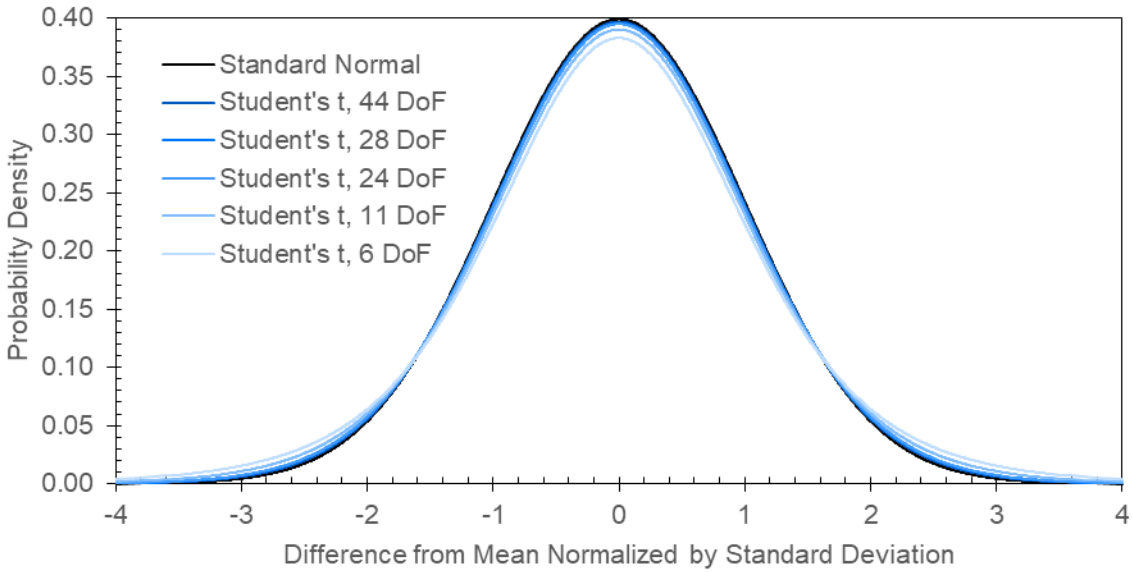

Figure 46: Convergence of Student's t and Normal Probability Density Functions

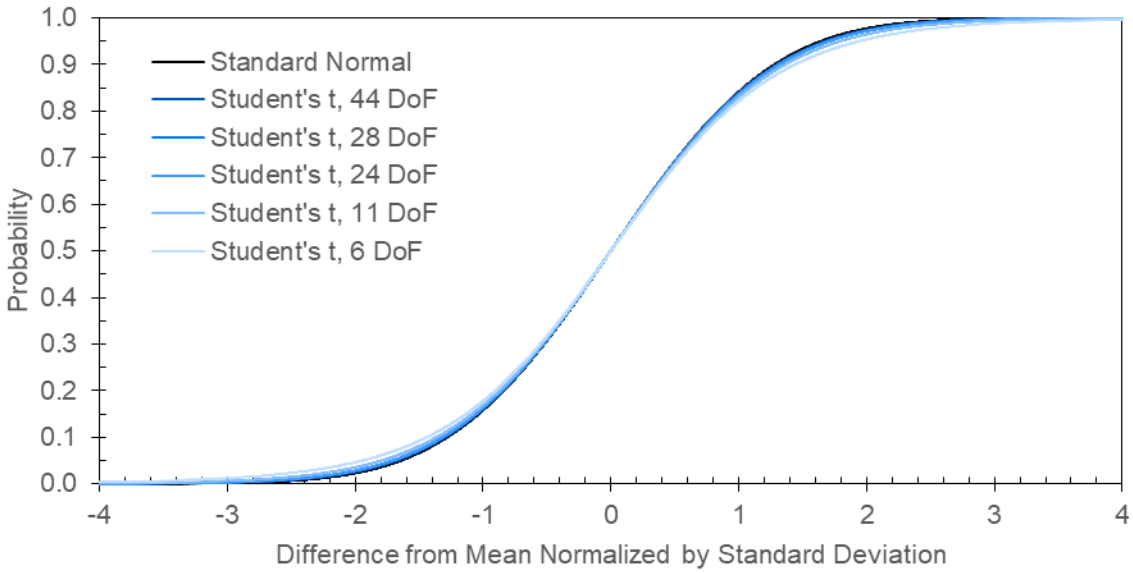

Figure 47: Convergence of Student's t and Normal Cumulative Distribution Functions

The PDF can be written (Ref. 9, p. 274, Eq. 8.4.2)

$$f(x) = \frac{\Gamma\left(\frac{\nu+1}{2}\right)}{\Gamma\left(\frac{\nu}{2}\right)\sqrt{\pi\nu\left(1+\frac{x^2}{\nu}\right)^{\nu+1}}} = \frac{\Gamma\left(\frac{\nu+1}{2}\right)}{\sqrt{\pi\nu}\,\Gamma\left(\frac{\nu}{2}\right)}\left(1+\frac{x^2}{\nu}\right)^{-\frac{\nu+1}{2}} \tag{22}$$

or

$$f(x) = \frac{1}{B\left(\frac{1}{2},\frac{\nu}{2}\right)\sqrt{\nu\left(1+\frac{x^2}{\nu}\right)^{\nu+1}}} = \frac{1}{\sqrt{\nu}\,B\left(\frac{1}{2},\frac{\nu}{2}\right)}\left(1+\frac{x^2}{\nu}\right)^{-\frac{\nu+1}{2}} \tag{23}$$

The gamma function in Equation 22 is (Ref. 8, p. 222; Ref. 9, p. 111, Eq. 3.3.4)

$$\Gamma(\gamma) = \int_0^\infty u^{\gamma-1}e^{-u}du \tag{24}$$

and the beta function in Equation 23 is (Ref. 8, p. 226)

$$B(\beta_1,\beta_2) = \int_0^1 u^{\beta_1-1}(1-u)^{\beta_2-1}du \tag{25}$$

The CDF is the integral of the PDF from negative infinity to the non-dimensional limit parameter t and may be written in terms of gamma functions by placing Equation 22 in the integral or in terms of beta functions by substituting $u = \frac{\nu}{x^2+\nu}$ into Equation 23.

$$p = C = \frac{\Gamma\left(\frac{\nu+1}{2}\right)}{\sqrt{\pi\nu}\,\Gamma\left(\frac{\nu}{2}\right)}\int_{-\infty}^{t}\left(1+\frac{x^2}{\nu}\right)^{-\frac{\nu+1}{2}}dx \tag{26}$$

or

$$p = C = \begin{cases} \dfrac{\int_0^{\frac{\nu}{t^2+\nu}} u^{\frac{\nu}{2}-1}(1-u)^{-\frac{1}{2}}du}{2\int_0^1 u^{\frac{\nu}{2}-1}(1-u)^{-\frac{1}{2}}du} & t < 0 \\ 1 - \dfrac{\int_0^{\frac{\nu}{t^2+\nu}} u^{\frac{\nu}{2}-1}(1-u)^{-\frac{1}{2}}du}{2\int_0^1 u^{\frac{\nu}{2}-1}(1-u)^{-\frac{1}{2}}du} & t \geq 0 \end{cases} \quad (27)$$

The probability (p) at which the CDF is evaluated equals the confidence (C) because a one-tailed bound is desired with that probability of bounding future observations. The objective is to make accurate predictions, so the desired probability is between 0.5 and 1. One of Equations 27 or 26 is solved for the parameter t, which is positive for any probability greater than 0.5. The confidence interval for the logarithm of the coefficient is (Ref. 7, p. 134, Eq. 4.35)

$$\log b_L = \log K - t\, S_F \leq \log K \leq \log K + t\, S_F = \log b_U \quad (28)$$

The lower bound on the coefficient (K) simplifies to

$$b_L = \frac{K}{10^{t\, S_F}} \quad (29)$$

Tables 19 through 21 list the Student's t parameter and the coefficient at several specific confidence levels, which are uniquely calculated with the parameters of the empirical model that are derived from data for a particular probe shape. The bounding probability refers to the chance that a future test performed under identical conditions would result in a lower energy value than the model predicts with the calculated coefficient. The value at which the standard normal cumulative distribution function equals the confidence is provided for comparison to the parameter t; the relative difference is the effect of the limited sample size. Probabilities of one per million or billion are included because they define screening thresholds in Reference 10, page 2.

Table 19: Lower Bounds of Confidence Intervals on Coefficient Optimized to Linear Equation and Flat-End Probe Data

Probability of Lower Future Observation		Confidence	Standard Normal Distribution	Student's t Parameter	Relative Difference	Coefficient, K
500E-3	50%	50%	0	0	0%	4.784
100E-3	10%	90%	1.2816	1.3011	1.52%	3.406
50E-3	5%	95%	1.6449	1.6802	2.2%	3.085
10E-3	1%	99%	2.326	2.414	3.8%	2.547
1E-3	0.1%	99.9%	3.090	3.286	6.3%	2.029
1E-6	0.0001%	99.9999%	4.753	5.472	15.1%	1.1465
1E-9	0.0000001%	99.9999999%	5.998	7.519	25%	0.6720

Table 20: Lower Bounds of Confidence Intervals on Coefficient Optimized to Linear Equation and Semi-spherical Probe Data

Probability of Lower Future Observation		Confidence	Standard Normal Distribution	Student's t Parameter	Relative Difference	Coefficient, K
500E-3	50%	50%	0	0	0%	7.234
100E-3	10%	90%	1.2816	1.3125	2.4%	5.179
50E-3	5%	95%	1.6449	1.7011	3.4%	4.691
10E-3	1%	99%	2.326	2.467	6.1%	3.860
1E-3	0.1%	99.9%	3.090	3.408	10.3%	3.038
1E-6	0.0001%	99.9999%	4.753	5.967	26%	1.5835
1E-9	0.0000001%	99.9999999%	5.998	8.677	45%	0.7943

Table 21: Lower Bounds of Confidence Intervals on Coefficient Optimized to Linear Equation and Tri-corner Probe Data

Probability of Lower Future Observation		Confidence	Standard Normal Distribution	Student's t Parameter	Relative Difference	Coefficient, K
500E-3	50%	50%	0	0	0%	9.011
100E-3	10%	90%	1.2816	1.3178	2.8%	6.807
50E-3	5%	95%	1.6449	1.7109	4.0%	6.261
10E-3	1%	99%	2.326	2.492	7.1%	5.302
1E-3	0.1%	99.9%	3.090	3.467	12.2%	4.309
1E-6	0.0001%	99.9999%	4.753	6.218	31%	2.399
1E-9	0.0000001%	99.9999999%	5.998	9.297	55%	1.2457

Figures 48 through 50 plot the three empirical models with the parameters in Tables 18 through 21 at several confidence levels. The experimental data are plotted with solid circles. In order to display multiple confidence levels on two-dimensional plots, the model and data are expressed in terms of the diameter-to-thickness ratio (M) and the normalized energy (E_n). Figures 51 through 53 plot the mitigated energy (E) as a function of the specimen thickness (t) and probe diameter (d), but only with the median values of the coefficient (K) so that these plots are also two-dimensional. Note that the data tend to be at opposite ends of the abscissas in these two sets of plots because the abscissa in the first set (Fig. 48–50) is inversely related to the thickness, whereas the abscissa in the second set (Fig. 51–53) is the thickness. The median curves appear to match the data more closely in the plots with non-dimensional axes (Fig. 48–50) than in the ones with units of length and energy (Fig. 51–53). The differences in the quality of each curve fit are slight except for the flat-end probes with 25.40-mm (1-in) diameters and 6.35-mm-thick (0.250-in-thick) specimens (diameter-to-thickness ratio of 4). This is simply due to the method of optimizing the parameters to the non-dimensional linear equation (Eq. 14) rather than the non-linear equation (Eq. 10) for the empirical model.

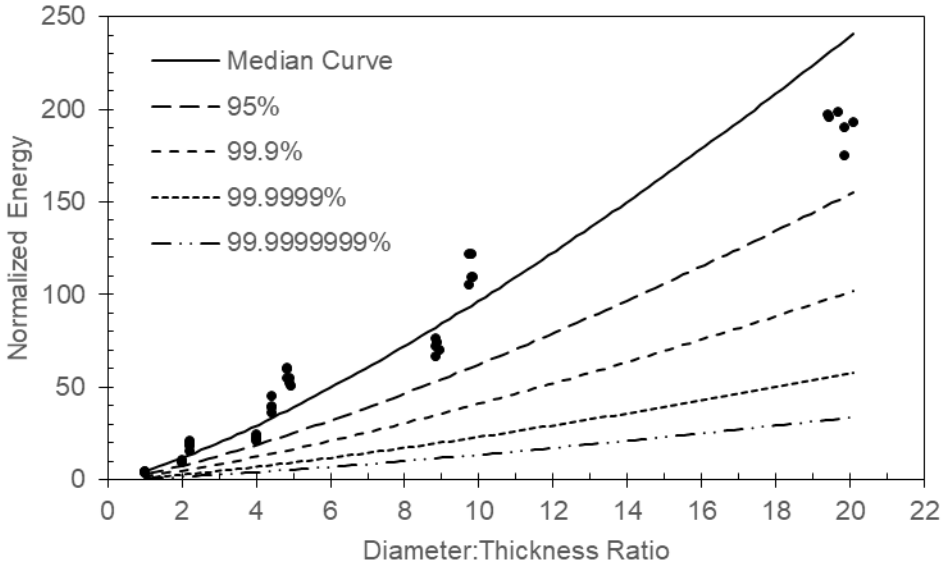

Figure 48: Empirical Model for Flat-End Probe Puncturing 7075-T651 Bar

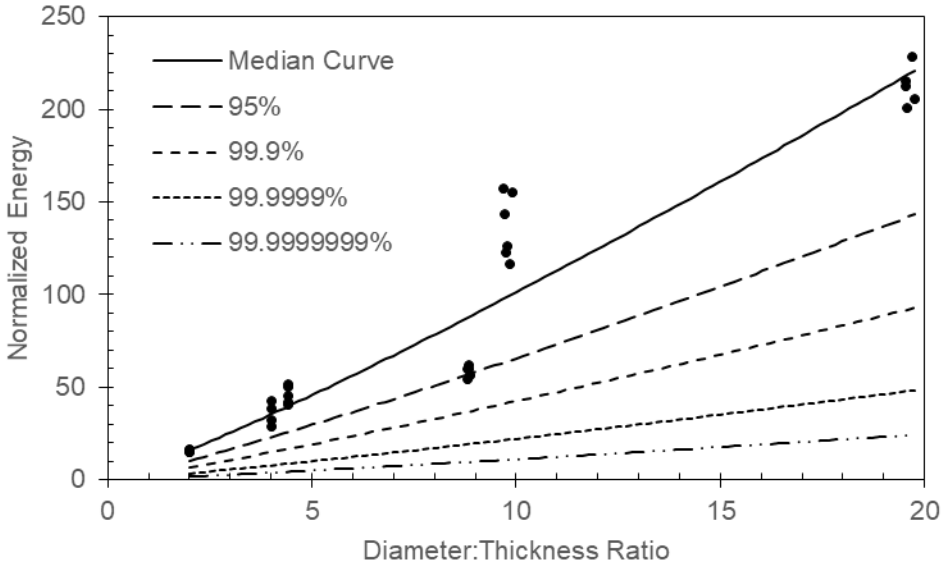

Figure 49: Empirical Model for Semi-spherical Probe Puncturing 7075-T651 Bar

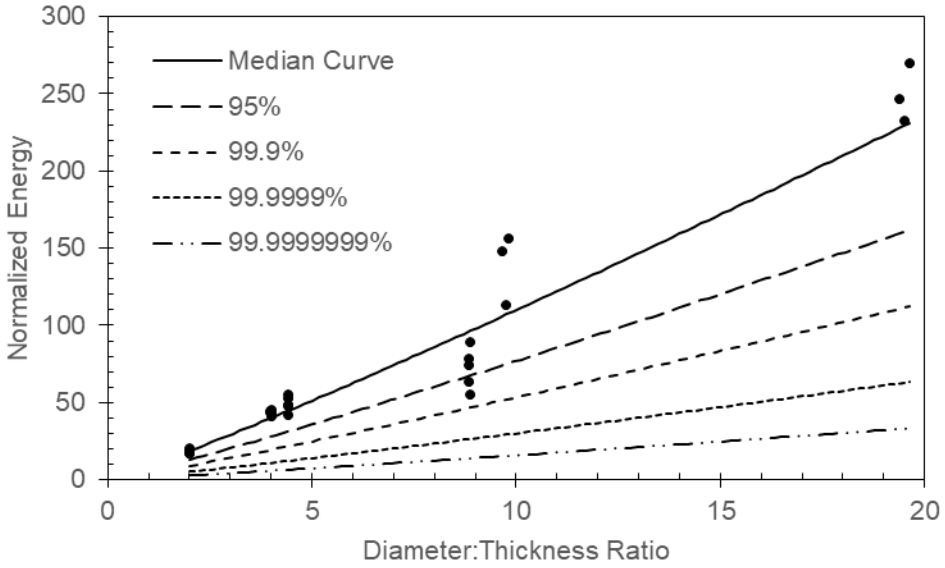

Figure 50: Empirical Model for Tri-corner Probe Puncturing 7075-T651 Bar

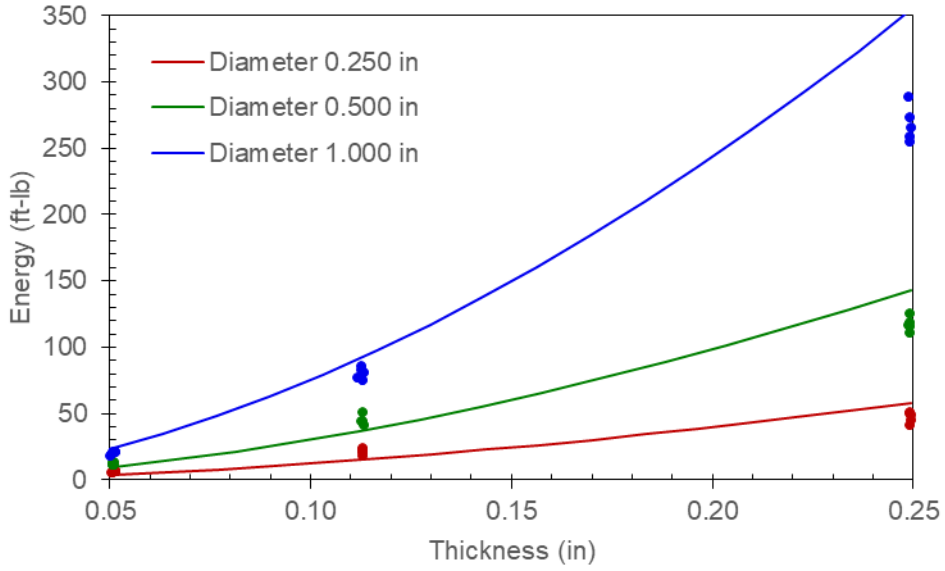

Figure 51: Empirical Model with Linearly Optimized Parameters Compared to Actual Mitigated Energy for Flat-End Probes

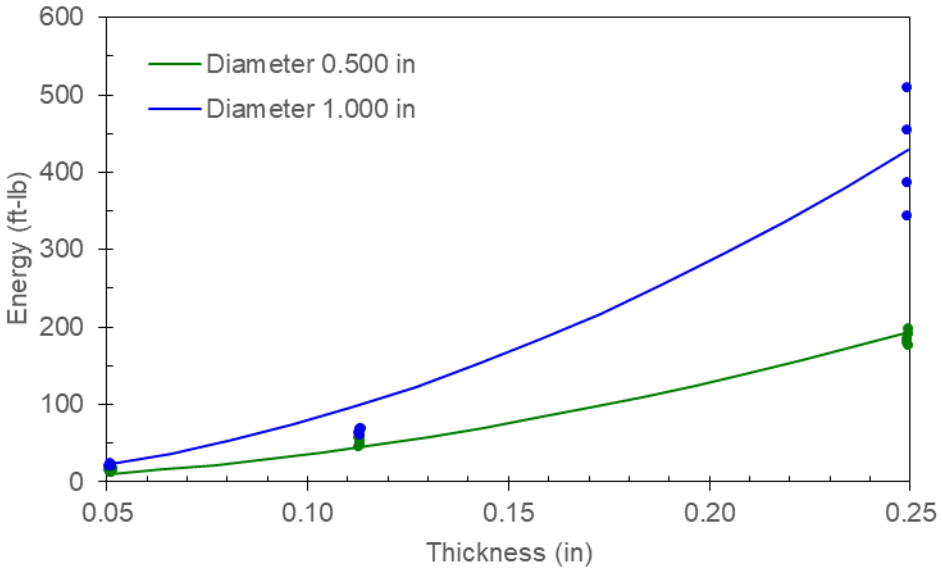

Figure 52: Empirical Model with Linearly Optimized Parameters Compared to Actual Mitigated Energy for Semi-spherical Probes

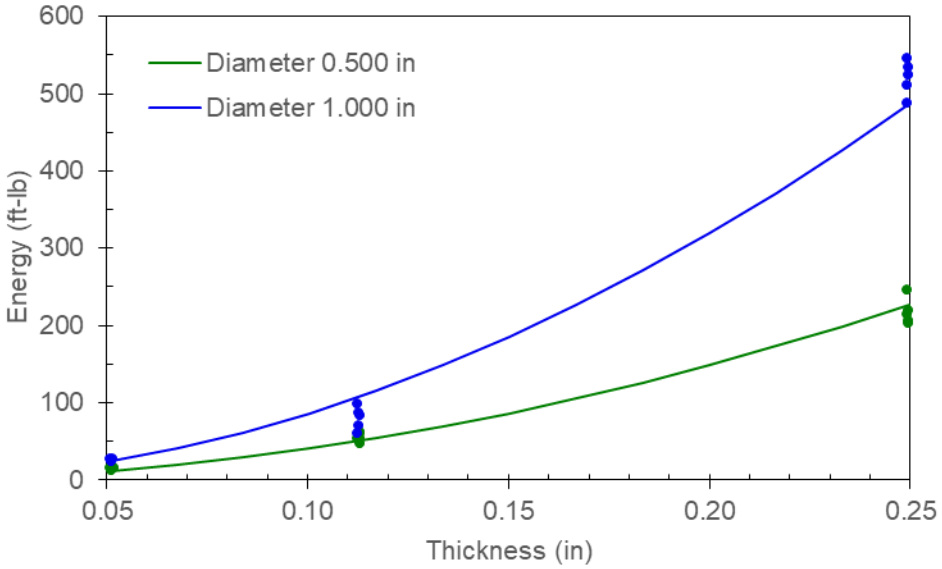

Figure 53: Empirical Model with Linearly Optimized Parameters Compared to Actual Mitigated Energy for Tri-corner Probes

The calibration of the empirical model alleviates error due to the simplicity of the equation. It does not reduce uncertainty in the dimensions and material properties that are provided as inputs. The statistical confidence intervals encompass differences between the properties of each specimen that was tested and the boundary conditions of the experiments that comprise the data set. However, differences between the experimental boundary conditions and those of an intended application are not accounted for. The confidence limits only bound the experiments that form the basis of the model. Engineering judgement is required to apply the results of the empirical model to specific applications.

Optimal Parameters of Non-linear Equation for Mitigated Energy

Numerical methods exist for multi-variate non-linear optimization such that the coefficient (K) and exponent (c) in Equation 10 may be found without writing it in non-dimensional linear form (Eq. 14), but they are too lengthy to present here. An alternate set of coefficients and exponents is provided in Table 22 that minimize the sum of the squares of the residuals of the mitigated energy relative to the data in Tables 14 through 16. Table 23 lists the lower bounds for the coefficient at several specific confidence levels, which are calculated with Equations 20, 26, and 29.

Table 22: Optimal Parameters of Non-linear Equation for Empirical Model

Probe End Geometry	Coefficient, K	Exponent, c
Flat	3.750	1.2991
Partial Sphere with 50% Larger Radius than Probe	7.760	1.0673
Three Orthogonal Planes Meeting at Corner	9.011	1.1061

Table 23: Lower Bounds of Confidence Intervals on Coefficient Optimized to Non-linear Equation

Probability of Lower Future Observation		Confidence	Coefficient, K, for Each Probe Shape		
			Flat-End	Semi-spherical	Tri-corner
500E-3	50%	50%	3.750	7.760	9.011
100E-3	10%	90%	2.322	5.422	6.807
50E-3	5%	95%	2.019	4.876	6.261
10E-3	1%	99%	1.5410	3.956	5.302
1E-3	0.1%	99.9%	1.1177	3.059	4.309
1E-6	0.0001%	99.9999%	0.4995	1.5211	2.399
1E-9	0.0000001%	99.9999999%	0.2351	0.7257	1.2457

Figures 54 through 56 plot the empirical models for the three probe shapes in terms of the diameter-to-thickness ratio (M) and the normalized energy (E_n) at several confidence levels, based on the parameters in Tables 22 and 23; the solid circles are the experimental data. Figures 57 through 59 plot the empirical models in terms of the mitigated energy (E), specimen thickness (t), and probe diameter (d), but only with the parameters in Table 22, which include the median values of the coefficient (K). With the parameters optimized to the non-linear equation (Eq. 10), the median curves appear to match the data more closely in the plots with units of length and energy (Fig. 57–59) than in the ones with non-dimensional axes (Fig. 54–56). The differences in the quality of each fit are slight between these two methods for presenting the data.

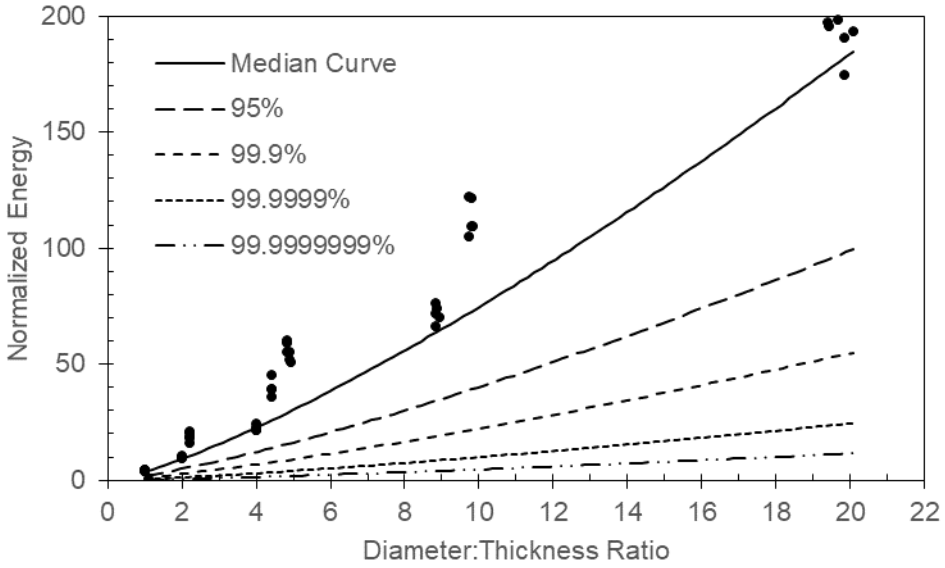

Figure 54: Empirical Model with Non-linearly Optimized Parameters for Flat-End Probe Puncturing 7075-T651 Bar

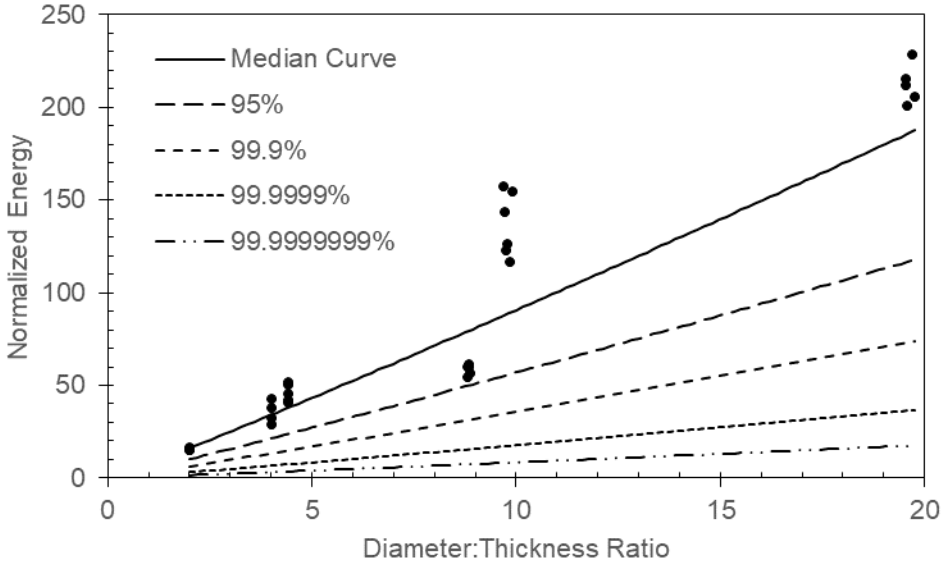

Figure 55: Empirical Model with Non-linearly Optimized Parameters for Semi-spherical Probe Puncturing 7075-T651 Bar

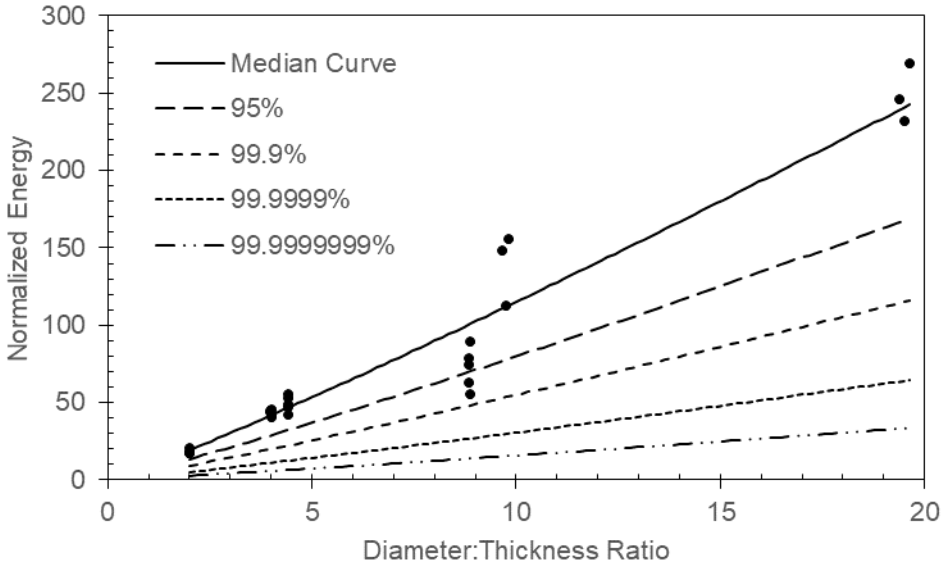

Figure 56: Empirical Model with Non-linearly Optimized Parameters for Tri-corner Probe Puncturing 7075-T651 Bar

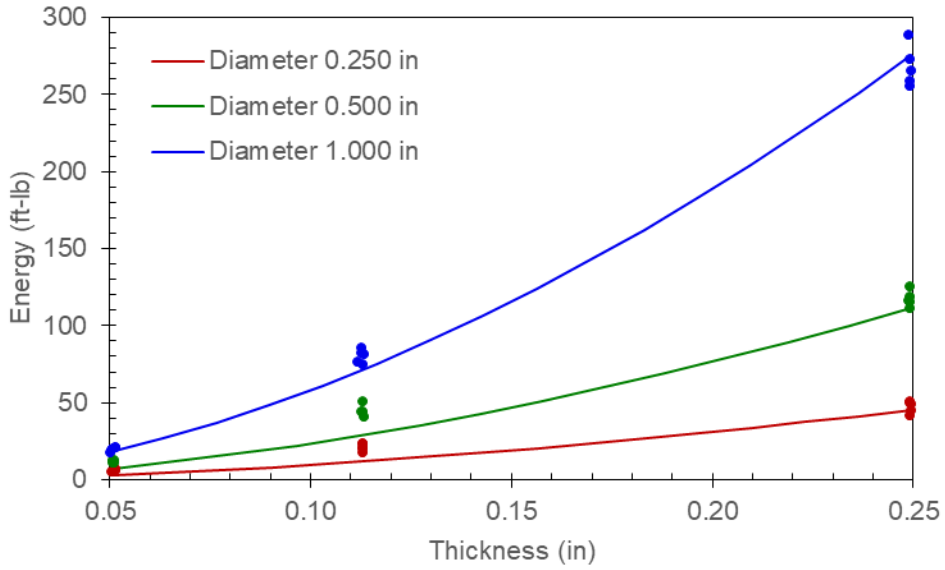

Figure 57: Empirical Model with Non-linearly Optimized Parameters Compared to Actual Mitigated Energy for Flat-End Probes

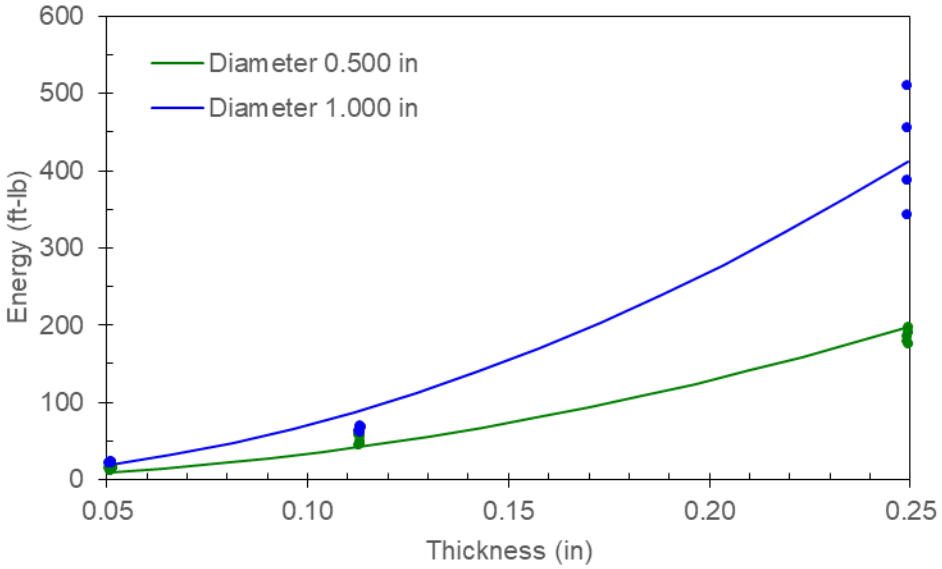

Figure 58: Empirical Model with Non-linearly Optimized Parameters Compared to Actual Mitigated Energy for Semi-spherical Probes

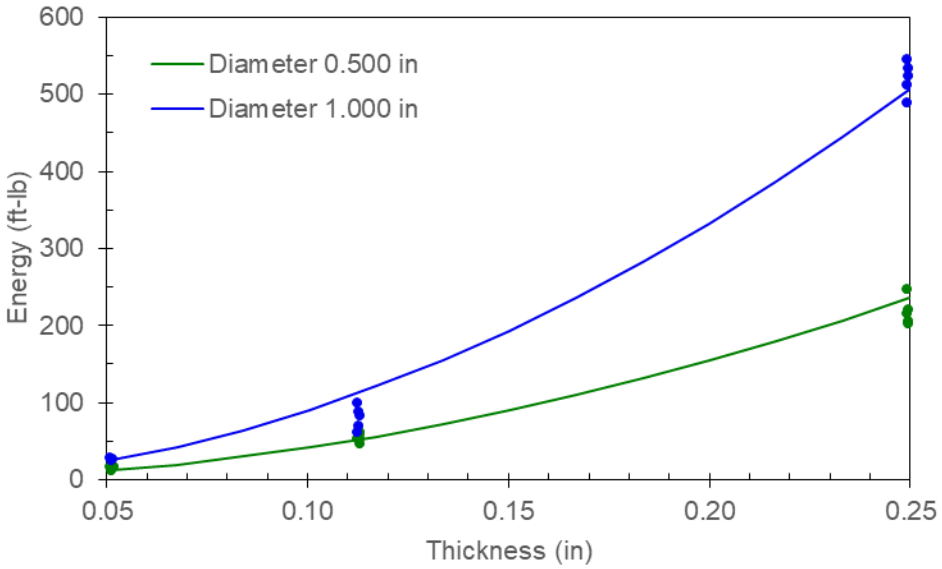

Figure 59: Empirical Model with Non-linearly Optimized Parameters Compared to Actual Mitigated Energy Tri-corner Probes

With the parameter values reported in Table 18, which are optimized to the linear equation (Eq. 14), the median curves show a closer fit to the data in Figures 48 through 50 than in Figures 54 through 56. All of these plots have non-dimensional axes and concentrate the mitigated energy data from the thickest specimens in the lower-left region. With the parameter values presented in Table 22, which are optimized to the non-linear equation (Eq. 10), the median curves show a closer fit to the data in Figures 57 through 59 than in Figures 51 through 53. These plots have axes with units of length and energy, so the data from the thickest specimens appear on the right. The differences in the quality of each fit are slight because the parameters in Tables 18 and 22 are similar. The non-linear optimization method weights the data differently than the linear regression method, which normalizes the mitigated energy data with Equation 11 and applies a logarithmic transformation with

Equation 14 prior to computing the residuals in Equation 20. Each method minimizes the sum of the squares of the residuals between the empirical model and the data, but the cube of the thickness in Equation 11 and the logarithm function in Equation 14 affect the residuals. Terms in Equation 11 (σ_u, ε_u) that do not vary between tests have no effect on the optimization process. Dividing the mitigated energy by the cube of the specimen thickness gives more weight to thin specimens. Taking the logarithm of the normalized energy gives less weight to large normalized energy values, which correspond to large probe diameters and thin specimens. Although the results differ, both methods are acceptable.

Conclusion

Experiments were performed to measure the total energy mitigated by specimens of 7075-T651 bar as cylindrical bars of AISI 4340 steel punctured them. The specimens were all cut from the same stock material but with three thicknesses in the zone where the probes penetrated them: 1.30 mm, 2.90 mm, and 6.35 mm (0.051 in, 0.114 in, and 0.250 in). The puncture probes were all circular cylinders but had three diameters and three shapes for the leading surface. The probes with a flat leading surface included all three diameters: 6.35 mm, 12.70 mm, and 25.40 mm (¼ in, ½ in, and 1 in). The probes with a semi-spherical leading surface had spherical radii that were larger than the cylinder radii by a factor of 1.25 (0.625 multiplied by the diameters): the spherical radii were 7.94 mm and 15.88 mm (0.313 in and 0.625 in) and the cylinder diameters were 12.70 mm and 25.40 mm (½ in and 1 in). The probes with a tri-corner leading surface were cut by three orthogonal planes arranged symmetrically around the axis of the cylinder such that a sharp point like the corner of a flat plate contacted the specimen first. The tri-corner probes were made with diameters of 12.70 mm and 25.40 mm (½ in and 1 in). The remaining geometric parameters of the specimens and boundary conditions were nominally equal in all of the experiments.

The experimental data are processed to determine the total energy (potential and kinetic) that was mitigated by each specimen as the probe passed through it. An empirical model (Eq. 10) is calibrated to the data for each probe shape in order to predict the energy mitigated by intermediate combinations of specimen thickness and probe diameter. The model accounts for the variation in these inputs by applying exponents to them and ensuring that the exponents sum to the required number of length dimensions. This constraint reduces the empirical fit parameters to one coefficient and one exponent. The model combines the specimen thickness and probe diameter with two material properties, the ultimate strength and strain, such that the output is the mitigated energy. Tables 24 through 26 summarize the lower bounds on the optimal parameters for both the linear and non-linear forms of the empirical model (Eq. 14 and 13, respectively). Probabilities of one per thousand, million, or billion are included for convenience; however, these lower bounds are considered uncertain because they would change significantly if additional specimens were tested. The exponent is included in the tables for completeness, although it is a constant.

Table 24: Parameters of Empirical Model for Energy Mitigated by 7075-T651 Bar When Punctured by Flat-End Probe

		Optimized to Linear Equation		Optimized to Non-linear Equation	
Bounding Probability	Confidence	Coefficient, K	Exponent, c	Coefficient, K	Exponent, c
Median	50%	4.784	1.3060	3.750	1.2991
One in Ten	90%	3.406	1.3060	2.322	1.2991
One in Twenty	95%	3.085	1.3060	2.019	1.2991
One in One Hundred	99%	2.547	1.3060	1.5410	1.2991
One in One Thousand	99.9%	2.029	1.3060	1.1177	1.2991
One in One Million	99.9999%	1.1465	1.3060	0.4995	1.2991
One in One Billion	99.9999999%	0.6720	1.3060	0.2351	1.2991

Table 25: Parameters of Empirical Model for Energy Mitigated by 7075-T651 Bar When Punctured by Semi-spherical Probe

		Optimized to Linear Equation		Optimized to Non-linear Equation	
Bounding Probability	Confidence	Coefficient, K	Exponent, c	Coefficient, K	Exponent, c
Median	50%	7.234	1.1458	7.760	1.0673
One in Ten	90%	5.179	1.1458	5.422	1.0673
One in Twenty	95%	4.691	1.1458	4.876	1.0673
One in One Hundred	99%	3.860	1.1458	3.956	1.0673
One in One Thousand	99.9%	3.038	1.1458	3.059	1.0673
One in One Million	99.9999%	1.5835	1.1458	1.5211	1.0673
One in One Billion	99.9999999%	0.7943	1.1458	0.7257	1.0673

Table 26: Parameters of Empirical Model for Energy Mitigated by 7075-T651 Bar When Punctured by Tri-corner Probe

		Optimized to Linear Equation		Optimized to Non-linear Equation	
Bounding Probability	Confidence	Coefficient, K	Exponent, c	Coefficient, K	Exponent, c
Median	50%	8.707	1.1012	9.011	1.1061
One in Ten	90%	6.618	1.1012	6.807	1.1061
One in Twenty	95%	6.099	1.1012	6.261	1.1061
One in One Hundred	99%	5.183	1.1012	5.302	1.1061
One in One Thousand	99.9%	4.232	1.1012	4.309	1.1061
One in One Million	99.9999%	2.387	1.1012	2.399	1.1061
One in One Billion	99.9999999%	1.2574	1.1012	1.2457	1.1061

Uncertainty in the measurements of the energy mitigated by each specimen is due to the accuracy of the laser interferometers, machining tolerances, spatial variation in material properties (non-homogeneity), and the stochastic nature of ductile fracture. The acceleration data serves as a trigger for selecting the time ranges over which to average the total energy, but the energy is calculated solely from position data, and the trigger times are adjusted such that the intervals appear reasonable on the total energy plot. Therefore, error in the accelerometer has no influence on the test results. The specimens are manufactured with reasonable tolerances and surface roughness limits for milling operations. The variation in thickness can be as much as 2% and remain within tolerance limits. The hardness of a similar aluminum alloy (6061-T651) has been shown to vary by 9% through the thickness of

a plate (Ref. 11). Ductile fracture occurs when voids form in the material and coalesce into cracks. The locations of voids and the reduction in the engineering strength as they grow and combine depend on the microstructure, which is not known before a component fractures and is, therefore, assumed to be homogeneous. Uncertainty about the microstructure makes the crack paths appear random although they follow patterns based on the boundary conditions.

There is also uncertainty in applying the empirical model to metal alloys of particular ultimate strengths and strains. There is measurement error in determining the material properties, both of the alloy that was tested and the subject to which the empirical model is applied. These errors may augment or reduce each other. The form of the stress-strain relation varies from one alloy to another, and the empirical model does not account for it. The experiments were performed with specimens from the same stock material, so they experienced the same heat treatments. This minimized the variance and maximized the energy at each confidence level; however, it also neglected differences between heat treatment lots and material production batches. Evaluating the empirical model with parameters fit to data from multiple sources, as in Reference 5, would reduce this unconservative bias.

References

1. Landry, D., Pfeifer, N., Neeley, D., and Settecerri, R., "Puncture Test Summary—SHK_5572 (07/31/2023–08/10/2023)," Sandia National Laboratories, 29 August 2023.
2. Boresi, A. P., Schmidt, R. J., and Sidebottom, O. M., *Advanced Mechanics of Materials*, 5th ed., John Wiley & Sons, 1993.
3. Shigley, J. E., and Mischke, C. R., *Mechanical Engineering Design*, McGraw-Hill, 2001.
4. Battelle Memorial Institute, MMPDS-17, "Metallic Materials Properties Development and Standardization (MMPDS)," 1 July 2022.
5. Corona, E., SAND2020-12660R, "Empirical Formula for Puncture Energy of Flat Plates by a Cylindrical Punch," Sandia National Laboratories, 6 November 2020.
6. Lay, D. C., *Linear Algebra and its Applications*, 1st ed., Addison-Wesley, 1994.
7. Figliola, R. S., and Beasley, D. E., *Theory and Design for Mechanical Measurements*, 3rd ed., John Wiley & Sons, 2000.
8. Ross, S., *A First Course in Probability*, 5th ed., Prentice Hall, 1998.
9. Bain, L. J., and Engelhardt, M., *Introduction to Probability and Mathematical Statistics*, 2nd ed., Duxbury Press, 1992.
10. Department of Energy, DOE-NA-STD-3016-2023, "Hazard Analysis Reports for Nuclear Explosive Operations," 2023.
11. Kramer, S., Antoun, B., Lu, W., Jones, A., Sanborn, B., Song, B., Jin, H., and Deibler, L., SAND2019-10152PE, "DE L2 Milestone Presentation: Ductile Failure," Sandia National Laboratories, 21 August 2019.

Appendix A: Acceleration

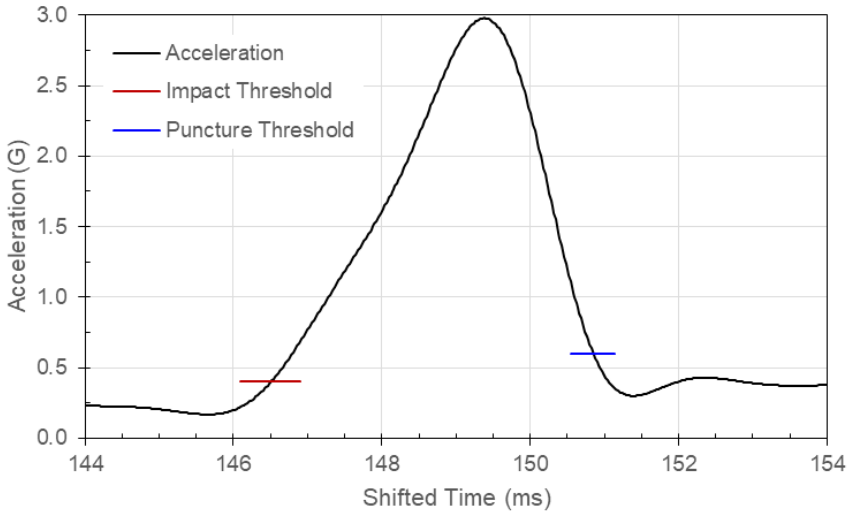

Figure 60: Carriage Acceleration, Test 11, Specimen T051-24, 0.250-Inch Flat Probe

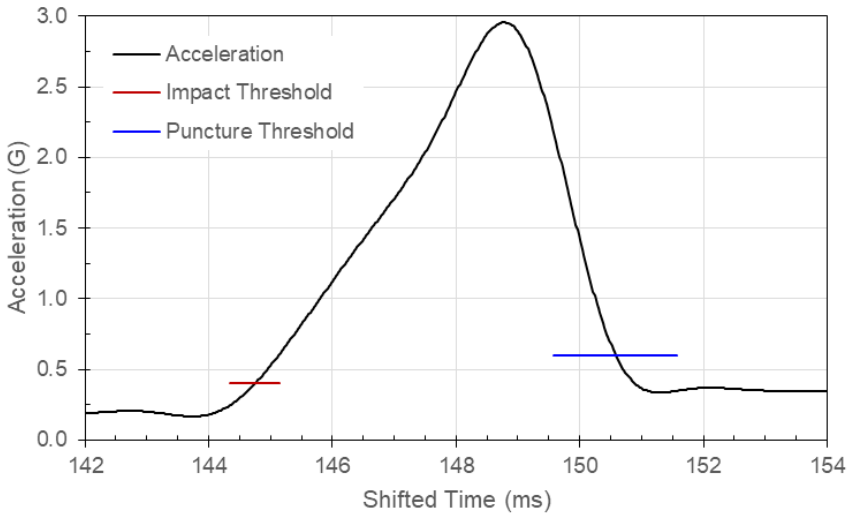

Figure 61: Carriage Acceleration, Test 12, Specimen T051-26, 0.250-Inch Flat Probe

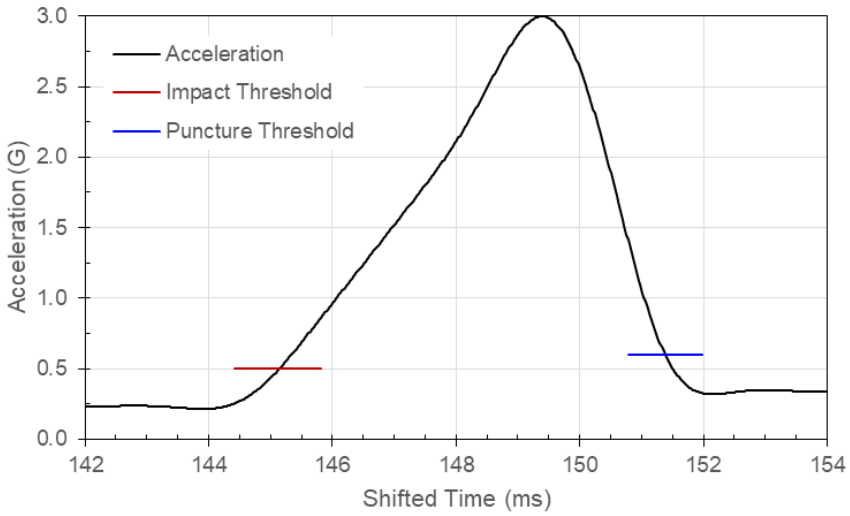

Figure 62: Carriage Acceleration, Test 16, Specimen T051-28, 0.250-Inch Flat Probe

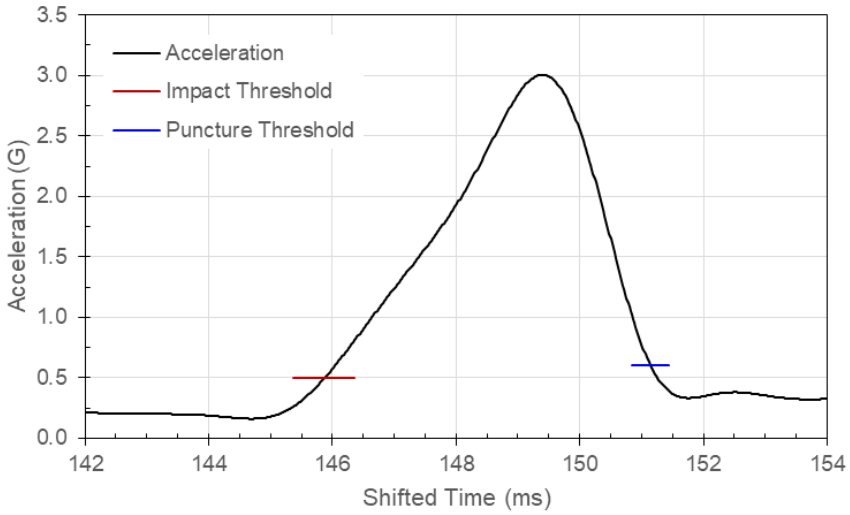

Figure 63: Carriage Acceleration, Test 17, Specimen T051-29, 0.250-Inch Flat Probe

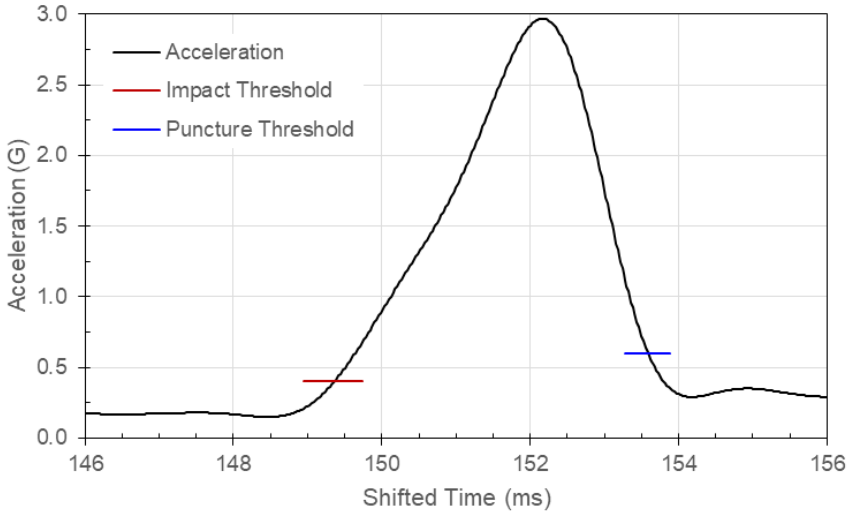

Figure 64: Carriage Acceleration, Test 6, Specimen T051-30, 0.250-Inch Flat Probe

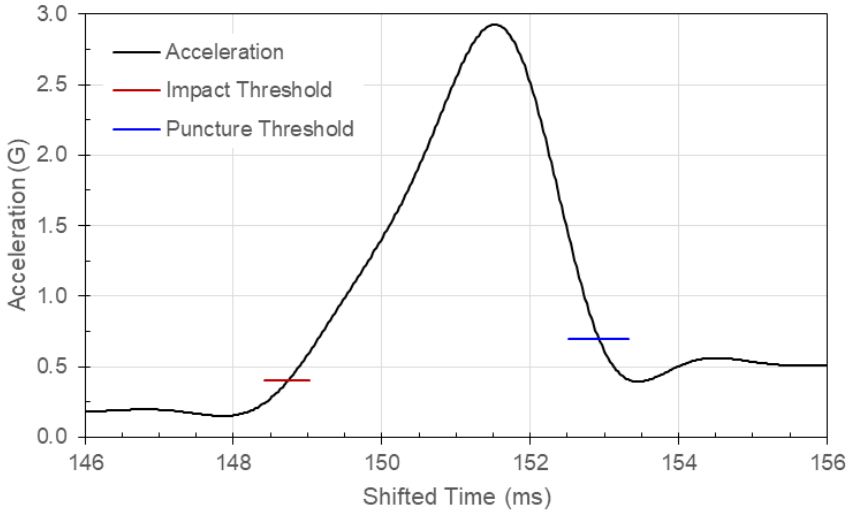

Figure 65: Carriage Acceleration, Test 5, Specimen T051-32, 0.250-Inch Flat Probe

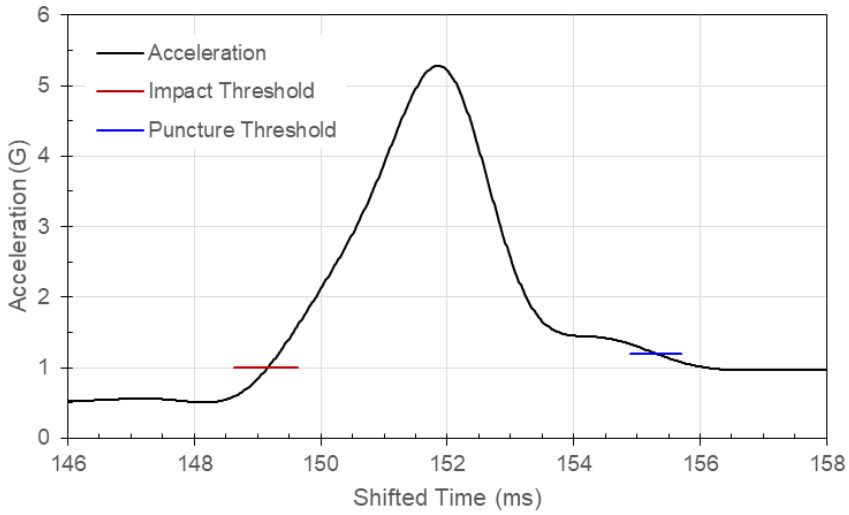

Figure 66: Carriage Acceleration, Test 28, Specimen T051-03, 0.500-Inch Flat Probe

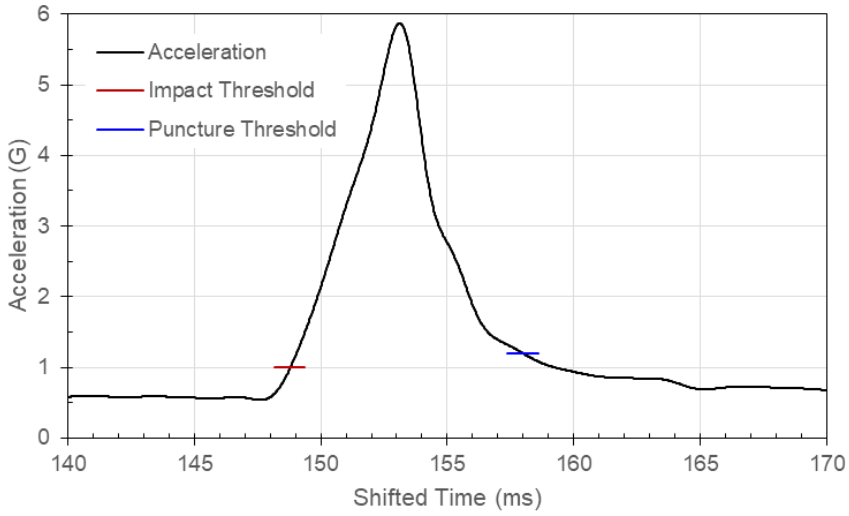

Figure 67: Carriage Acceleration, Test 29, Specimen T051-08, 0.500-Inch Flat Probe

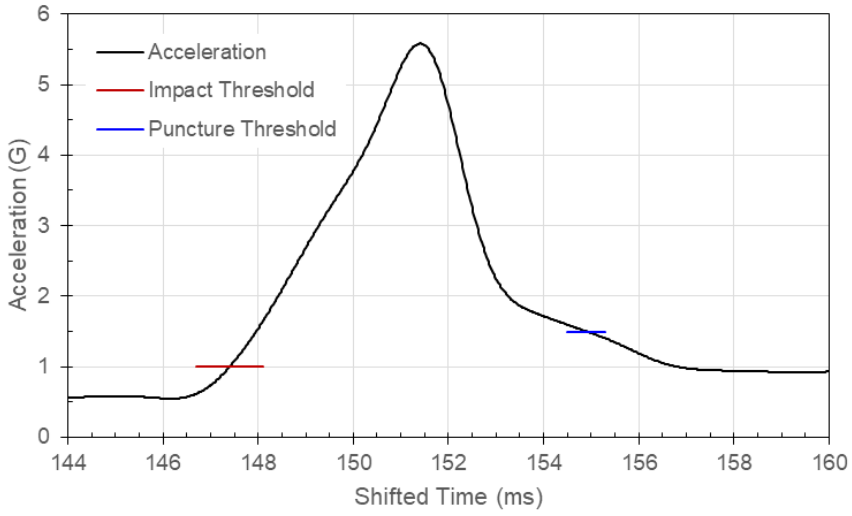

Figure 68: Carriage Acceleration, Test 30, Specimen T051-10, 0.500-Inch Flat Probe

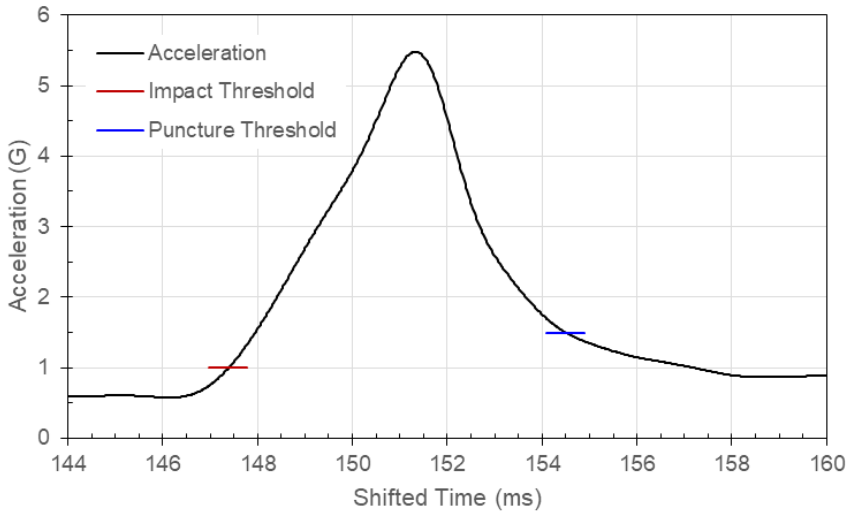

Figure 69: Carriage Acceleration, Test 31, Specimen T051-21, 0.500-Inch Flat Probe

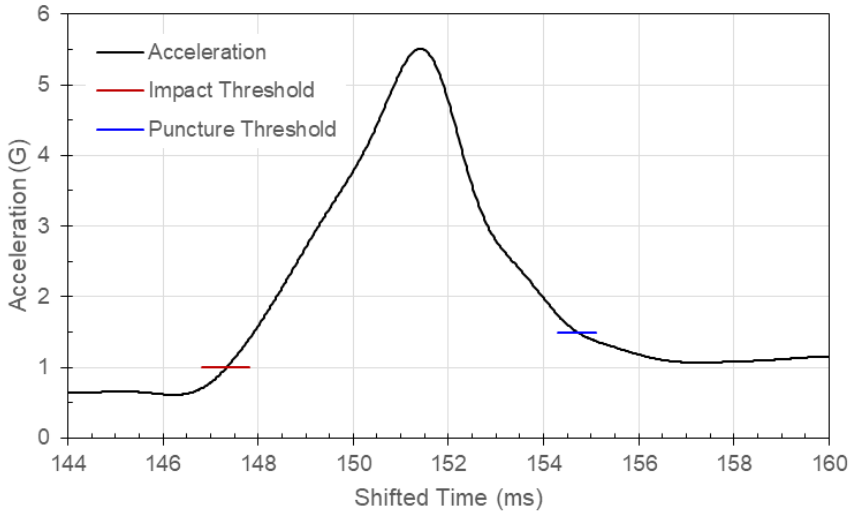

Figure 70: Carriage Acceleration, Test 32, Specimen T051-27, 0.500-Inch Flat Probe

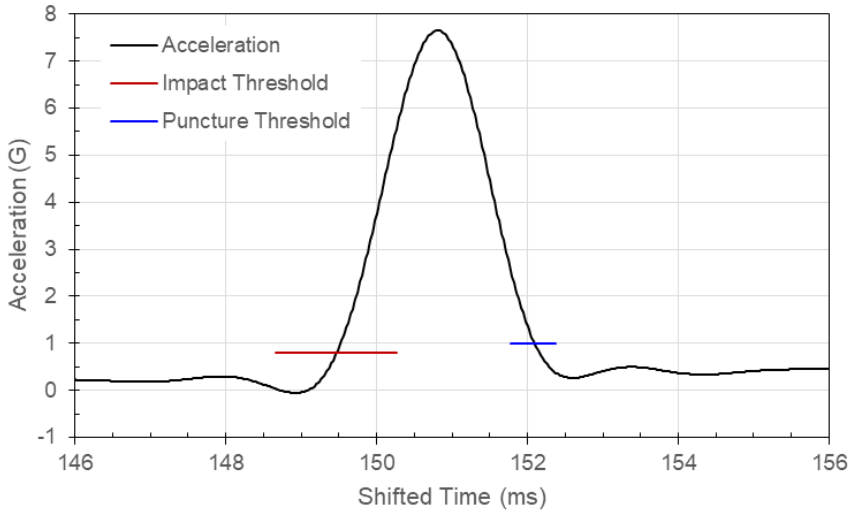

Figure 71: Carriage Acceleration, Test 44, Specimen T051-14, 1.000-Inch Flat Probe

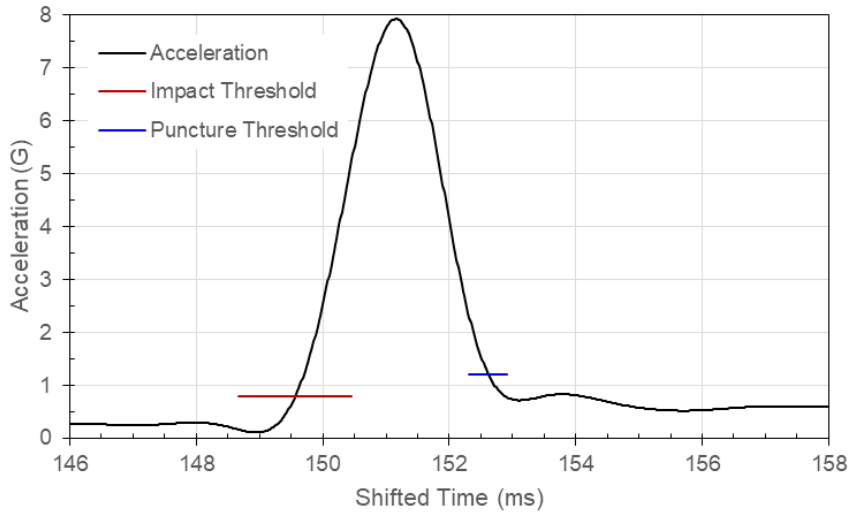

Figure 72: Carriage Acceleration, Test 45, Specimen T051-15, 1.000-Inch Flat Probe

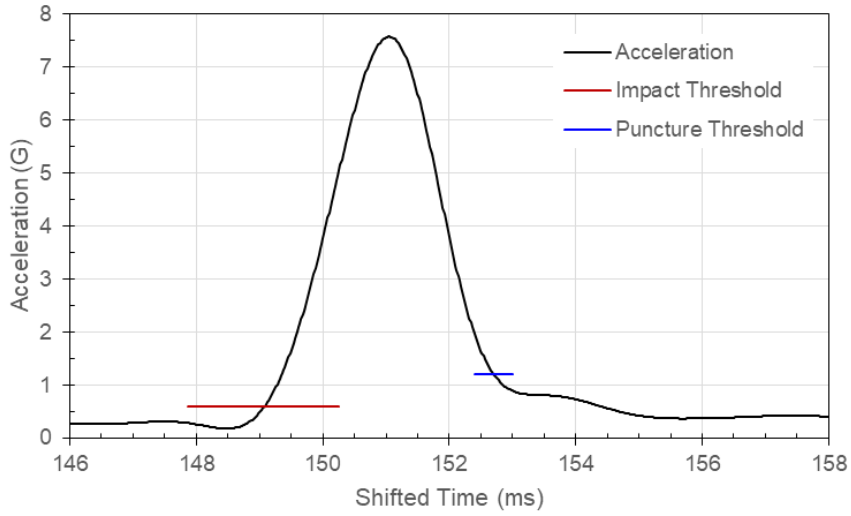

Figure 73: Carriage Acceleration, Test 46, Specimen T051-16, 1.000-Inch Flat Probe

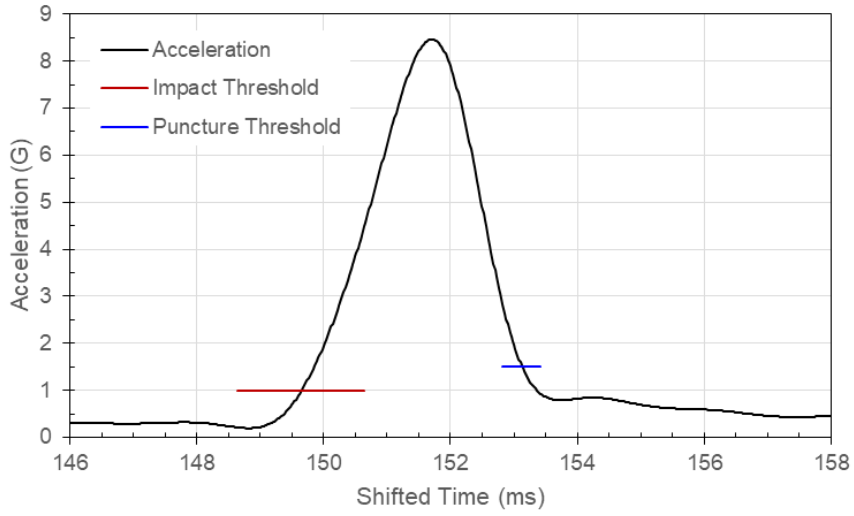

Figure 74: Carriage Acceleration, Test 48, Specimen T051-17, 1.000-Inch Flat Probe

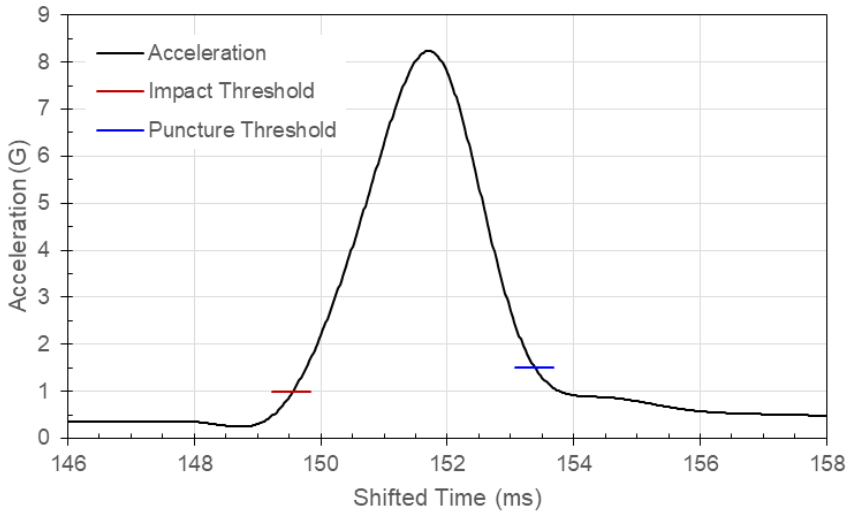

Figure 75: Carriage Acceleration, Test 49, Specimen T051-20, 1.000-Inch Flat Probe

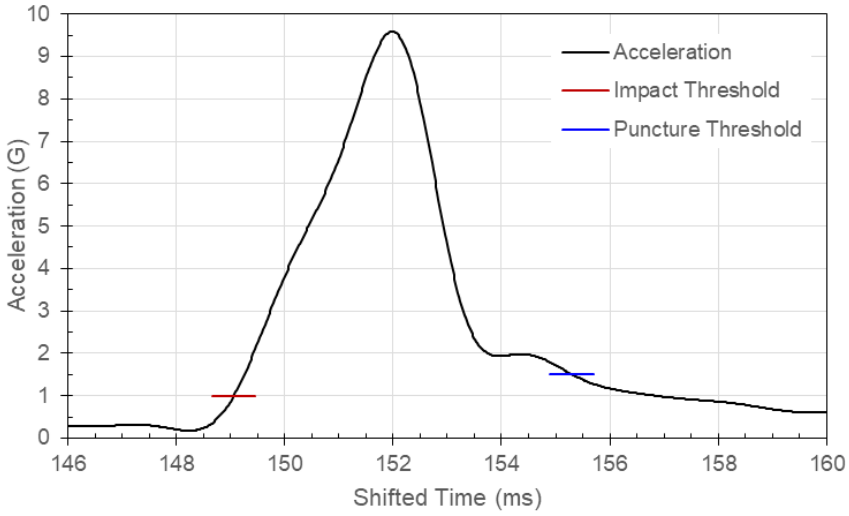

Figure 76: Carriage Acceleration, Test 47, Specimen T051-35, 1.000-Inch Flat Probe

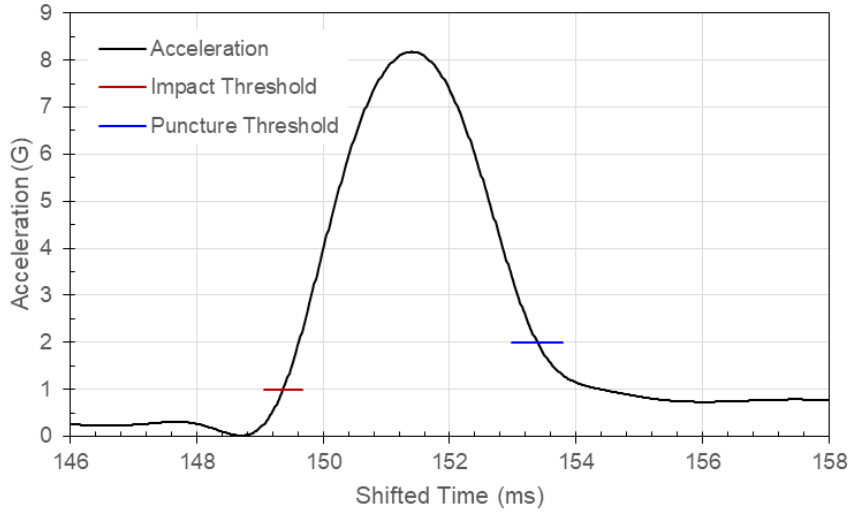

Figure 77: Carriage Acceleration, Test 18, Specimen T114-08, 0.250-Inch Flat Probe

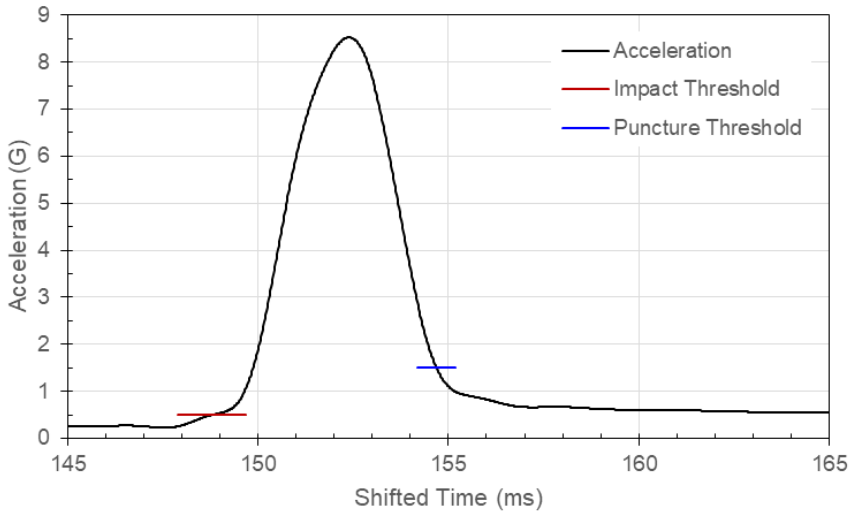

Figure 78: Carriage Acceleration, Test 19, Specimen T114-16, 0.250-Inch Flat Probe

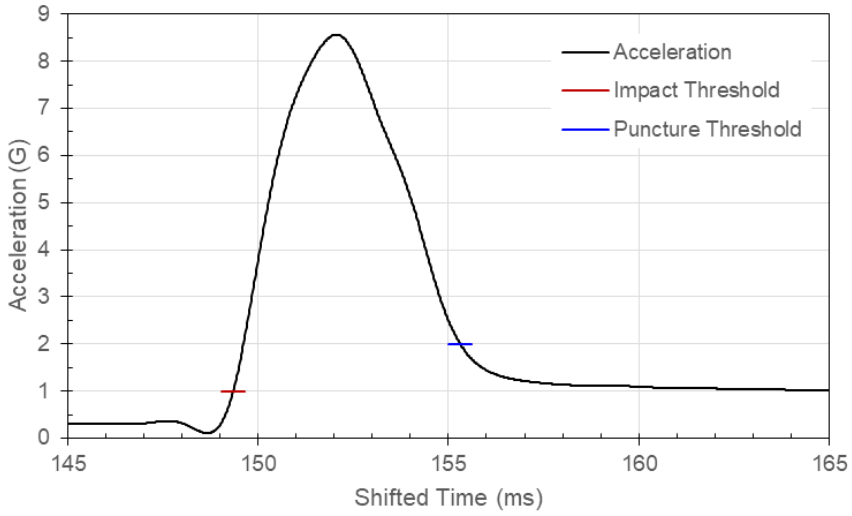

Figure 79: Carriage Acceleration, Test 20, Specimen T114-17, 0.250-Inch Flat Probe

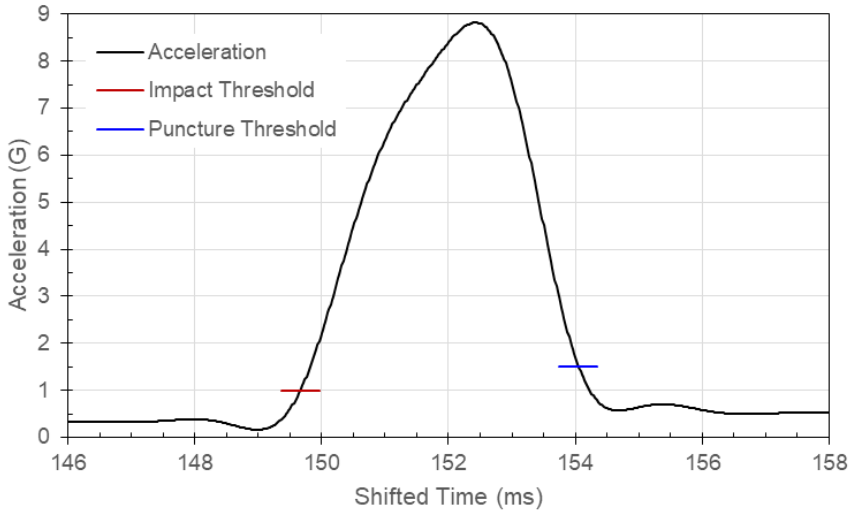

Figure 80: Carriage Acceleration, Test 21, Specimen T114-23, 0.250-Inch Flat Probe

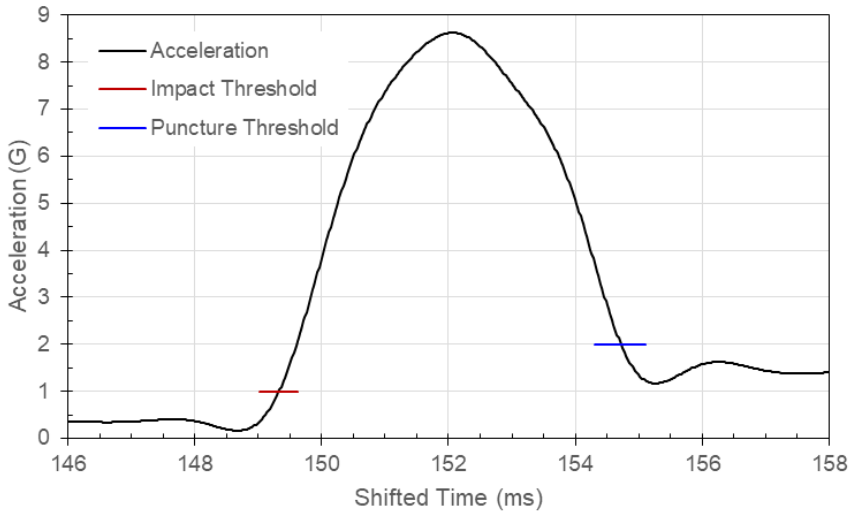

Figure 81: Carriage Acceleration, Test 22, Specimen T114-24, 0.250-Inch Flat Probe

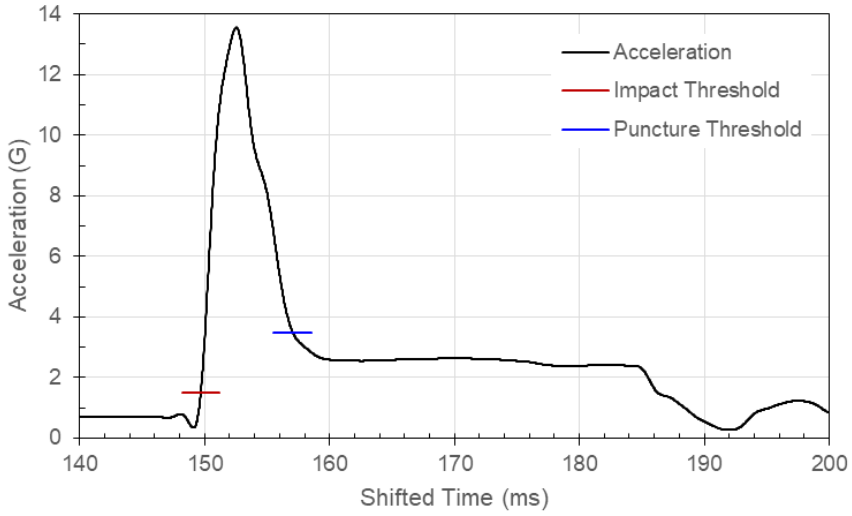

Figure 82: Carriage Acceleration, Test 33, Specimen T114-07, 0.500-Inch Flat Probe

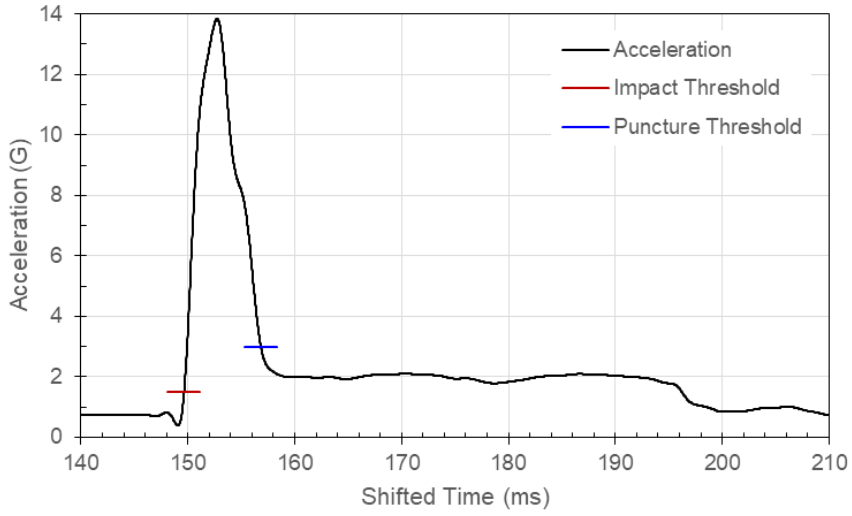

Figure 83: Carriage Acceleration, Test 35, Specimen T114-09, 0.500-Inch Flat Probe

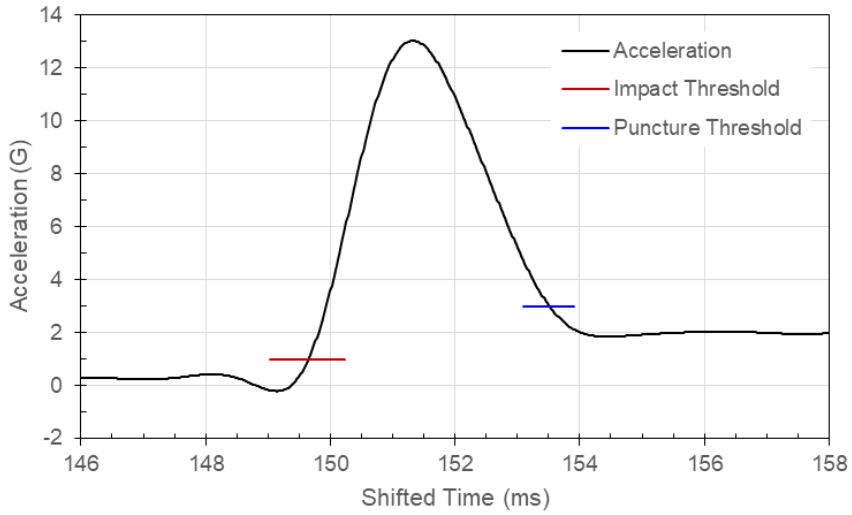

Figure 84: Carriage Acceleration, Test 37, Specimen T114-27, 0.500-Inch Flat Probe

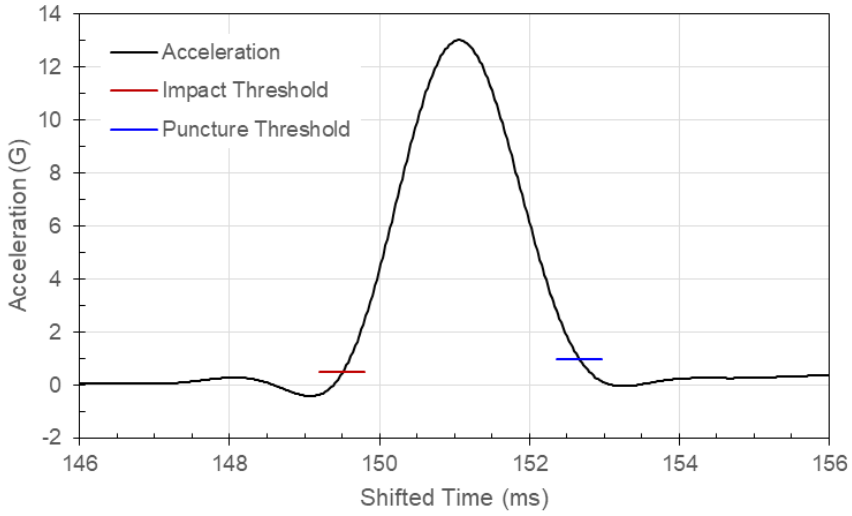

Figure 85: Carriage Acceleration, Test 38, Specimen T114-30, 0.500-Inch Flat Probe

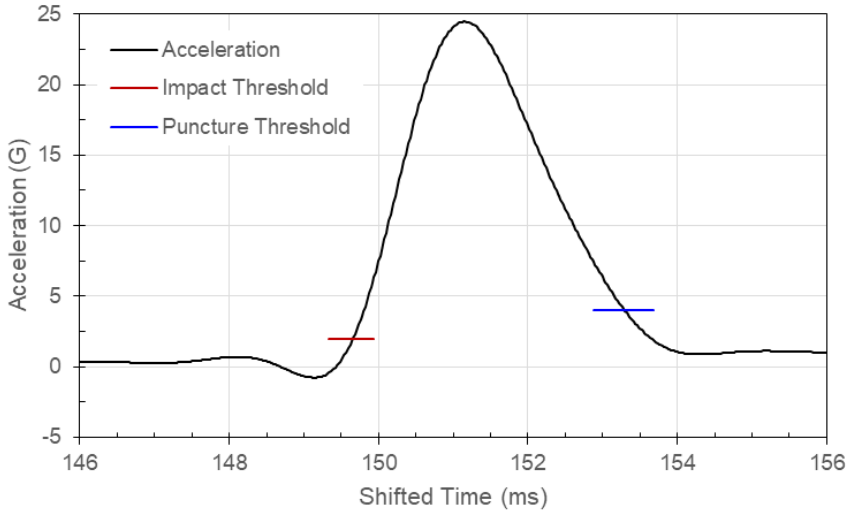

Figure 86: Carriage Acceleration, Test 50, Specimen T114-05, 1.000-Inch Flat Probe

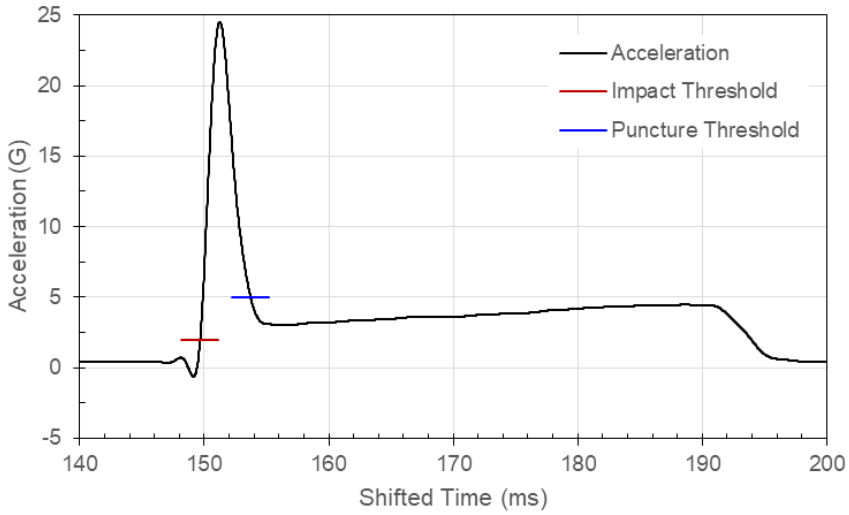

Figure 87: Carriage Acceleration, Test 51, Specimen T114-13, 1.000-Inch Flat Probe

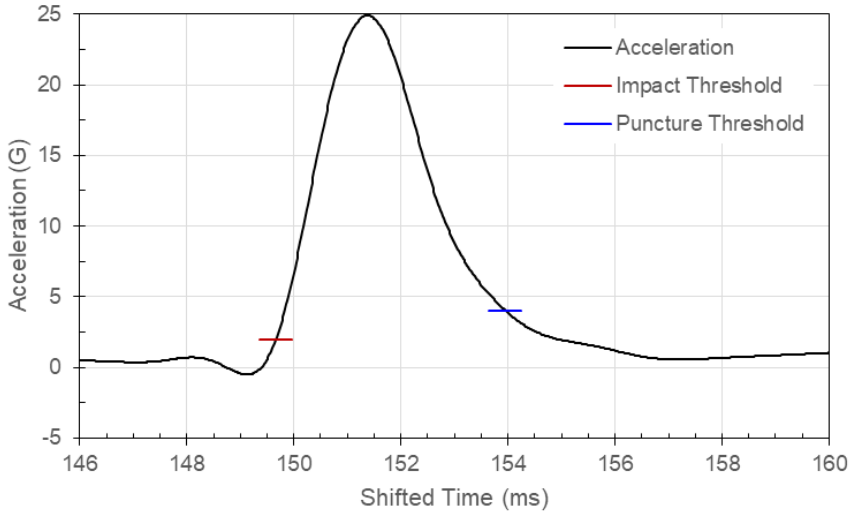

Figure 88: Carriage Acceleration, Test 52, Specimen T114-14, 1.000-Inch Flat Probe

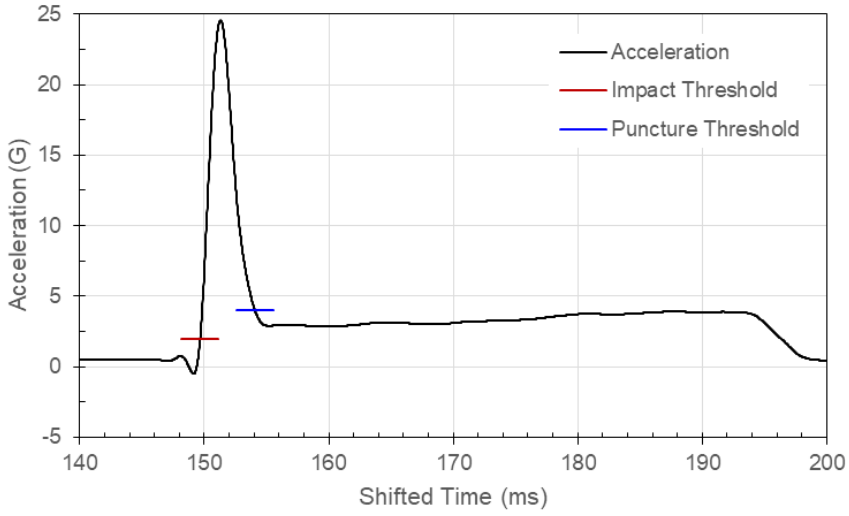

Figure 89: Carriage Acceleration, Test 53, Specimen T114-21, 1.000-Inch Flat Probe

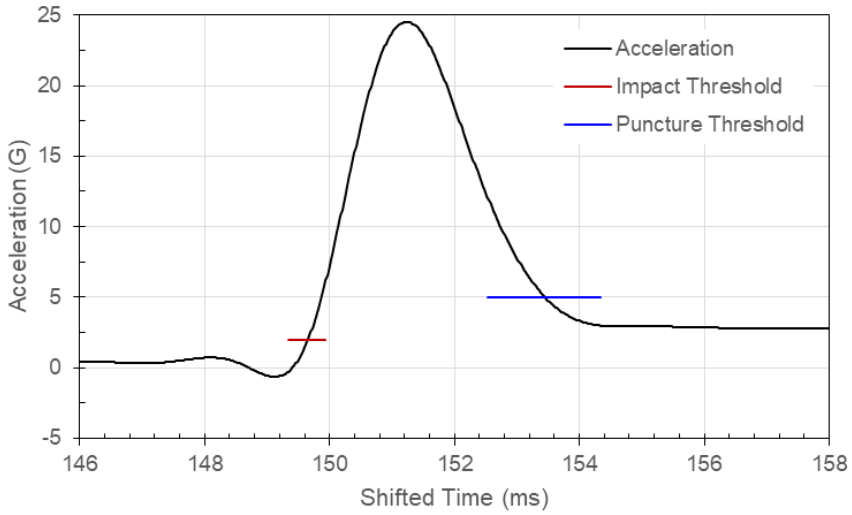

Figure 90: Carriage Acceleration, Test 54, Specimen T114-29, 1.000-Inch Flat Probe

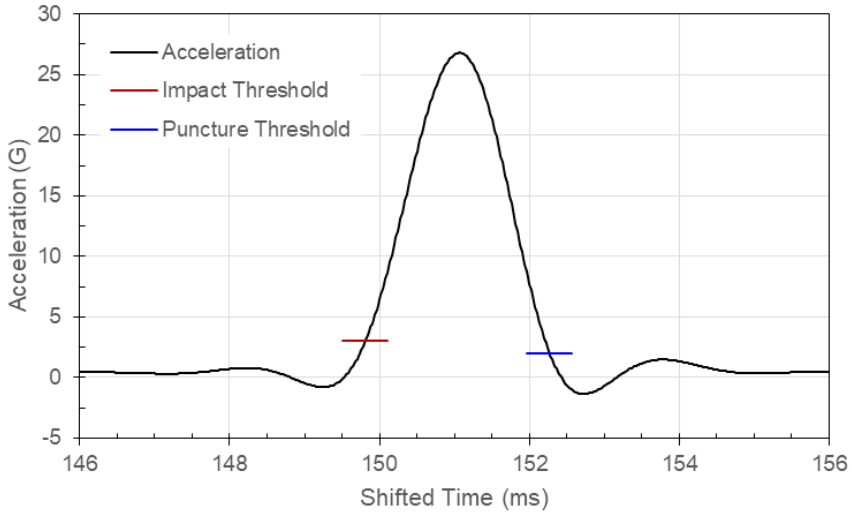

Figure 91: Carriage Acceleration, Test 23, Specimen T250-08, 0.250-Inch Flat Probe

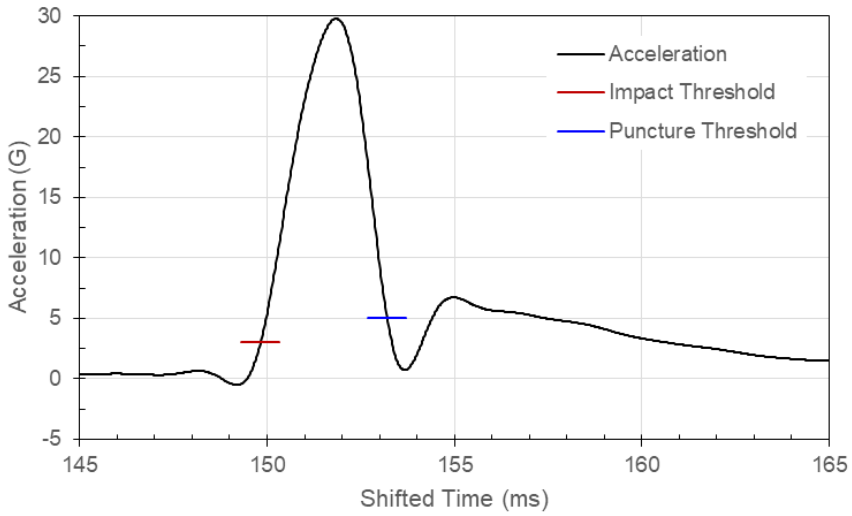

Figure 92: Carriage Acceleration, Test 24, Specimen T250-16, 0.250-Inch Flat Probe

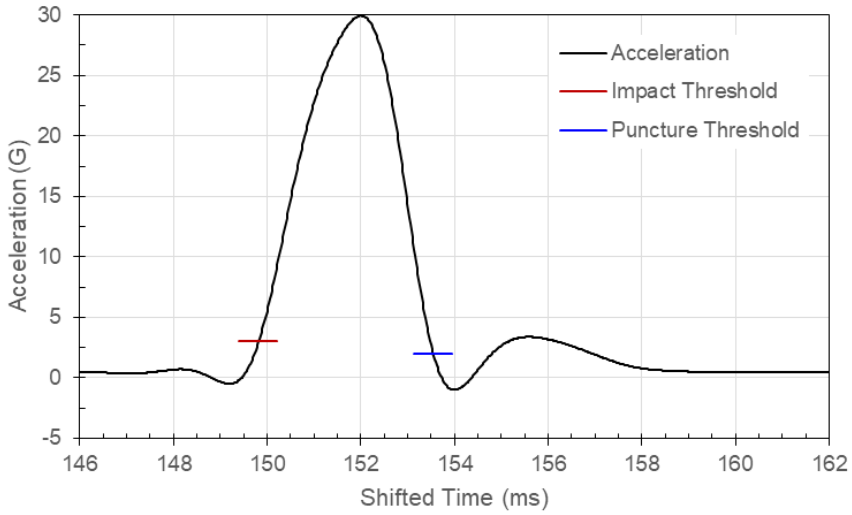

Figure 93: Carriage Acceleration, Test 25, Specimen T250-17, 0.250-Inch Flat Probe

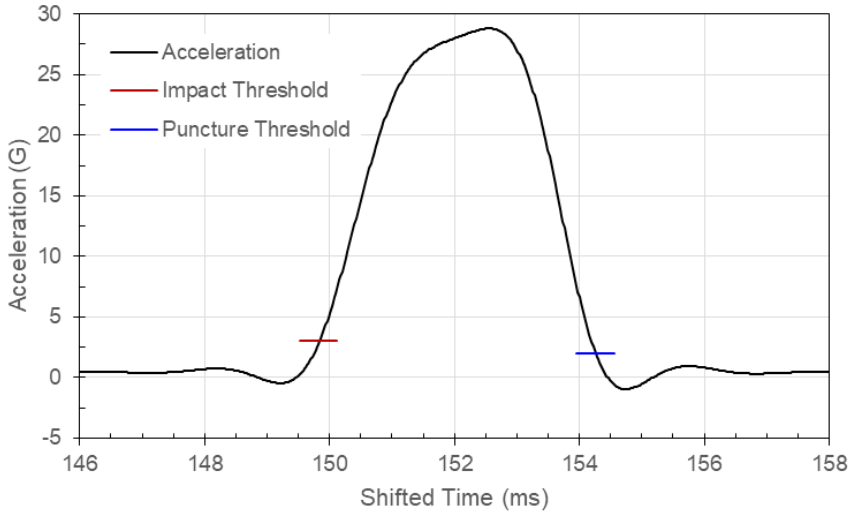

Figure 94: Carriage Acceleration, Test 26, Specimen T250-23, 0.250-Inch Flat Probe

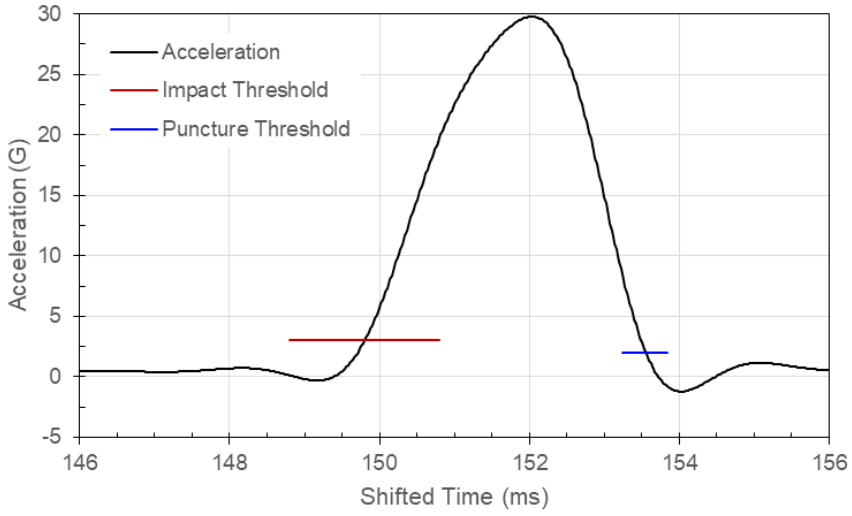

Figure 95: Carriage Acceleration, Test 27, Specimen T250-29, 0.250-Inch Flat Probe

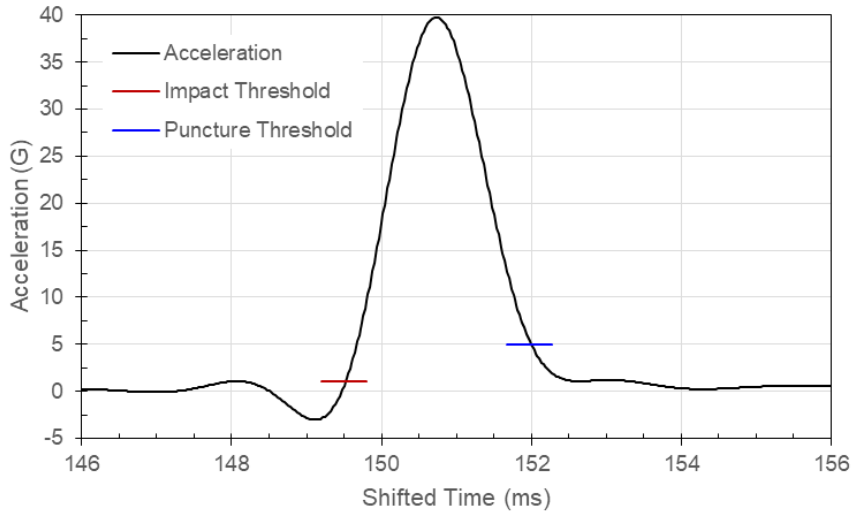

Figure 96: Carriage Acceleration, Test 39, Specimen T250-07, 0.500-Inch Flat Probe

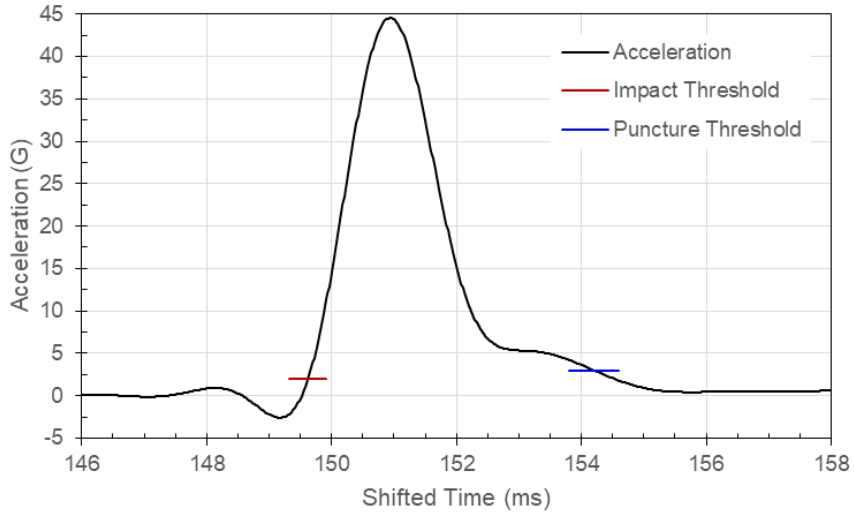

Figure 97: Carriage Acceleration, Test 40, Specimen T250-09, 0.500-Inch Flat Probe

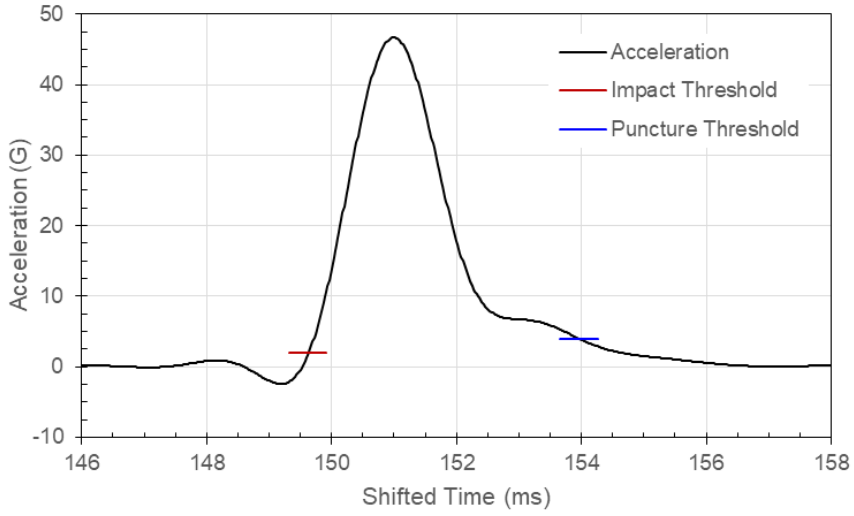

Figure 98: Carriage Acceleration, Test 41, Specimen T250-18, 0.500-Inch Flat Probe

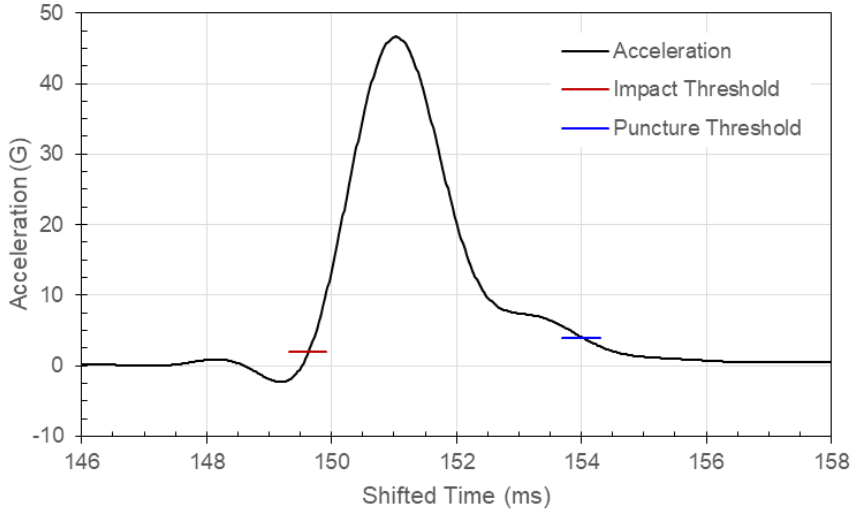

Figure 99: Carriage Acceleration, Test 42, Specimen T250-24, 0.500-Inch Flat Probe

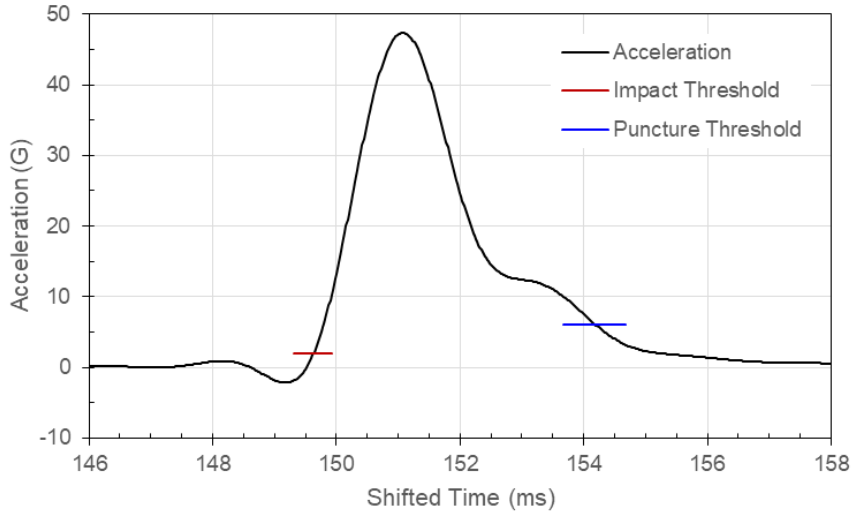

Figure 100: Carriage Acceleration, Test 43, Specimen T250-30, 0.500-Inch Flat Probe

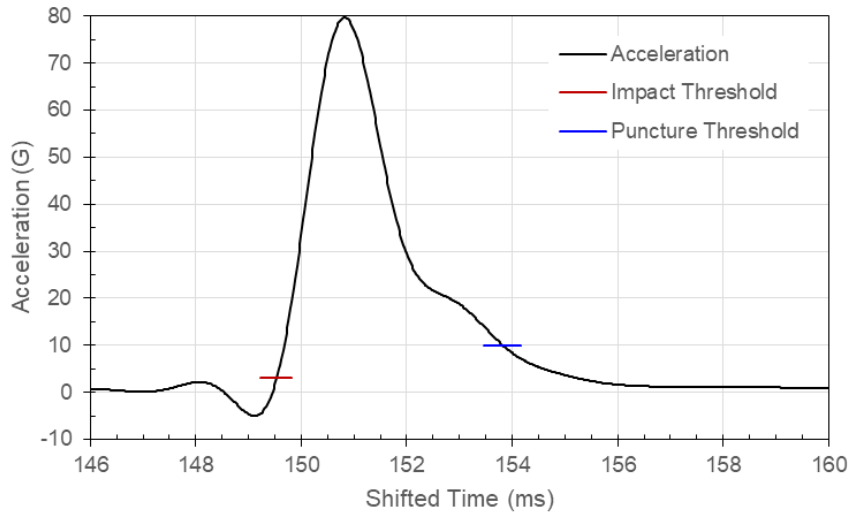

Figure 101: Carriage Acceleration, Test 55, Specimen T250-06, 1.000-Inch Flat Probe

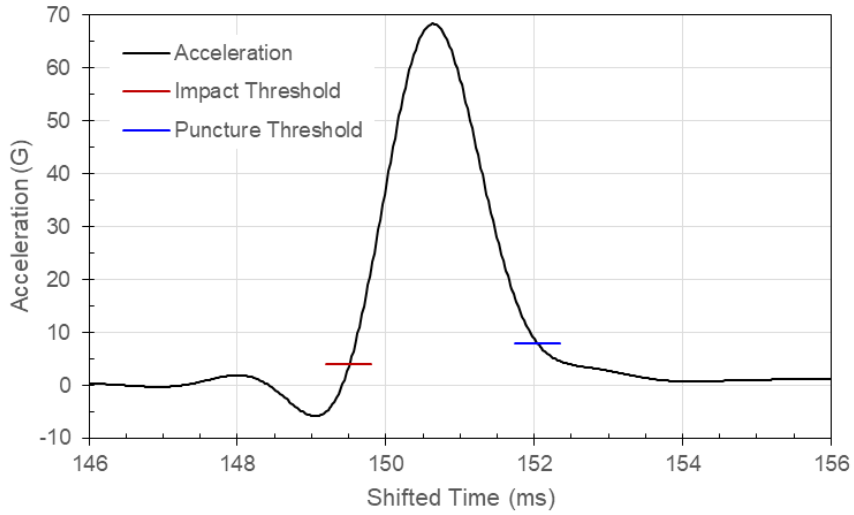

Figure 102: Carriage Acceleration, Test 56, Specimen T250-15, 1.000-Inch Flat Probe

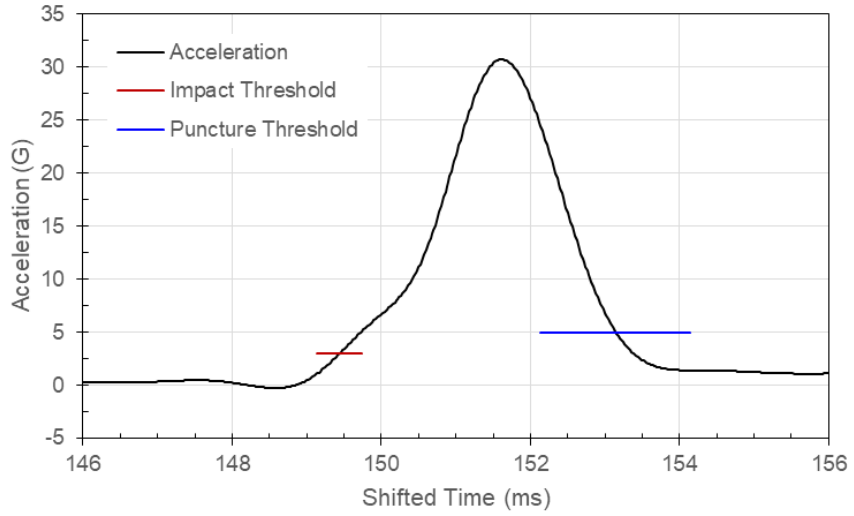

Figure 103: Carriage Acceleration, Test 57, Specimen T250-28, 1.000-Inch Flat Probe

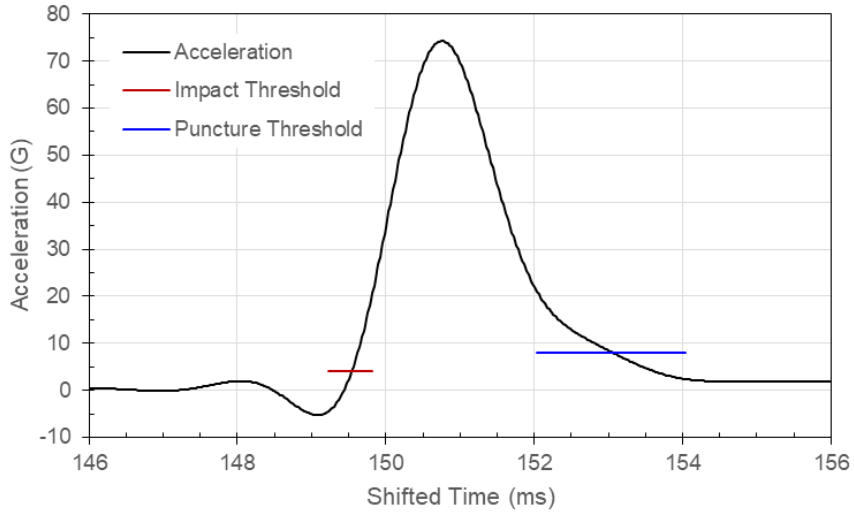

Figure 104: Carriage Acceleration, Test 58, Specimen T250-34, 1.000-Inch Flat Probe

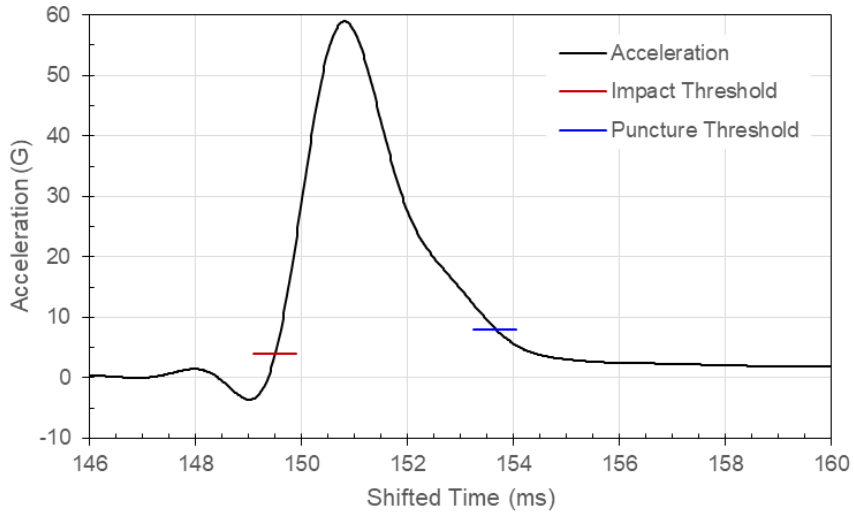

Figure 105: Carriage Acceleration, Test 59, Specimen T250-35, 1.000-Inch Flat Probe

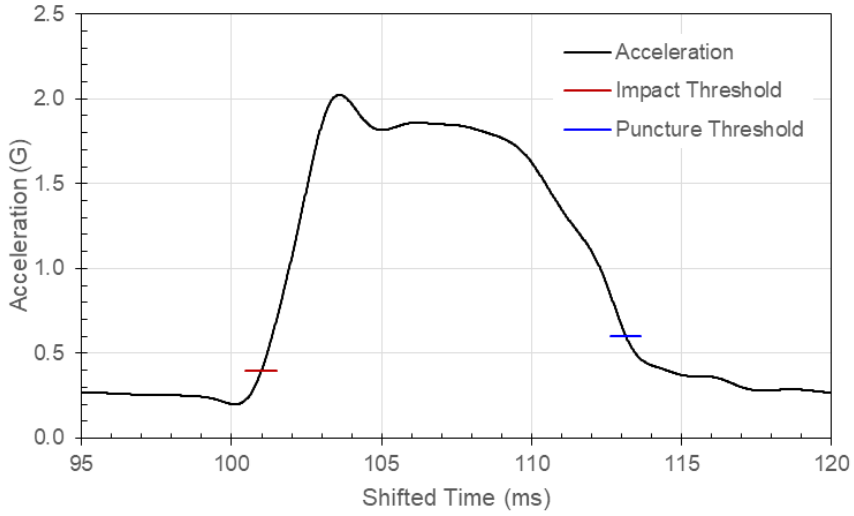

Figure 106: Carriage Acceleration, Test 61, Specimen T051-06, 0.500-Inch Semi-spherical Probe

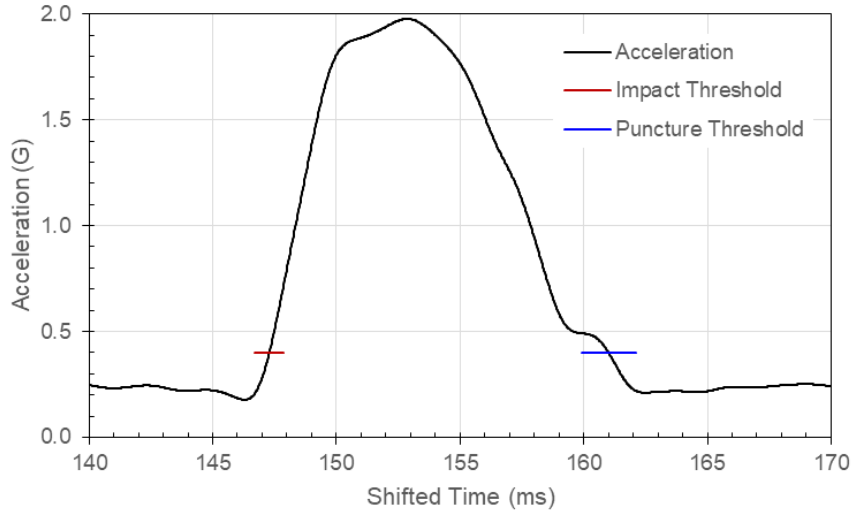

Figure 107: Carriage Acceleration, Test 62, Specimen T051-07, 0.500-Inch Semi-spherical Probe

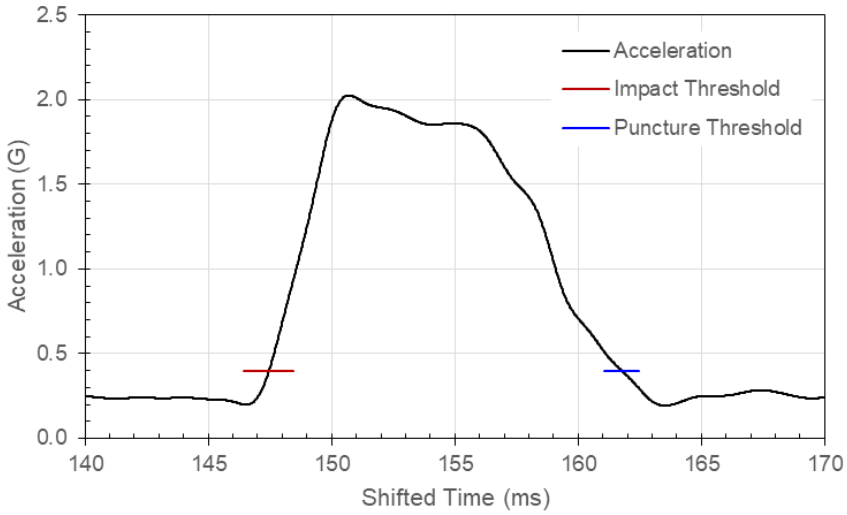

Figure 108: Carriage Acceleration, Test 63, Specimen T051-11, 0.500-Inch Semi-spherical Probe

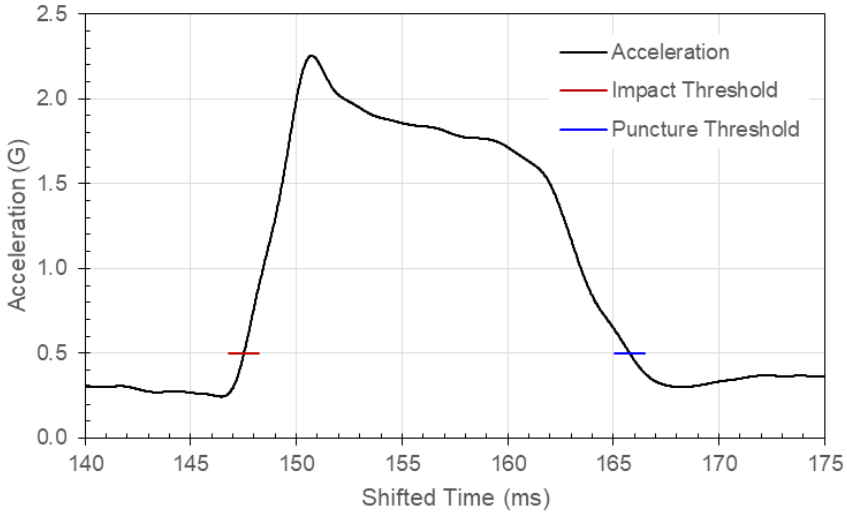

Figure 109: Carriage Acceleration, Test 64, Specimen T051-13, 0.500-Inch Semi-spherical Probe

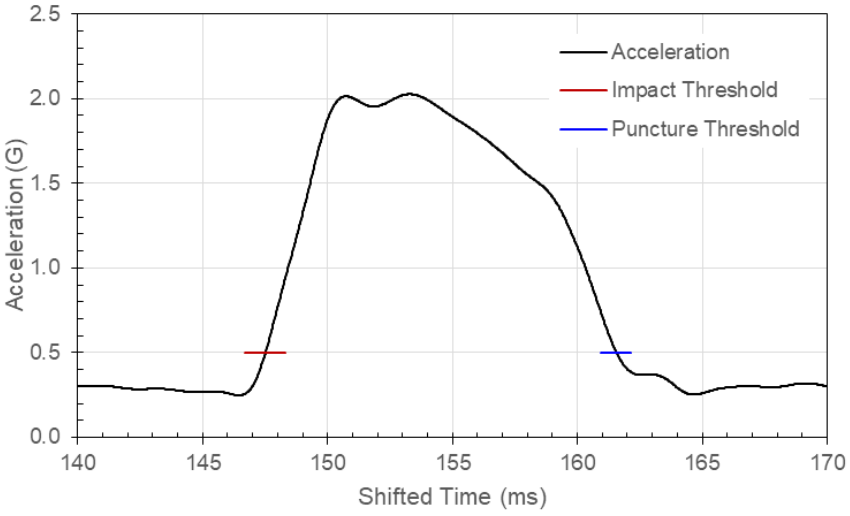

Figure 110: Carriage Acceleration, Test 65, Specimen T051-23, 0.500-Inch Semi-spherical Probe

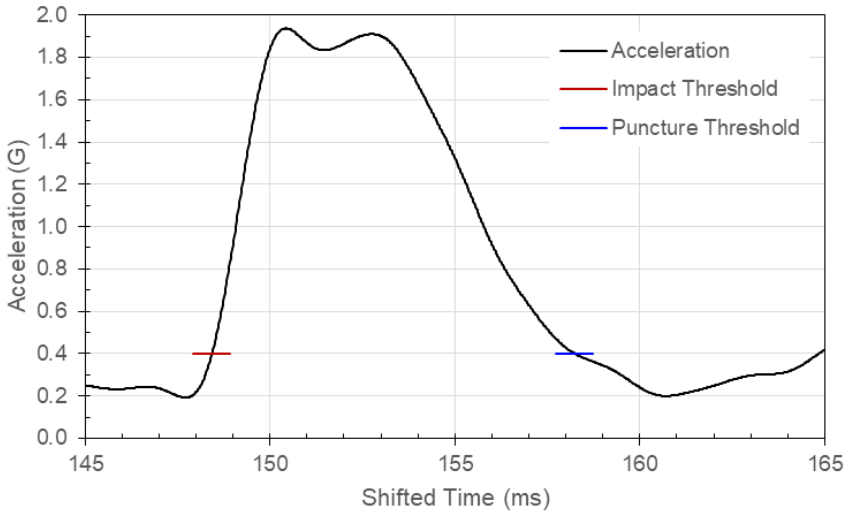

Figure 111: Carriage Acceleration, Test 60, Specimen T051-34, 0.500-Inch Semi-spherical Probe

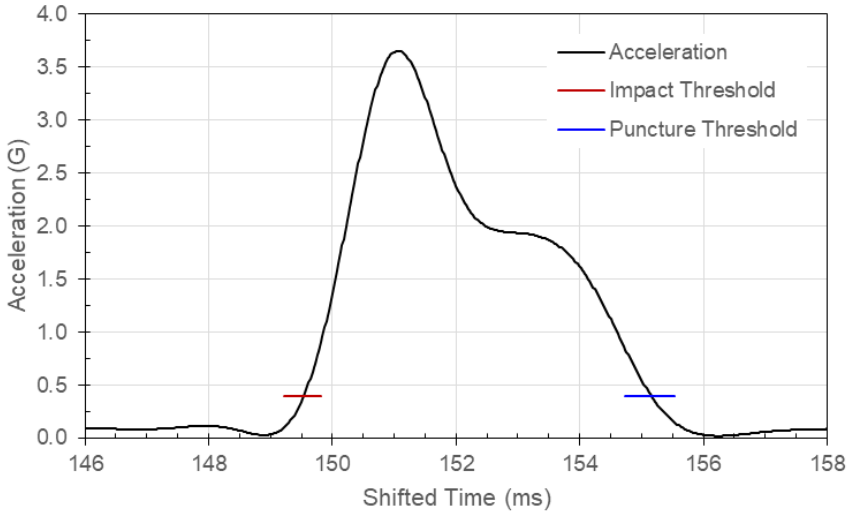

Figure 112: Carriage Acceleration, Test 76, Specimen T051-09, 1.000-Inch Semi-spherical Probe

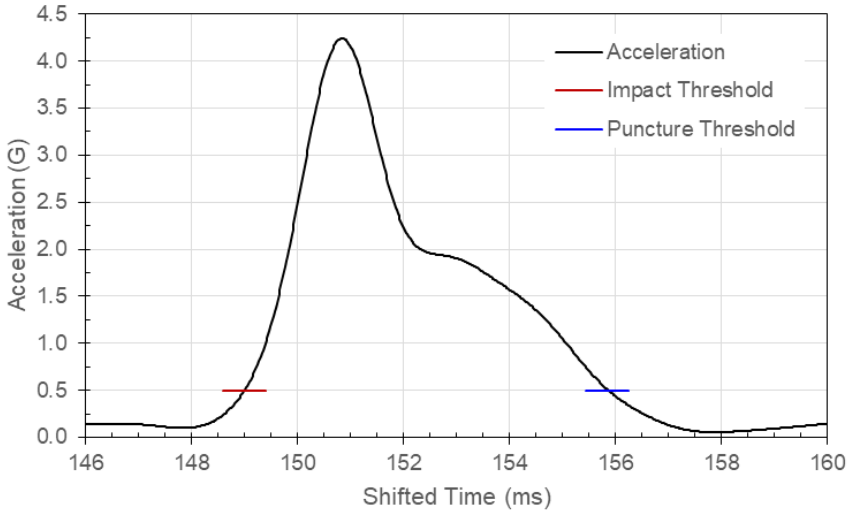

Figure 113: Carriage Acceleration, Test 77, Specimen T051-12, 1.000-Inch Semi-spherical Probe

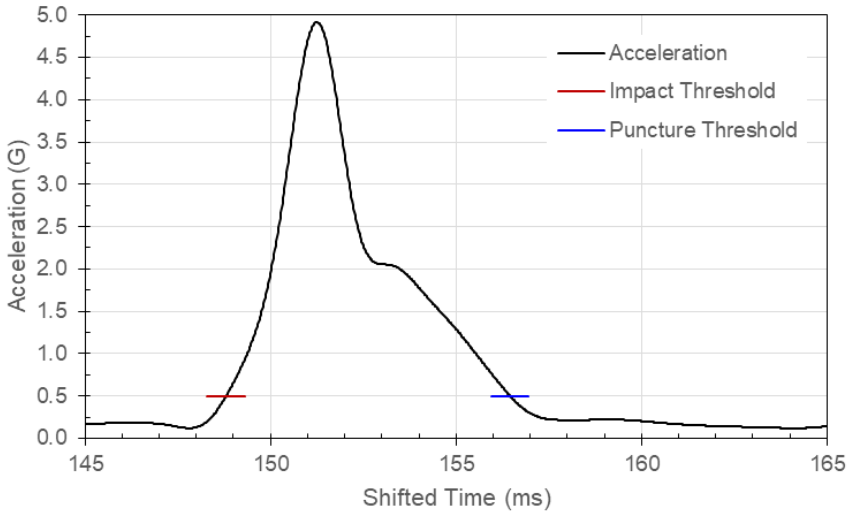

Figure 114: Carriage Acceleration, Test 78, Specimen T051-18, 1.000-Inch Semi-spherical Probe

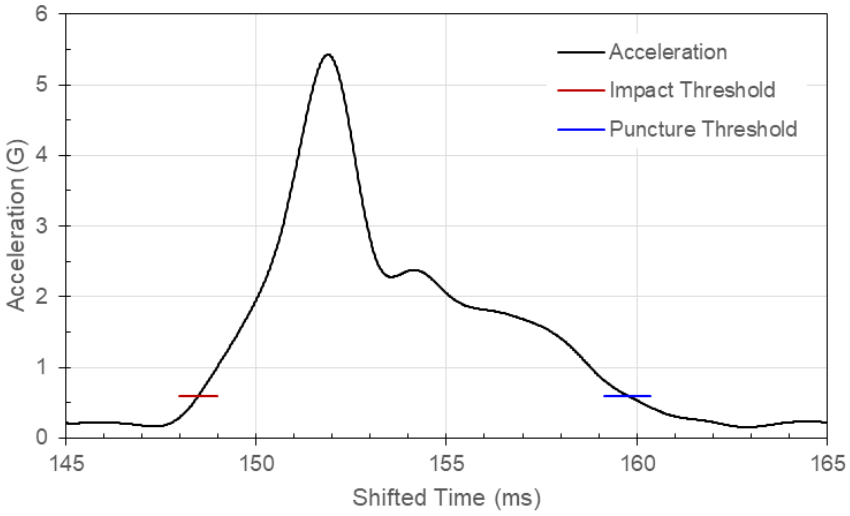

Figure 115: Carriage Acceleration, Test 79, Specimen T051-19, 1.000-Inch Semi-spherical Probe

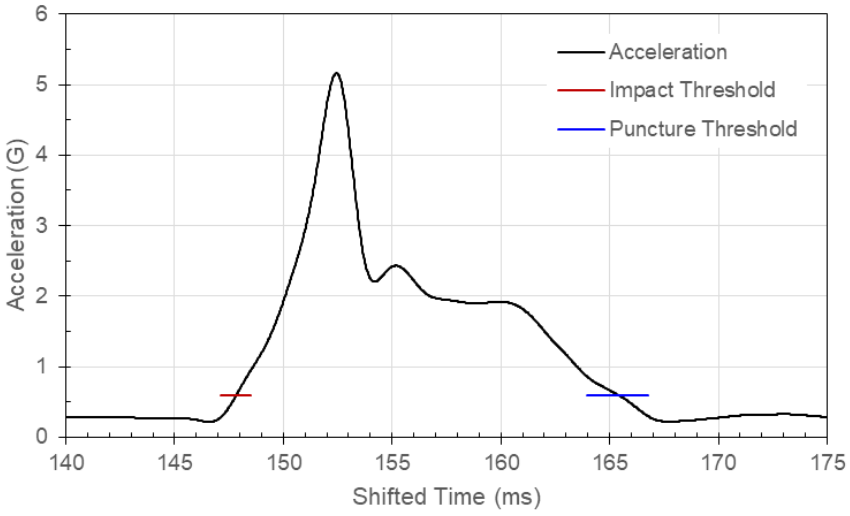

Figure 116: Carriage Acceleration, Test 80, Specimen T051-22, 1.000-Inch Semi-spherical Probe

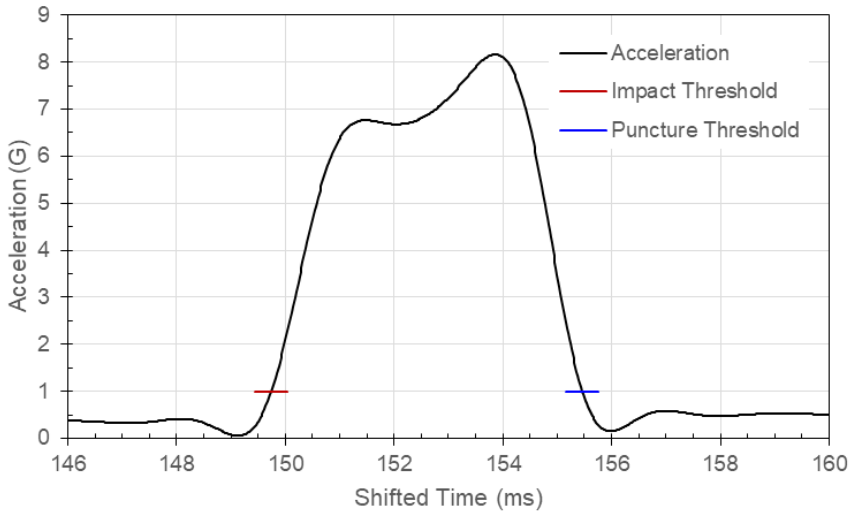

Figure 117: Carriage Acceleration, Test 66, Specimen T114-04, 0.500-Inch Semi-spherical Probe

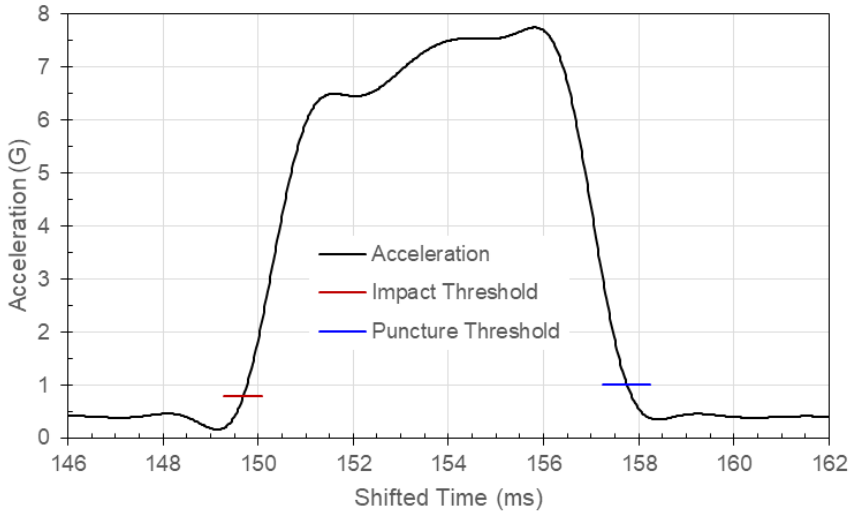

Figure 118: Carriage Acceleration, Test 67, Specimen T114-22, 0.500-Inch Semi-spherical Probe

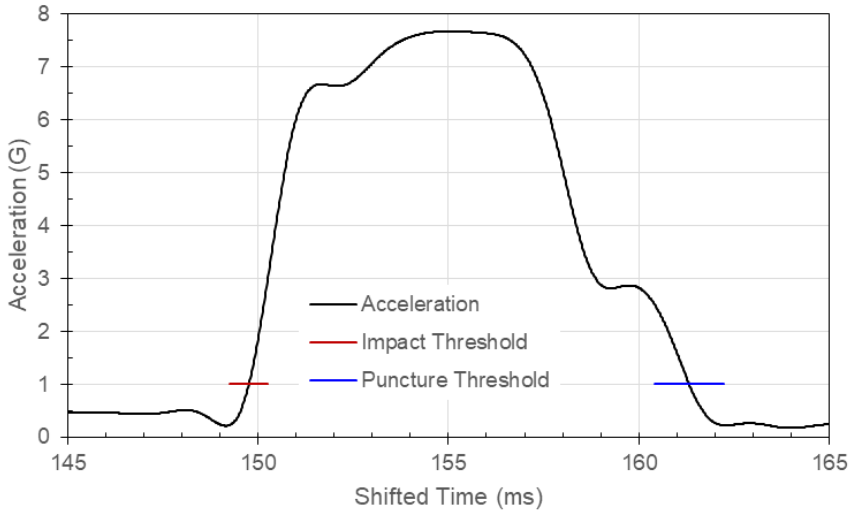

Figure 119: Carriage Acceleration, Test 68, Specimen T114-25, 0.500-Inch Semi-spherical Probe

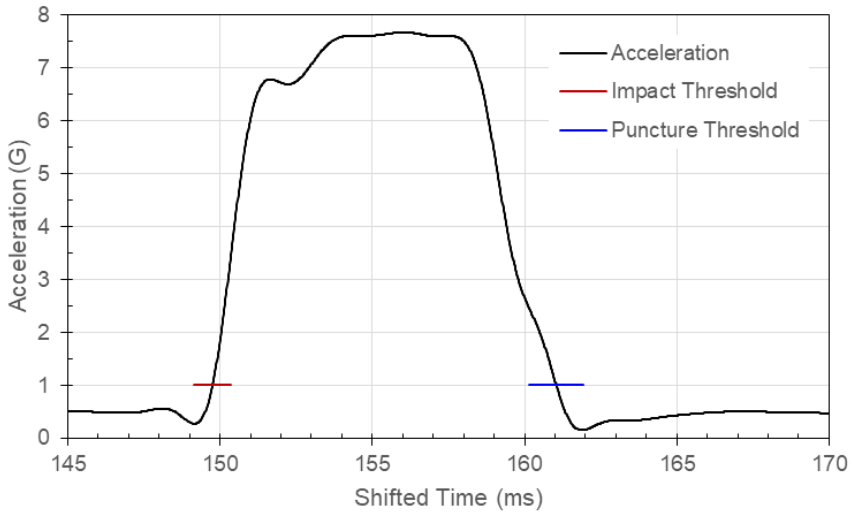

Figure 120: Carriage Acceleration, Test 69, Specimen T114-33, 0.500-Inch Semi-spherical Probe

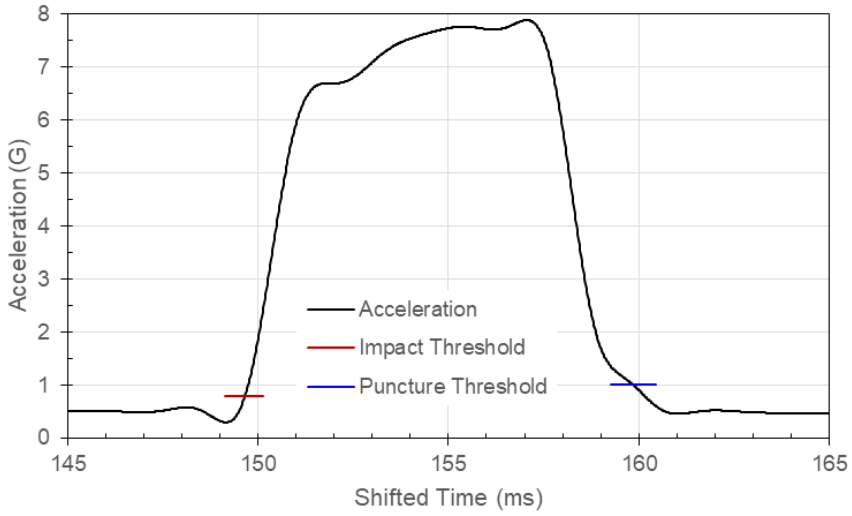

Figure 121: Carriage Acceleration, Test 70, Specimen T114-35, 0.500-Inch Semi-spherical Probe

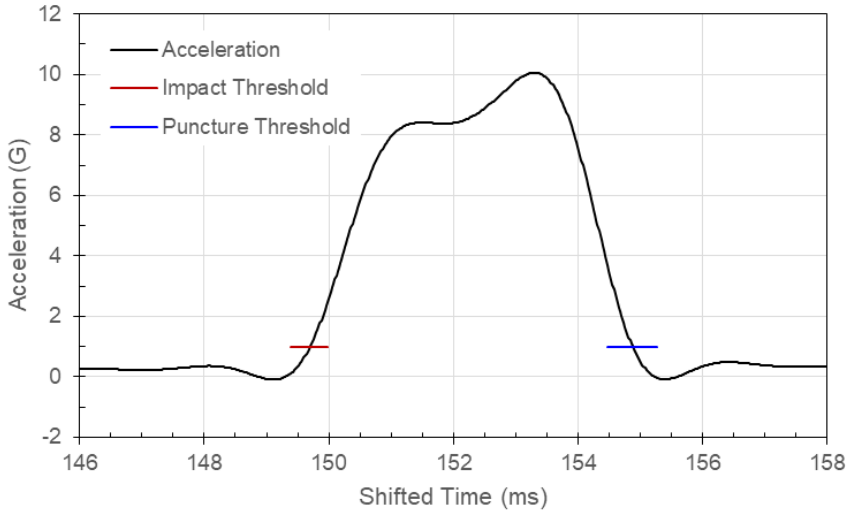

Figure 122: Carriage Acceleration, Test 81, Specimen T114-06, 1.000-Inch Semi-spherical Probe

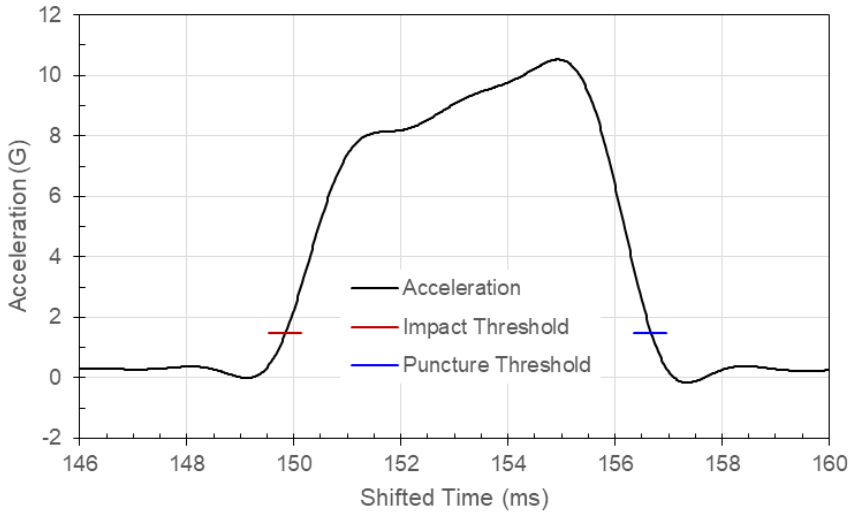

Figure 123: Carriage Acceleration, Test 82, Specimen T114-15, 1.000-Inch Semi-spherical Probe

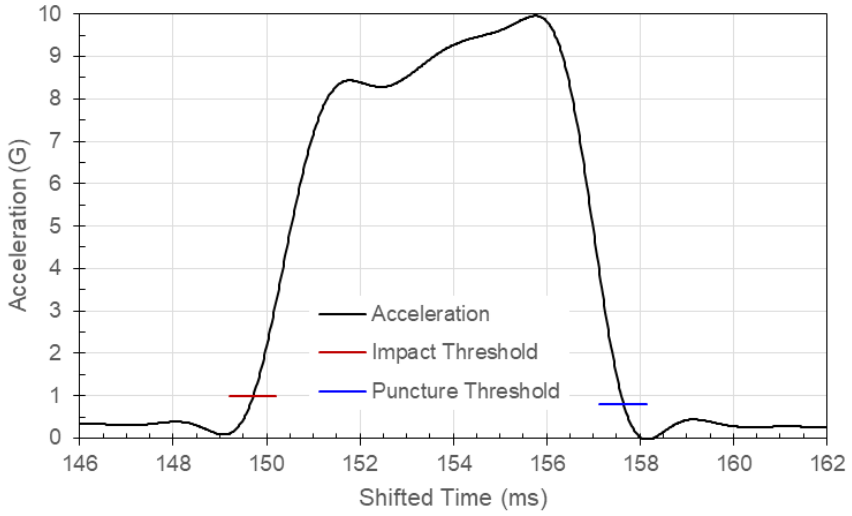

Figure 124: Carriage Acceleration, Test 83, Specimen T114-28, 1.000-Inch Semi-spherical Probe

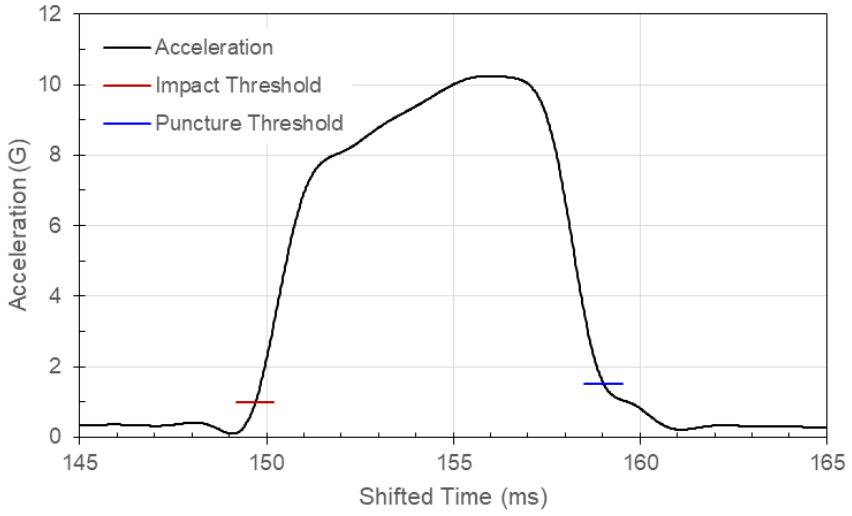

Figure 125: Carriage Acceleration, Test 84, Specimen T114-31, 1.000-Inch Semi-spherical Probe

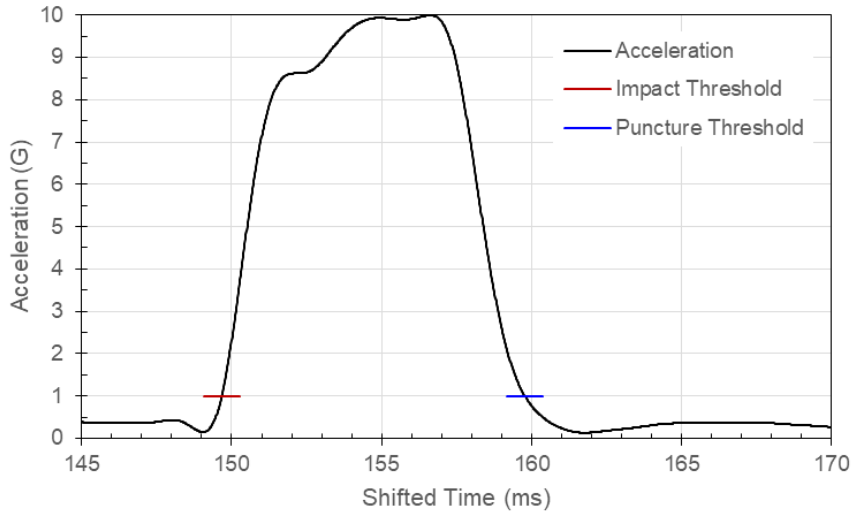

Figure 126: Carriage Acceleration, Test 85, Specimen T114-32, 1.000-Inch Semi-spherical Probe

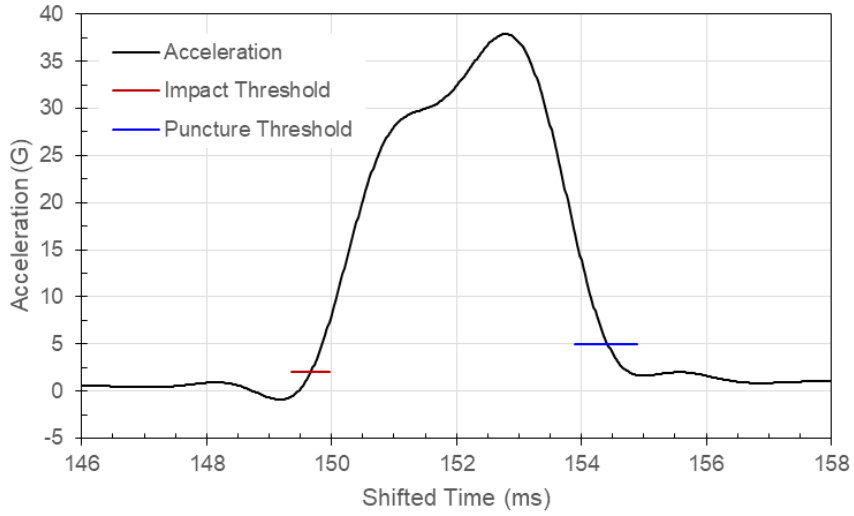

Figure 127: Carriage Acceleration, Test 71, Specimen T250-05, 0.500-Inch Semi-spherical Probe

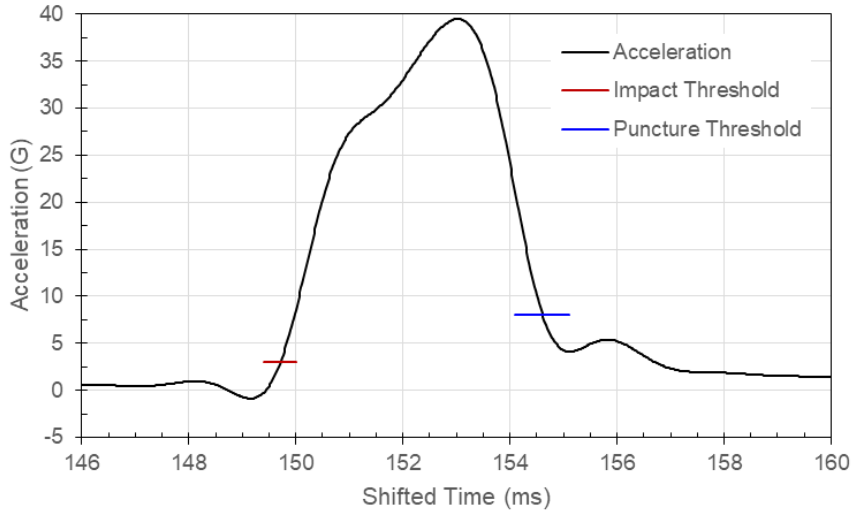

Figure 128: Carriage Acceleration, Test 72, Specimen T250-14, 0.500-Inch Semi-spherical Probe

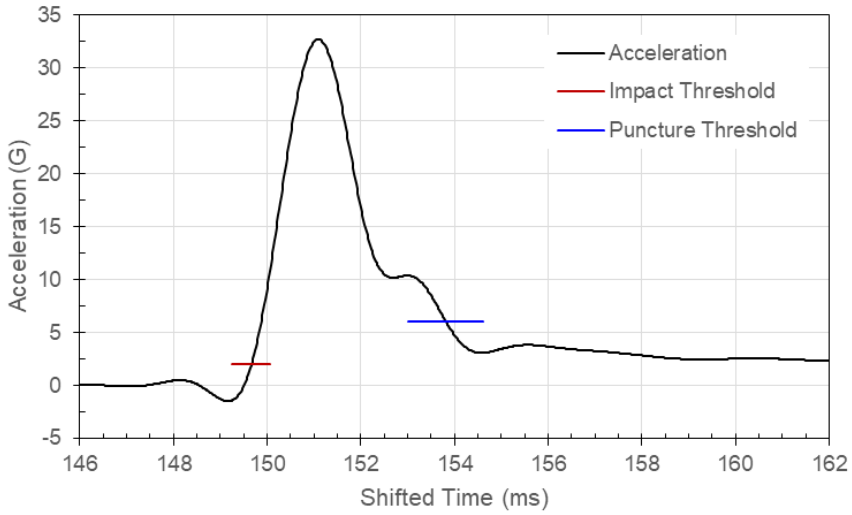

Figure 129: Carriage Acceleration, Test 73, Specimen T250-22, 0.500-Inch Semi-spherical Probe

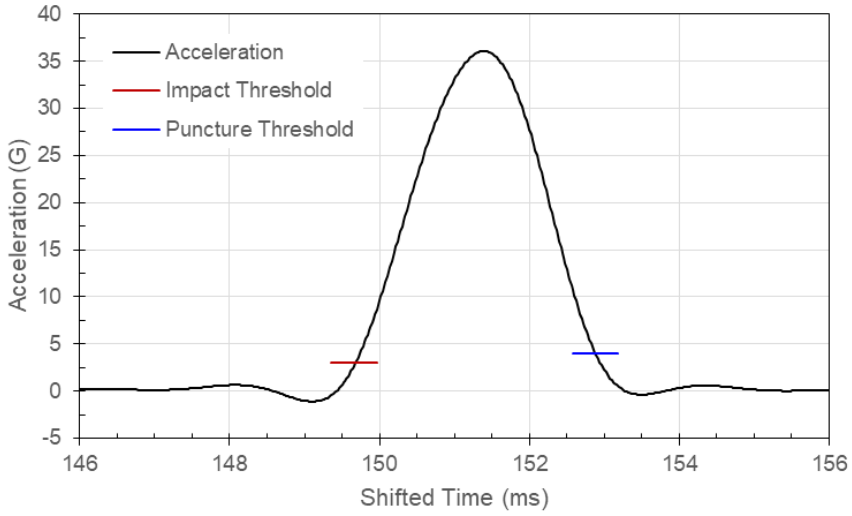

Figure 130: Carriage Acceleration, Test 74, Specimen T250-32, 0.500-Inch Semi-spherical Probe

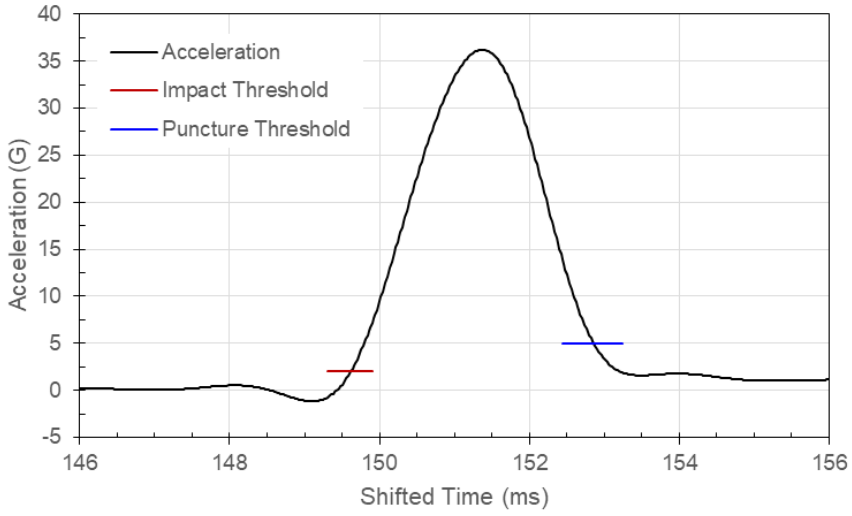

Figure 131: Carriage Acceleration, Test 75, Specimen T250-33, 0.500-Inch Semi-spherical Probe

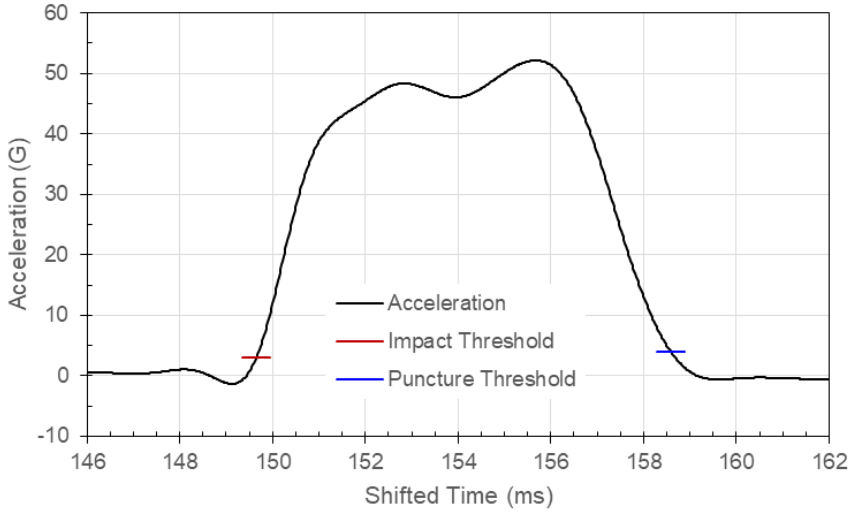

Figure 132: Carriage Acceleration, Test 87, Specimen T250-13, 1.000-Inch Semi-spherical Probe

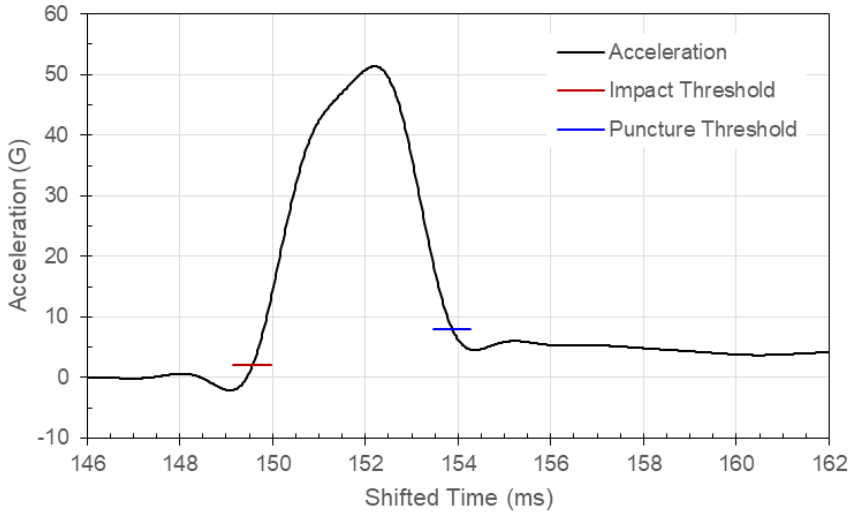

Figure 133: Carriage Acceleration, Test 89, Specimen T250-20, 1.000-Inch Semi-spherical Probe

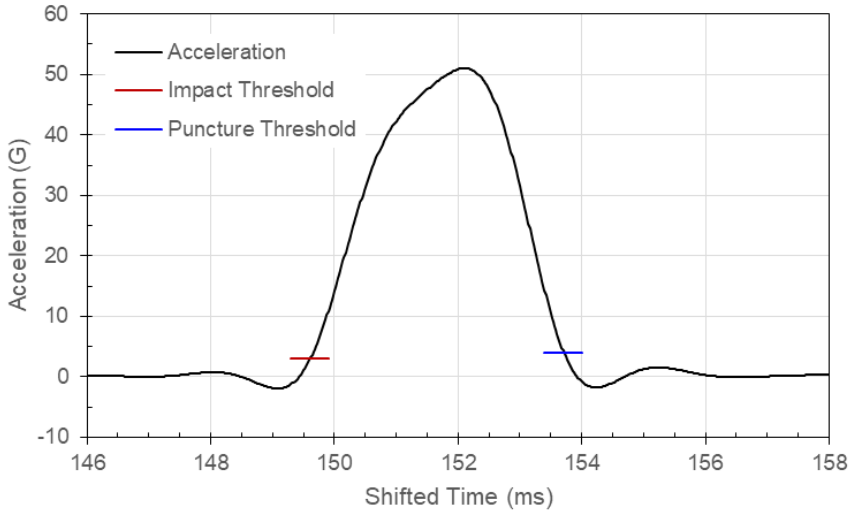

Figure 134: Carriage Acceleration, Test 90, Specimen T250-21, 1.000-Inch Semi-spherical Probe

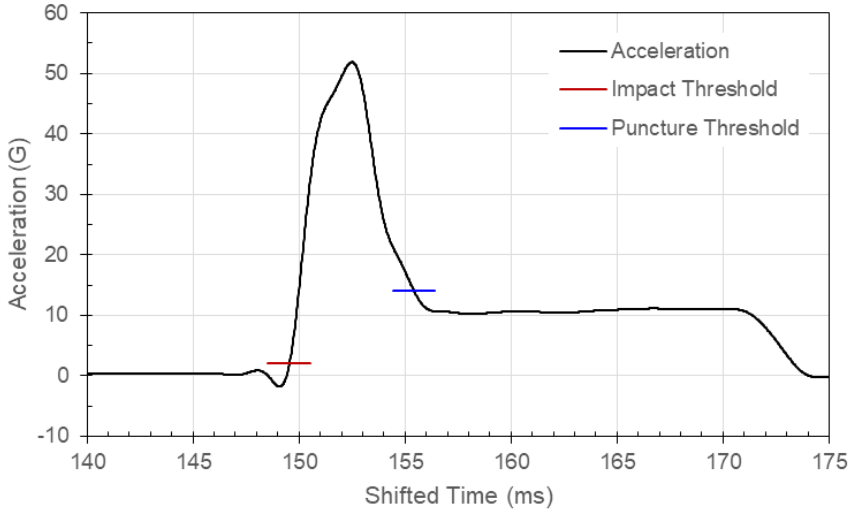

Figure 135: Carriage Acceleration, Test 91, Specimen T250-27, 1.000-Inch Semi-spherical Probe

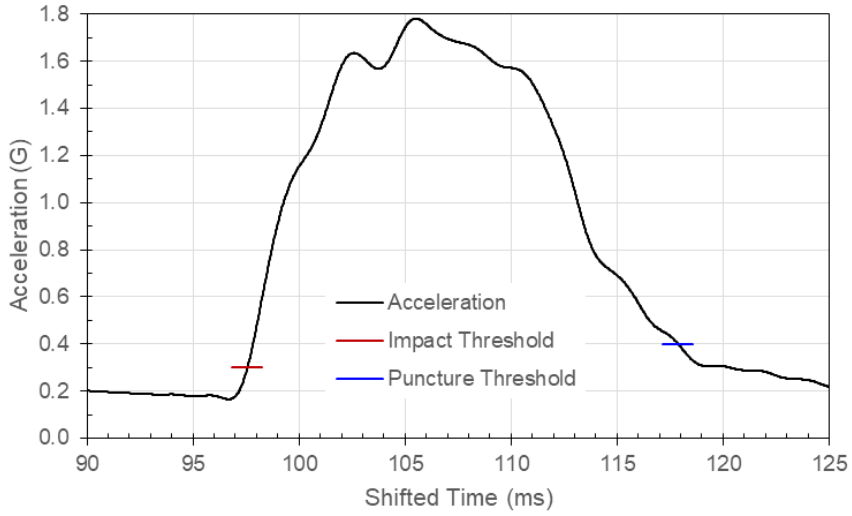

Figure 136: Carriage Acceleration, Test 103, Specimen T051-01, 0.500-Inch Tri-corner Probe

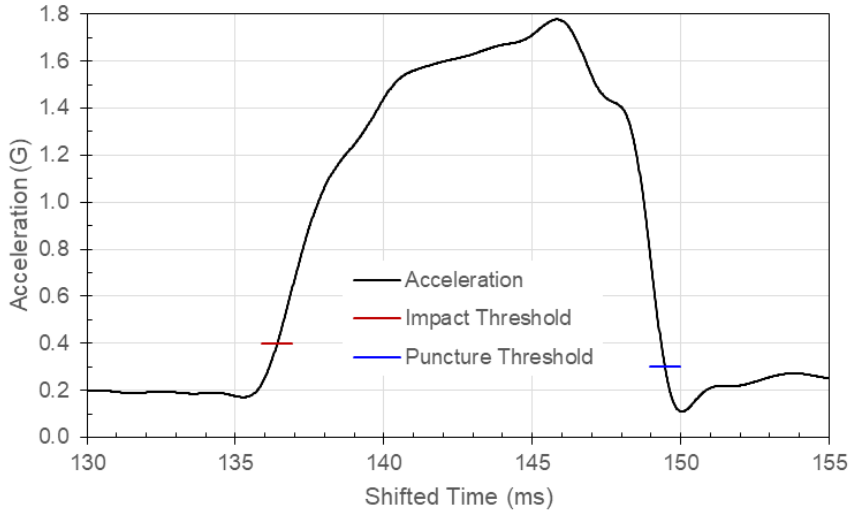

Figure 137: Carriage Acceleration, Test 104, Specimen T051-02, 0.500-Inch Tri-corner Probe

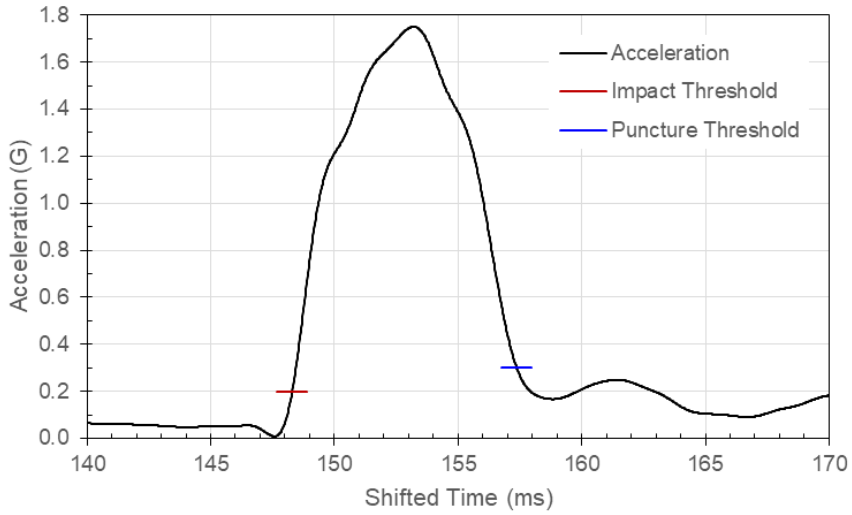

Figure 138: Carriage Acceleration, Test 4, Specimen T051-31, 0.500-Inch Tri-corner Probe

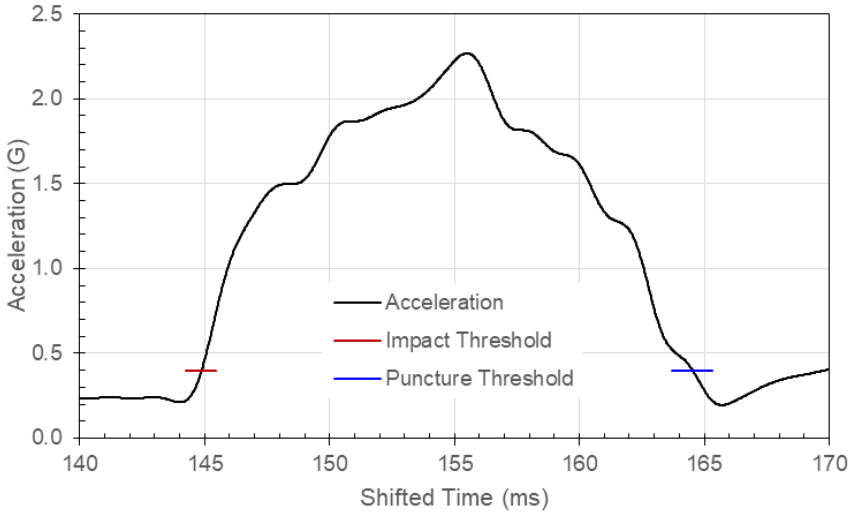

Figure 139: Carriage Acceleration, Test 105, Specimen T051-05, 1.000-Inch Tri-corner Probe

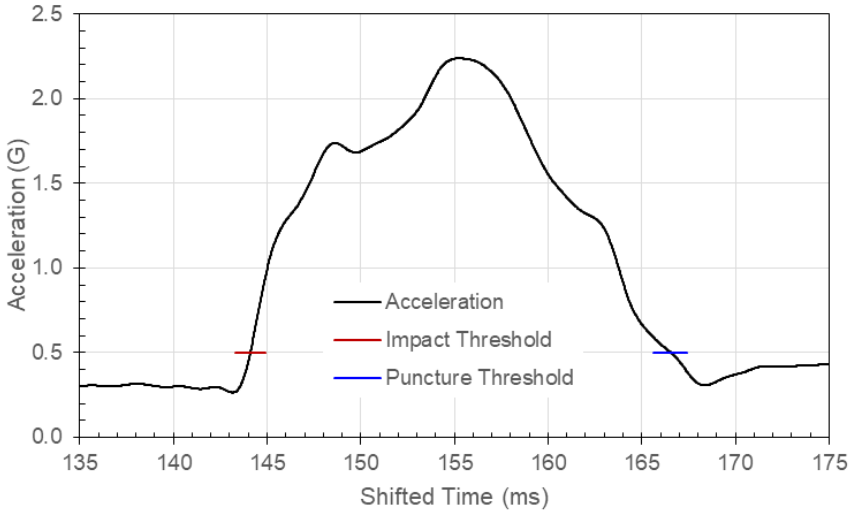

Figure 140: Carriage Acceleration, Test 106, Specimen T051-25, 1.000-Inch Tri-corner Probe

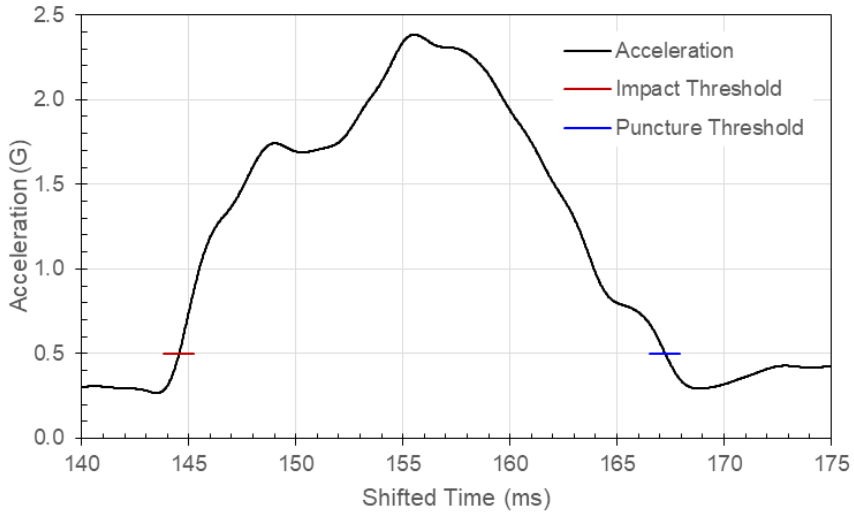

Figure 141: Carriage Acceleration, Test 107, Specimen T051-33, 1.000-Inch Tri-corner Probe

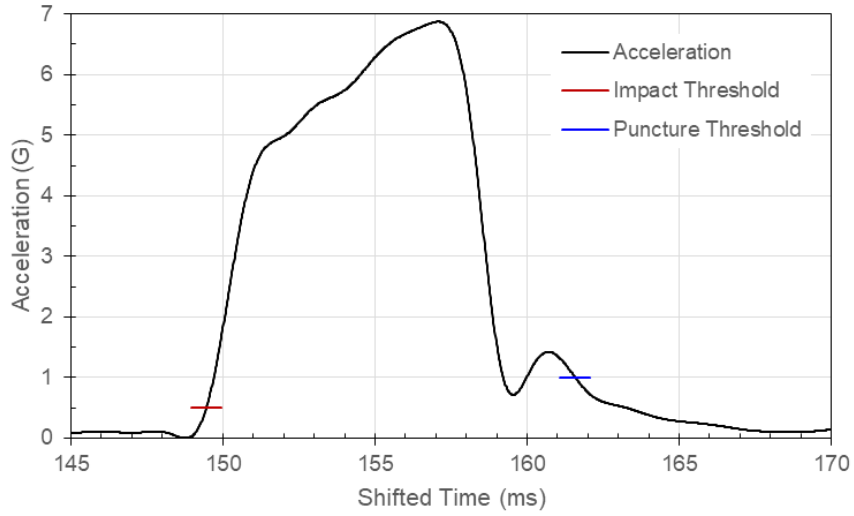

Figure 142: Carriage Acceleration, Test 92, Specimen T114-03, 0.500-Inch Tri-corner Probe

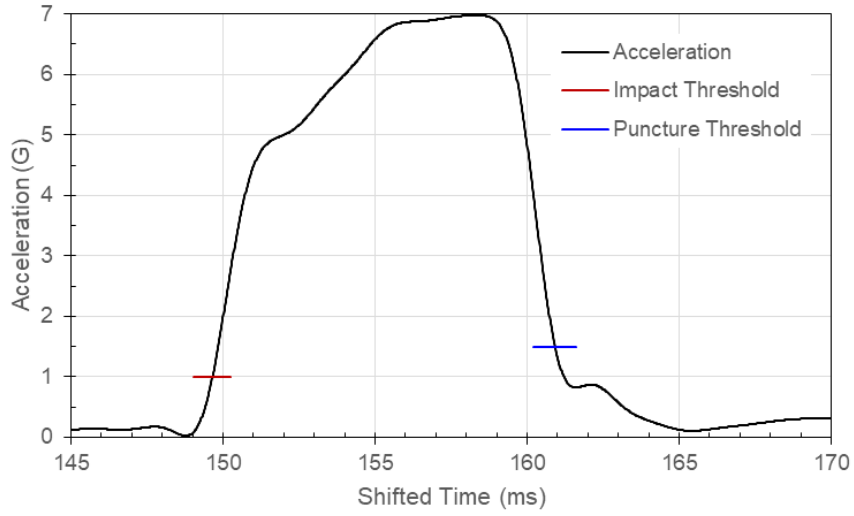

Figure 143: Carriage Acceleration, Test 93, Specimen T114-12, 0.500-Inch Tri-corner Probe

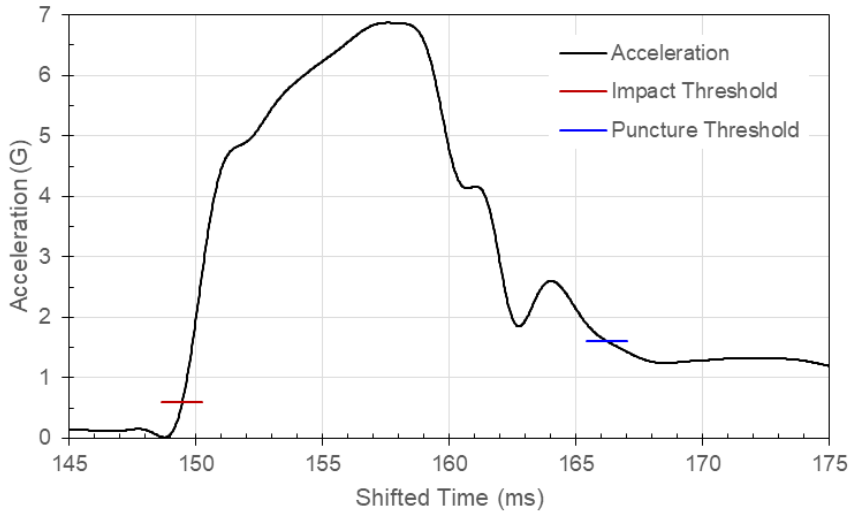

Figure 144: Carriage Acceleration, Test 94, Specimen T114-19, 0.500-Inch Tri-corner Probe

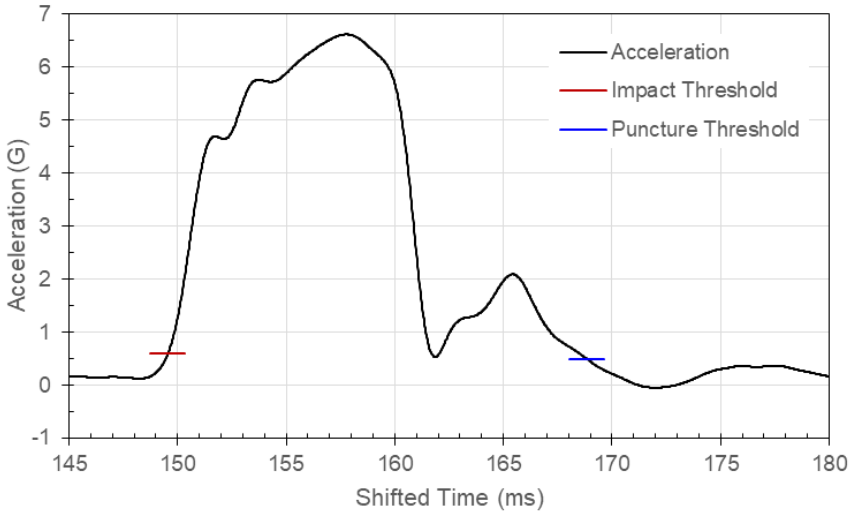

Figure 145: Carriage Acceleration, Test 95, Specimen T114-20, 0.500-Inch Tri-corner Probe

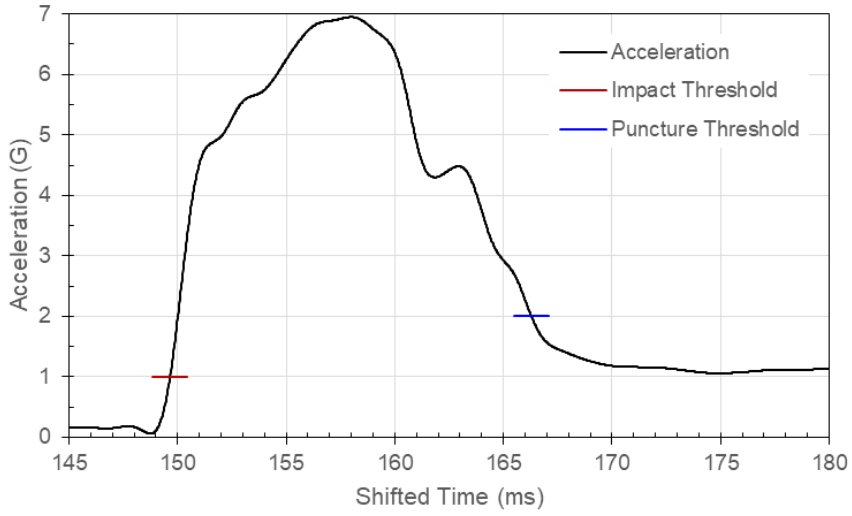

Figure 146: Carriage Acceleration, Test 96, Specimen T114-34, 0.500-Inch Tri-corner Probe

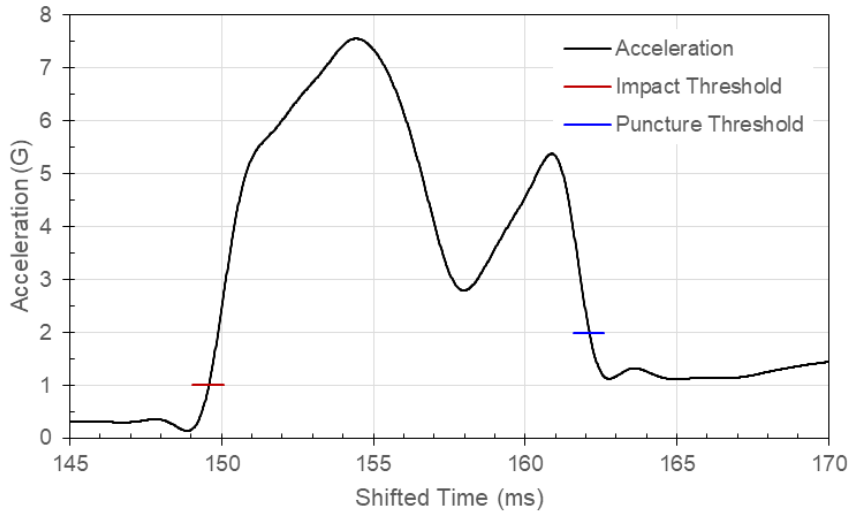

Figure 147: Carriage Acceleration, Test 108, Specimen T114-01, 1.000-Inch Tri-corner Probe

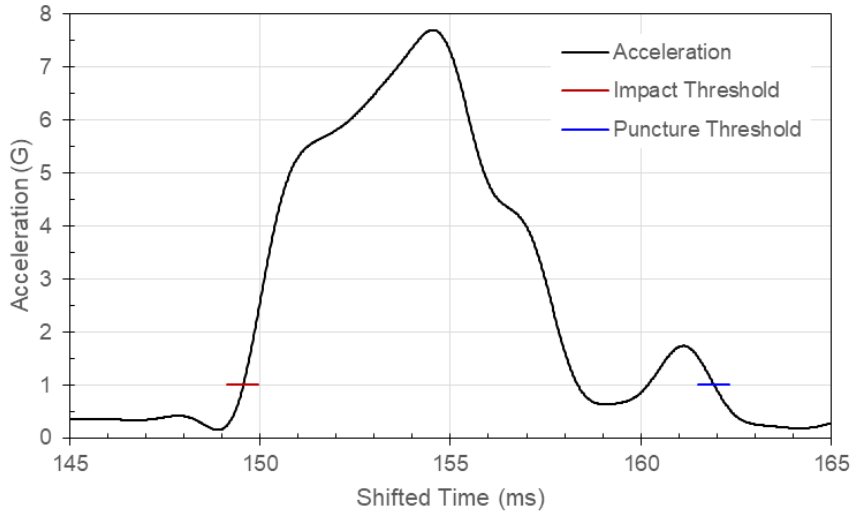

Figure 148: Carriage Acceleration, Test 109, Specimen T114-02, 1.000-Inch Tri-corner Probe

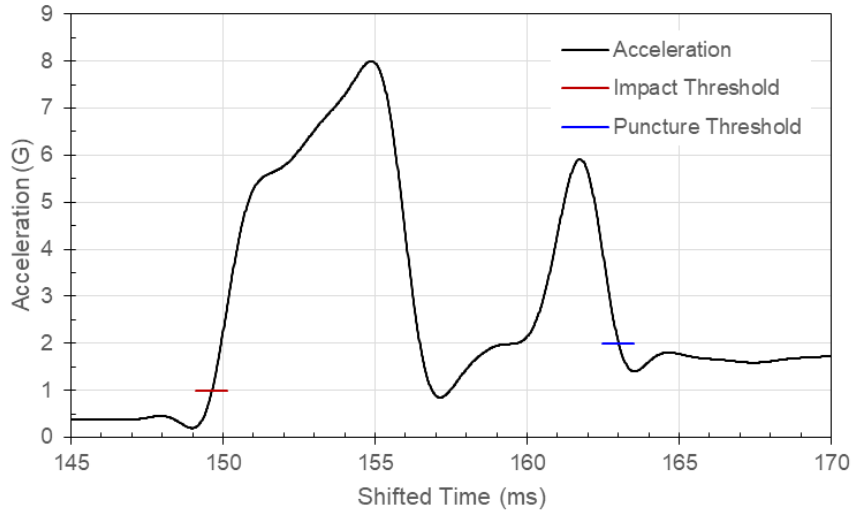

Figure 149: Carriage Acceleration, Test 110, Specimen T114-10, 1.000-Inch Tri-corner Probe

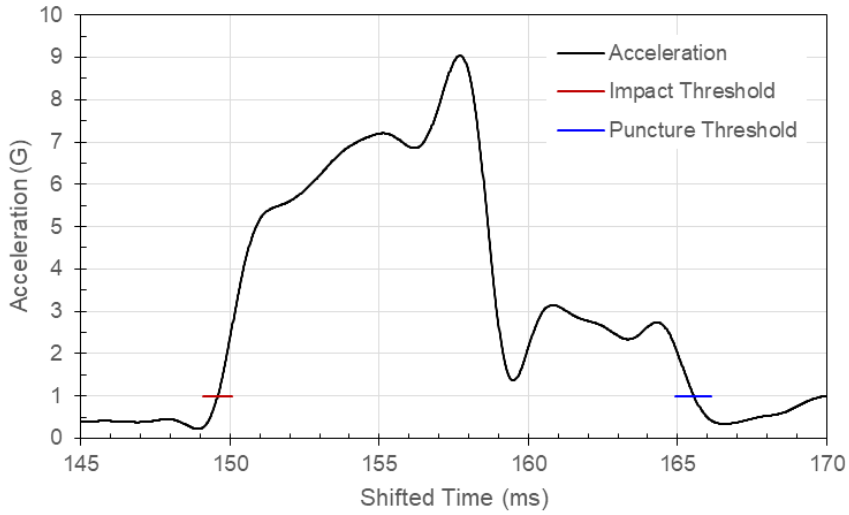

Figure 150: Carriage Acceleration, Test 111, Specimen T114-11, 1.000-Inch Tri-corner Probe

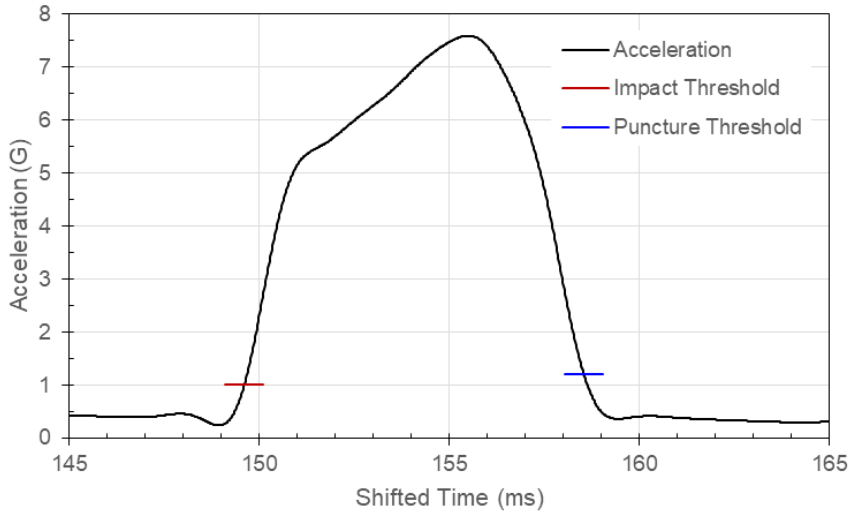

Figure 151: Carriage Acceleration, Test 112, Specimen T114-26, 1.000-Inch Tri-corner Probe

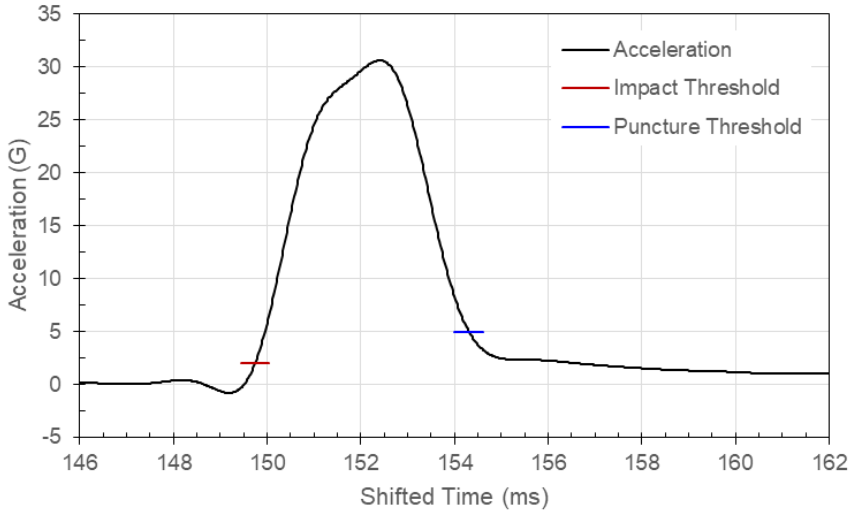

Figure 152: Carriage Acceleration, Test 98, Specimen T250-01, 0.500-Inch Tri-corner Probe

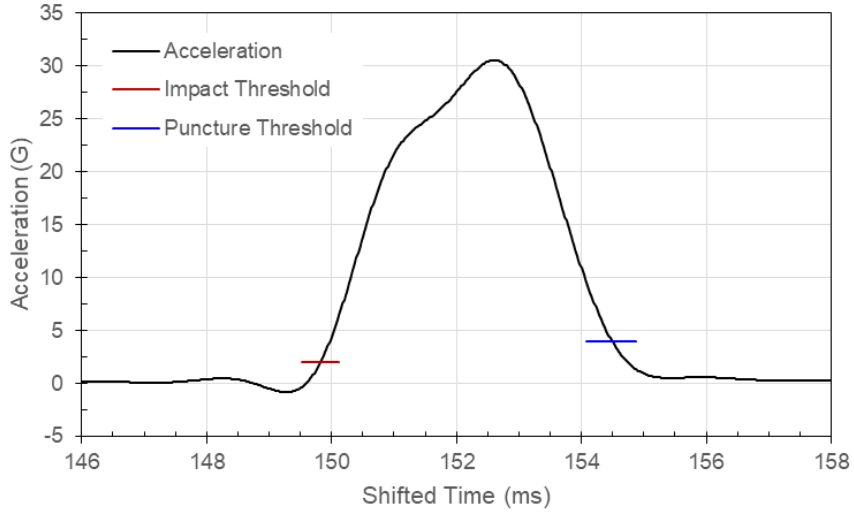

Figure 153: Carriage Acceleration, Test 99, Specimen T250-10, 0.500-Inch Tri-corner Probe

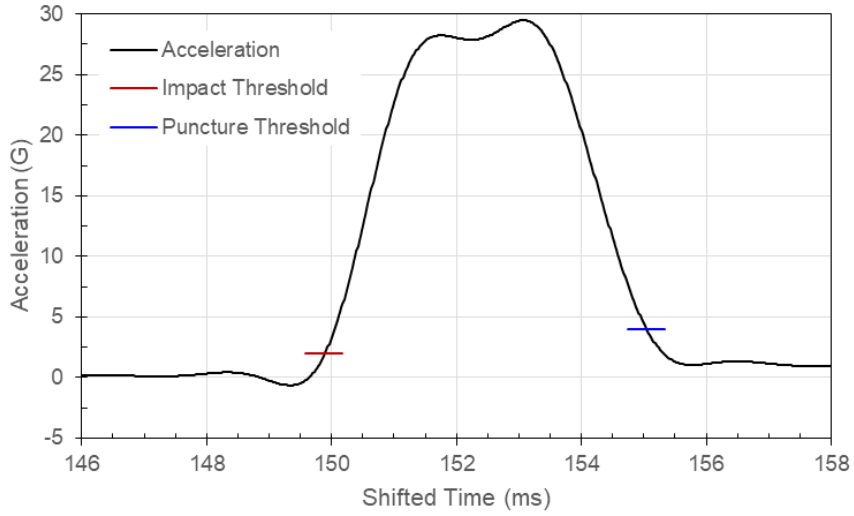

Figure 154: Carriage Acceleration, Test 100, Specimen T250-19, 0.500-Inch Tri-corner Probe

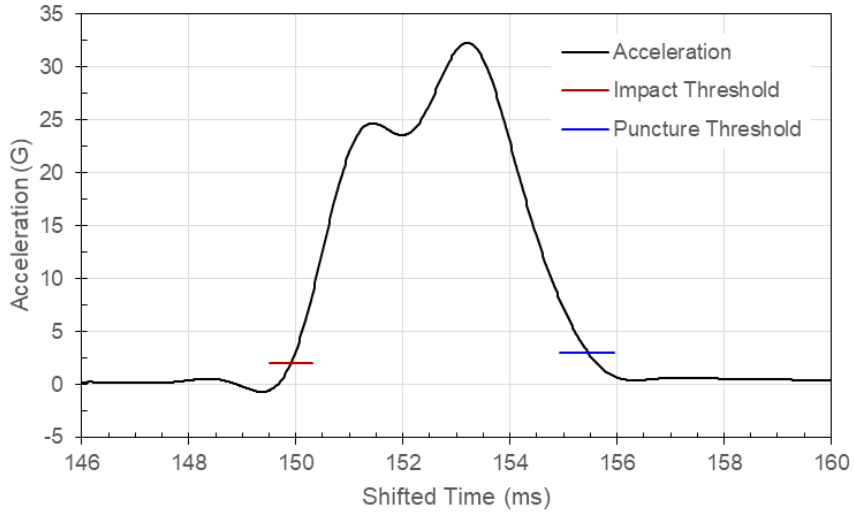

Figure 155: Carriage Acceleration, Test 101, Specimen T250-25, 0.500-Inch Tri-corner Probe

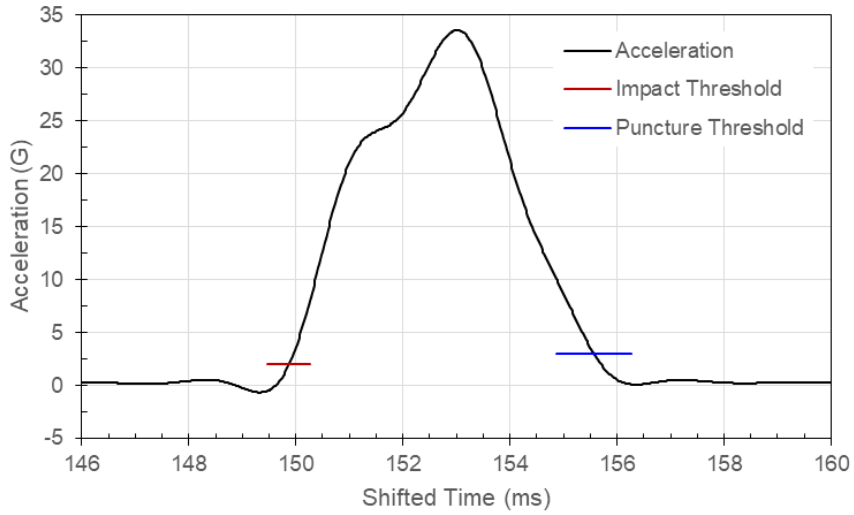

Figure 156: Carriage Acceleration, Test 102, Specimen T250-31, 0.500-Inch Tri-corner Probe

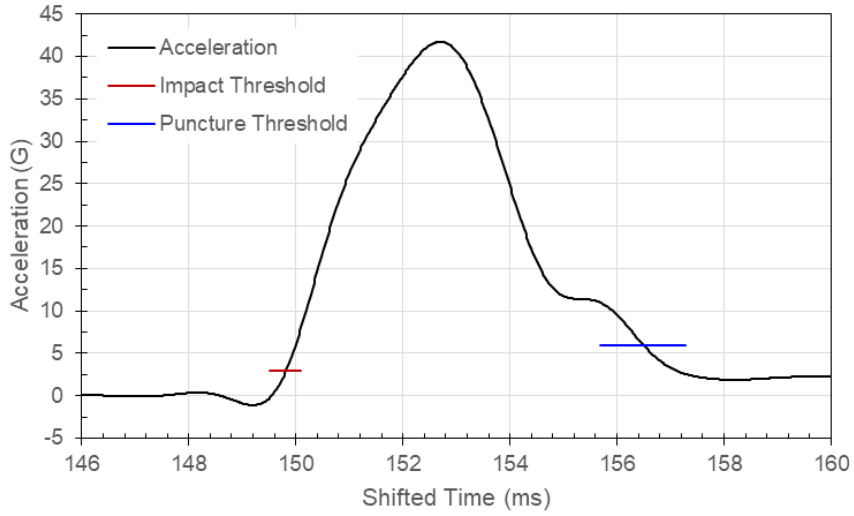

Figure 157: Carriage Acceleration, Test 113, Specimen T250-02, 1.000-Inch Tri-corner Probe

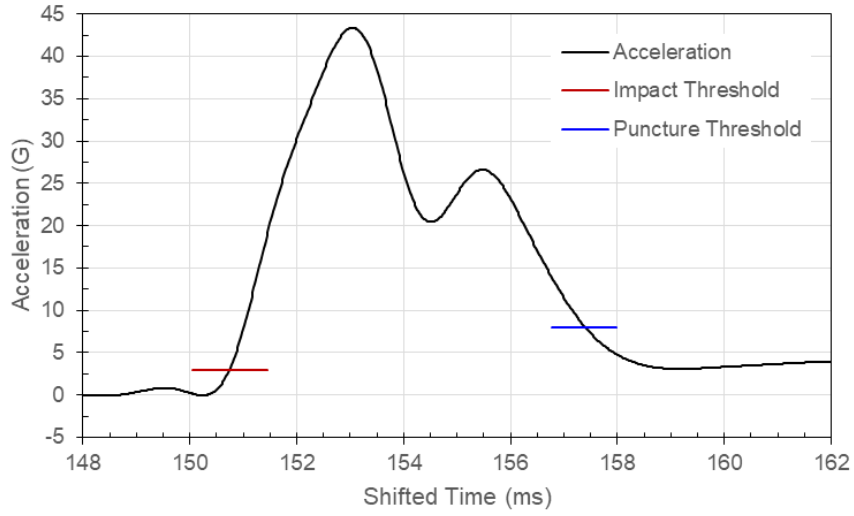

Figure 158: Carriage Acceleration, Test 114, Specimen T250-03, 1.000-Inch Tri-corner Probe

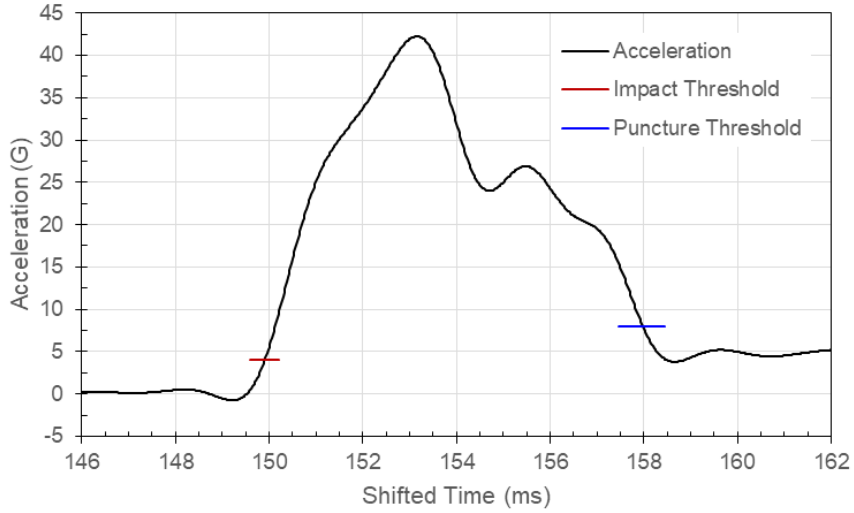

Figure 159: Carriage Acceleration, Test 115, Specimen T250-11, 1.000-Inch Tri-corner Probe

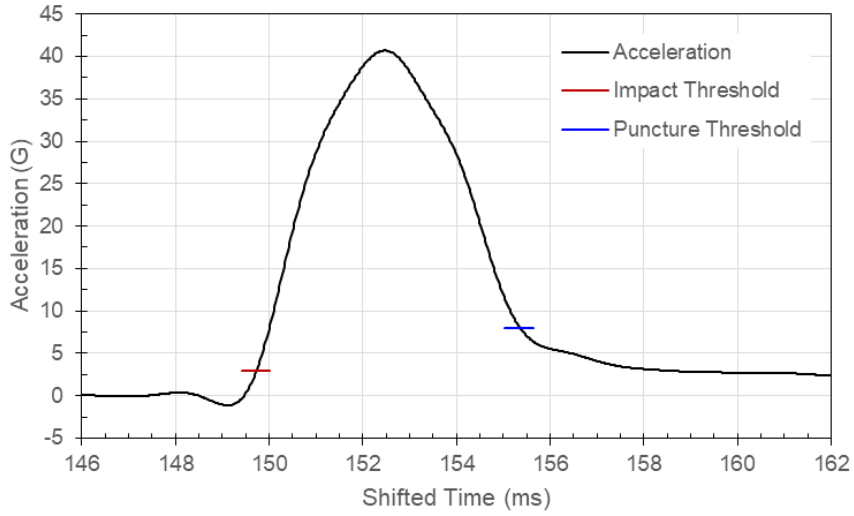

Figure 160: Carriage Acceleration, Test 116, Specimen T250-12, 1.000-Inch Tri-corner Probe

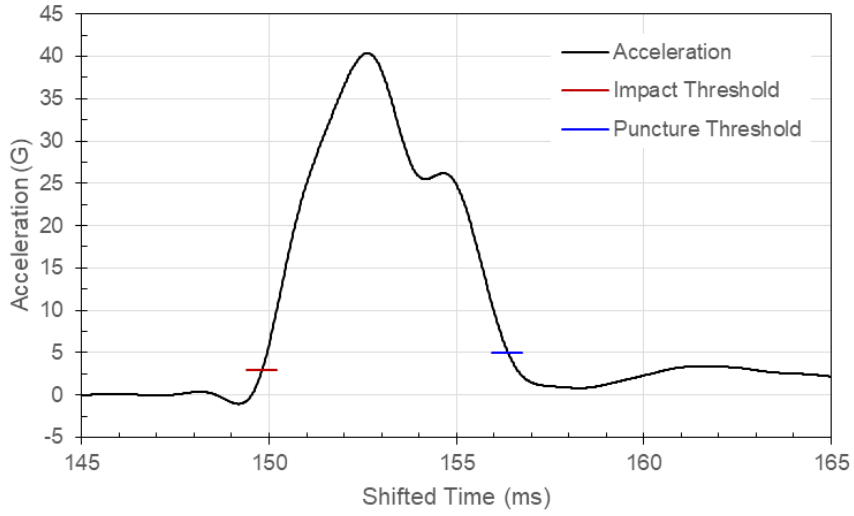

Figure 161: Carriage Acceleration, Test 117, Specimen T250-26, 1.000-Inch Tri-corner Probe

Appendix B: Total Energy

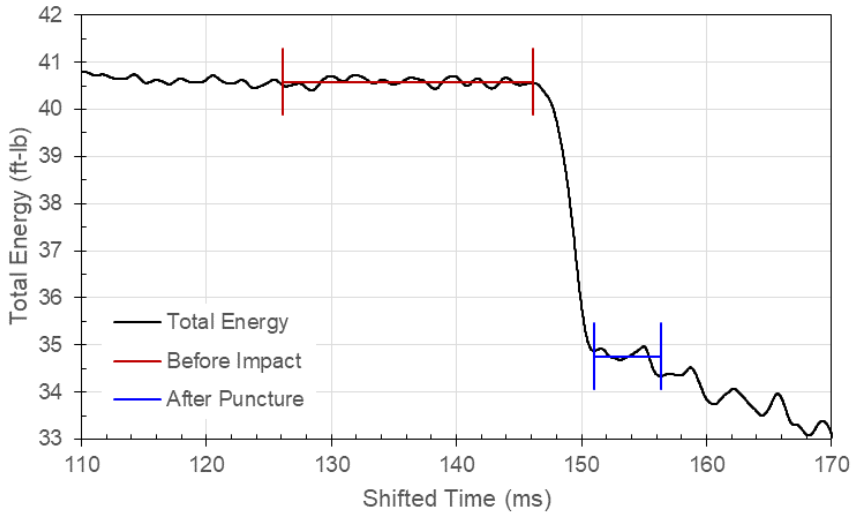

Figure 162: Total Energy, Test 11, Specimen T051-24, 0.250-Inch Flat Probe

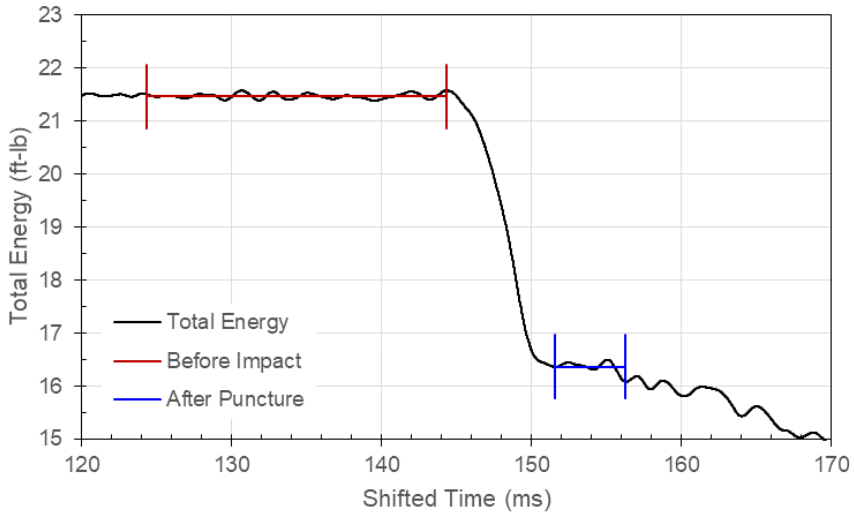

Figure 163: Total Energy, Test 12, Specimen T051-26, 0.250-Inch Flat Probe

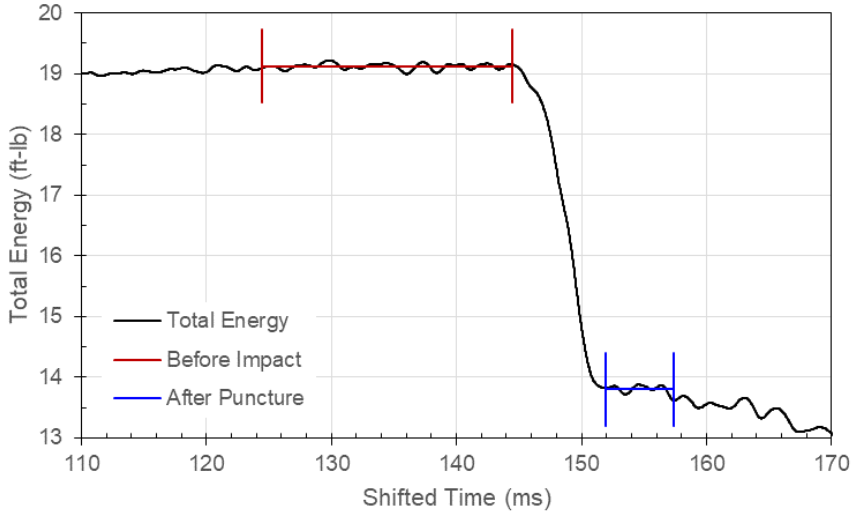

Figure 164: Total Energy, Test 16, Specimen T051-28, 0.250-Inch Flat Probe

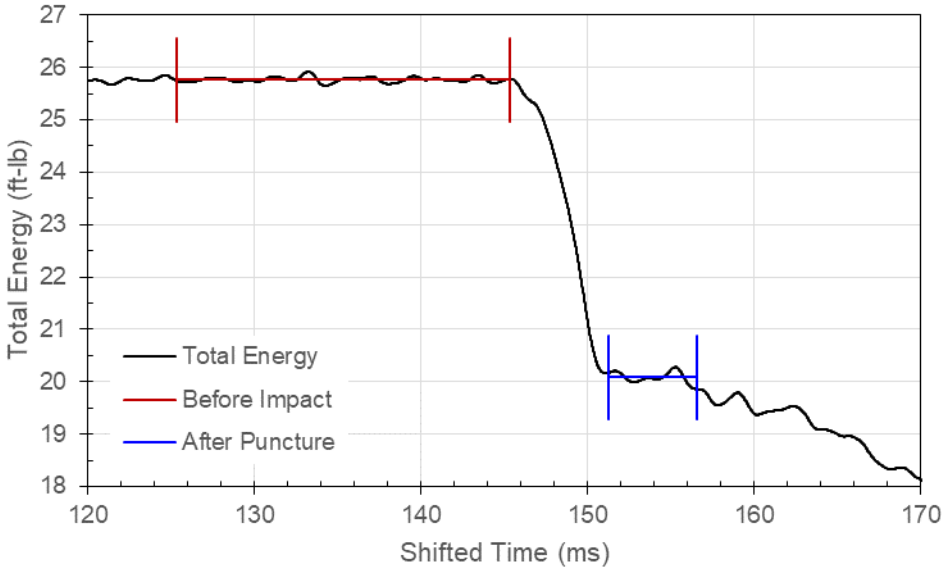

Figure 165: Total Energy, Test 17, Specimen T051-29, 0.250-Inch Flat Probe

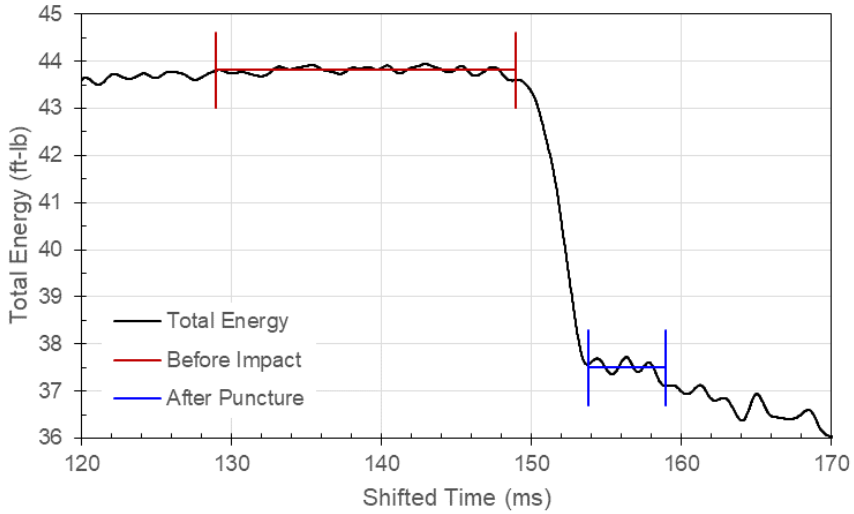

Figure 166: Total Energy, Test 6, Specimen T051-30, 0.250-Inch Flat Probe

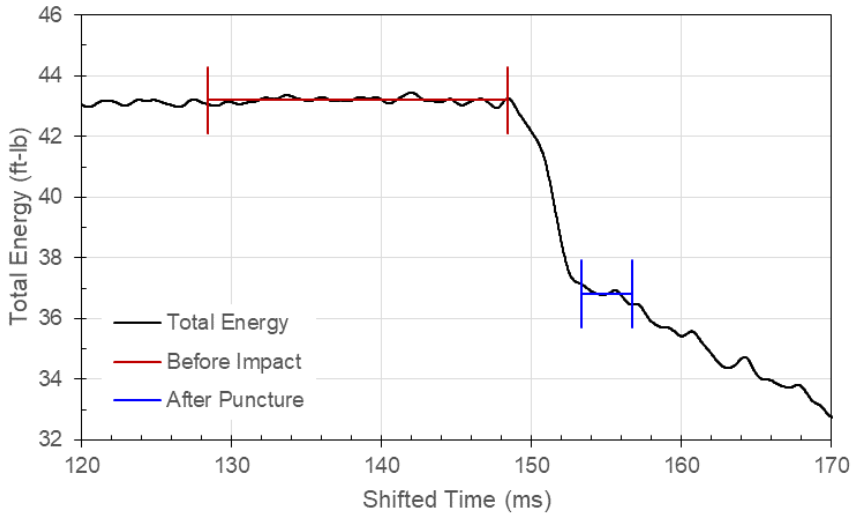

Figure 167: Total Energy, Test 5, Specimen T051-32, 0.250-Inch Flat Probe

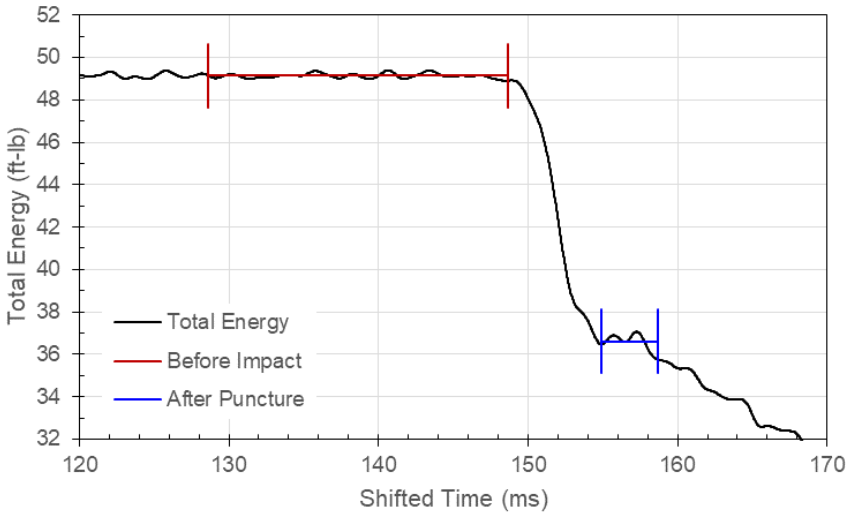

Figure 168: Total Energy, Test 28, Specimen T051-03, 0.500-Inch Flat Probe

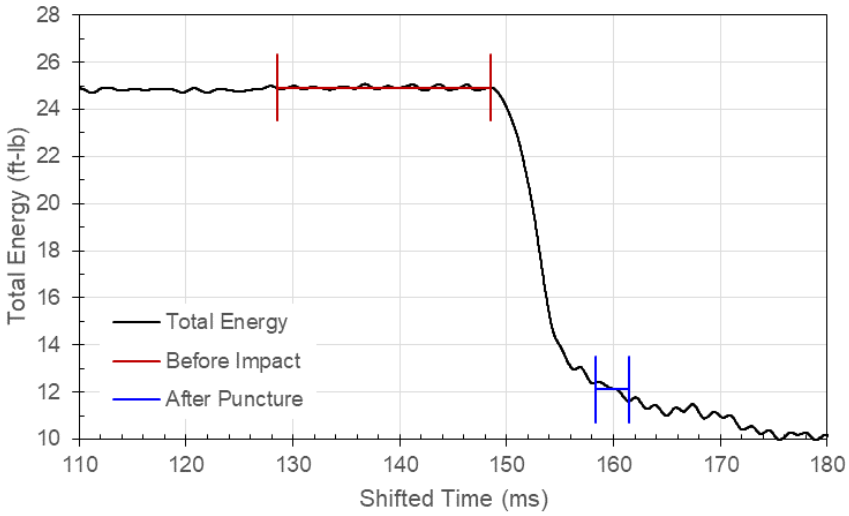

Figure 169: Total Energy, Test 29, Specimen T051-08, 0.500-Inch Flat Probe

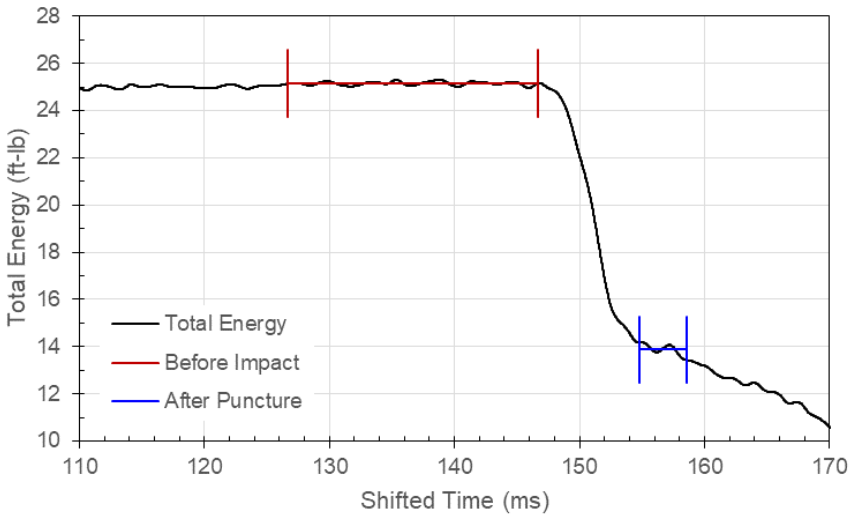

Figure 170: Total Energy, Test 30, Specimen T051-10, 0.500-Inch Flat Probe

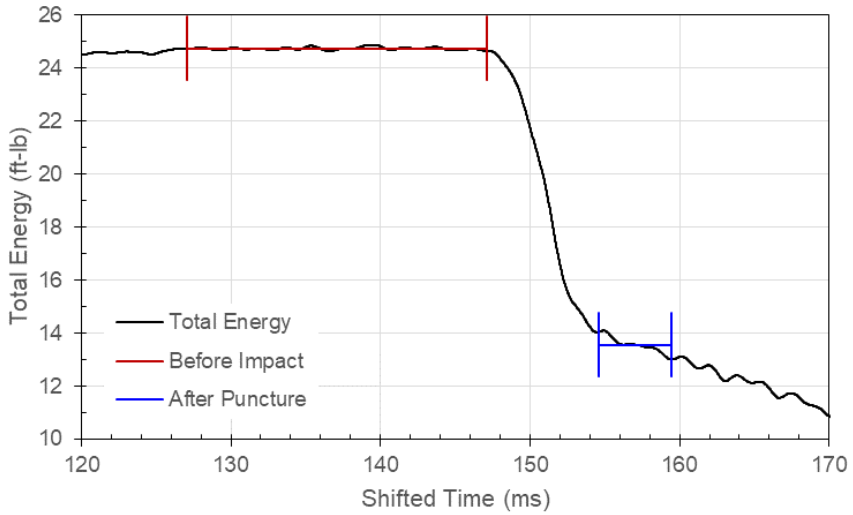

Figure 171: Total Energy, Test 31, Specimen T051-21, 0.500-Inch Flat Probe

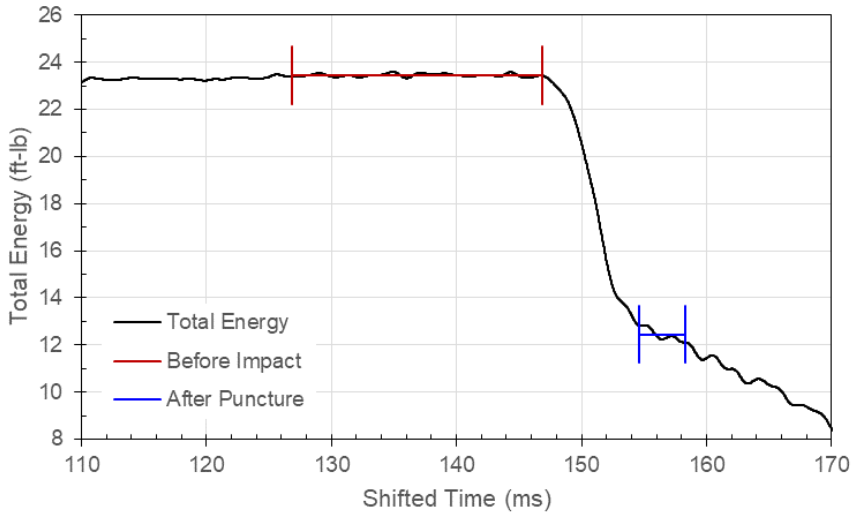

Figure 172: Total Energy, Test 32, Specimen T051-27, 0.500-Inch Flat Probe

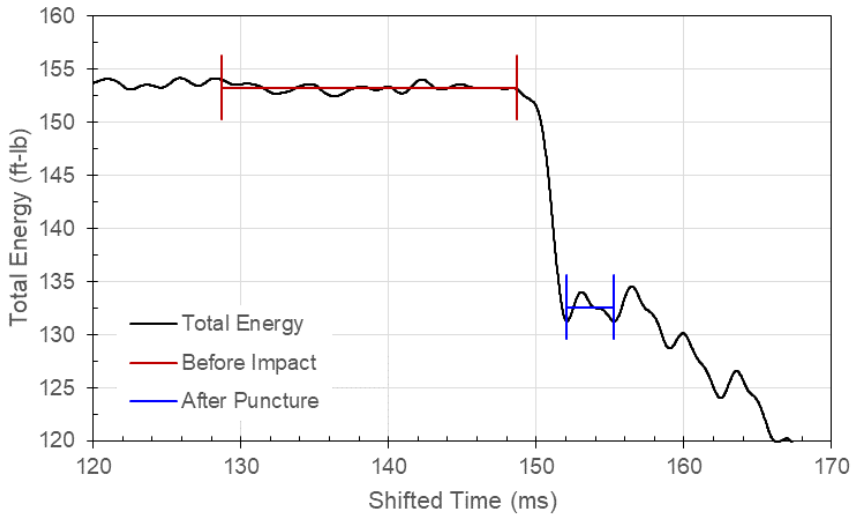

Figure 173: Total Energy, Test 44, Specimen T051-14, 1.000-Inch Flat Probe

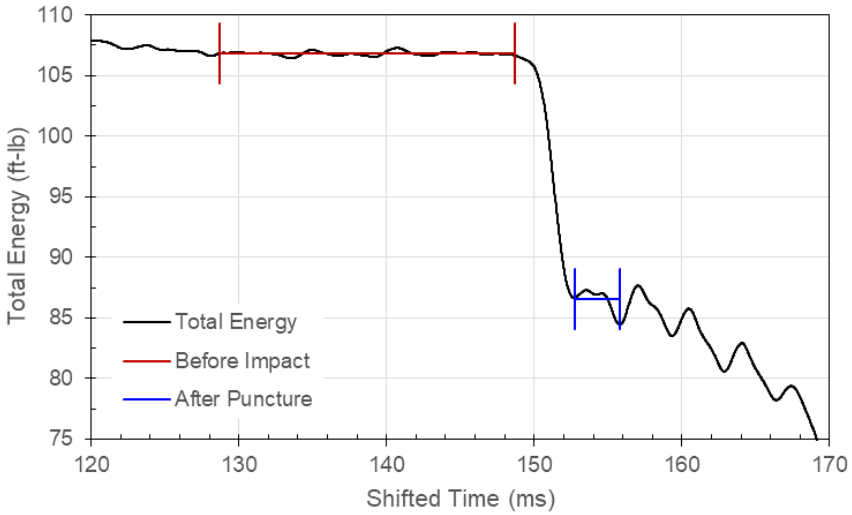

Figure 174: Total Energy, Test 45, Specimen T051-15, 1.000-Inch Flat Probe

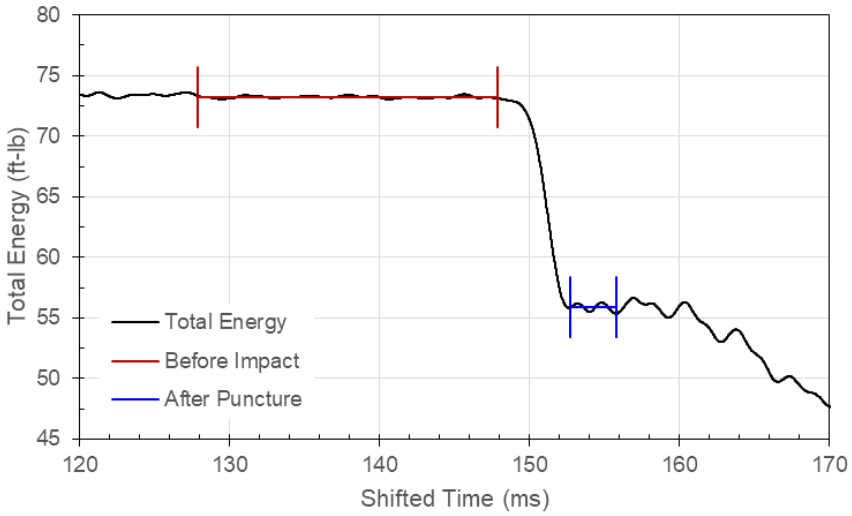

Figure 175: Total Energy, Test 46, Specimen T051-16, 1.000-Inch Flat Probe

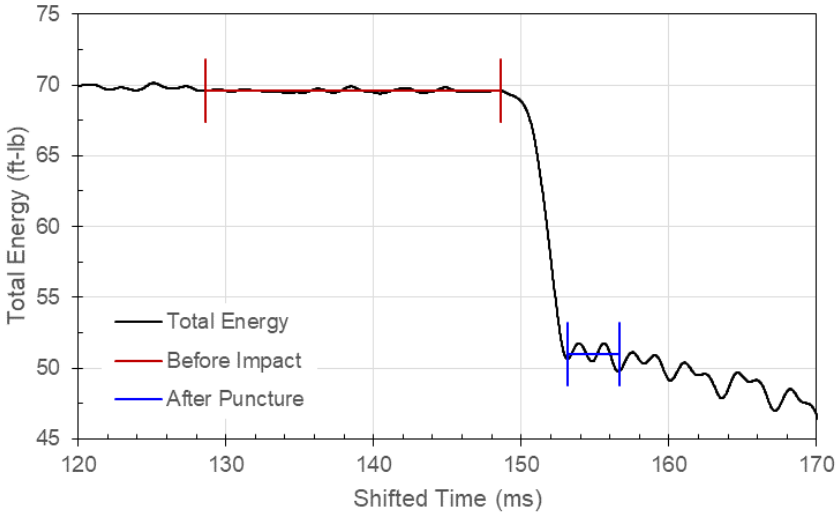

Figure 176: Total Energy, Test 48, Specimen T051-17, 1.000-Inch Flat Probe

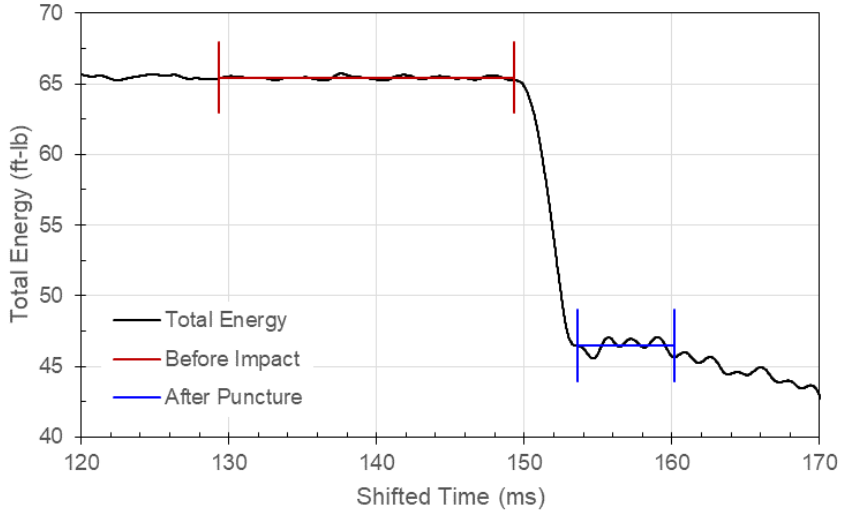

Figure 177: Total Energy, Test 49, Specimen T051-20, 1.000-Inch Flat Probe

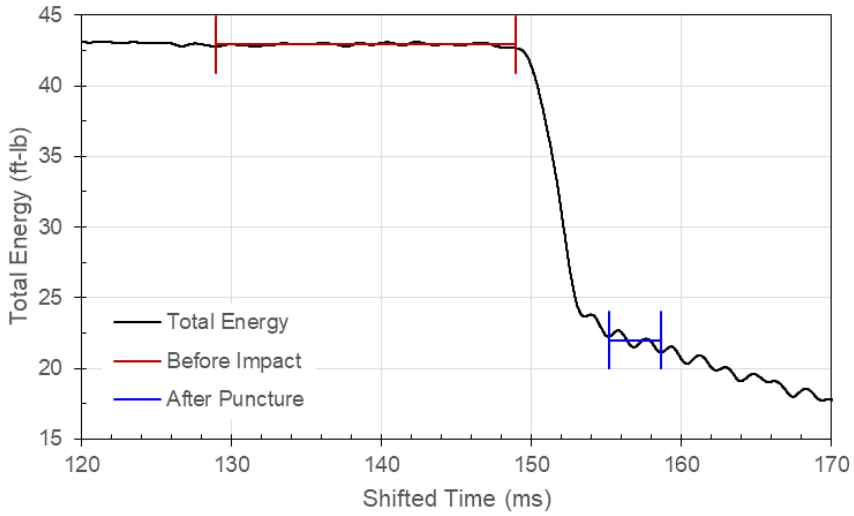

Figure 178: Total Energy, Test 47, Specimen T051-35, 1.000-Inch Flat Probe

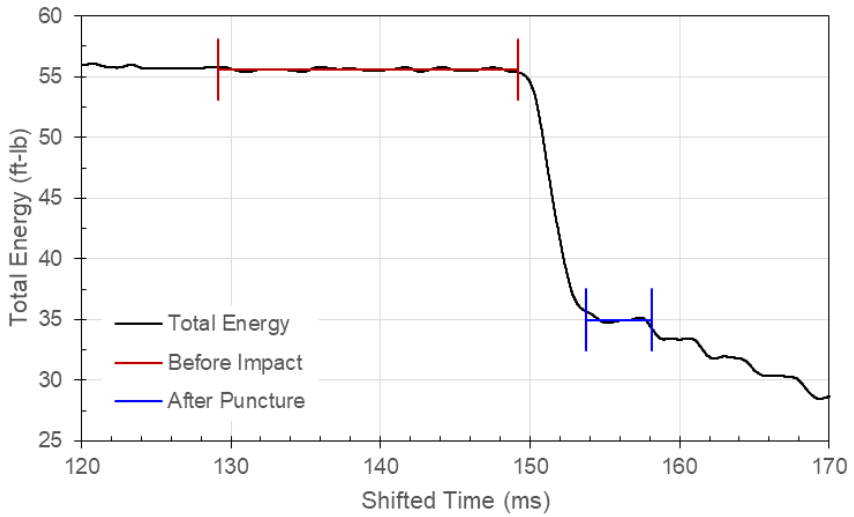

Figure 179: Total Energy, Test 18, Specimen T114-08, 0.250-Inch Flat Probe

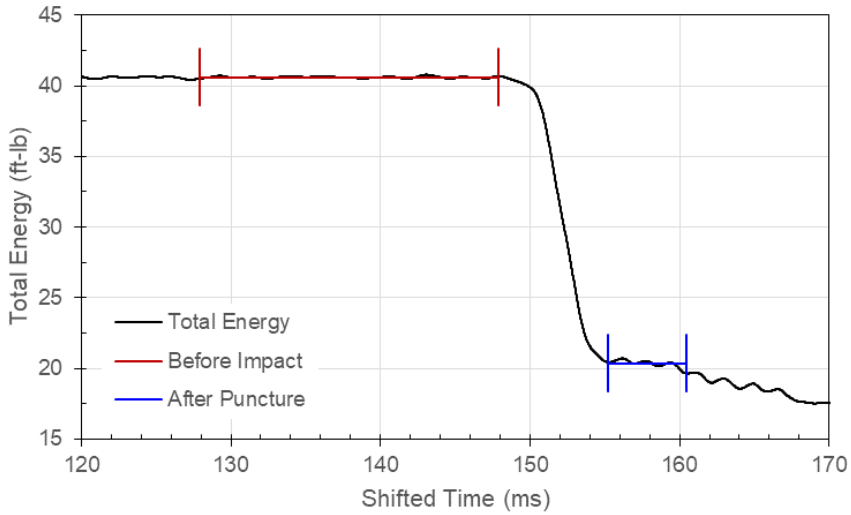

Figure 180: Total Energy, Test 19, Specimen T114-16, 0.250-Inch Flat Probe

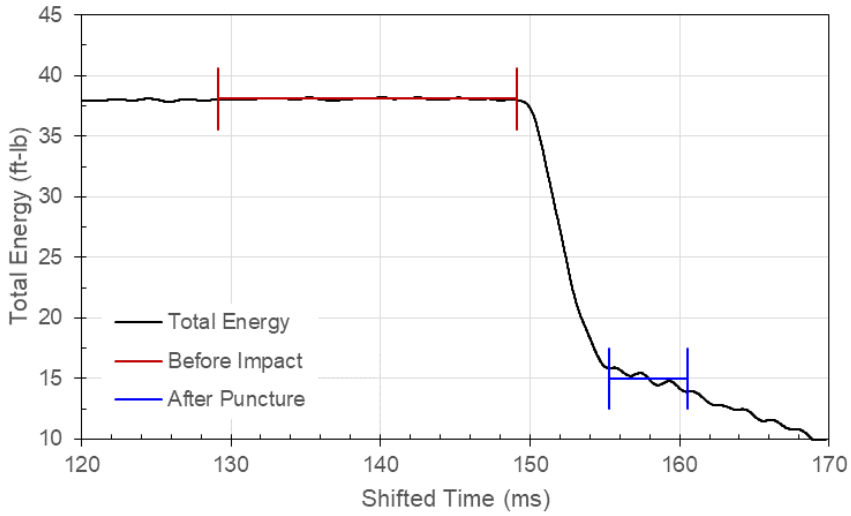

Figure 181: Total Energy, Test 20, Specimen T114-17, 0.250-Inch Flat Probe

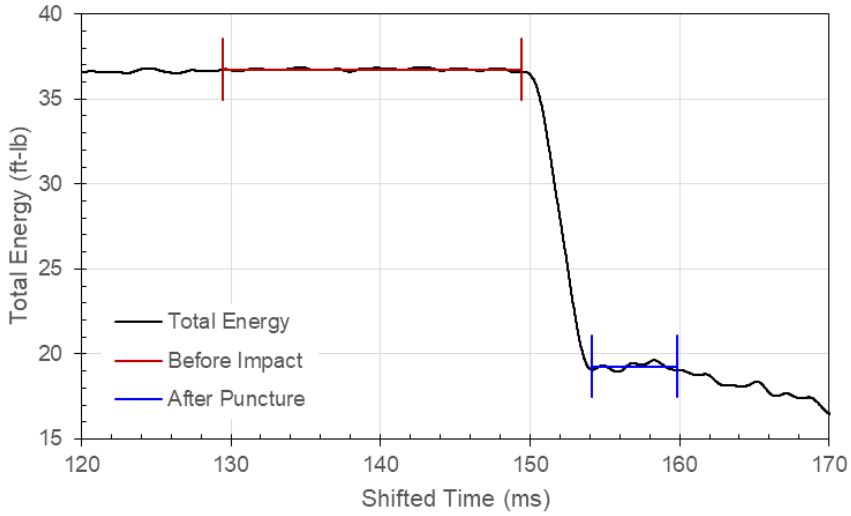

Figure 182: Total Energy, Test 21, Specimen T114-23, 0.250-Inch Flat Probe

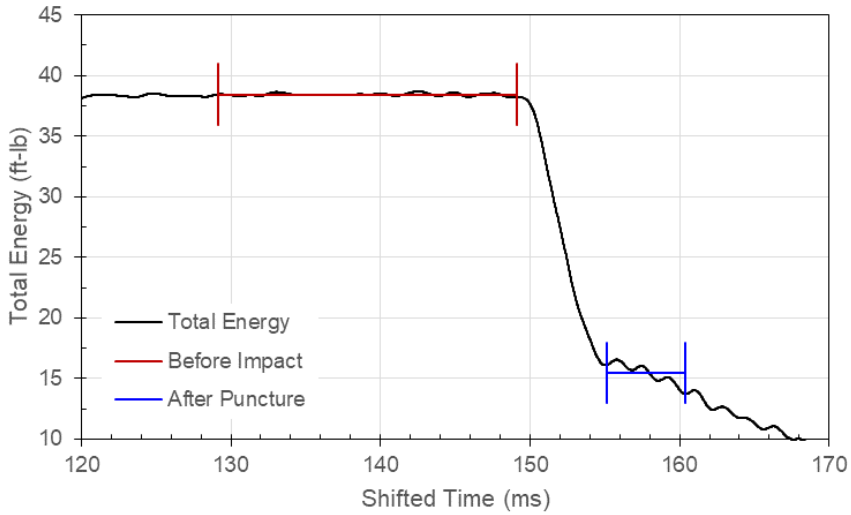

Figure 183: Total Energy, Test 22, Specimen T114-24, 0.250-Inch Flat Probe

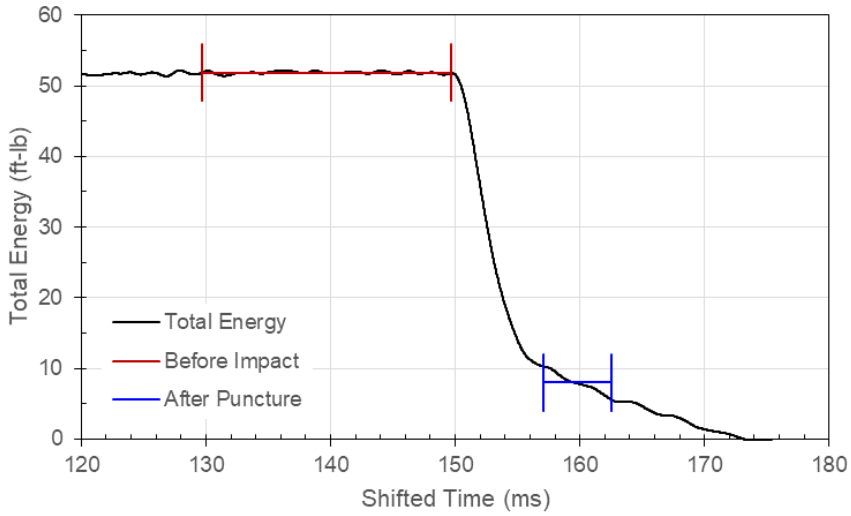

Figure 184: Total Energy, Test 33, Specimen T114-07, 0.500-Inch Flat Probe

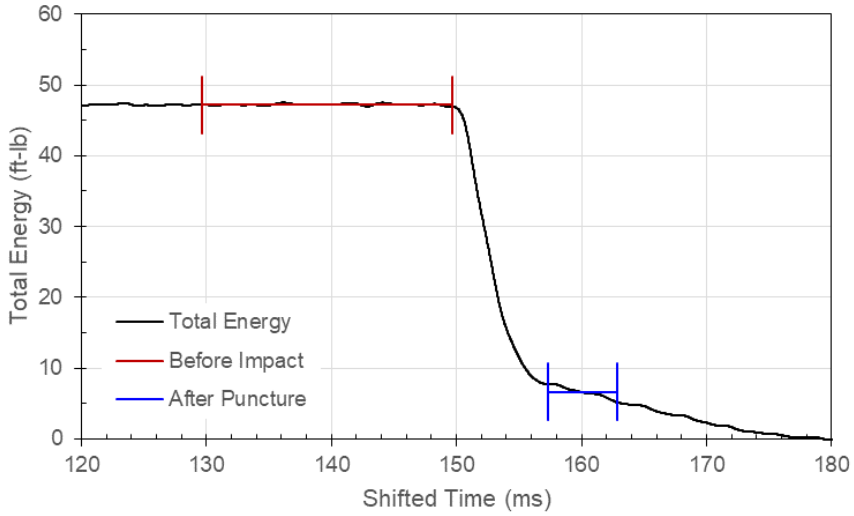

Figure 185: Total Energy, Test 35, Specimen T114-09, 0.500-Inch Flat Probe

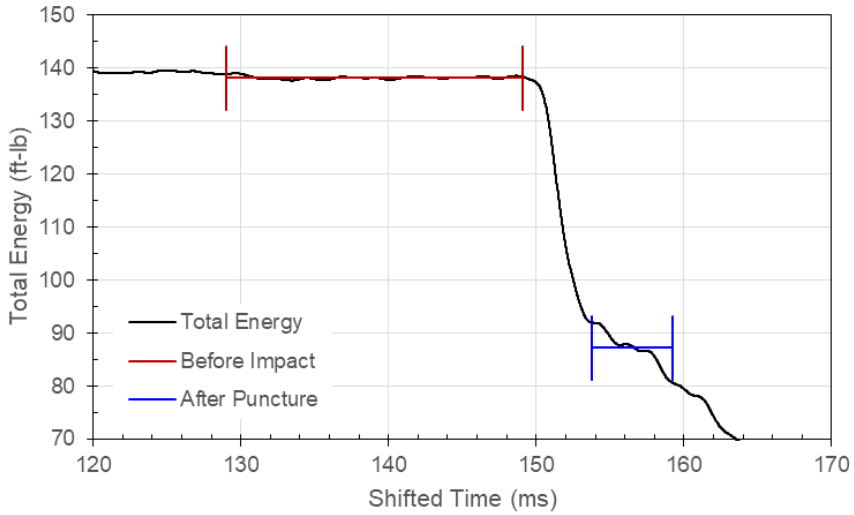

Figure 186: Total Energy, Test 37, Specimen T114-27, 0.500-Inch Flat Probe

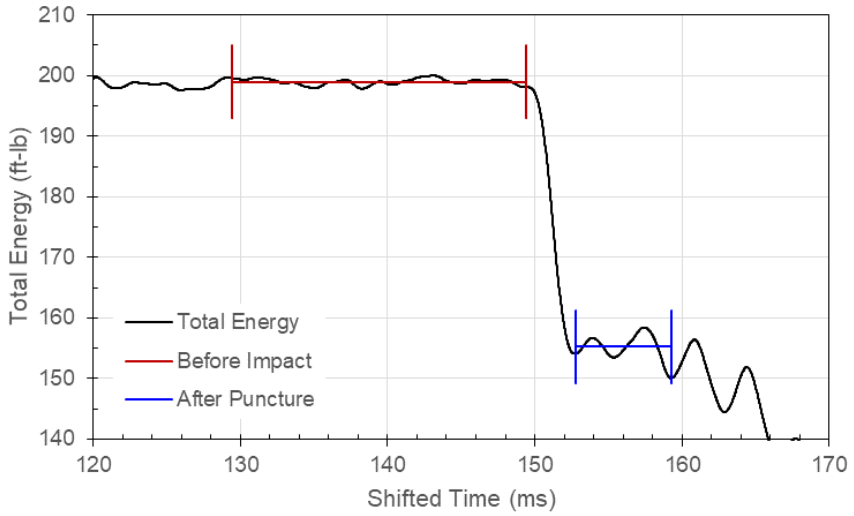

Figure 187: Total Energy, Test 38, Specimen T114-30, 0.500-Inch Flat Probe

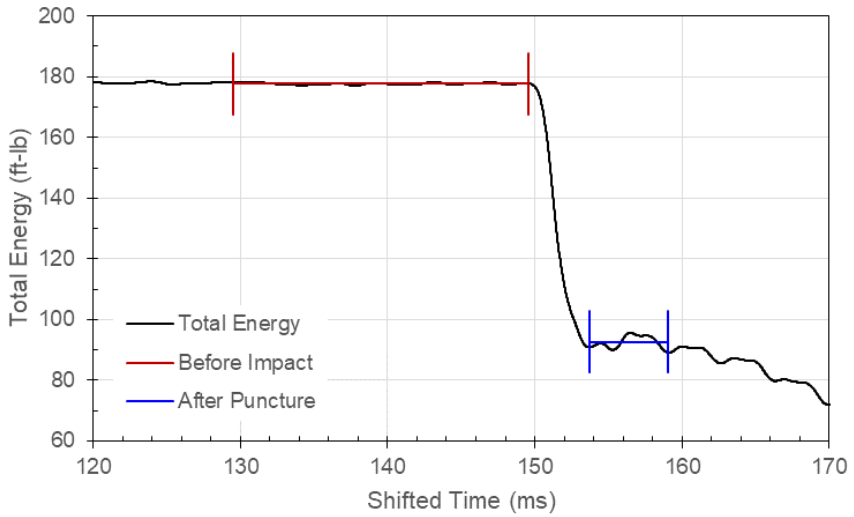

Figure 188: Total Energy, Test 50, Specimen T114-05, 1.000-Inch Flat Probe

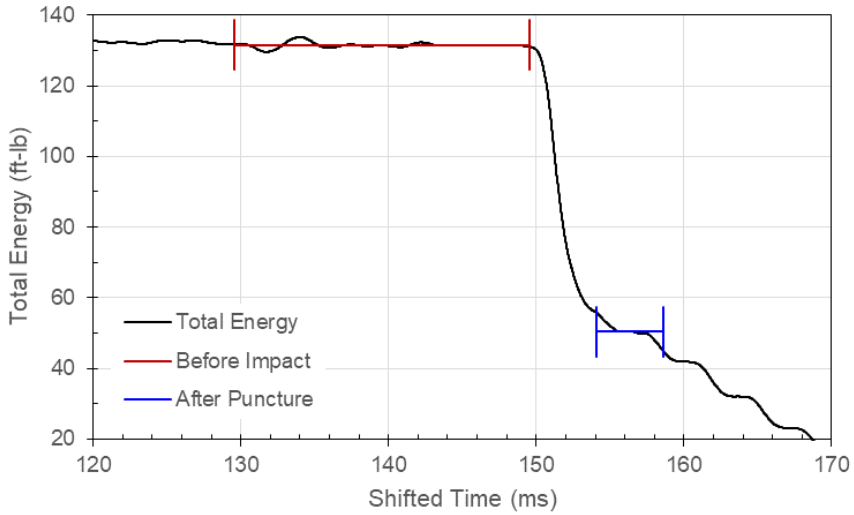

Figure 189: Total Energy, Test 51, Specimen T114-13, 1.000-Inch Flat Probe

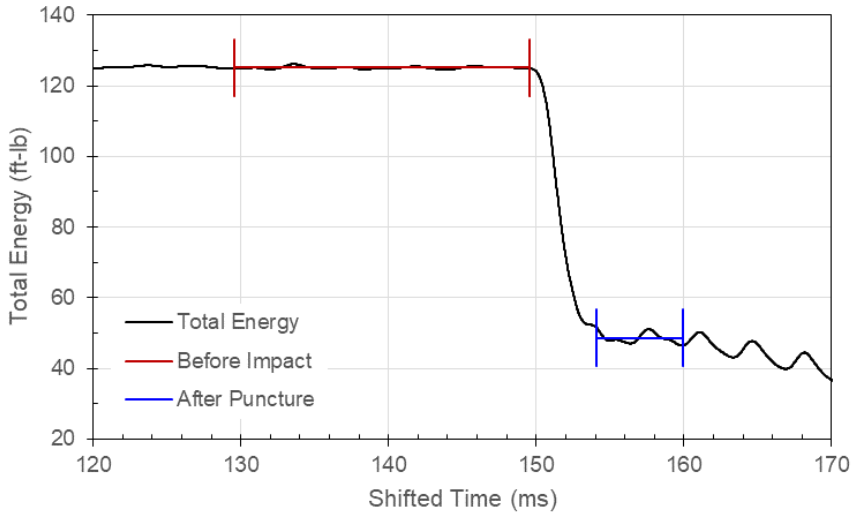

Figure 190: Total Energy, Test 52, Specimen T114-14, 1.000-Inch Flat Probe

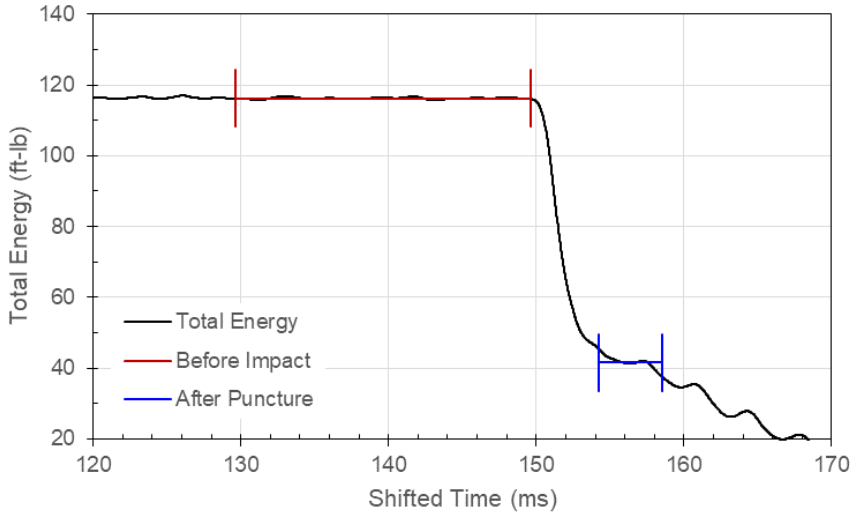

Figure 191: Total Energy, Test 53, Specimen T114-21, 1.000-Inch Flat Probe

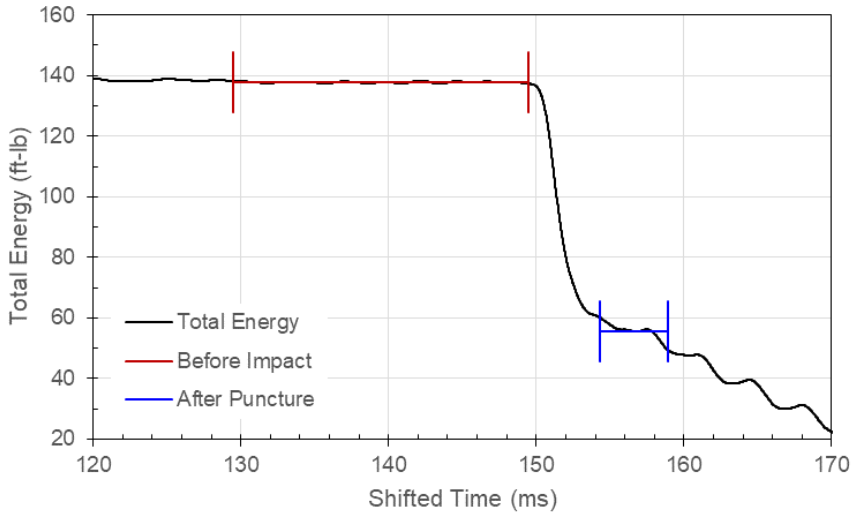

Figure 192: Total Energy, Test 54, Specimen T114-29, 1.000-Inch Flat Probe

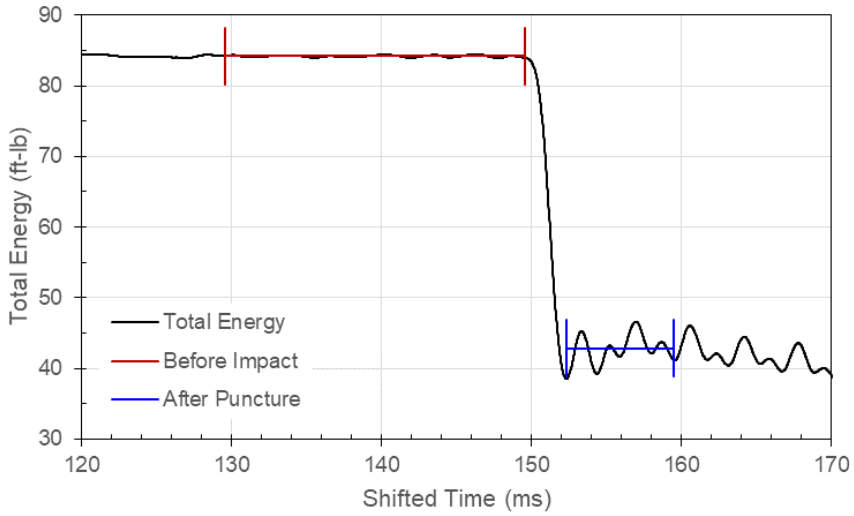

Figure 193: Total Energy, Test 23, Specimen T250-08, 0.250-Inch Flat Probe

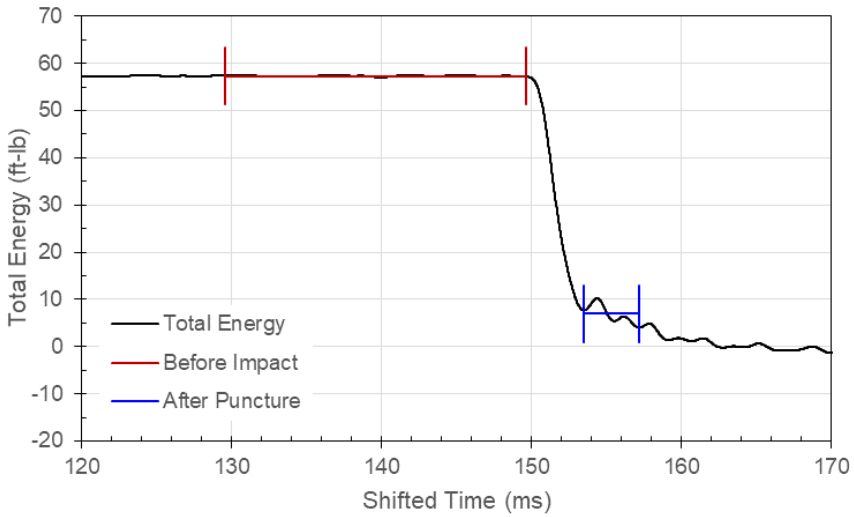

Figure 194: Total Energy, Test 24, Specimen T250-16, 0.250-Inch Flat Probe

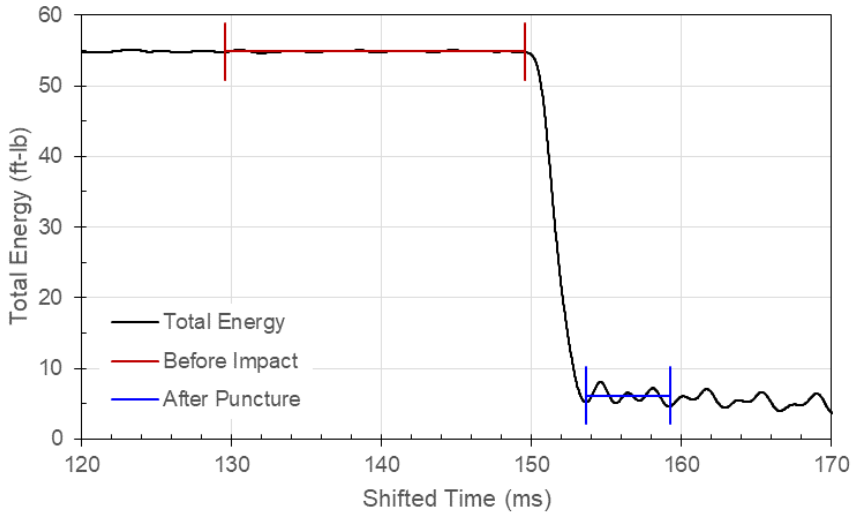

Figure 195: Total Energy, Test 25, Specimen T250-17, 0.250-Inch Flat Probe

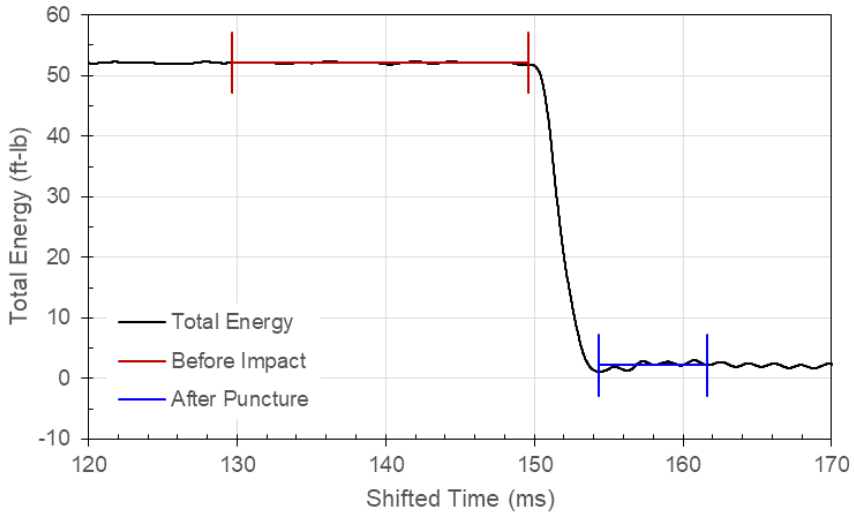

Figure 196: Total Energy, Test 26, Specimen T250-23, 0.250-Inch Flat Probe

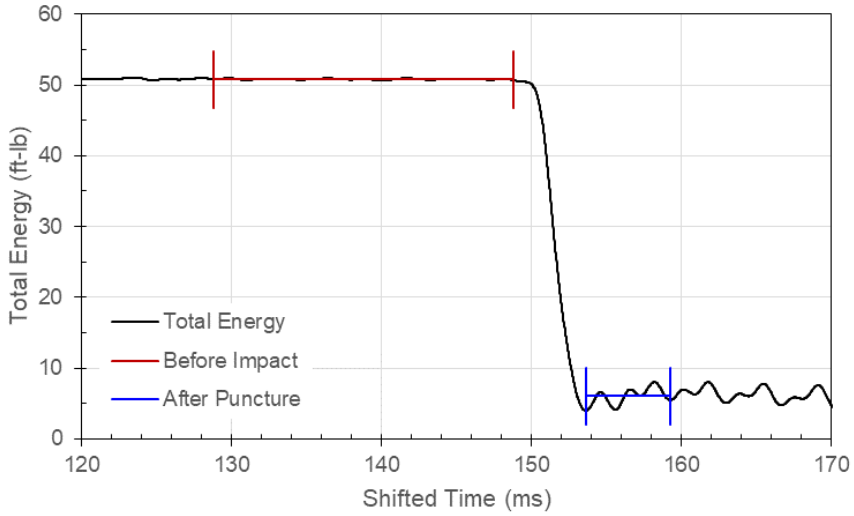

Figure 197: Total Energy, Test 27, Specimen T250-29, 0.250-Inch Flat Probe

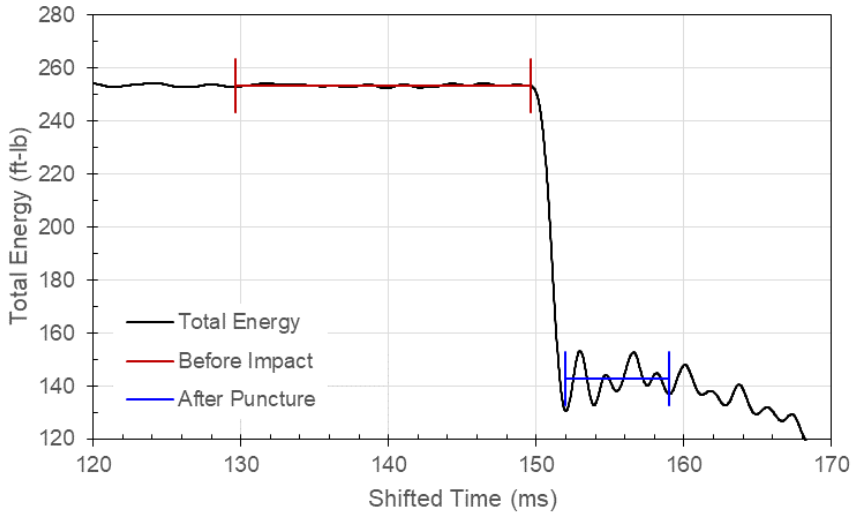

Figure 198: Total Energy, Test 39, Specimen T250-07, 0.500-Inch Flat Probe

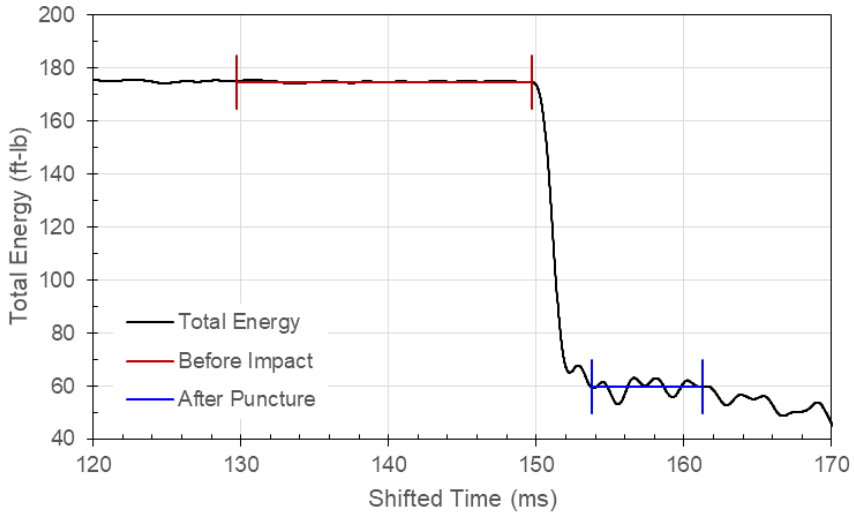

Figure 199: Total Energy, Test 40, Specimen T250-09, 0.500-Inch Flat Probe

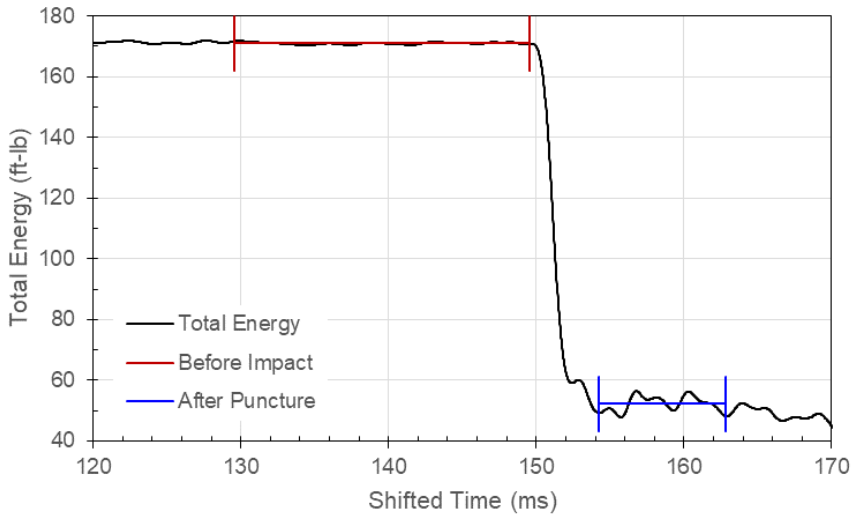

Figure 200: Total Energy, Test 41, Specimen T250-18, 0.500-Inch Flat Probe

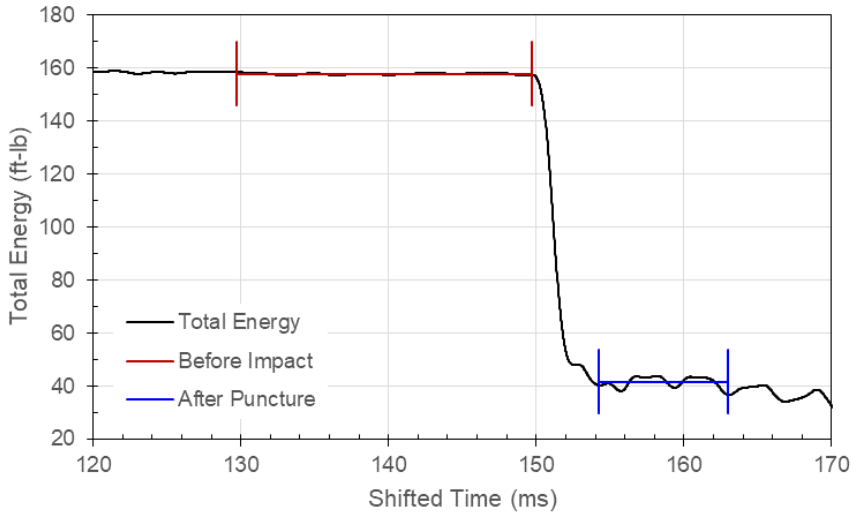

Figure 201: Total Energy, Test 42, Specimen T250-24, 0.500-Inch Flat Probe

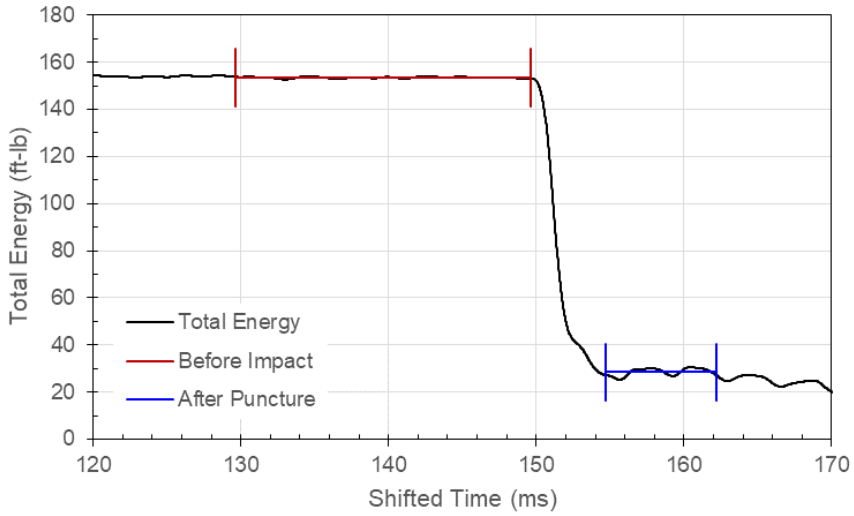

Figure 202: Total Energy, Test 43, Specimen T250-30, 0.500-Inch Flat Probe

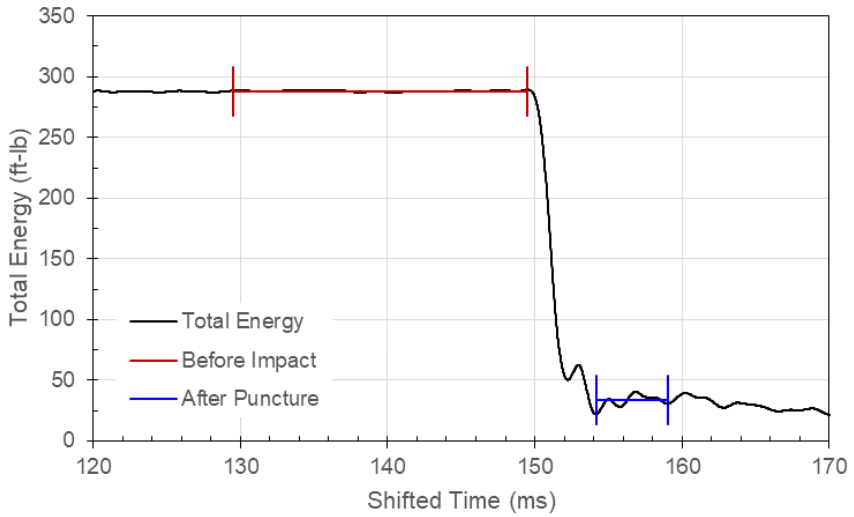

Figure 203: Total Energy, Test 55, Specimen T250-06, 1.000-Inch Flat Probe

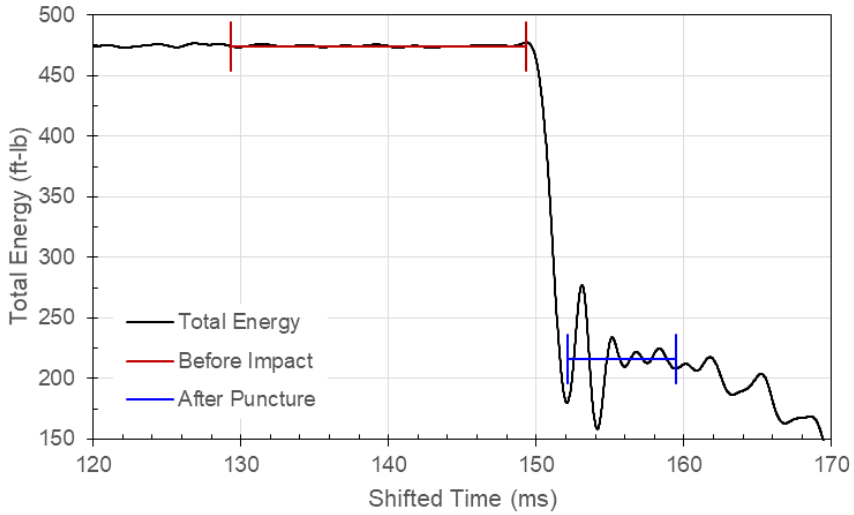

Figure 204: Total Energy, Test 56, Specimen T250-15, 1.000-Inch Flat Probe

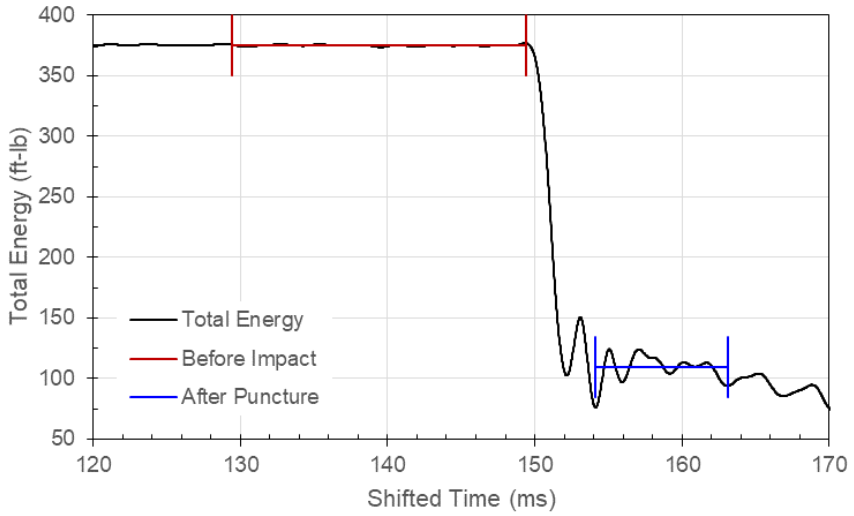

Figure 205: Total Energy, Test 57, Specimen T250-28, 1.000-Inch Flat Probe

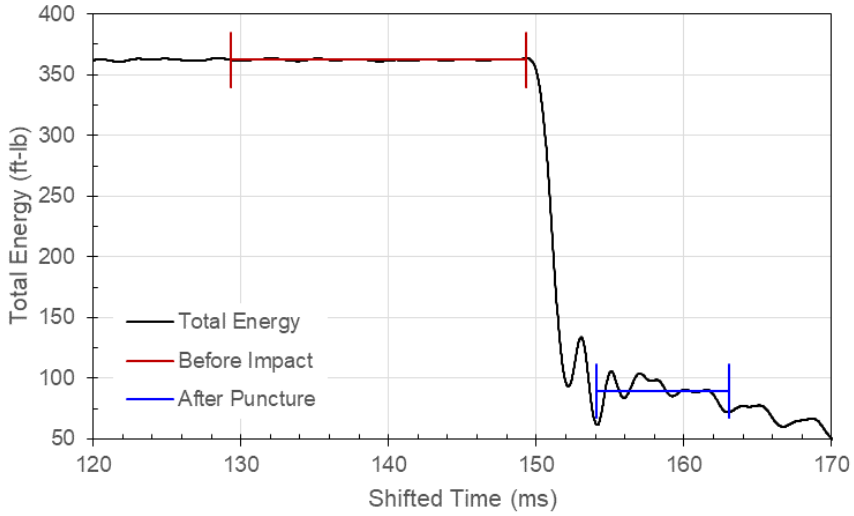

Figure 206: Total Energy, Test 58, Specimen T250-34, 1.000-Inch Flat Probe

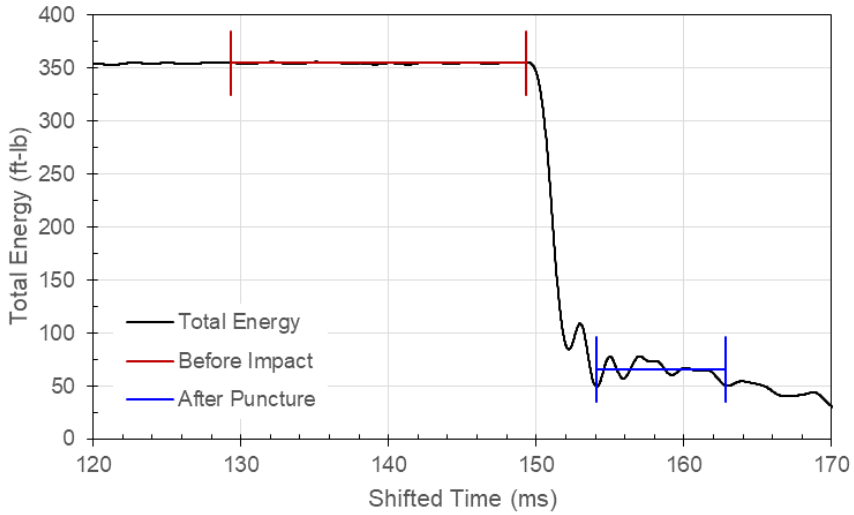

Figure 207: Total Energy, Test 59, Specimen T250-35, 1.000-Inch Flat Probe

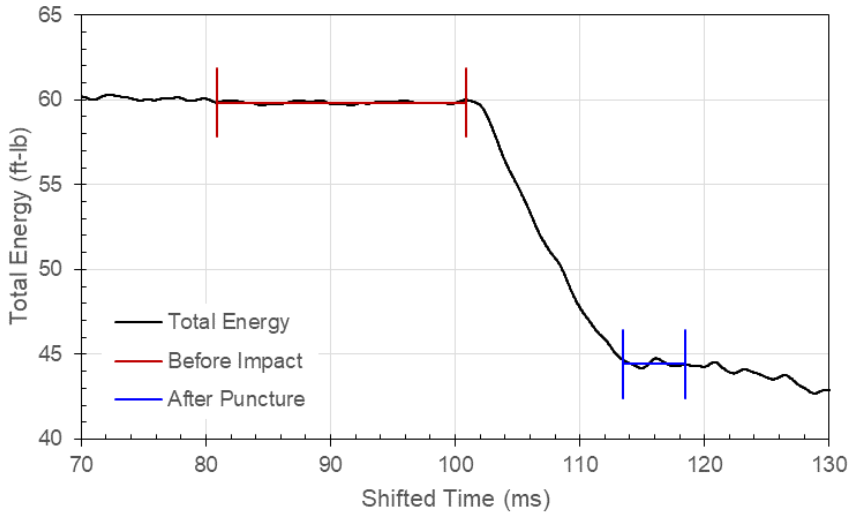

Figure 208: Total Energy, Test 61, Specimen T051-06, 0.500-Inch Semi-spherical Probe

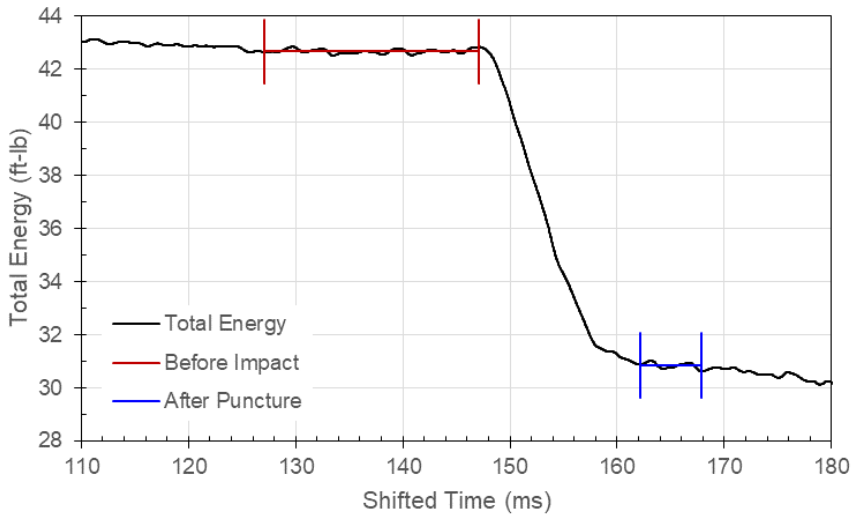

Figure 209: Total Energy, Test 62, Specimen T051-07, 0.500-Inch Semi-spherical Probe

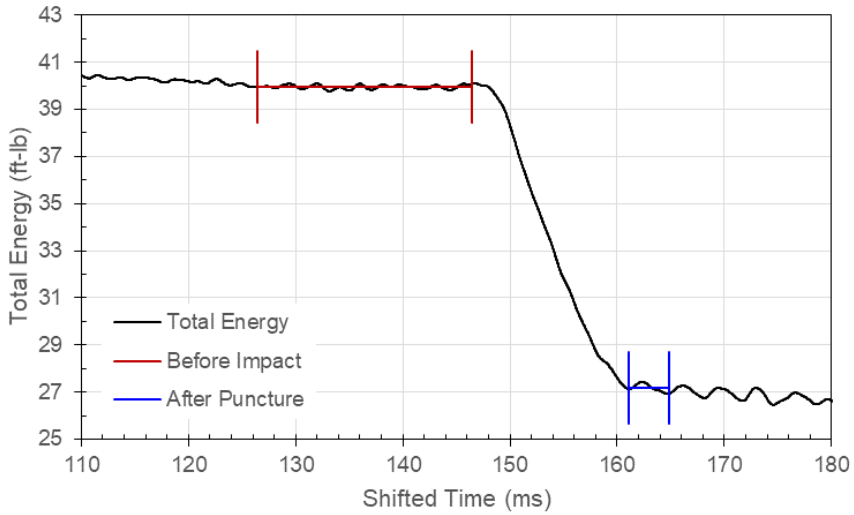

Figure 210: Total Energy, Test 63, Specimen T051-11, 0.500-Inch Semi-spherical Probe

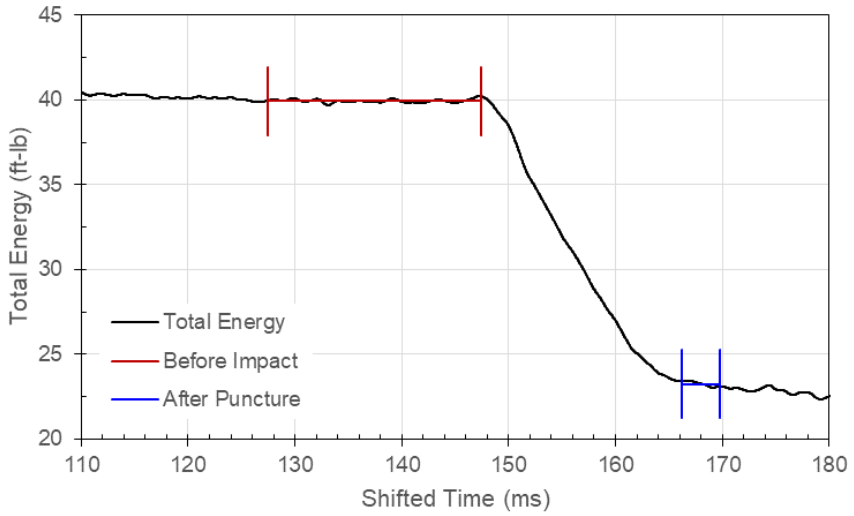

Figure 211: Total Energy, Test 64, Specimen T051-13, 0.500-Inch Semi-spherical Probe

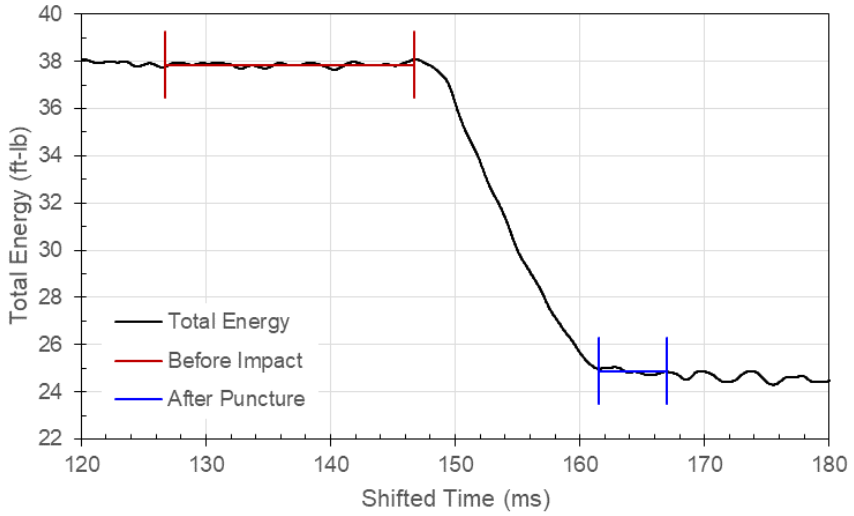

Figure 212: Total Energy, Test 65, Specimen T051-23, 0.500-Inch Semi-spherical Probe

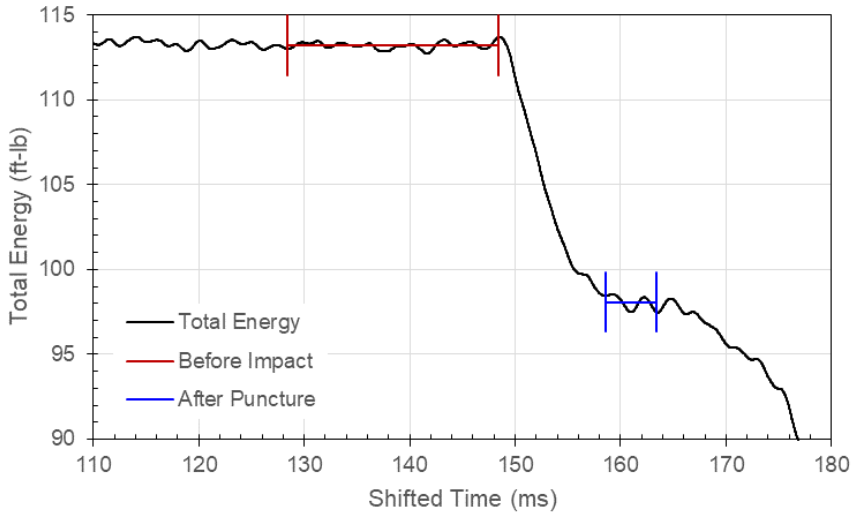

Figure 213: Total Energy, Test 60, Specimen T051-34, 0.500-Inch Semi-spherical Probe

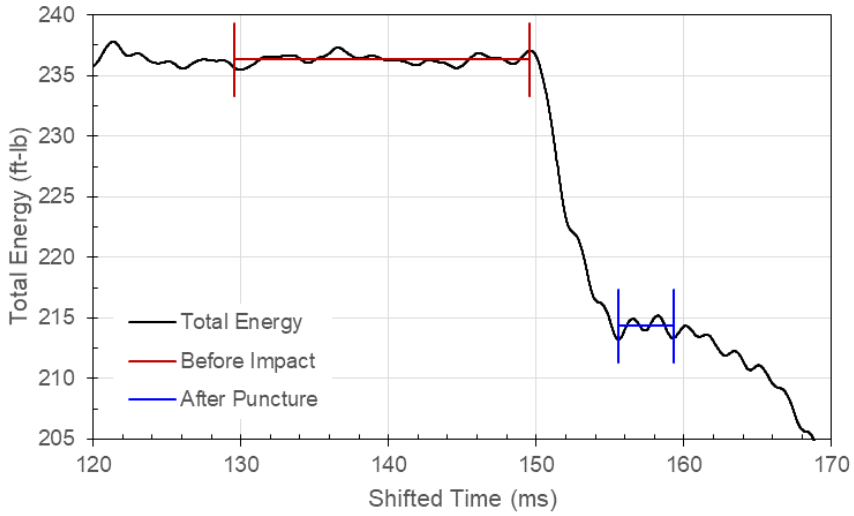

Figure 214: Total Energy, Test 76, Specimen T051-09, 1.000-Inch Semi-spherical Probe

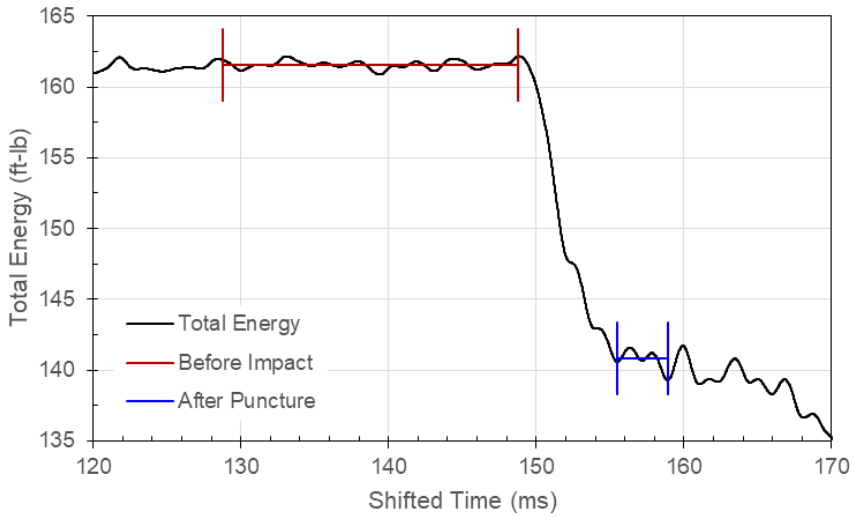

Figure 215: Total Energy, Test 77, Specimen T051-12, 1.000-Inch Semi-spherical Probe

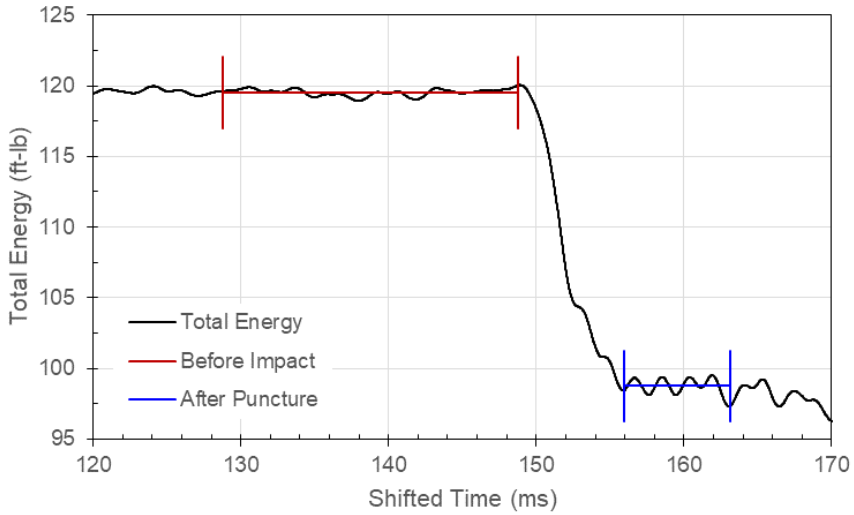

Figure 216: Total Energy, Test 78, Specimen T051-18, 1.000-Inch Semi-spherical Probe

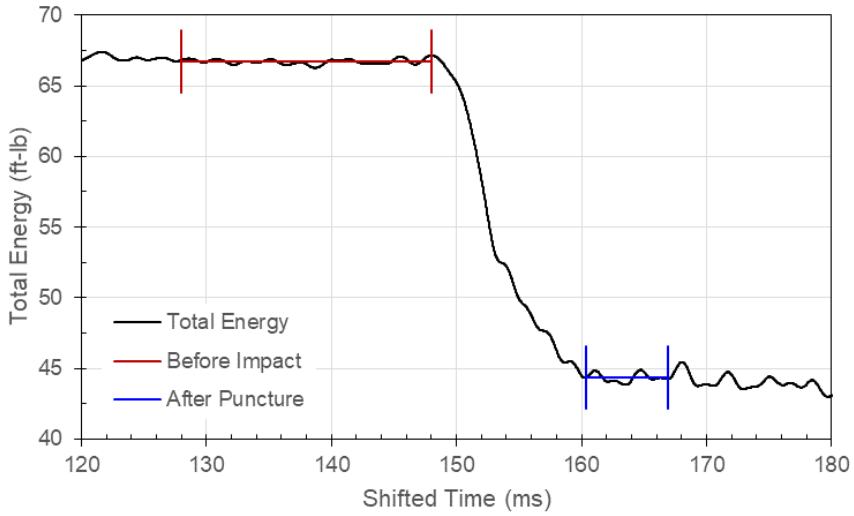

Figure 217: Total Energy, Test 79, Specimen T051-19, 1.000-Inch Semi-spherical Probe

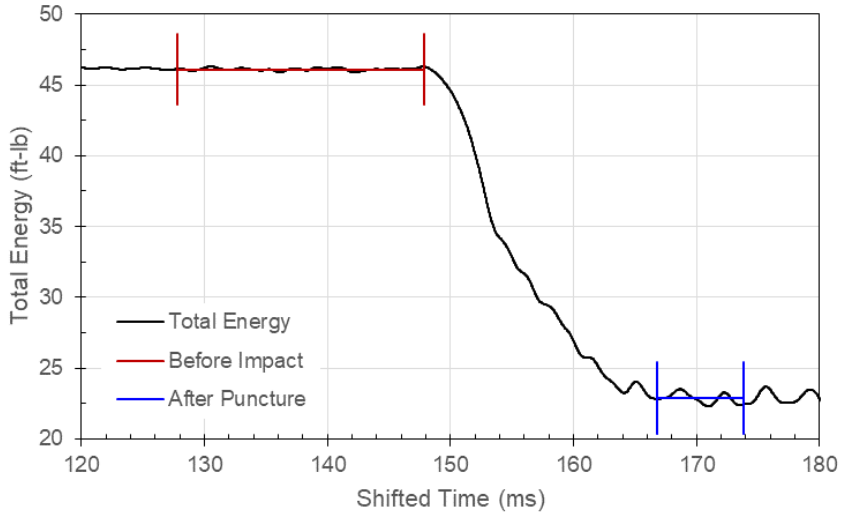

Figure 218: Total Energy, Test 80, Specimen T051-22, 1.000-Inch Semi-spherical Probe

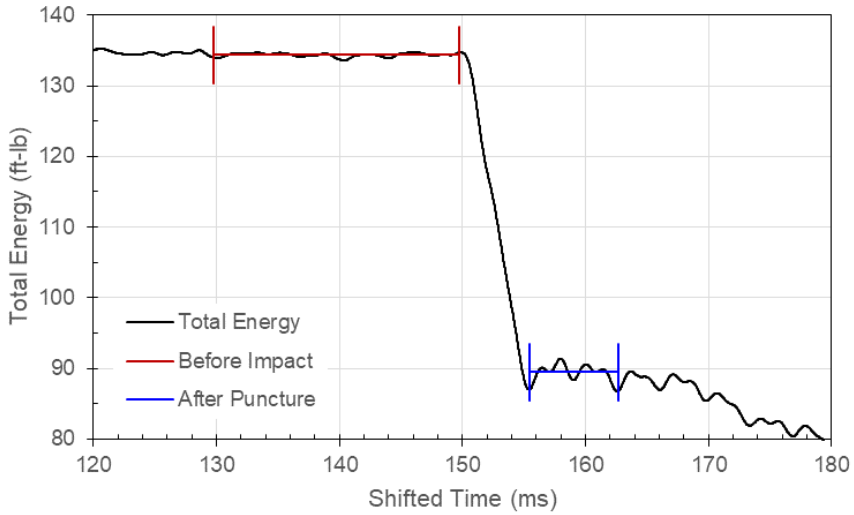

Figure 219: Total Energy, Test 66, Specimen T114-04, 0.500-Inch Semi-spherical Probe

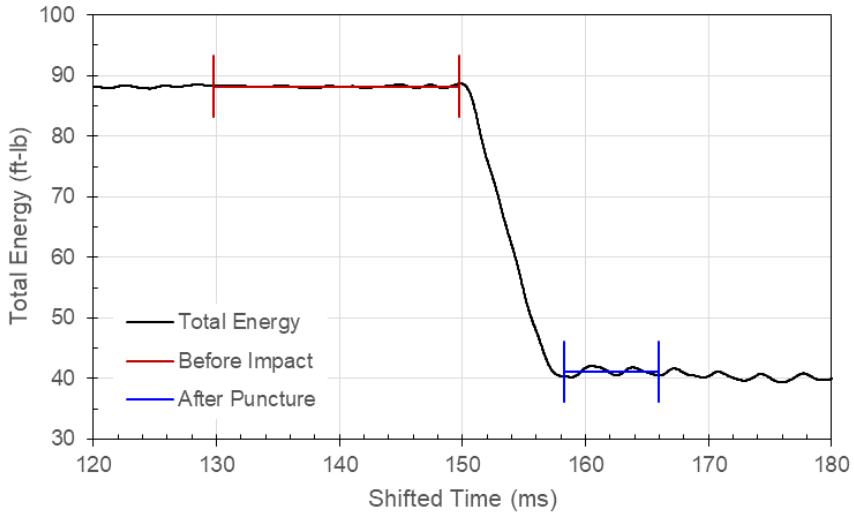

Figure 220: Total Energy, Test 67, Specimen T114-22, 0.500-Inch Semi-spherical Probe

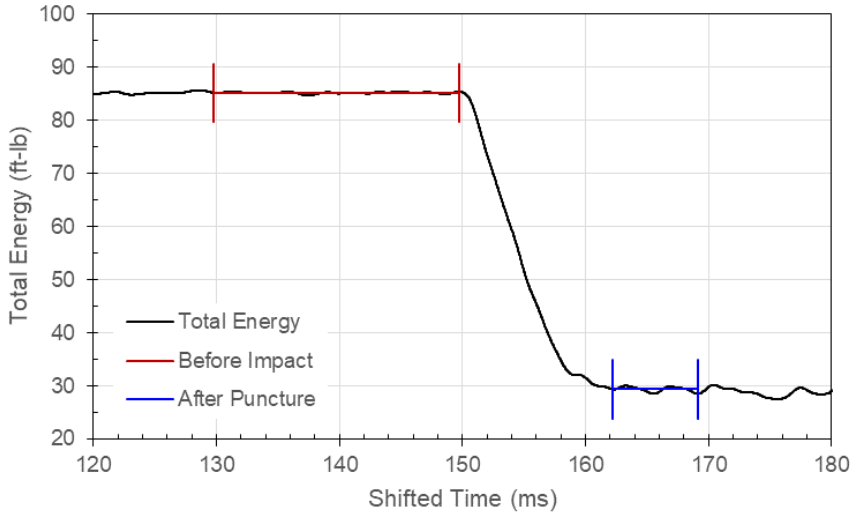

Figure 221: Total Energy, Test 68, Specimen T114-25, 0.500-Inch Semi-spherical Probe

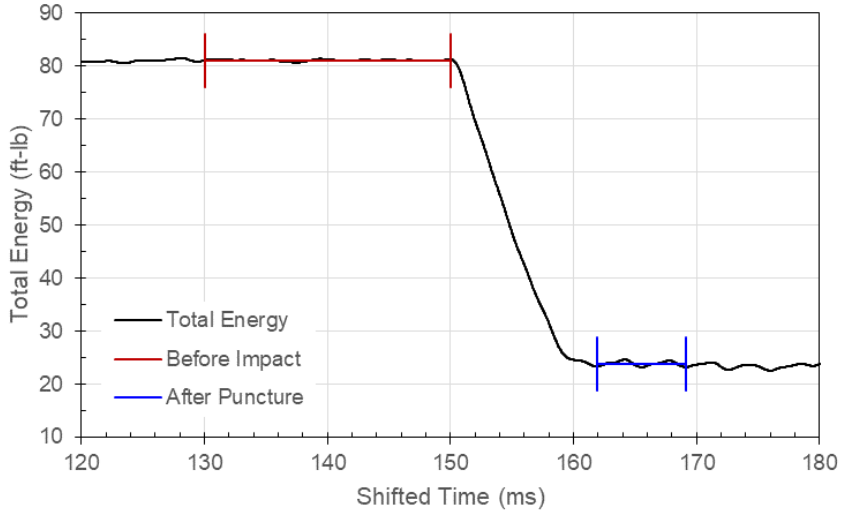

Figure 222: Total Energy, Test 69, Specimen T114-33, 0.500-Inch Semi-spherical Probe

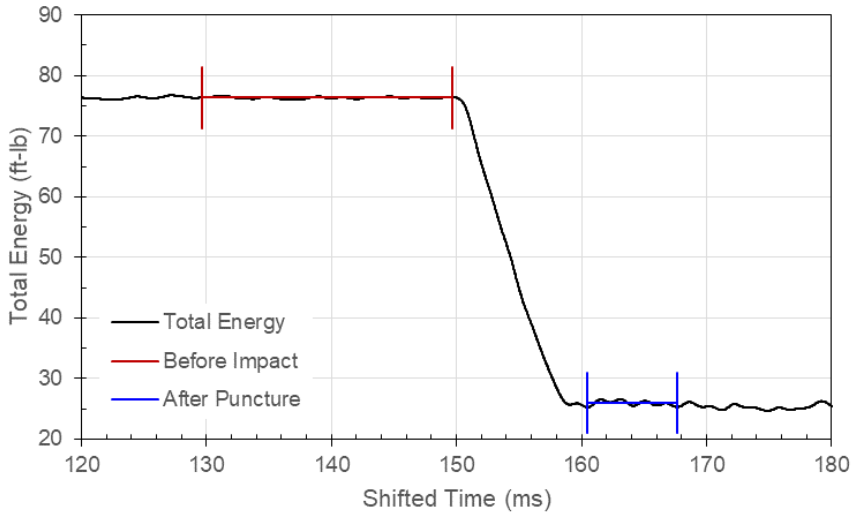

Figure 223: Total Energy, Test 70, Specimen T114-35, 0.500-Inch Semi-spherical Probe

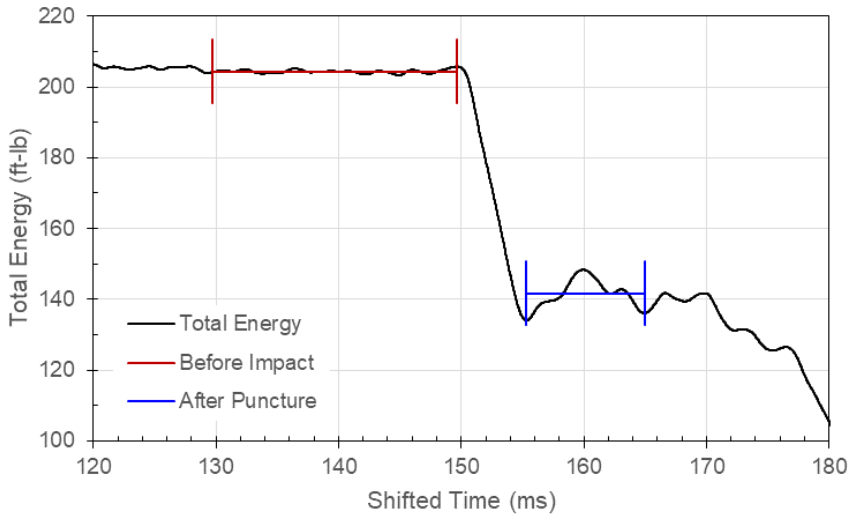

Figure 224: Total Energy, Test 81, Specimen T114-06, 1.000-Inch Semi-spherical Probe

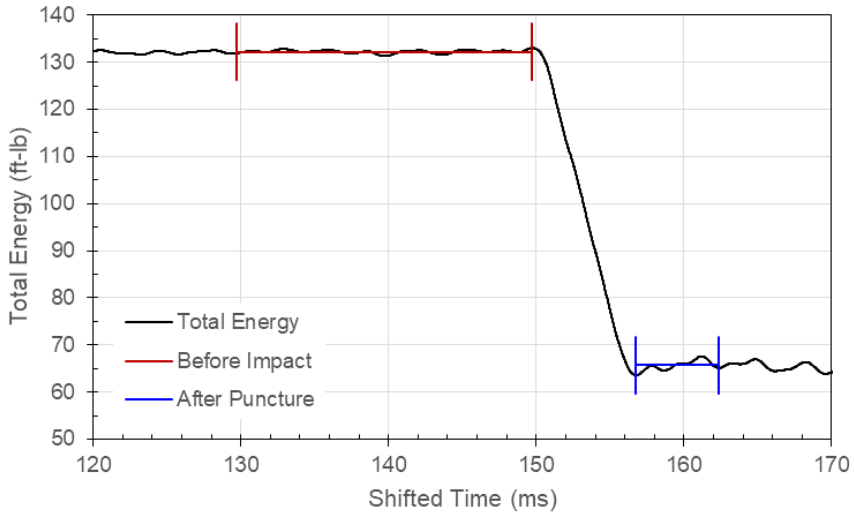

Figure 225: Total Energy, Test 82, Specimen T114-15, 1.000-Inch Semi-spherical Probe

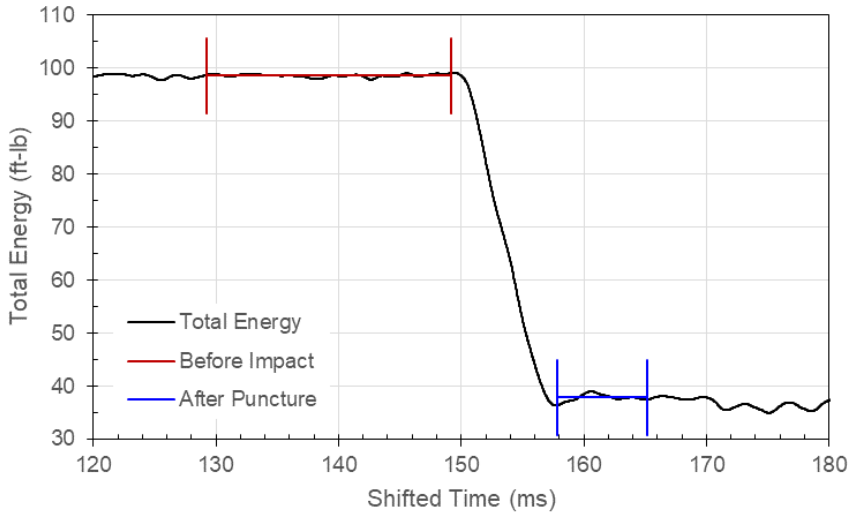

Figure 226: Total Energy, Test 83, Specimen T114-28, 1.000-Inch Semi-spherical Probe

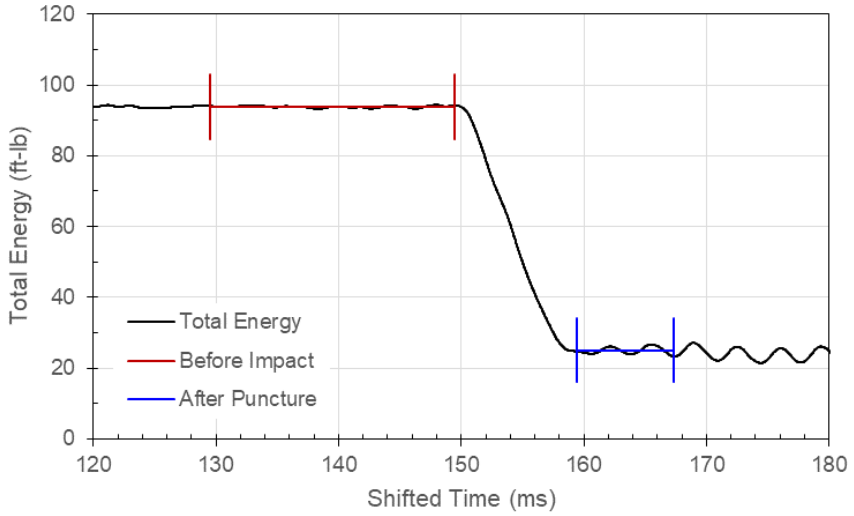

Figure 227: Total Energy, Test 84, Specimen T114-31, 1.000-Inch Semi-spherical Probe

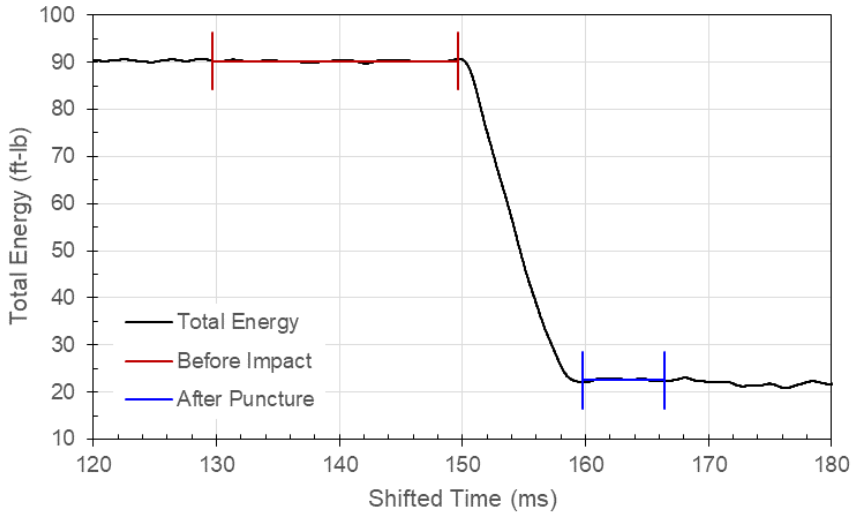

Figure 228: Total Energy, Test 85, Specimen T114-32, 1.000-Inch Semi-spherical Probe

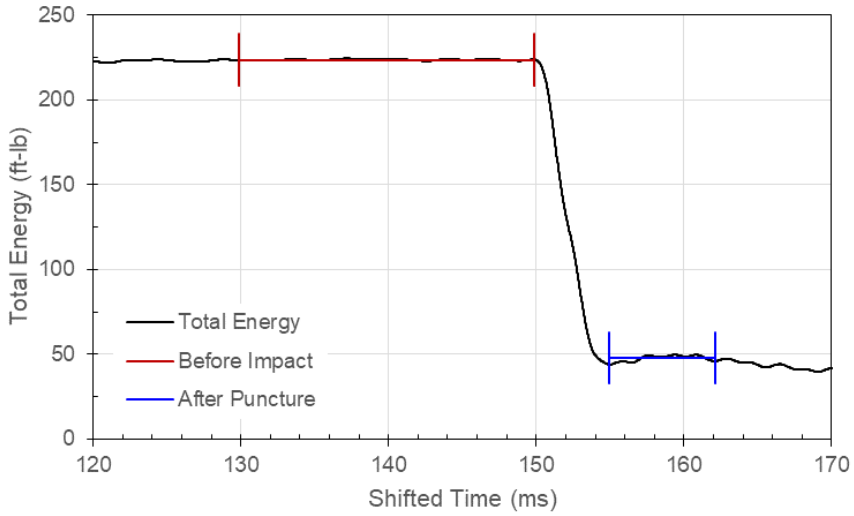

Figure 229: Total Energy, Test 71, Specimen T250-05, 0.500-Inch Semi-spherical Probe

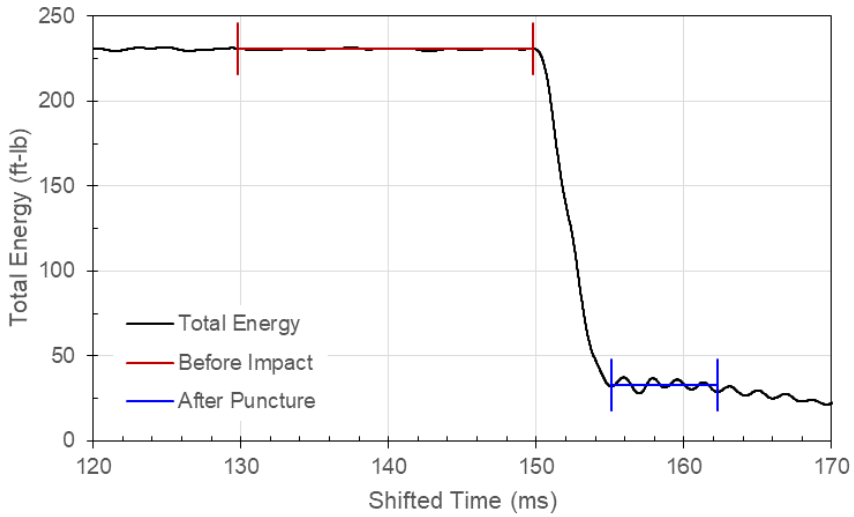

Figure 230: Total Energy, Test 72, Specimen T250-14, 0.500-Inch Semi-spherical Probe

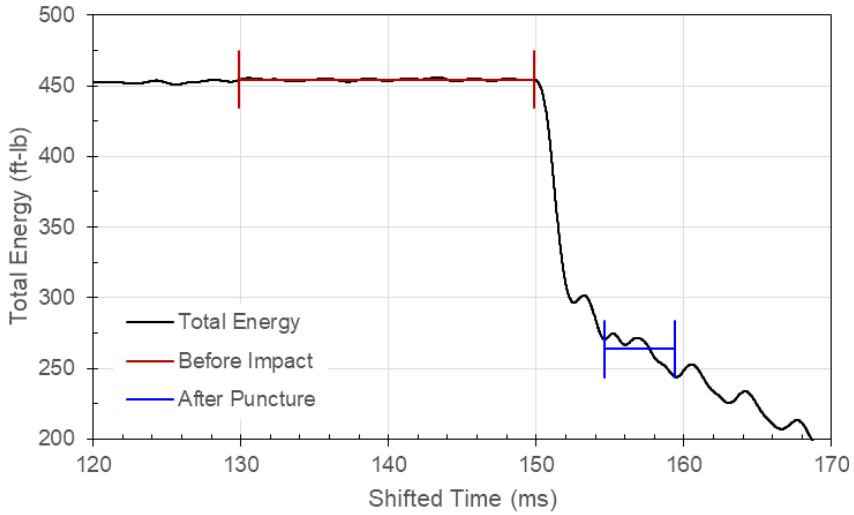

Figure 231: Total Energy, Test 73, Specimen T250-22, 0.500-Inch Semi-spherical Probe

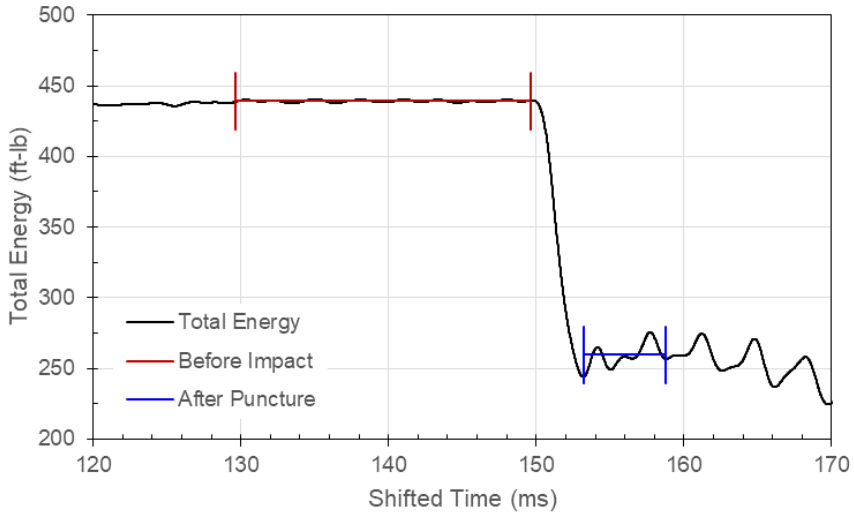

Figure 232: Total Energy, Test 74, Specimen T250-32, 0.500-Inch Semi-spherical Probe

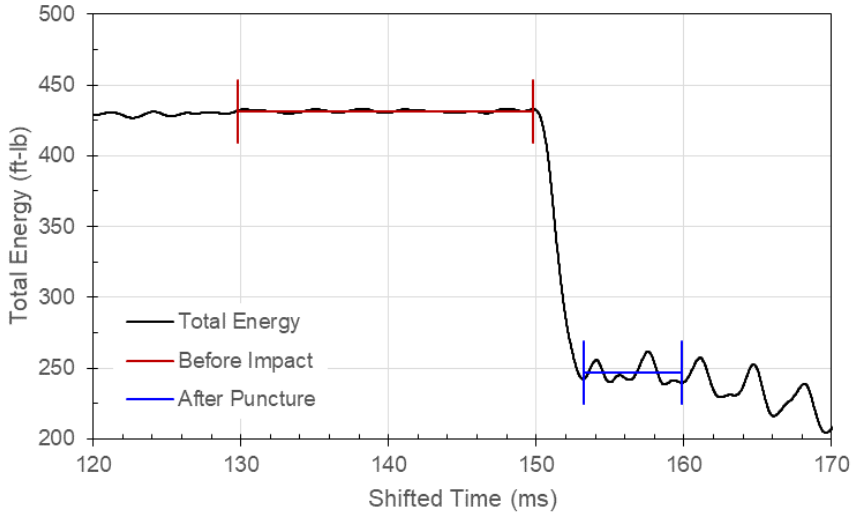

Figure 233: Total Energy, Test 75, Specimen T250-33, 0.500-Inch Semi-spherical Probe

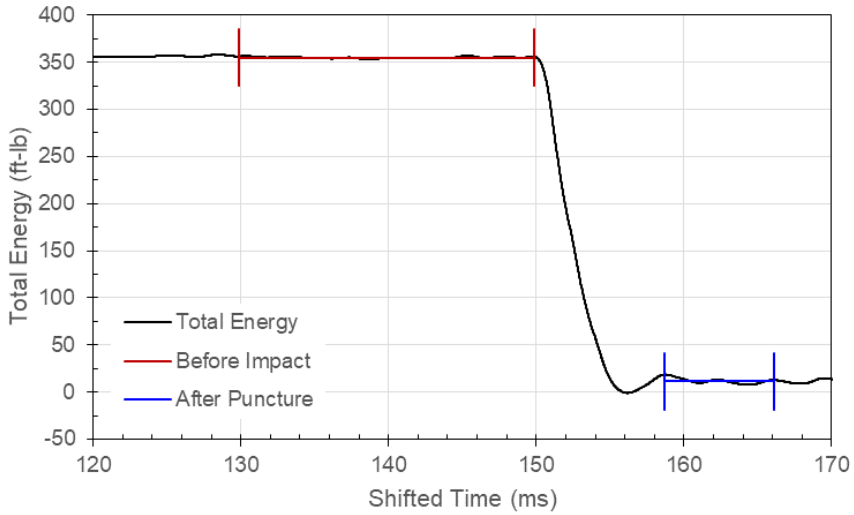

Figure 234: Total Energy, Test 87, Specimen T250-13, 1.000-Inch Semi-spherical Probe

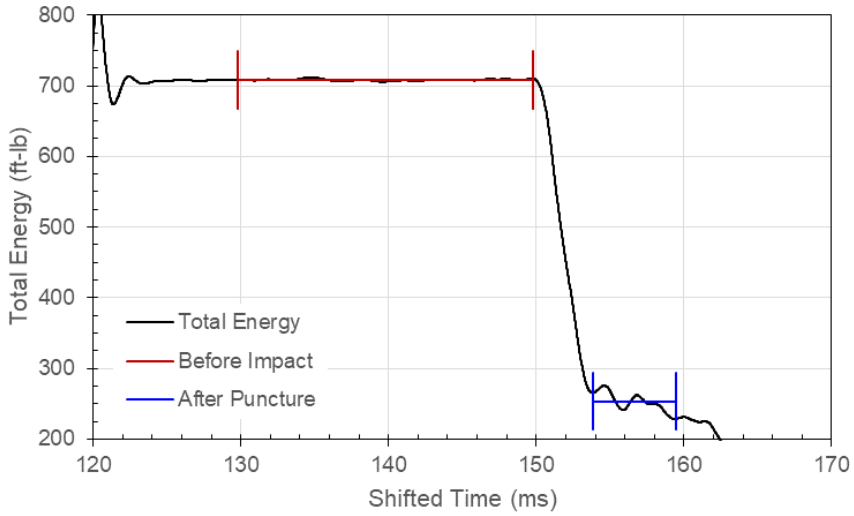

Figure 235: Total Energy, Test 89, Specimen T250-20, 1.000-Inch Semi-spherical Probe

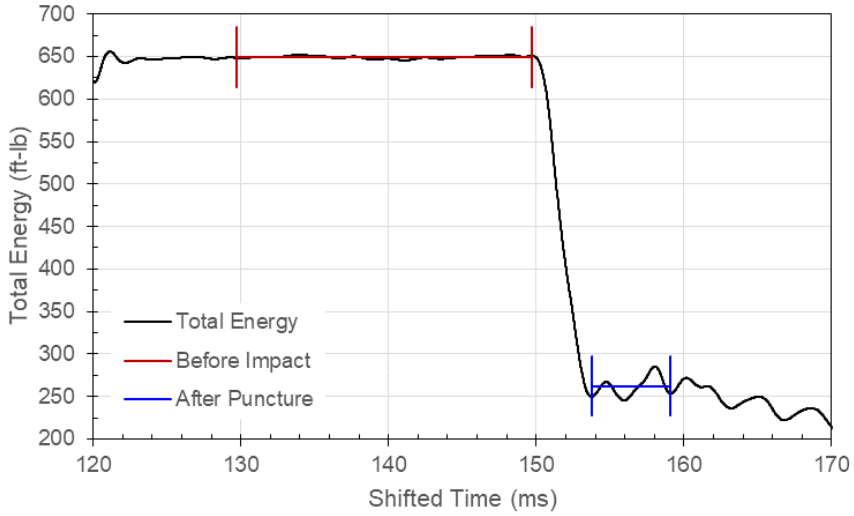

Figure 236: Total Energy, Test 90, Specimen T250-21, 1.000-Inch Semi-spherical Probe

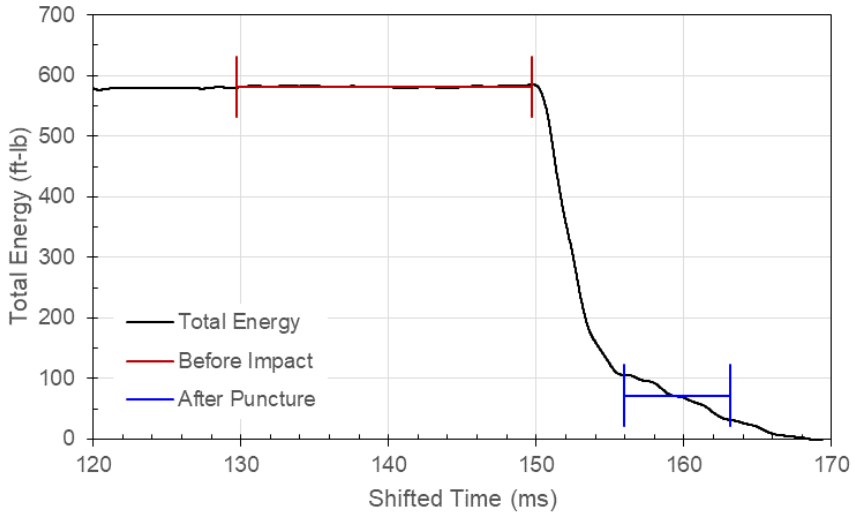

Figure 237: Total Energy, Test 91, Specimen T250-27, 1.000-Inch Semi-spherical Probe

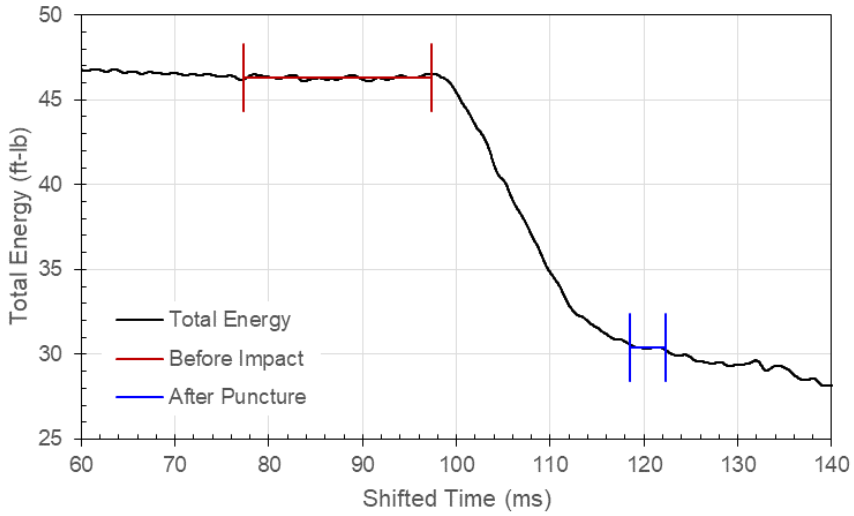

Figure 238: Total Energy, Test 103, Specimen T051-01, 0.500-Inch Tri-corner Probe

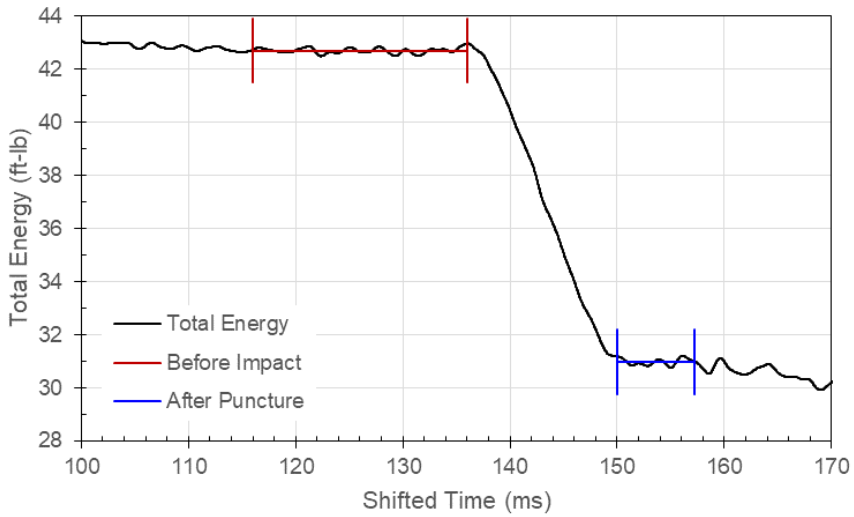

Figure 239: Total Energy, Test 104, Specimen T051-02, 0.500-Inch Tri-corner Probe

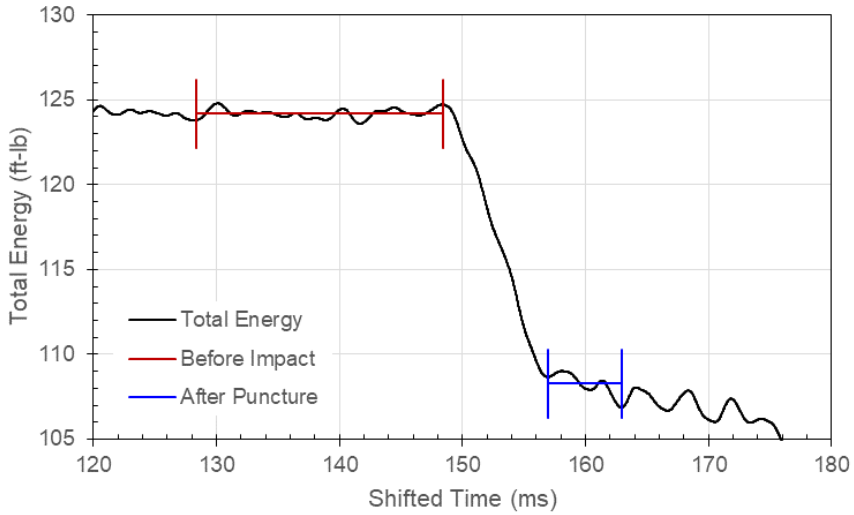

Figure 240: Total Energy, Test 4, Specimen T051-31, 0.500-Inch Tri-corner Probe

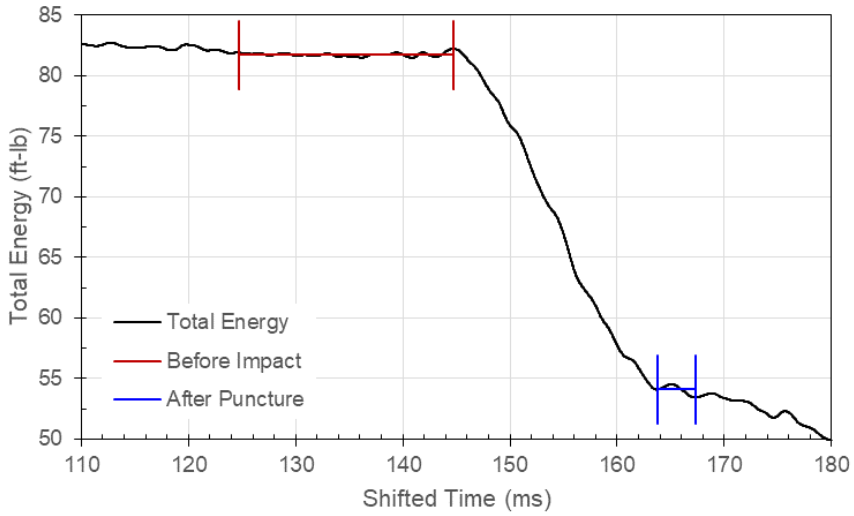

Figure 241: Total Energy, Test 105, Specimen T051-05, 1.000-Inch Tri-corner Probe

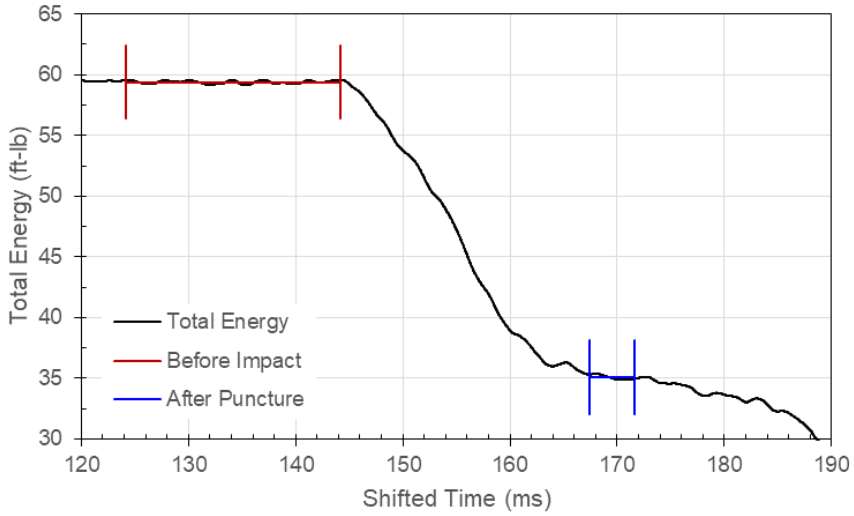

Figure 242: Total Energy, Test 106, Specimen T051-25, 1.000-Inch Tri-corner Probe

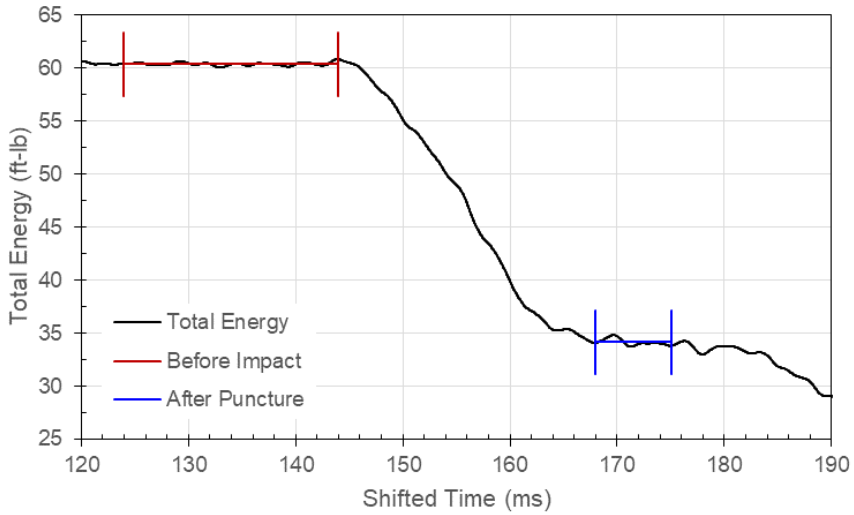

Figure 243: Total Energy, Test 107, Specimen T051-33, 1.000-Inch Tri-corner Probe

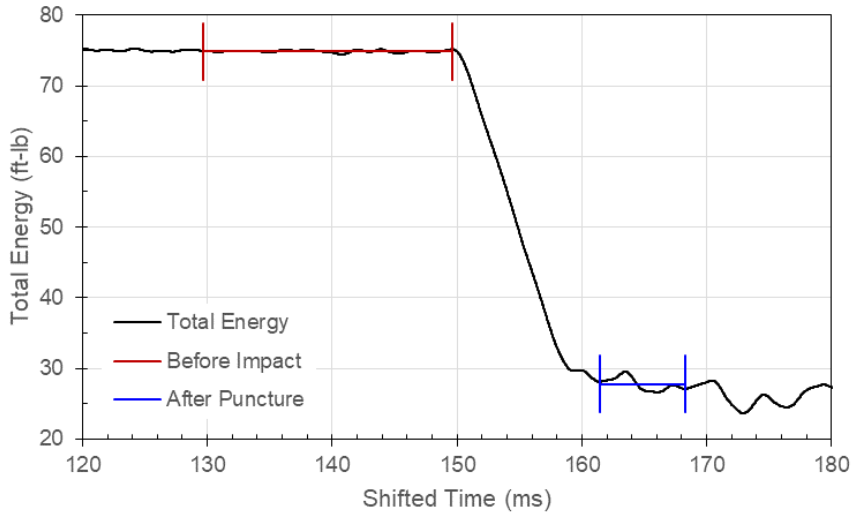

Figure 244: Total Energy, Test 92, Specimen T114-03, 0.500-Inch Tri-corner Probe

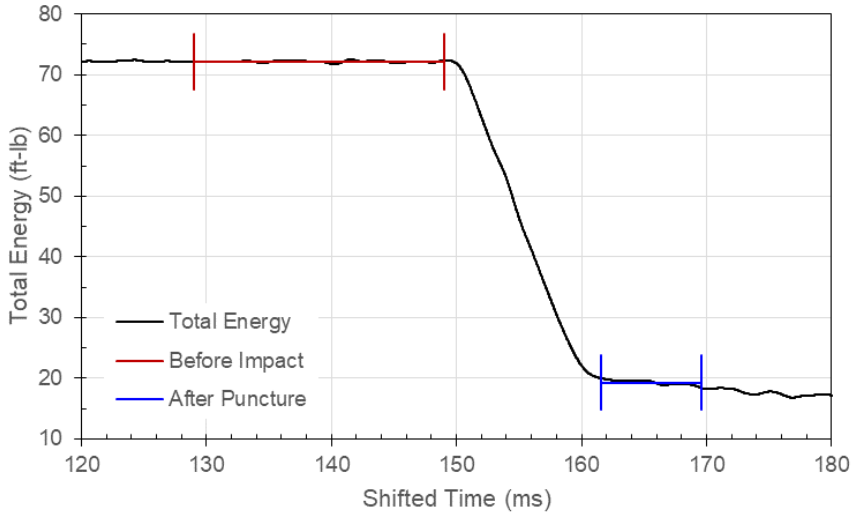

Figure 245: Total Energy, Test 93, Specimen T114-12, 0.500-Inch Tri-corner Probe

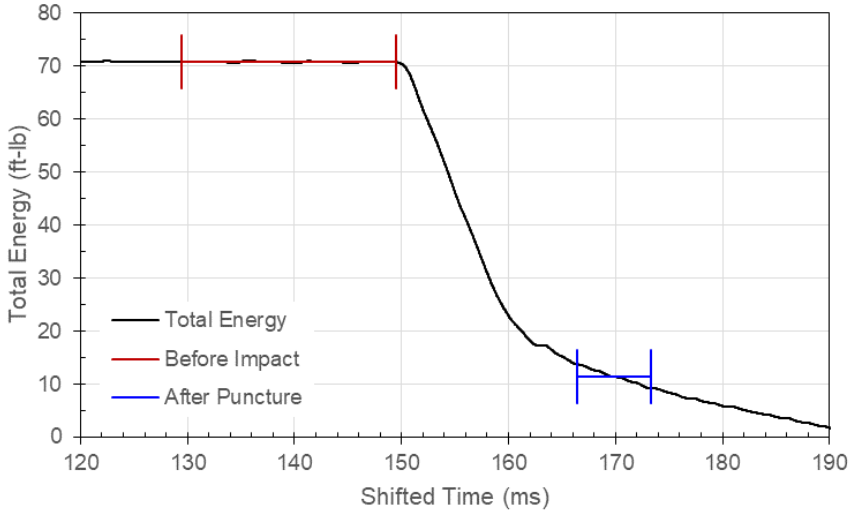

Figure 246: Total Energy, Test 94, Specimen T114-19, 0.500-Inch Tri-corner Probe

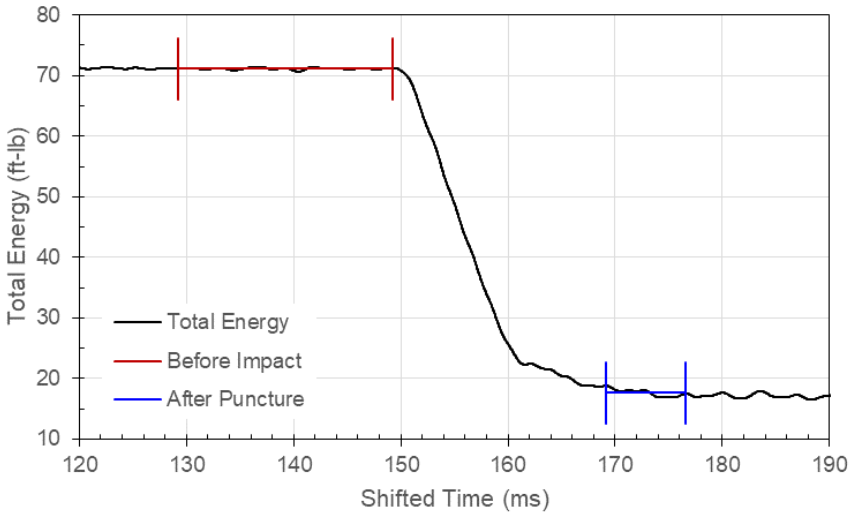

Figure 247: Total Energy, Test 95, Specimen T114-20, 0.500-Inch Tri-corner Probe

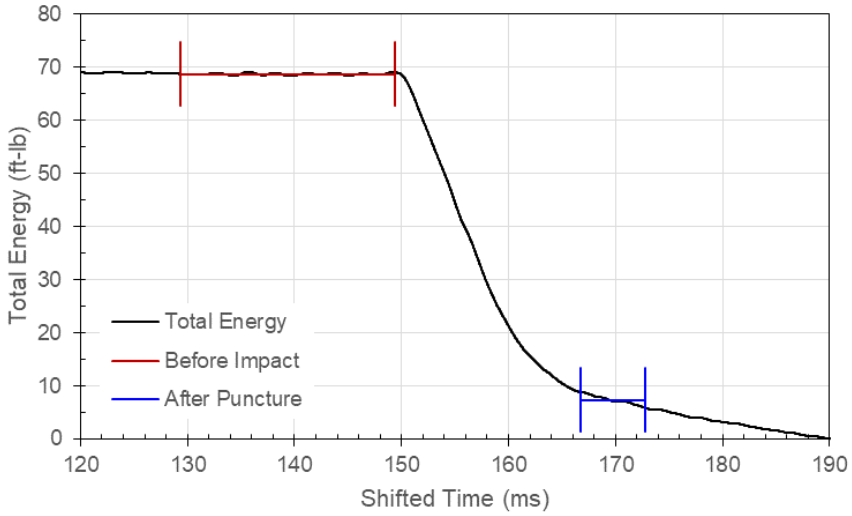

Figure 248: Total Energy, Test 96, Specimen T114-34, 0.500-Inch Tri-corner Probe

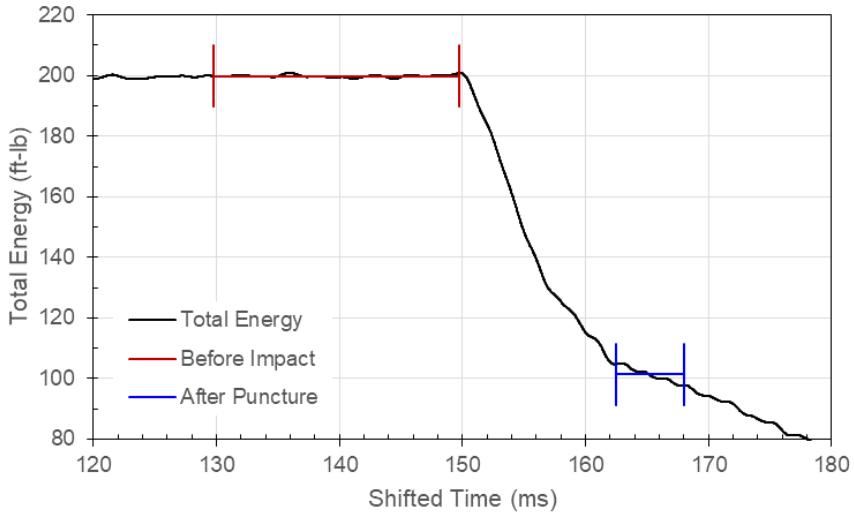

Figure 249: Total Energy, Test 108, Specimen T114-01, 1.000-Inch Tri-corner Probe

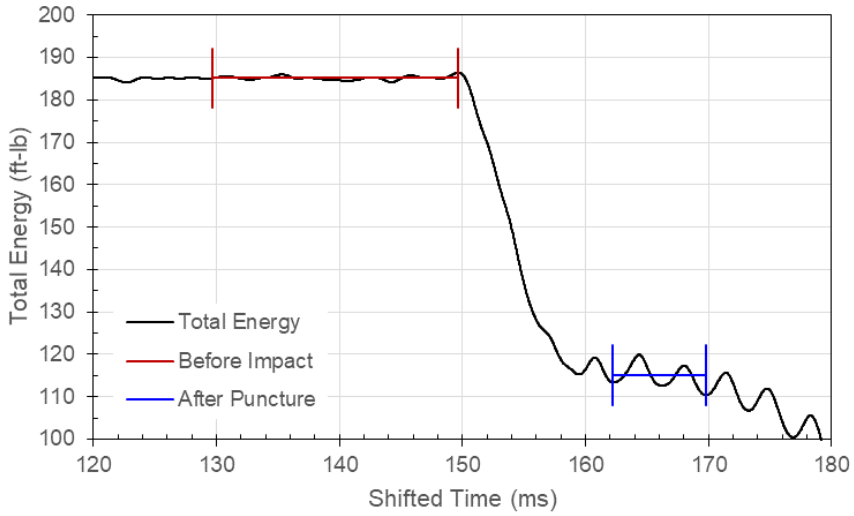

Figure 250: Total Energy, Test 109, Specimen T114-02, 1.000-Inch Tri-corner Probe

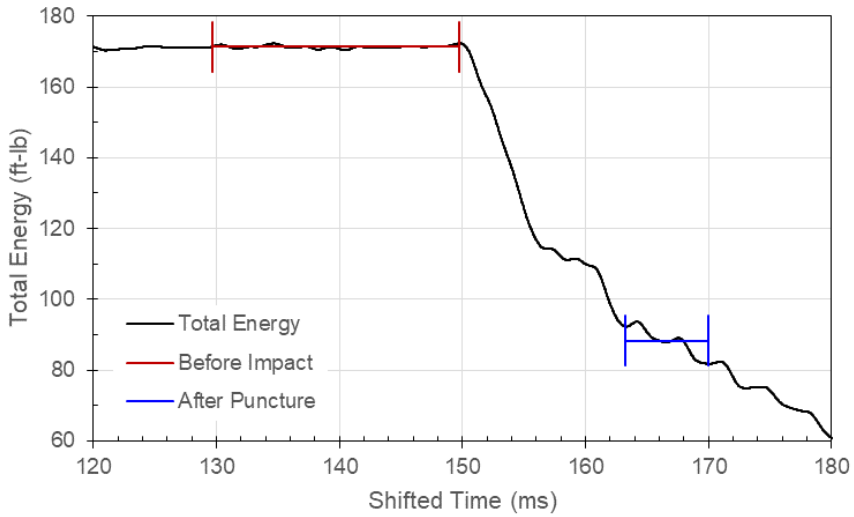

Figure 251: Total Energy, Test 110, Specimen T114-10, 1.000-Inch Tri-corner Probe

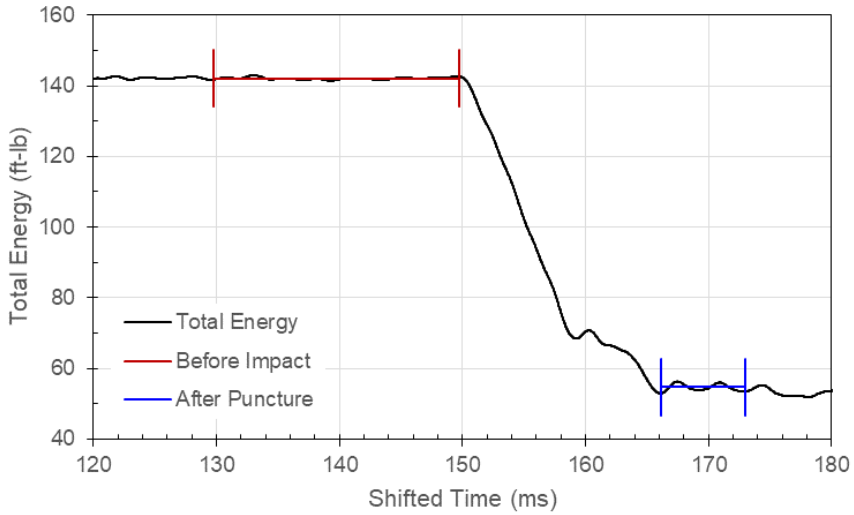

Figure 252: Total Energy, Test 111, Specimen T114-11, 1.000-Inch Tri-corner Probe

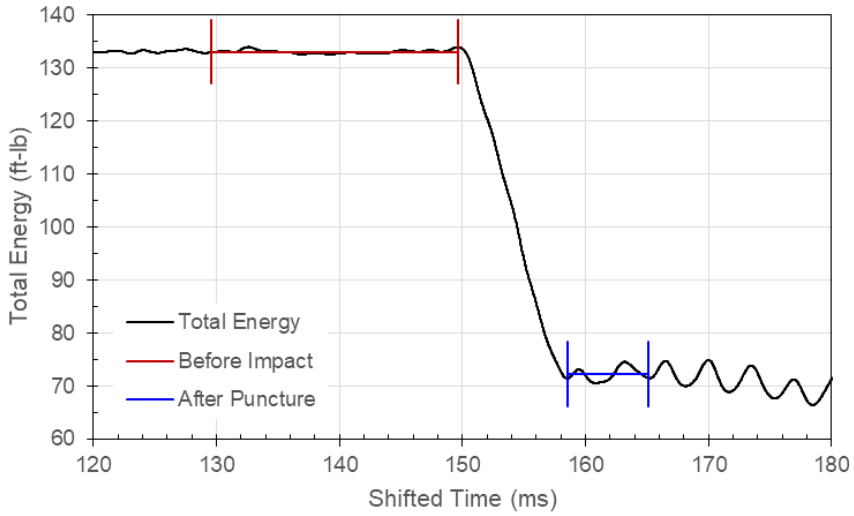

Figure 253: Total Energy, Test 112, Specimen T114-26, 1.000-Inch Tri-corner Probe

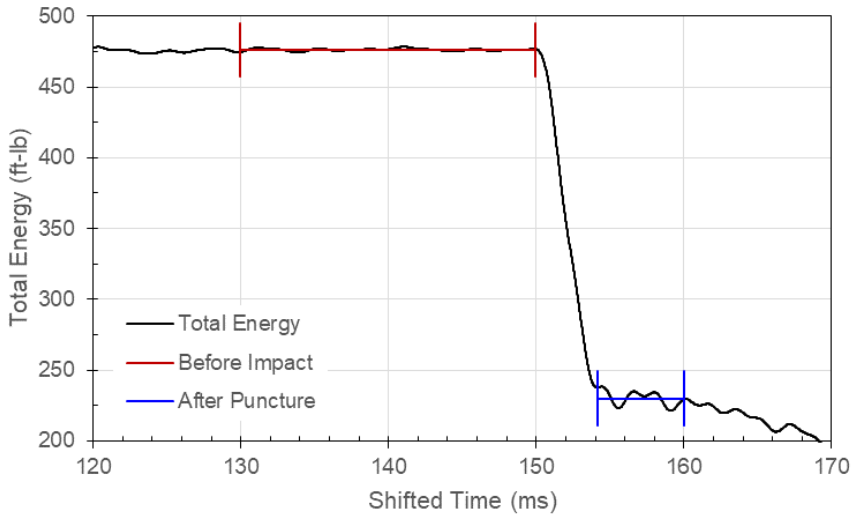

Figure 254: Total Energy, Test 98, Specimen T250-01, 0.500-Inch Tri-corner Probe

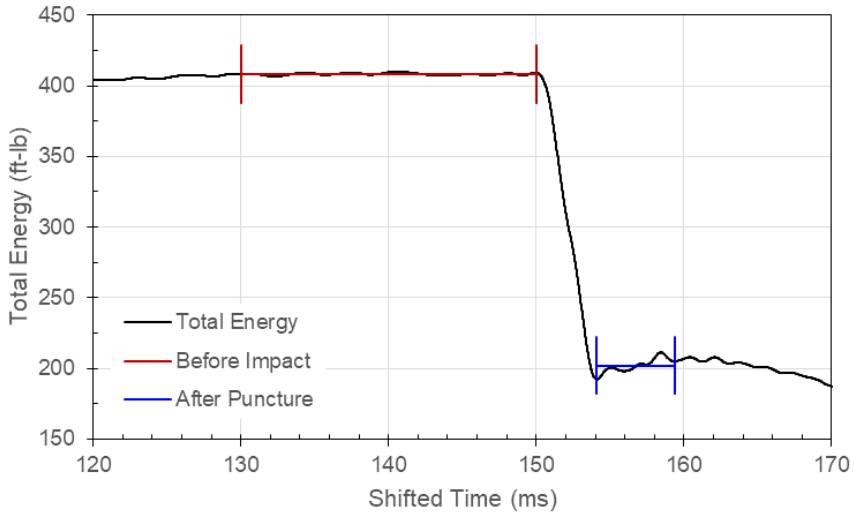

Figure 255: Total Energy, Test 99, Specimen T250-10, 0.500-Inch Tri-corner Probe

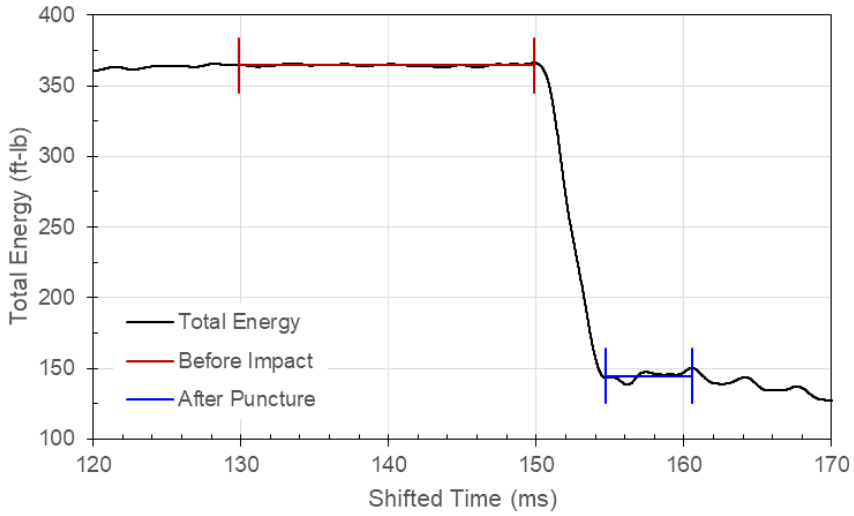

Figure 256: Total Energy, Test 100, Specimen T250-19, 0.500-Inch Tri-corner Probe

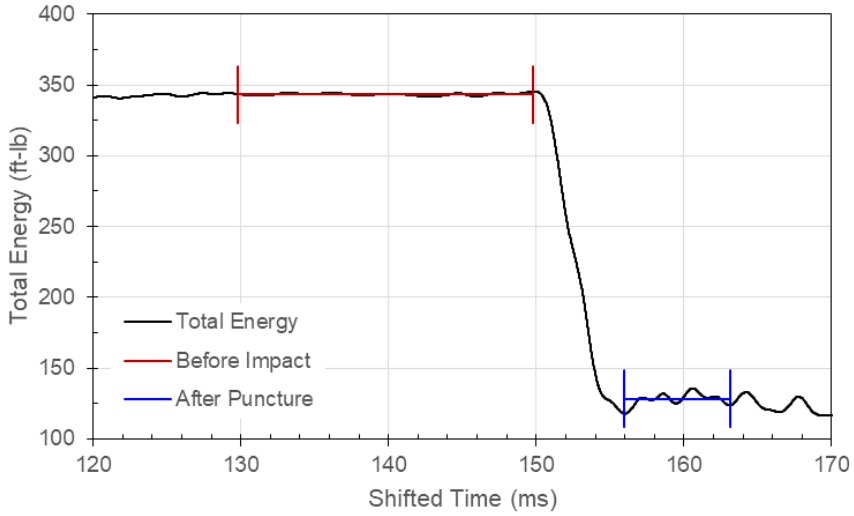

Figure 257: Total Energy, Test 101, Specimen T250-25, 0.500-Inch Tri-corner Probe

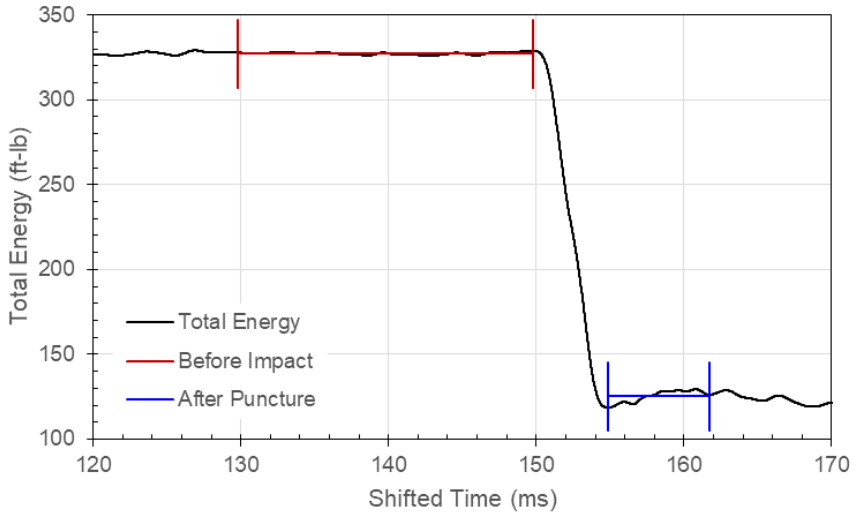

Figure 258: Total Energy, Test 102, Specimen T250-31, 0.500-Inch Tri-corner Probe

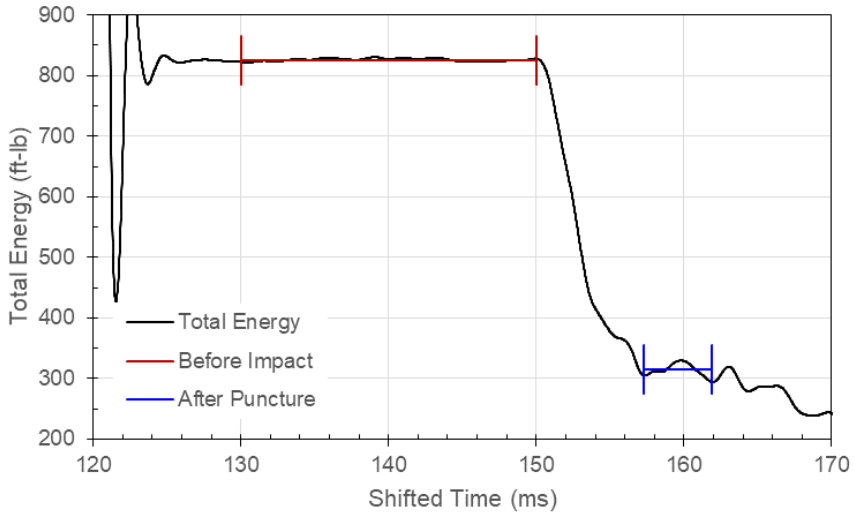

Figure 259: Total Energy, Test 113, Specimen T250-02, 1.000-Inch Tri-corner Probe

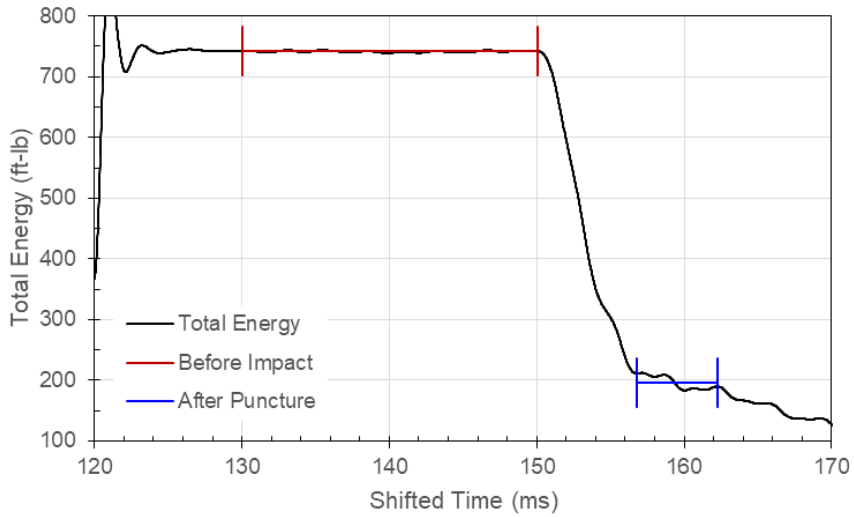

Figure 260: Total Energy, Test 114, Specimen T250-03, 1.000-Inch Tri-corner Probe

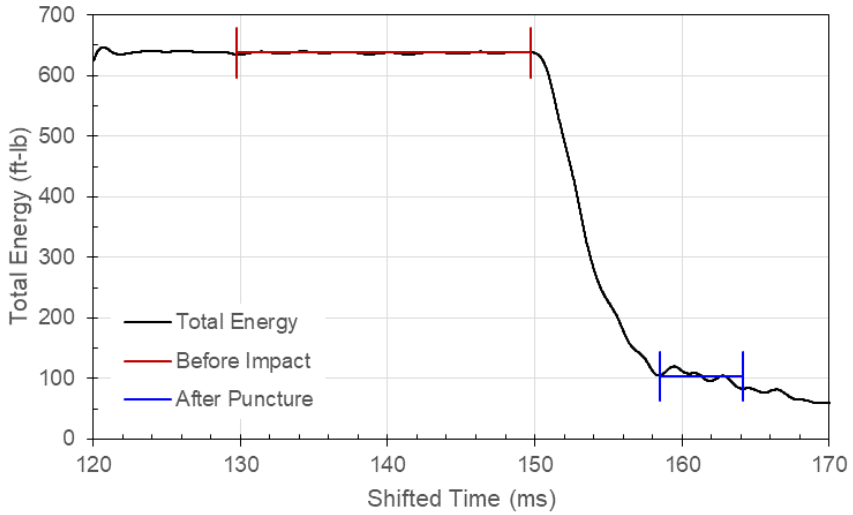

Figure 261: Total Energy, Test 115, Specimen T250-11, 1.000-Inch Tri-corner Probe

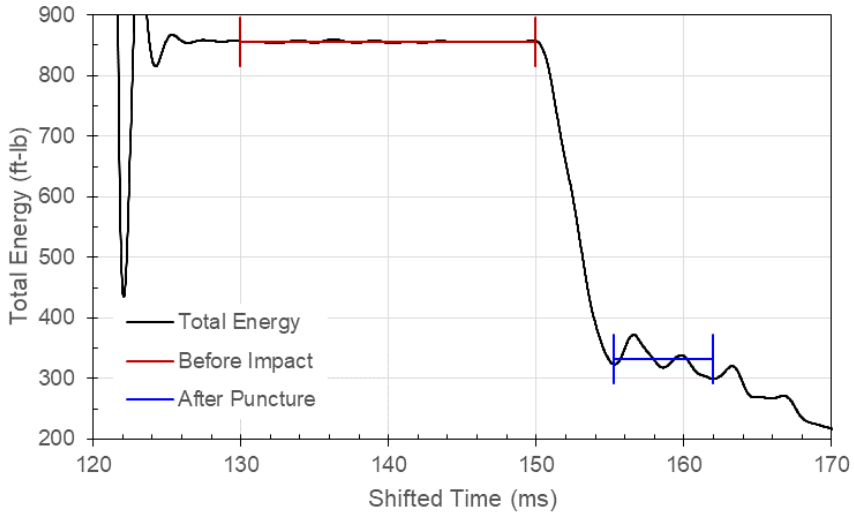

Figure 262: Total Energy, Test 116, Specimen T250-12, 1.000-Inch Tri-corner Probe

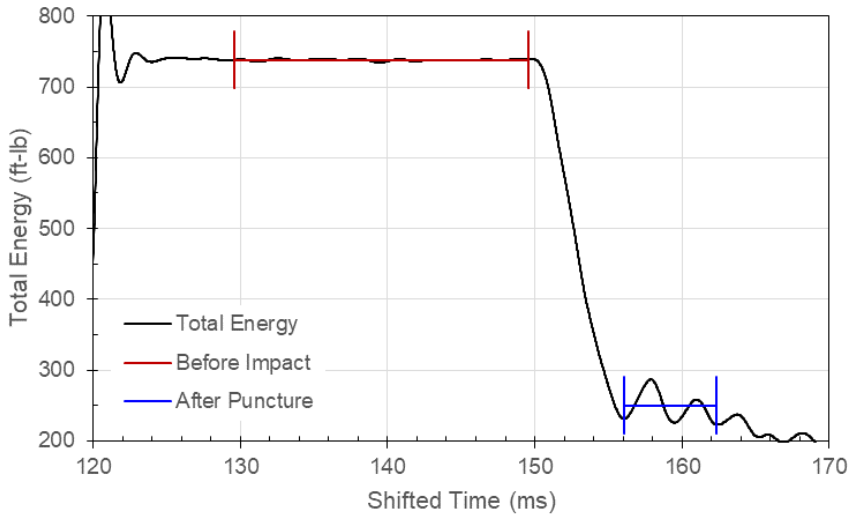

Figure 263: Total Energy, Test 117, Specimen T250-26, 1.000-Inch Tri-corner Probe

Appendix C: Velocity

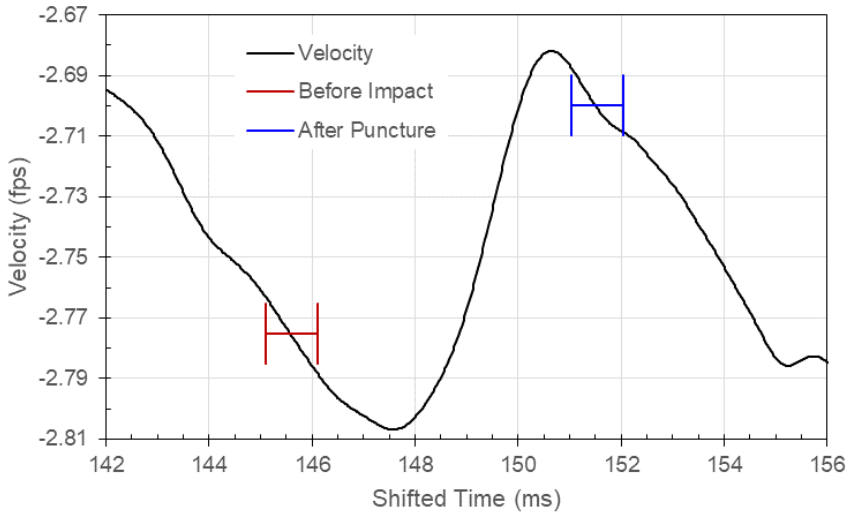

Figure 264: Carriage Velocity, Test 11, Specimen T051-24, 0.250-Inch Flat Probe

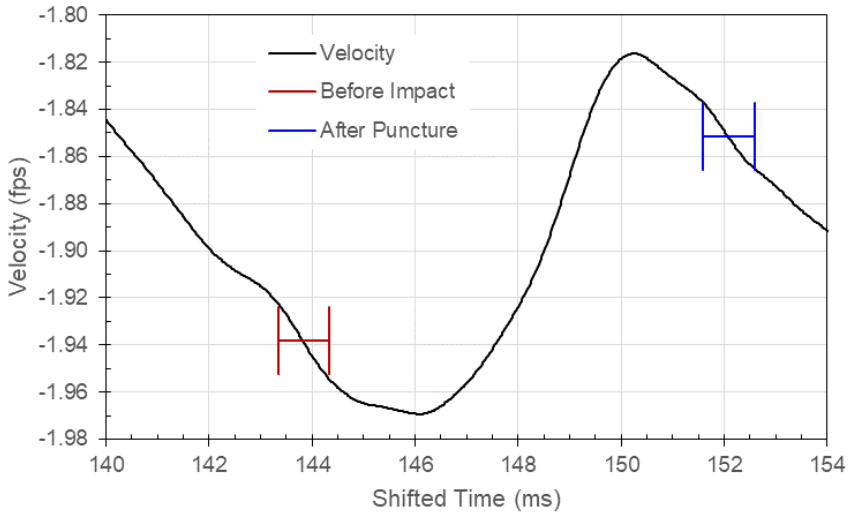

Figure 265: Carriage Velocity, Test 12, Specimen T051-26, 0.250-Inch Flat Probe

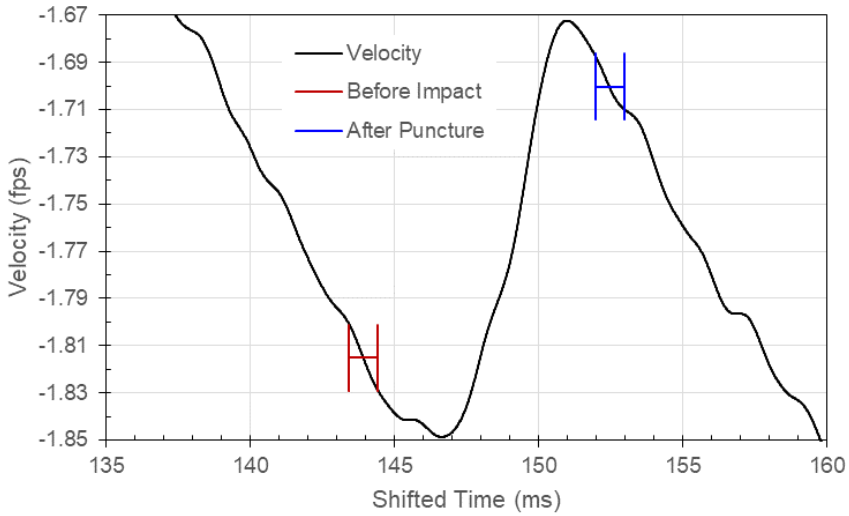

Figure 266: Carriage Velocity, Test 16, Specimen T051-28, 0.250-Inch Flat Probe

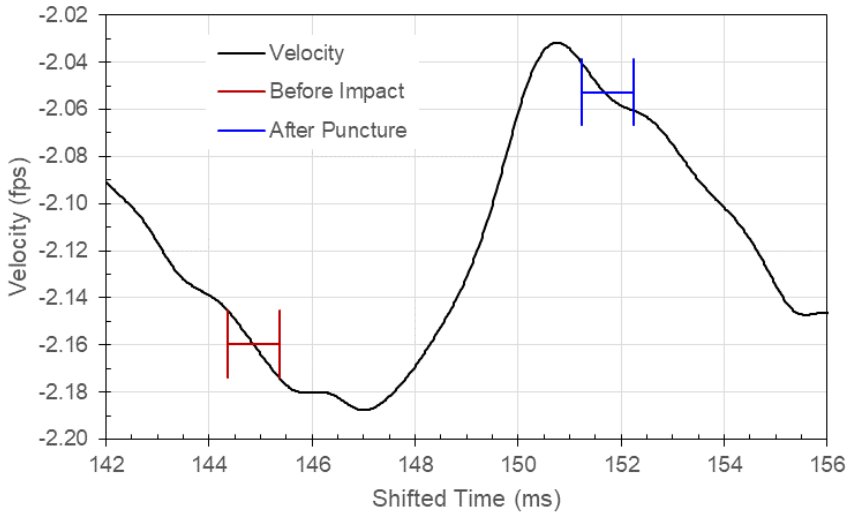

Figure 267: Carriage Velocity, Test 17, Specimen T051-29, 0.250-Inch Flat Probe

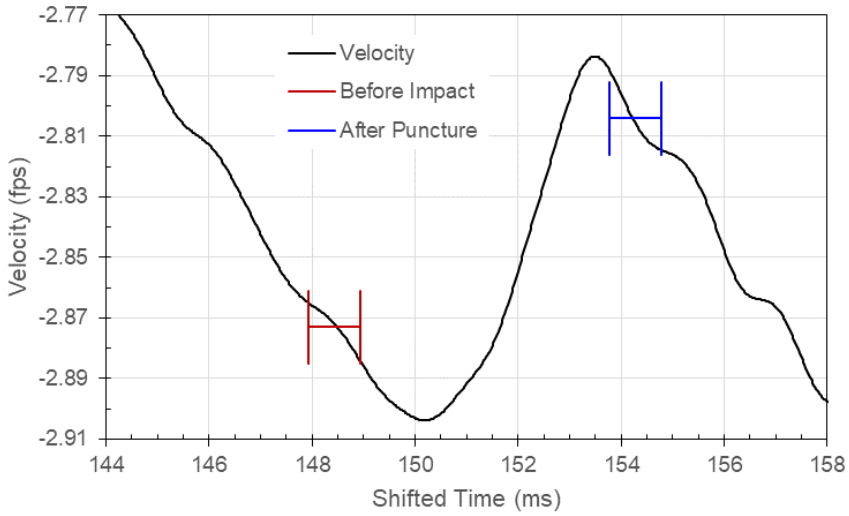

Figure 268: Carriage Velocity, Test 6, Specimen T051-30, 0.250-Inch Flat Probe

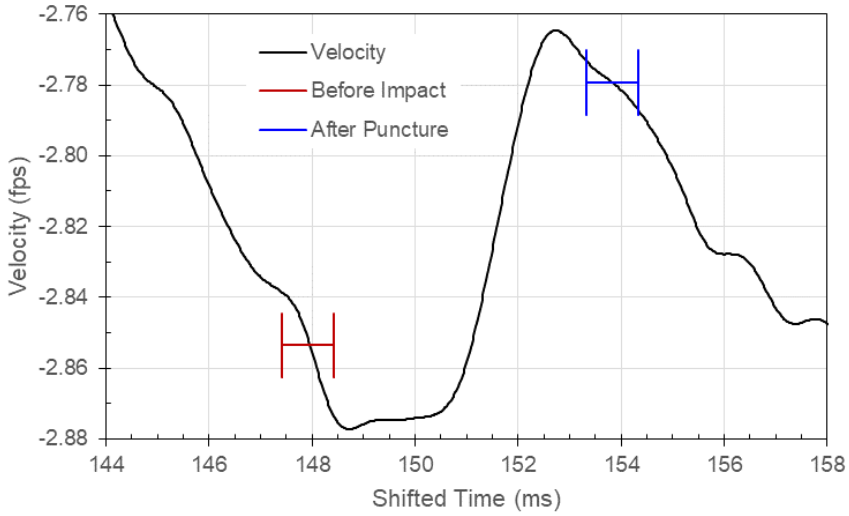

Figure 269: Carriage Velocity, Test 5, Specimen T051-32, 0.250-Inch Flat Probe

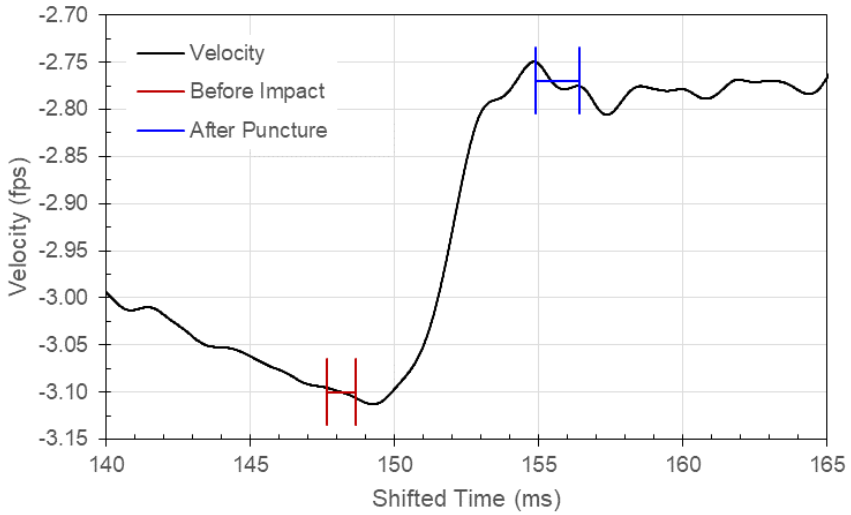

Figure 270: Carriage Velocity, Test 28, Specimen T051-03, 0.500-Inch Flat Probe

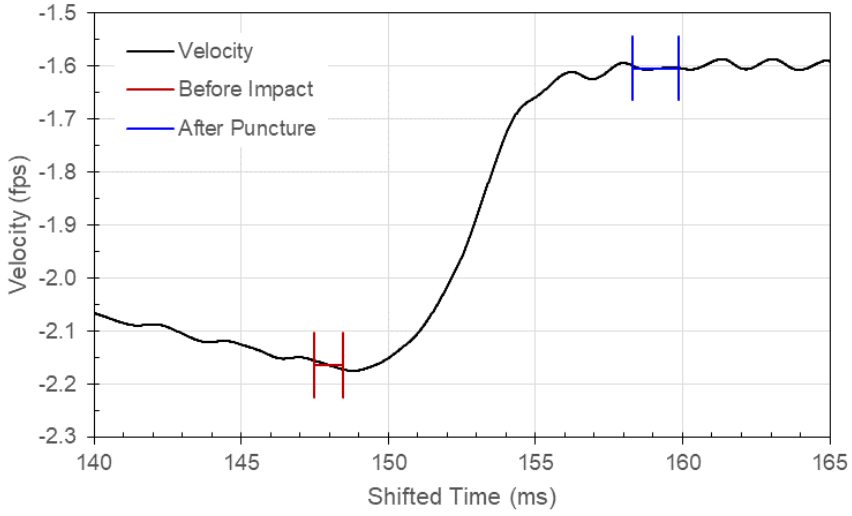

Figure 271: Carriage Velocity, Test 29, Specimen T051-08, 0.500-Inch Flat Probe

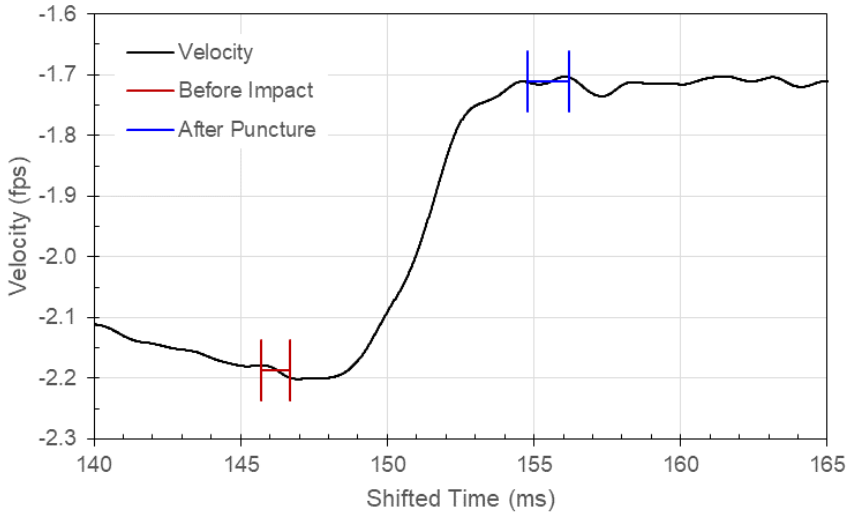

Figure 272: Carriage Velocity, Test 30, Specimen T051-10, 0.500-Inch Flat Probe

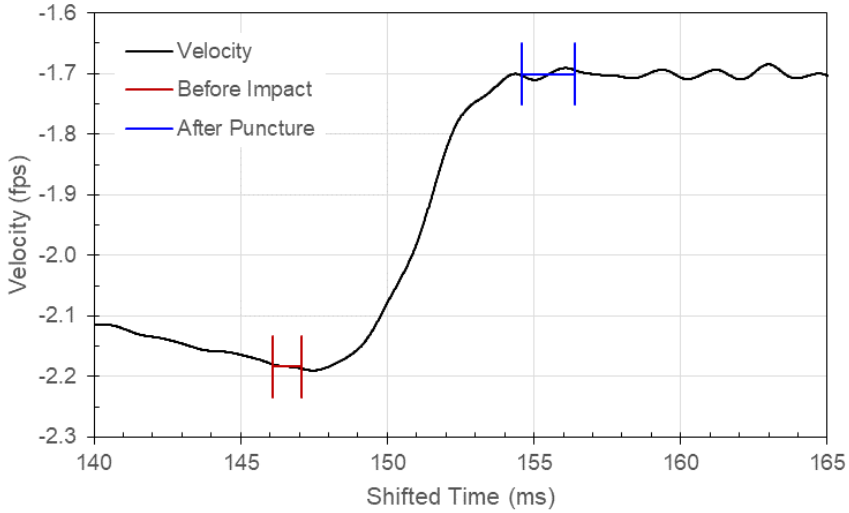

Figure 273: Carriage Velocity, Test 31, Specimen T051-21, 0.500-Inch Flat Probe

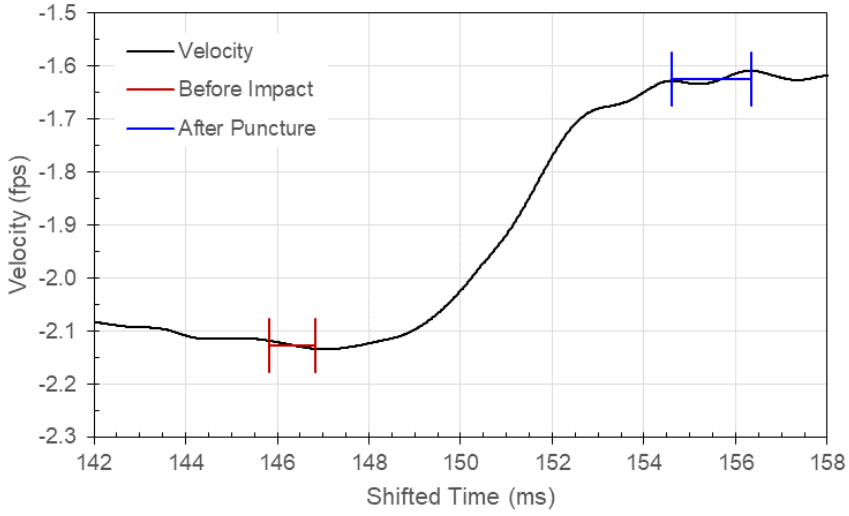

Figure 274: Carriage Velocity, Test 32, Specimen T051-27, 0.500-Inch Flat Probe

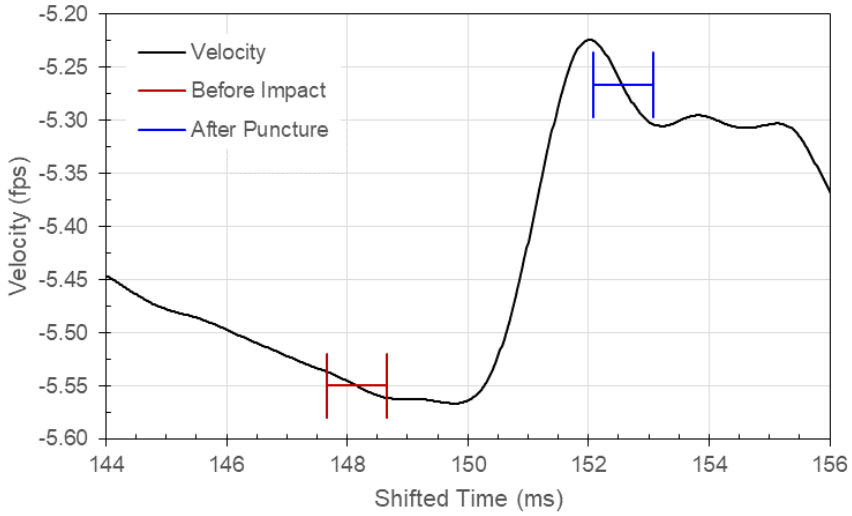

Figure 275: Carriage Velocity, Test 44, Specimen T051-14, 1.000-Inch Flat Probe

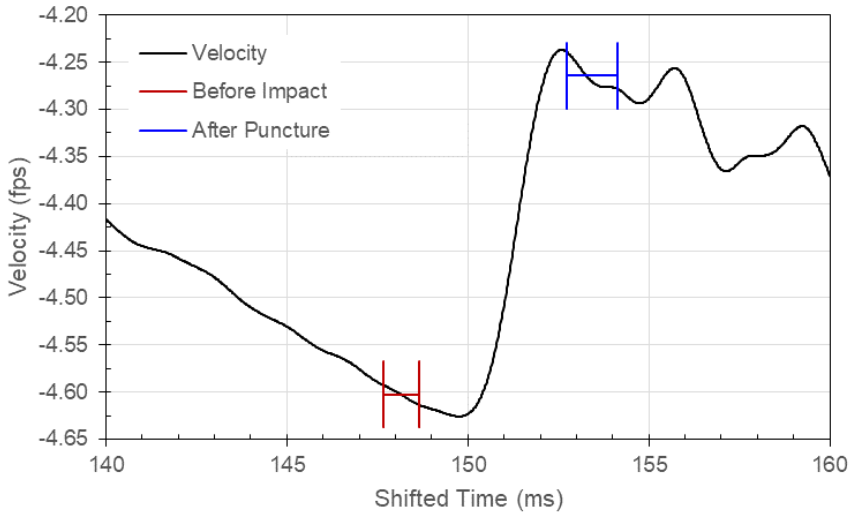

Figure 276: Carriage Velocity, Test 45, Specimen T051-15, 1.000-Inch Flat Probe

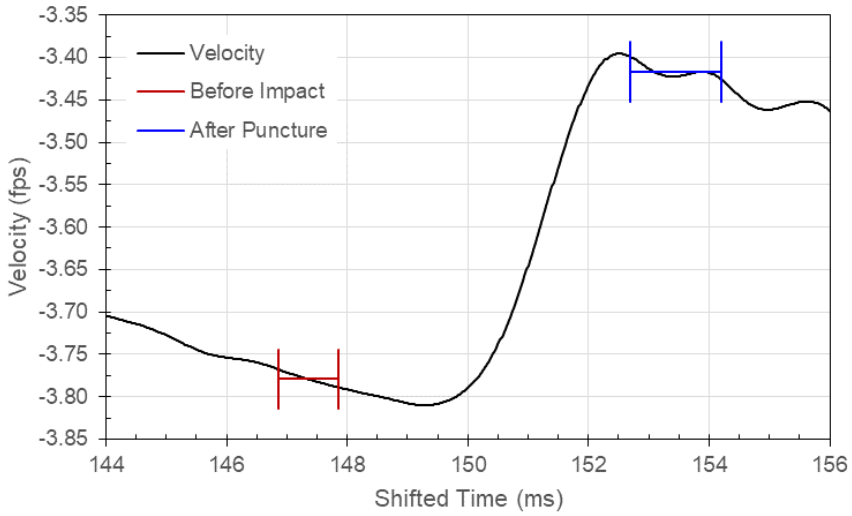

Figure 277: Carriage Velocity, Test 46, Specimen T051-16, 1.000-Inch Flat Probe

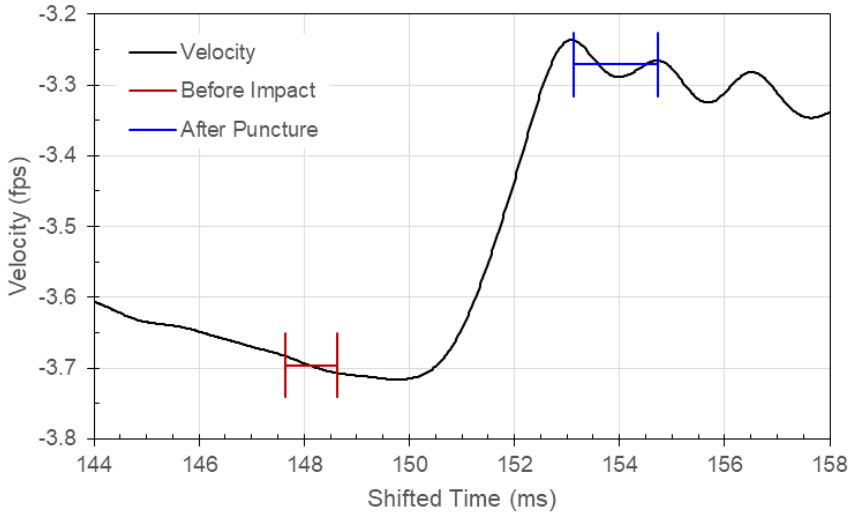

Figure 278: Carriage Velocity, Test 48, Specimen T051-17, 1.000-Inch Flat Probe

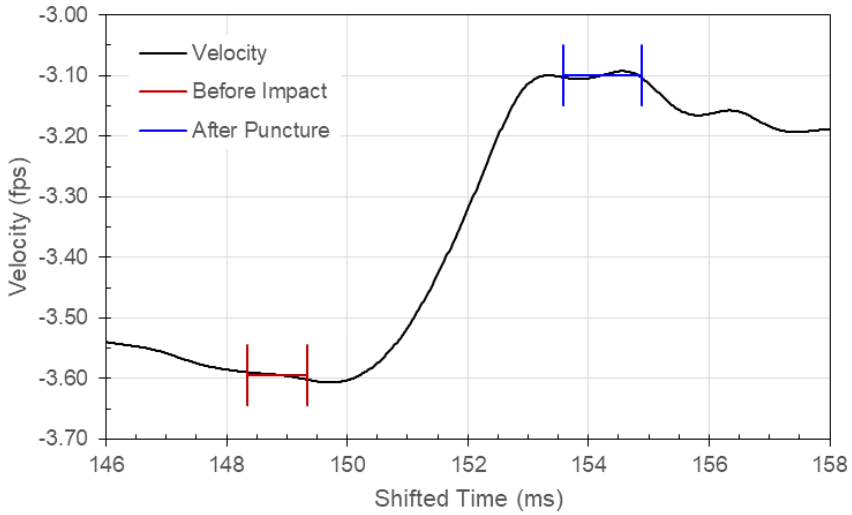

Figure 279: Carriage Velocity, Test 49, Specimen T051-20, 1.000-Inch Flat Probe

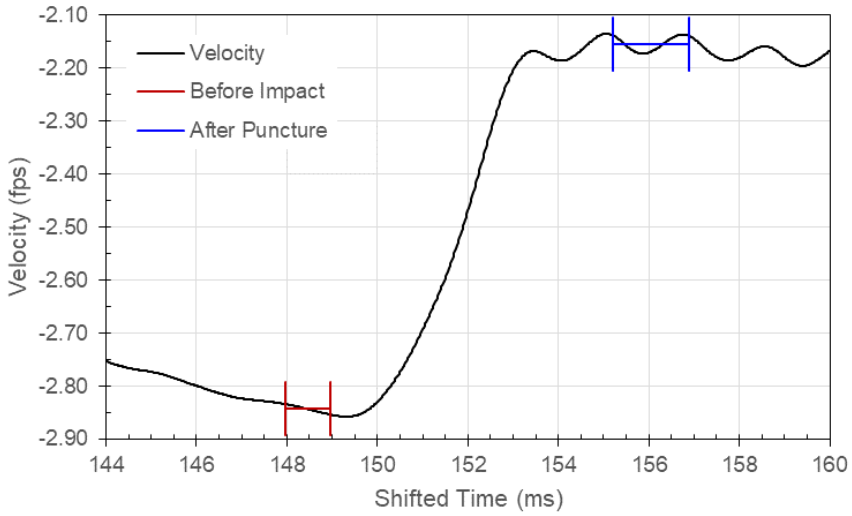

Figure 280: Carriage Velocity, Test 47, Specimen T051-35, 1.000-Inch Flat Probe

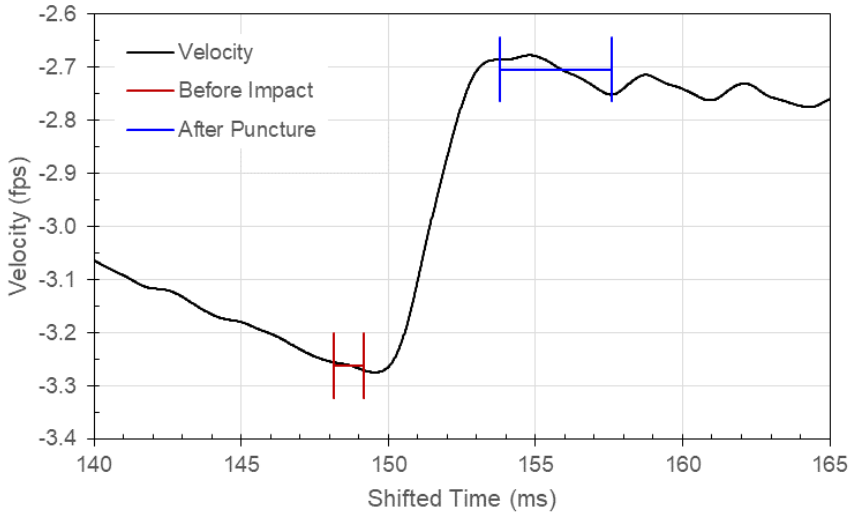

Figure 281: Carriage Velocity, Test 18, Specimen T114-08, 0.250-Inch Flat Probe

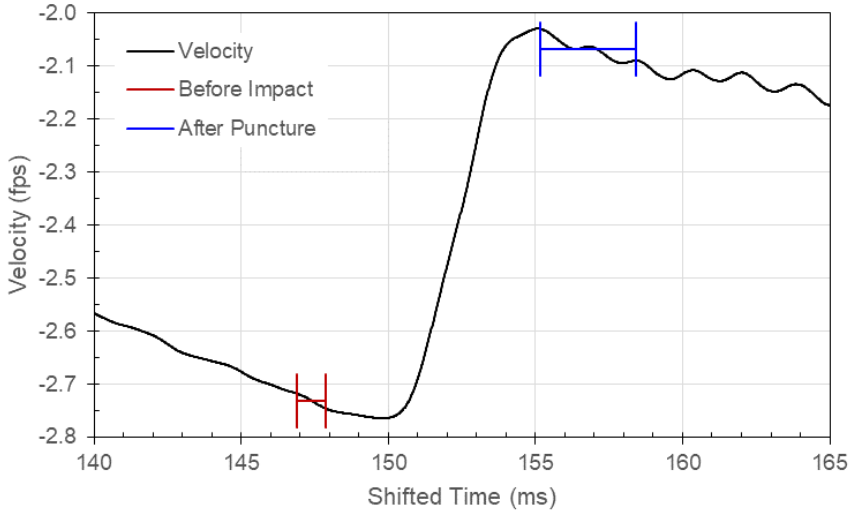

Figure 282: Carriage Velocity, Test 19, Specimen T114-16, 0.250-Inch Flat Probe

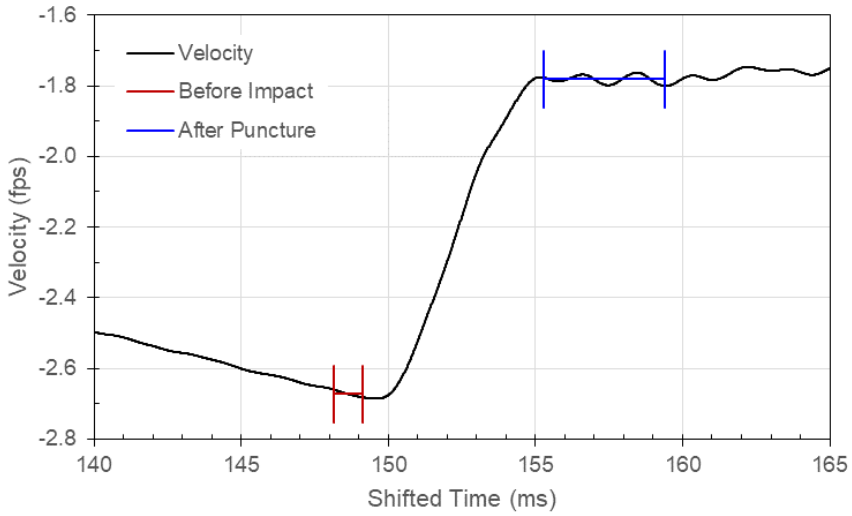

Figure 283: Carriage Velocity, Test 20, Specimen T114-17, 0.250-Inch Flat Probe

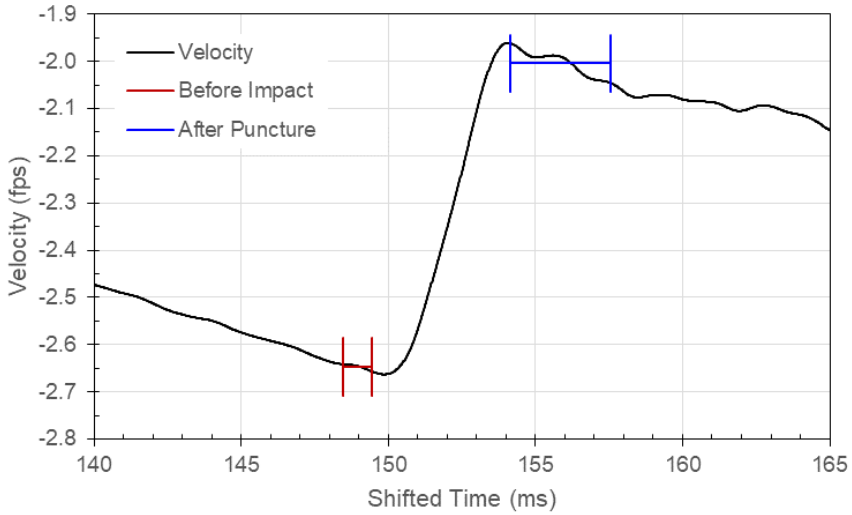

Figure 284: Carriage Velocity, Test 21, Specimen T114-23, 0.250-Inch Flat Probe

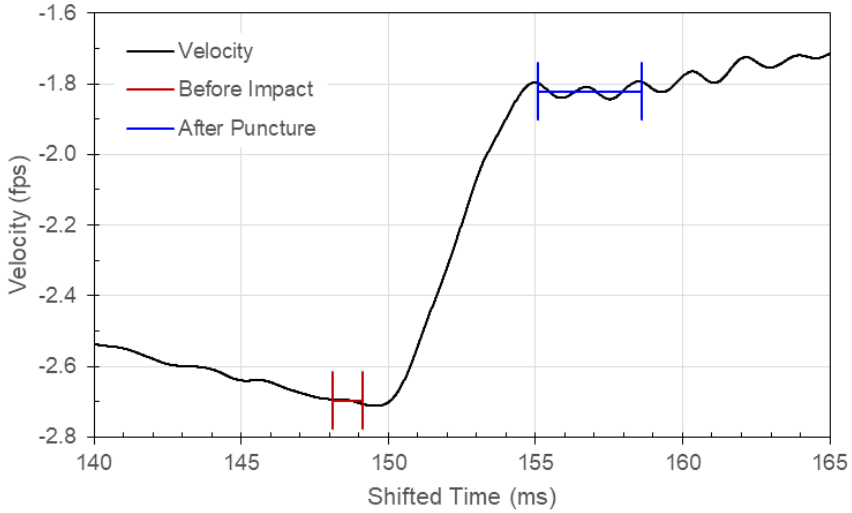

Figure 285: Carriage Velocity, Test 22, Specimen T114-24, 0.250-Inch Flat Probe

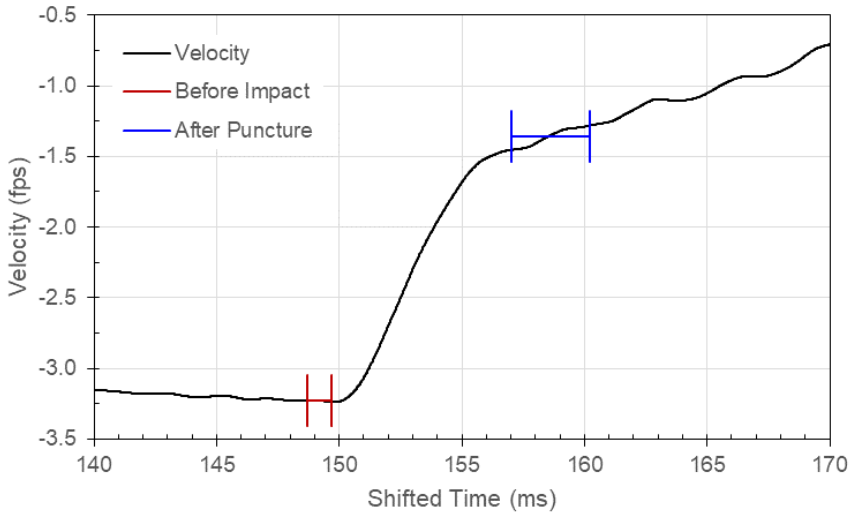

Figure 286: Carriage Velocity, Test 33, Specimen T114-07, 0.500-Inch Flat Probe

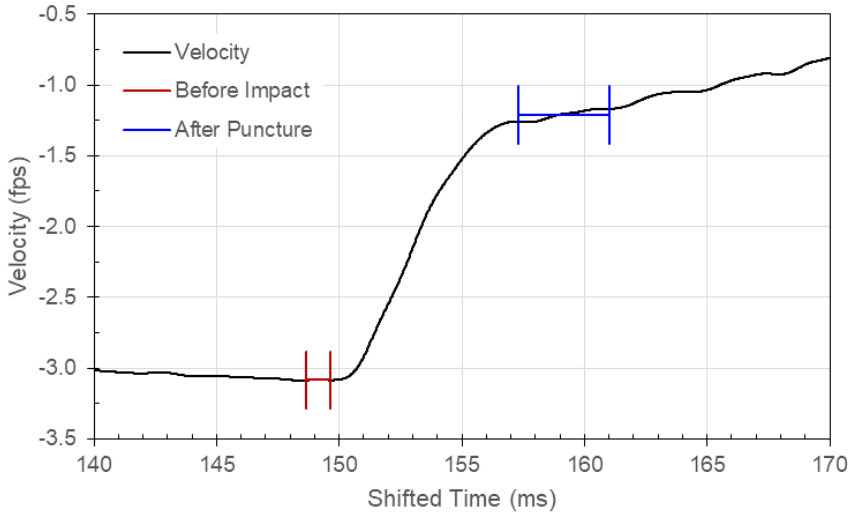

Figure 287: Carriage Velocity, Test 35, Specimen T114-09, 0.500-Inch Flat Probe

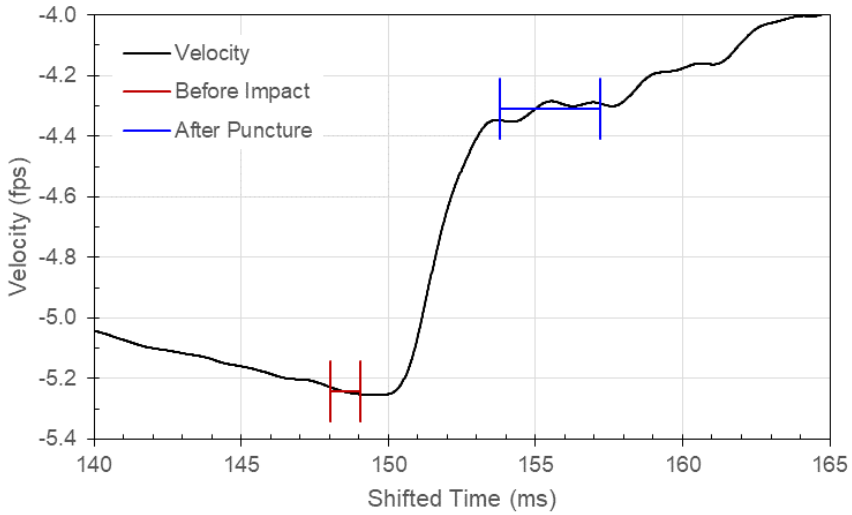

Figure 288: Carriage Velocity, Test 37, Specimen T114-27, 0.500-Inch Flat Probe

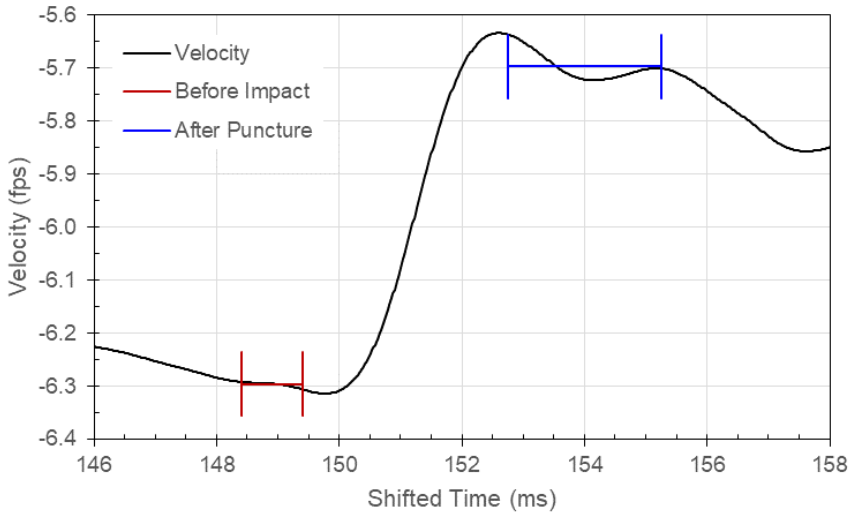

Figure 289: Carriage Velocity, Test 38, Specimen T114-30, 0.500-Inch Flat Probe

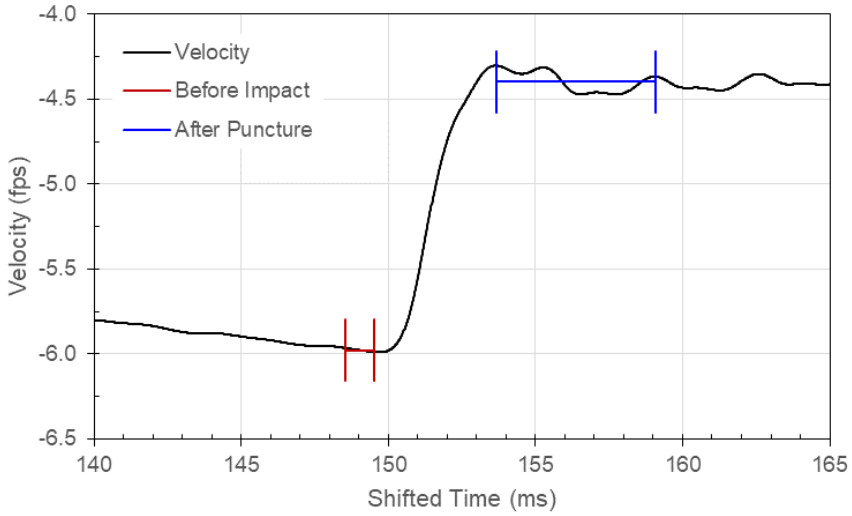

Figure 290: Carriage Velocity, Test 50, Specimen T114-05, 1.000-Inch Flat Probe

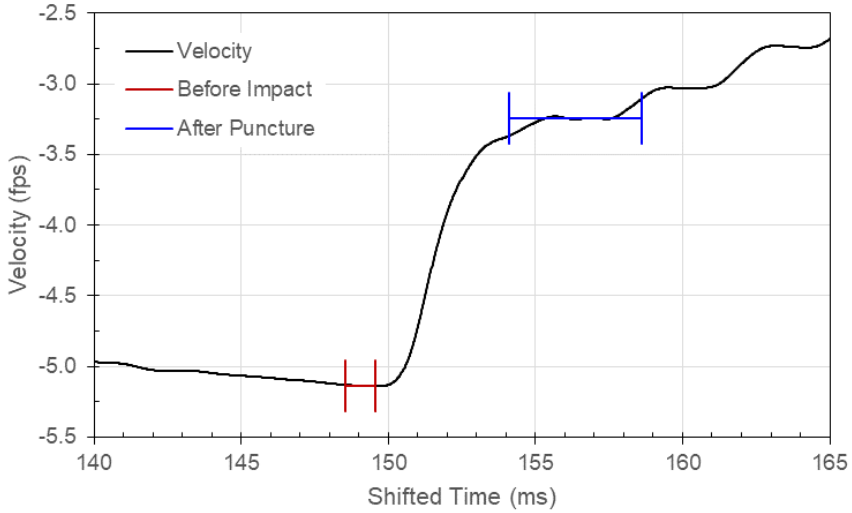

Figure 291: Carriage Velocity, Test 51, Specimen T114-13, 1.000-Inch Flat Probe

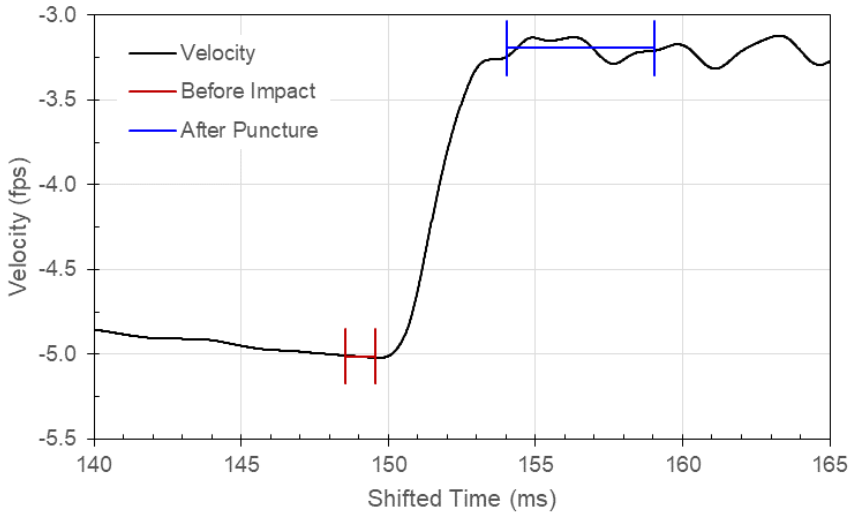

Figure 292: Carriage Velocity, Test 52, Specimen T114-14, 1.000-Inch Flat Probe

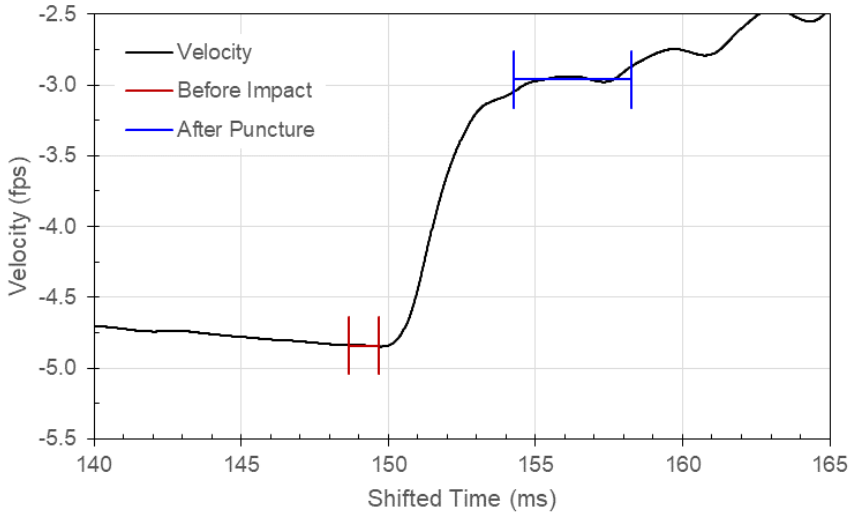

Figure 293: Carriage Velocity, Test 53, Specimen T114-21, 1.000-Inch Flat Probe

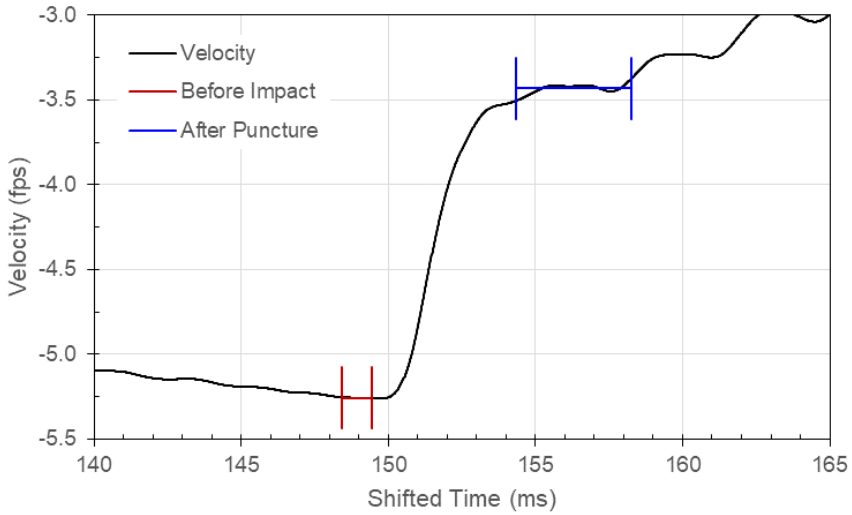

Figure 294: Carriage Velocity, Test 54, Specimen T114-29, 1.000-Inch Flat Probe

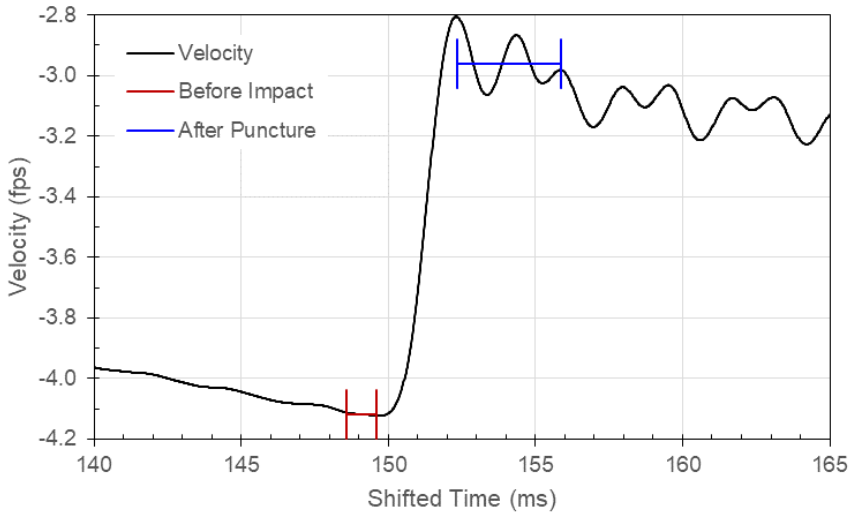

Figure 295: Carriage Velocity, Test 23, Specimen T250-08, 0.250-Inch Flat Probe

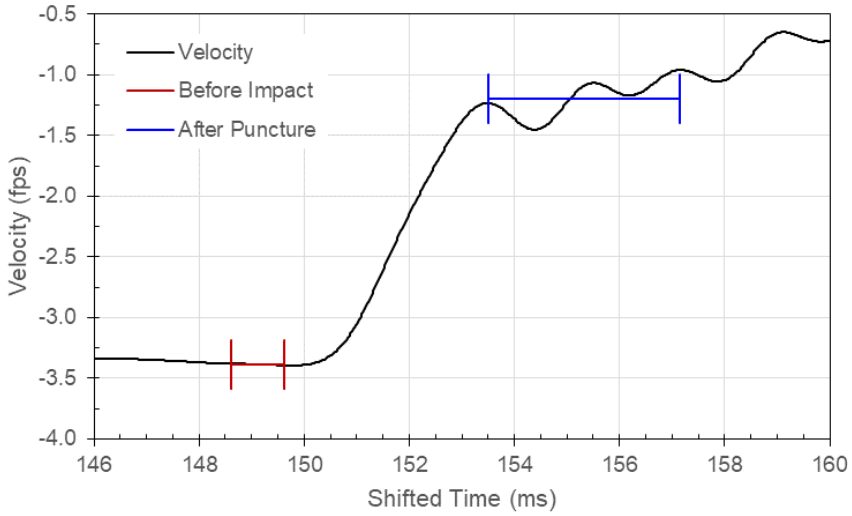

Figure 296: Carriage Velocity, Test 24, Specimen T250-16, 0.250-Inch Flat Probe

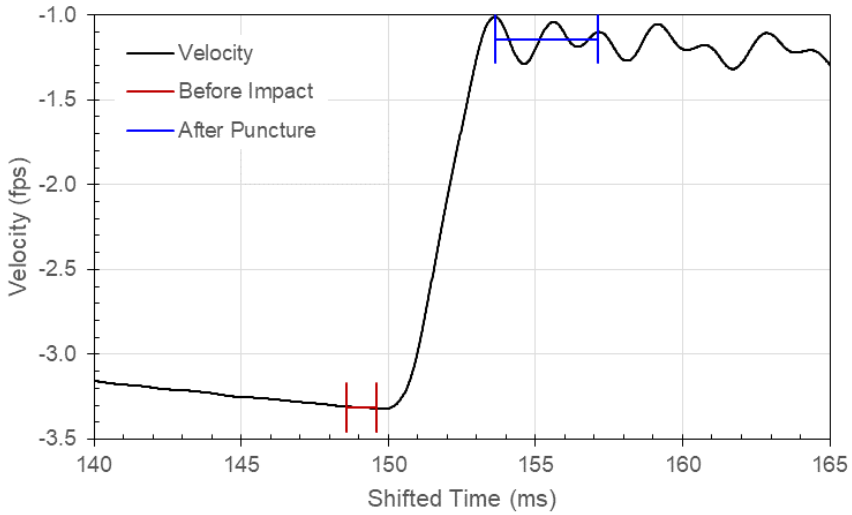

Figure 297: Carriage Velocity, Test 25, Specimen T250-17, 0.250-Inch Flat Probe

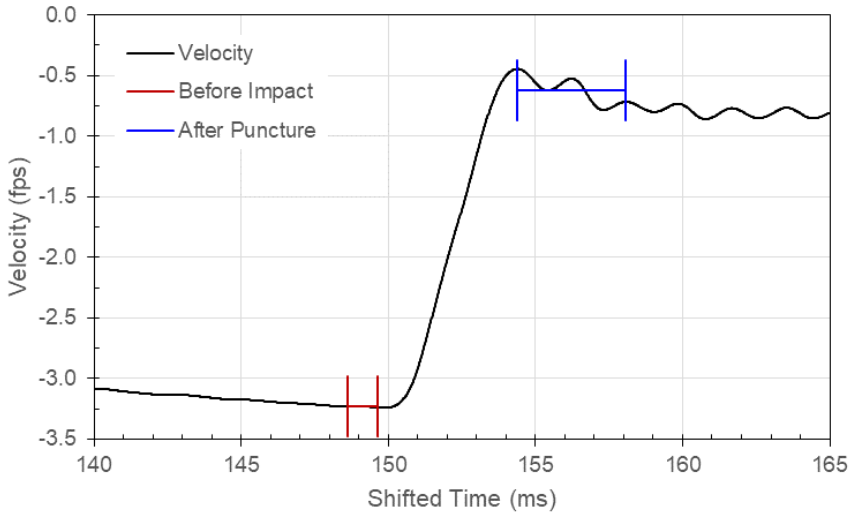

Figure 298: Carriage Velocity, Test 26, Specimen T250-23, 0.250-Inch Flat Probe

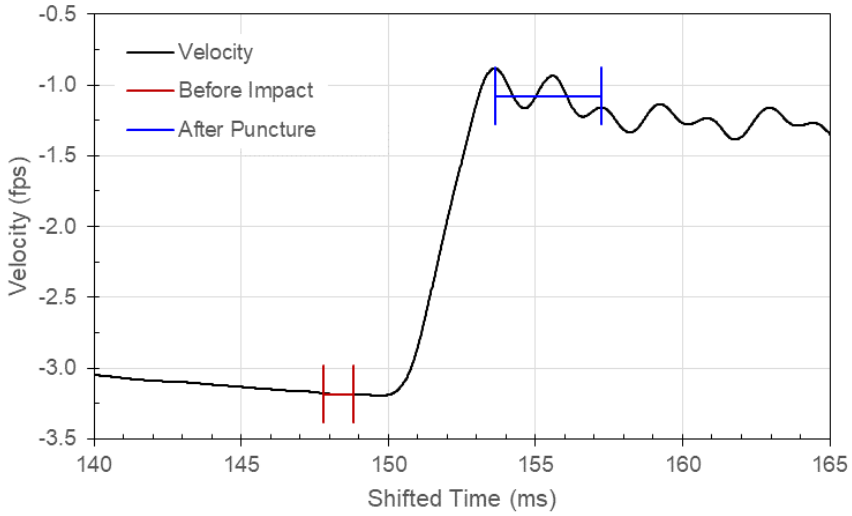

Figure 299: Carriage Velocity, Test 27, Specimen T250-29, 0.250-Inch Flat Probe

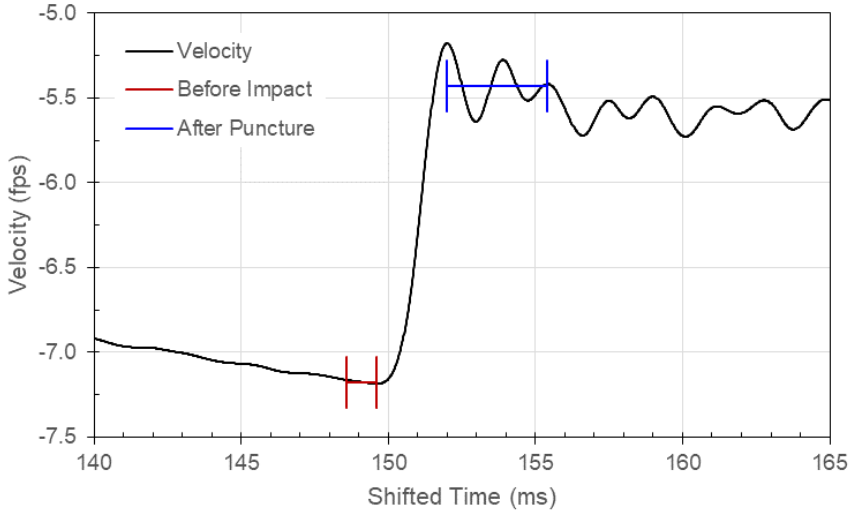

Figure 300: Carriage Velocity, Test 39, Specimen T250-07, 0.500-Inch Flat Probe

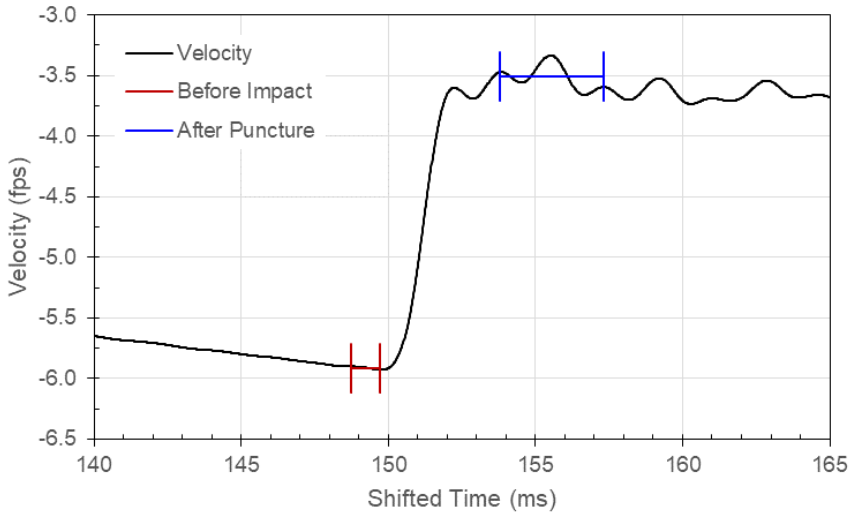

Figure 301: Carriage Velocity, Test 40, Specimen T250-09, 0.500-Inch Flat Probe

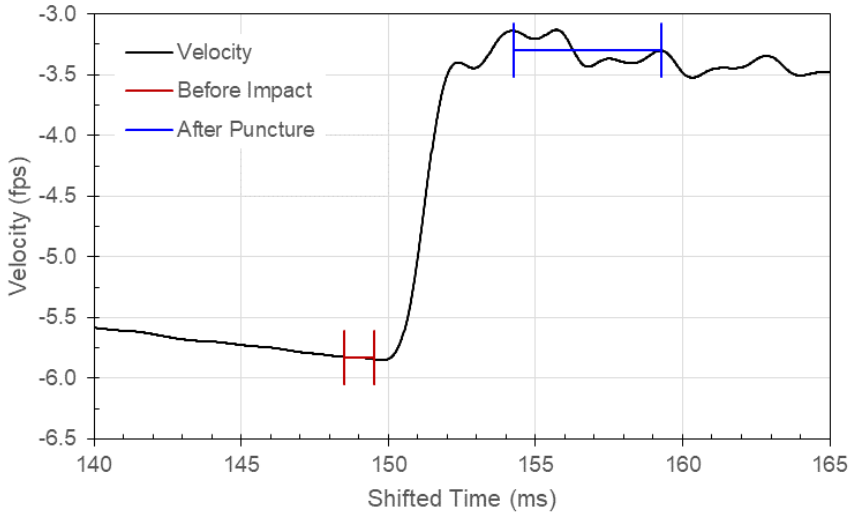

Figure 302: Carriage Velocity, Test 41, Specimen T250-18, 0.500-Inch Flat Probe

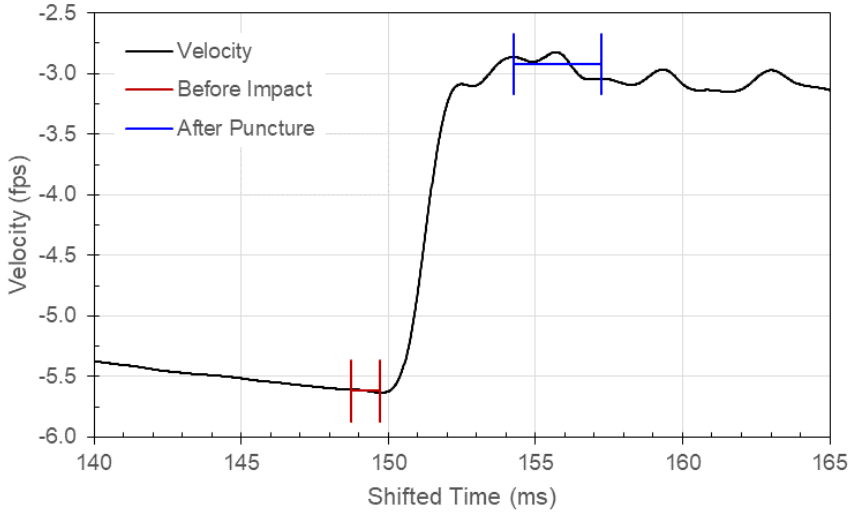

Figure 303: Carriage Velocity, Test 42, Specimen T250-24, 0.500-Inch Flat Probe

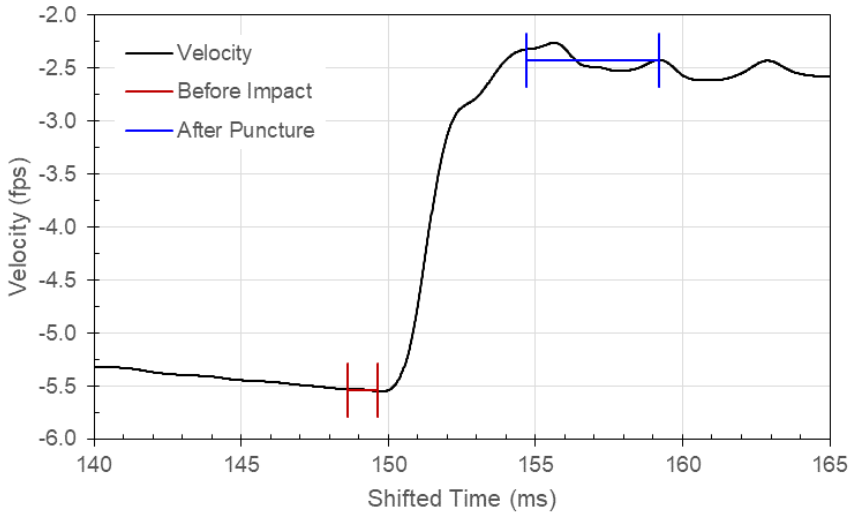

Figure 304: Carriage Velocity, Test 43, Specimen T250-30, 0.500-Inch Flat Probe

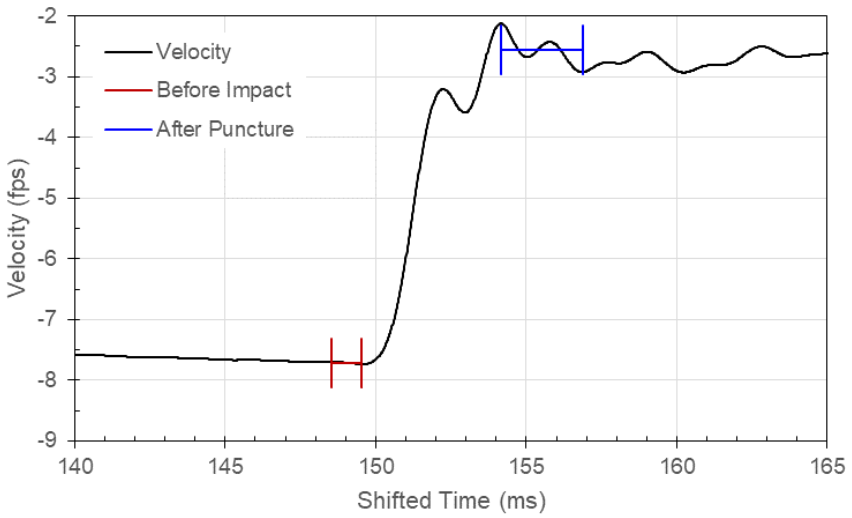

Figure 305: Carriage Velocity, Test 55, Specimen T250-06, 1.000-Inch Flat Probe

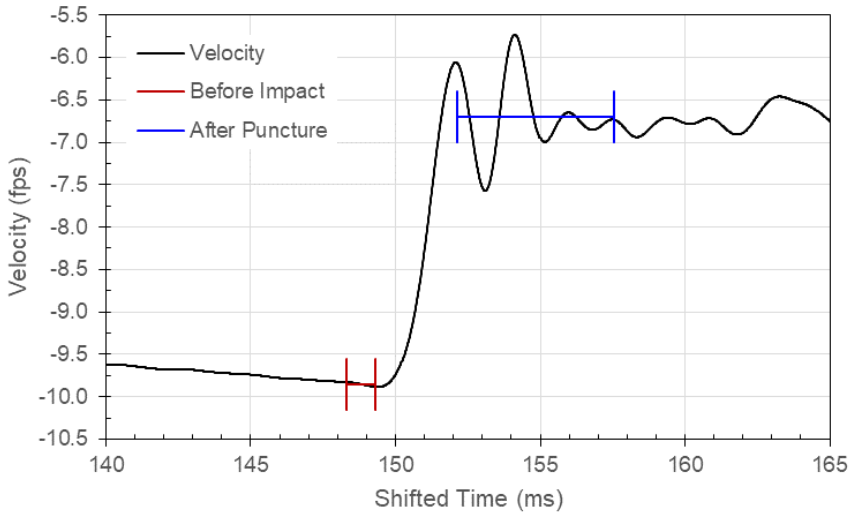

Figure 306: Carriage Velocity, Test 56, Specimen T250-15, 1.000-Inch Flat Probe

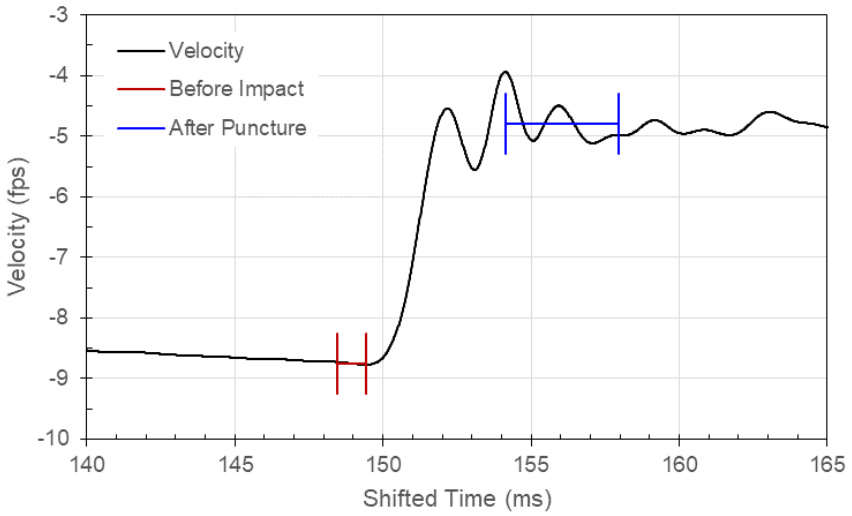

Figure 307: Carriage Velocity, Test 57, Specimen T250-28, 1.000-Inch Flat Probe

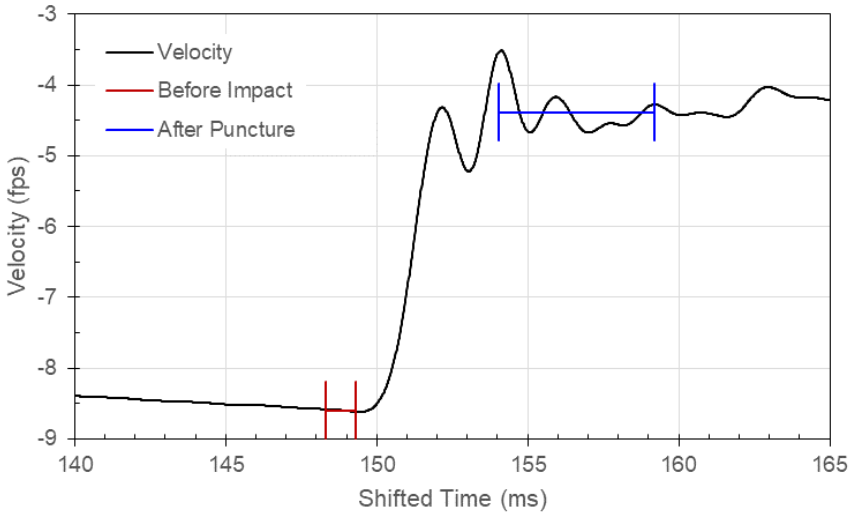

Figure 308: Carriage Velocity, Test 58, Specimen T250-34, 1.000-Inch Flat Probe

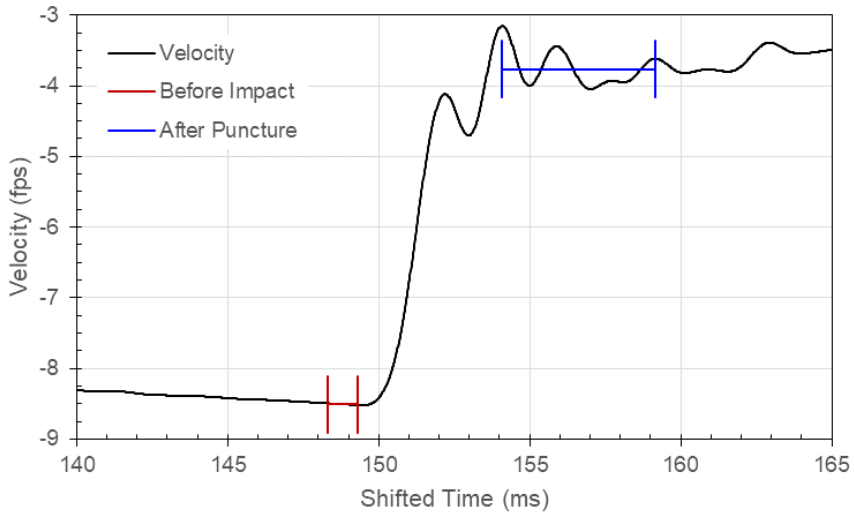

Figure 309: Carriage Velocity, Test 59, Specimen T250-35, 1.000-Inch Flat Probe

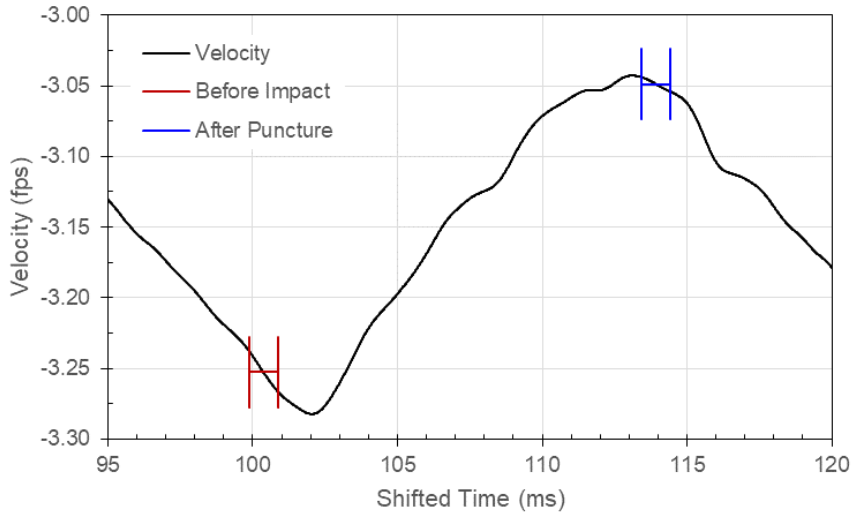

Figure 310: Carriage Velocity, Test 61, Specimen T051-06, 0.500-Inch Semi-spherical Probe

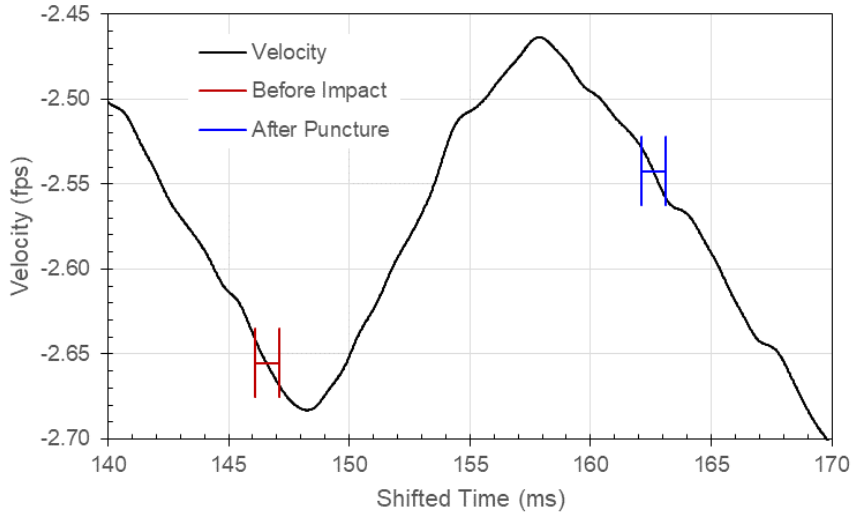

Figure 311: Carriage Velocity, Test 62, Specimen T051-07, 0.500-Inch Semi-spherical Probe

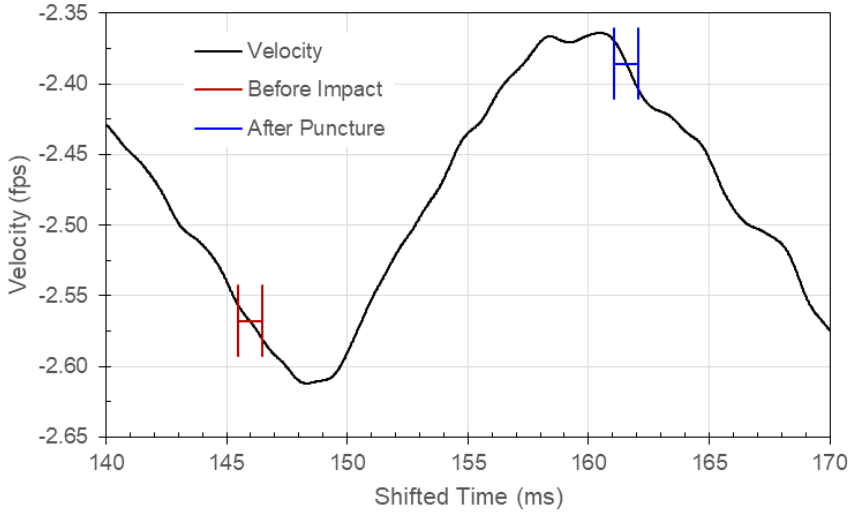

Figure 312: Carriage Velocity, Test 63, Specimen T051-11, 0.500-Inch Semi-spherical Probe

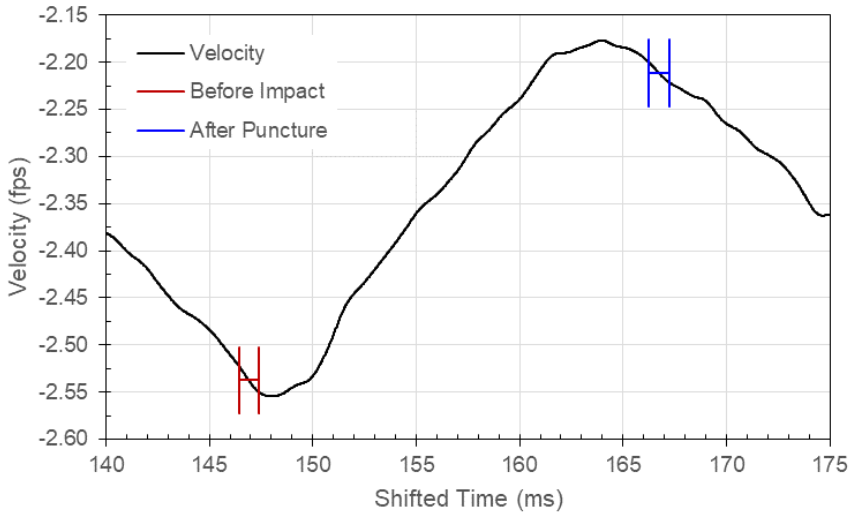

Figure 313: Carriage Velocity, Test 64, Specimen T051-13, 0.500-Inch Semi-spherical Probe

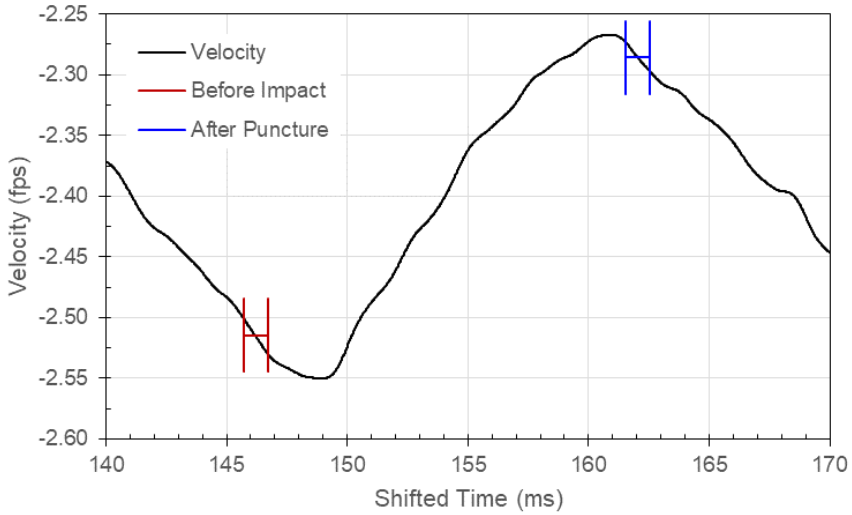

Figure 314: Carriage Velocity, Test 65, Specimen T051-23, 0.500-Inch Semi-spherical Probe

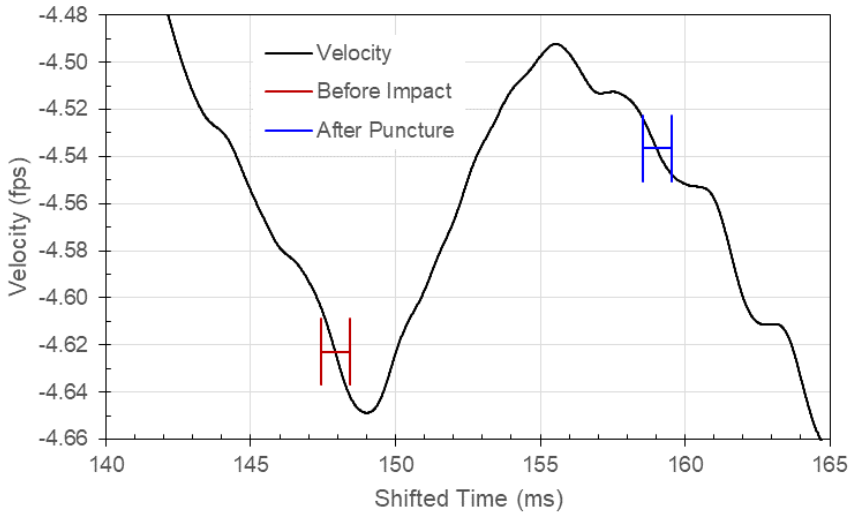

Figure 315: Carriage Velocity, Test 60, Specimen T051-34, 0.500-Inch Semi-spherical Probe

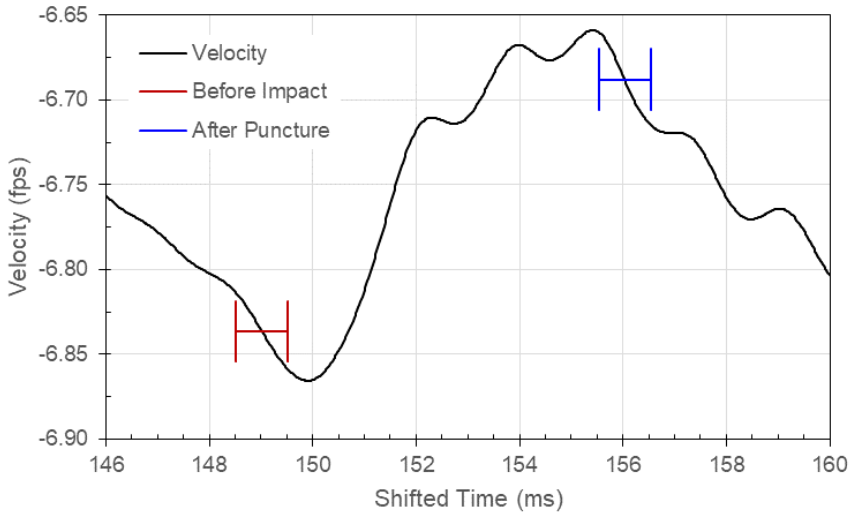

Figure 316: Carriage Velocity, Test 76, Specimen T051-09, 1.000-Inch Semi-spherical Probe

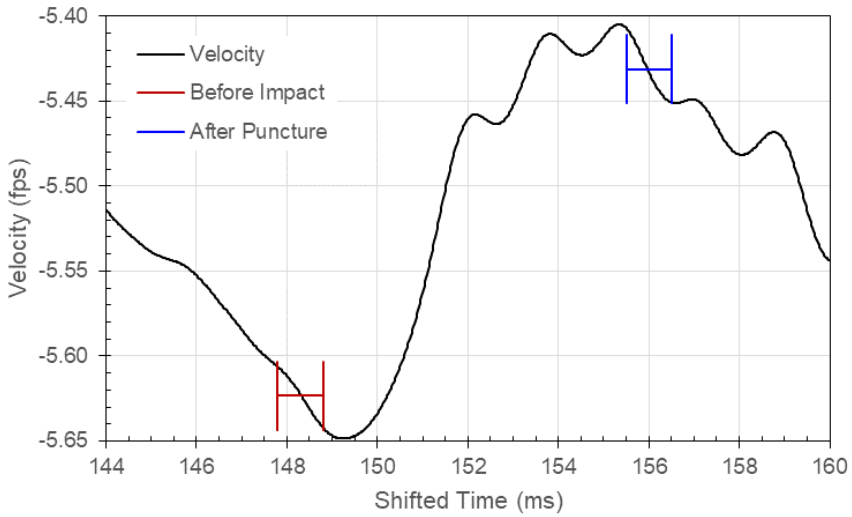

Figure 317: Carriage Velocity, Test 77, Specimen T051-12, 1.000-Inch Semi-spherical Probe

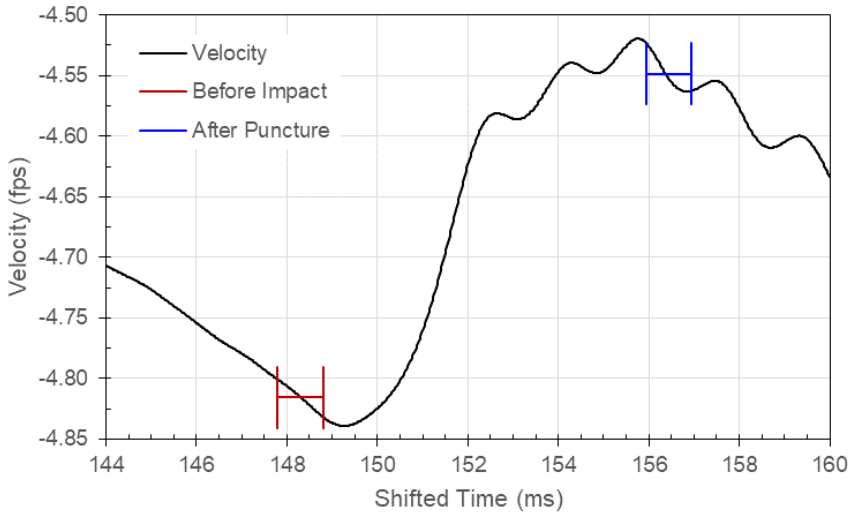

Figure 318: Carriage Velocity, Test 78, Specimen T051-18, 1.000-Inch Semi-spherical Probe

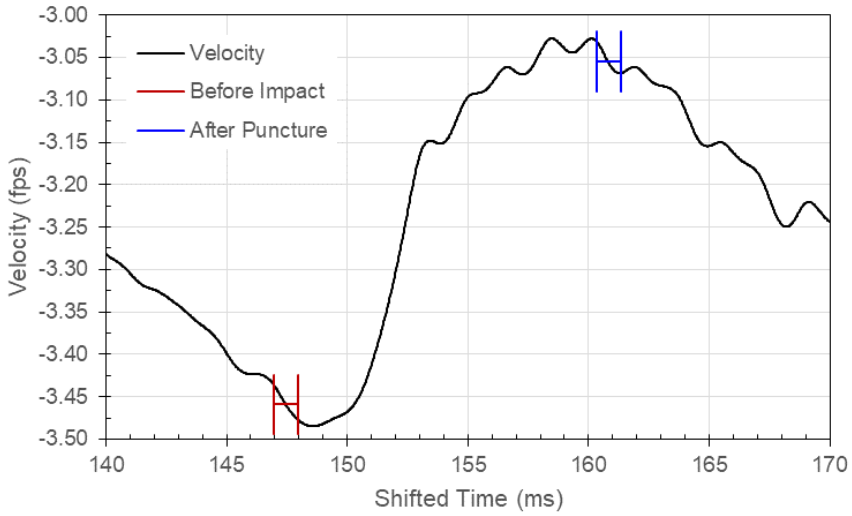

Figure 319: Carriage Velocity, Test 79, Specimen T051-19, 1.000-Inch Semi-spherical Probe

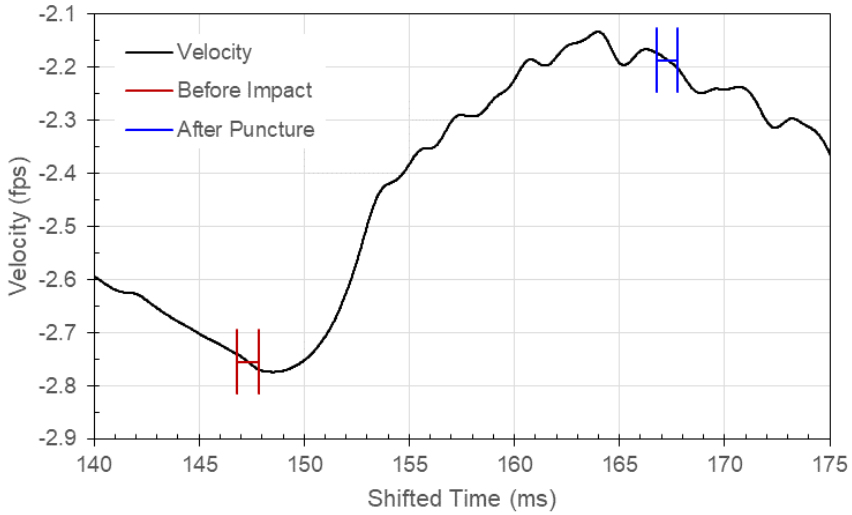

Figure 320: Carriage Velocity, Test 80, Specimen T051-22, 1.000-Inch Semi-spherical Probe

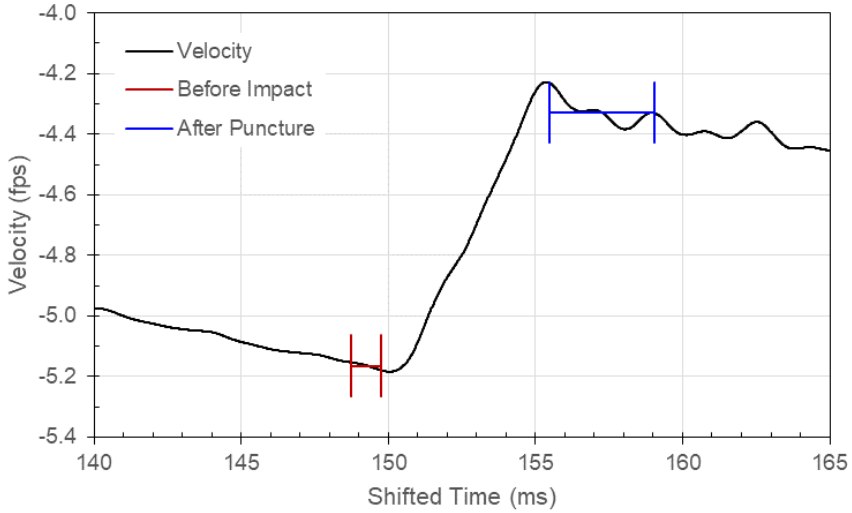

Figure 321: Carriage Velocity, Test 66, Specimen T114-04, 0.500-Inch Semi-spherical Probe

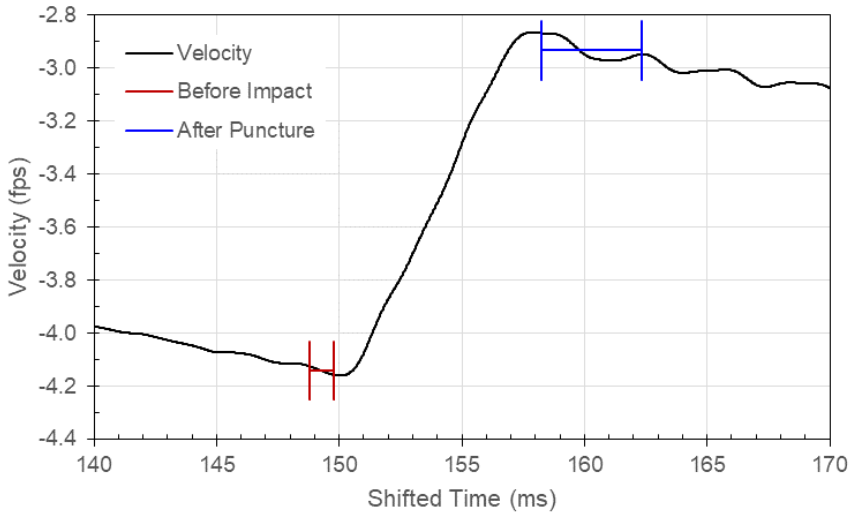

Figure 322: Carriage Velocity, Test 67, Specimen T114-22, 0.500-Inch Semi-spherical Probe

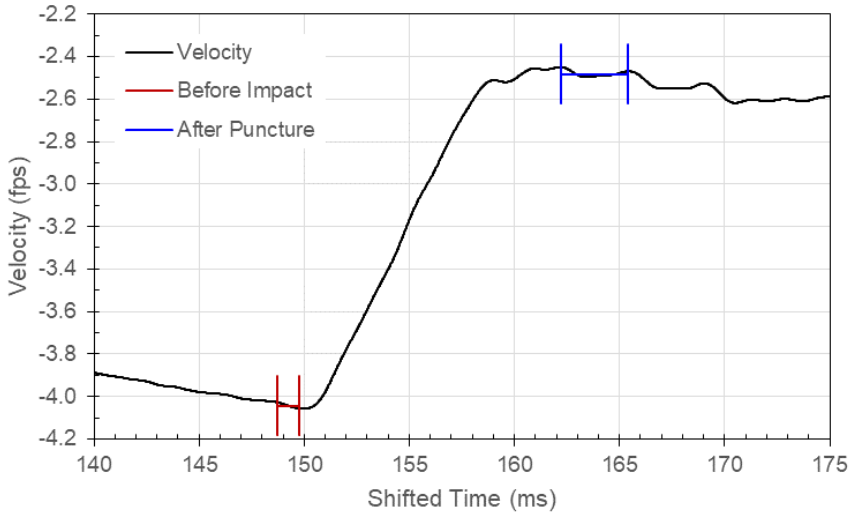

Figure 323: Carriage Velocity, Test 68, Specimen T114-25, 0.500-Inch Semi-spherical Probe

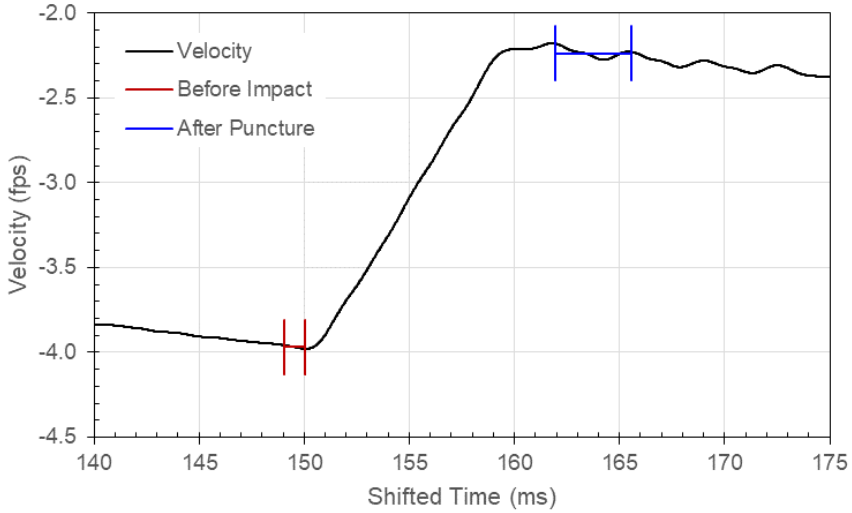

Figure 324: Carriage Velocity, Test 69, Specimen T114-33, 0.500-Inch Semi-spherical Probe

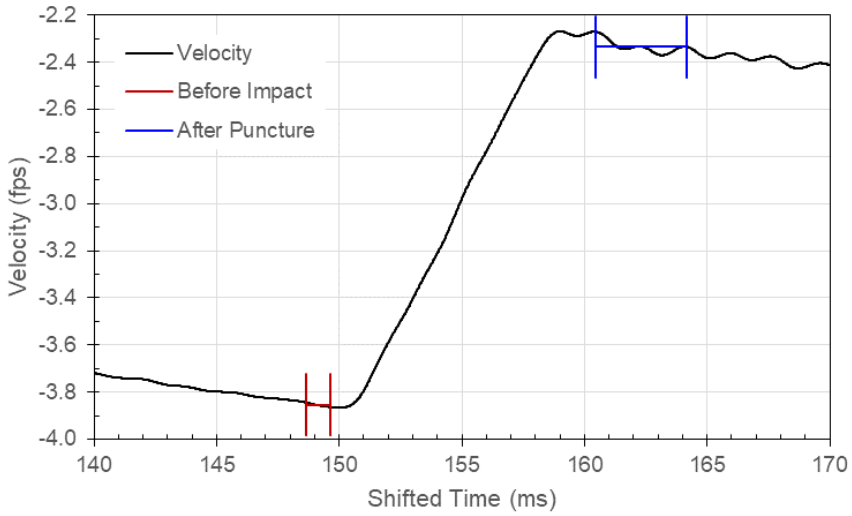

Figure 325: Carriage Velocity, Test 70, Specimen T114-35, 0.500-Inch Semi-spherical Probe

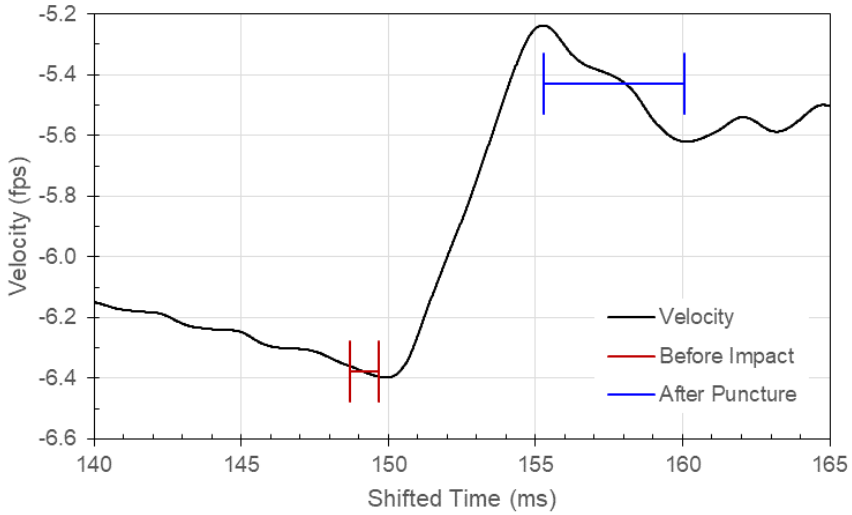

Figure 326: Carriage Velocity, Test 81, Specimen T114-06, 1.000-Inch Semi-spherical Probe

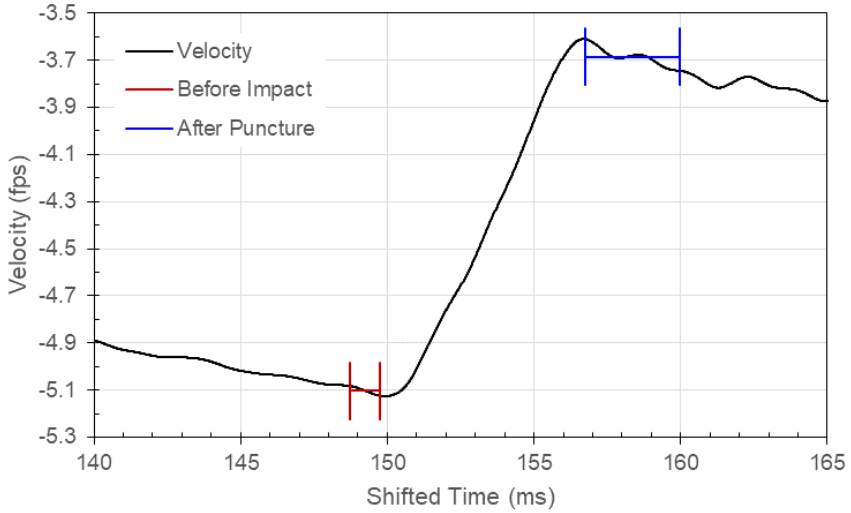

Figure 327: Carriage Velocity, Test 82, Specimen T114-15, 1.000-Inch Semi-spherical Probe

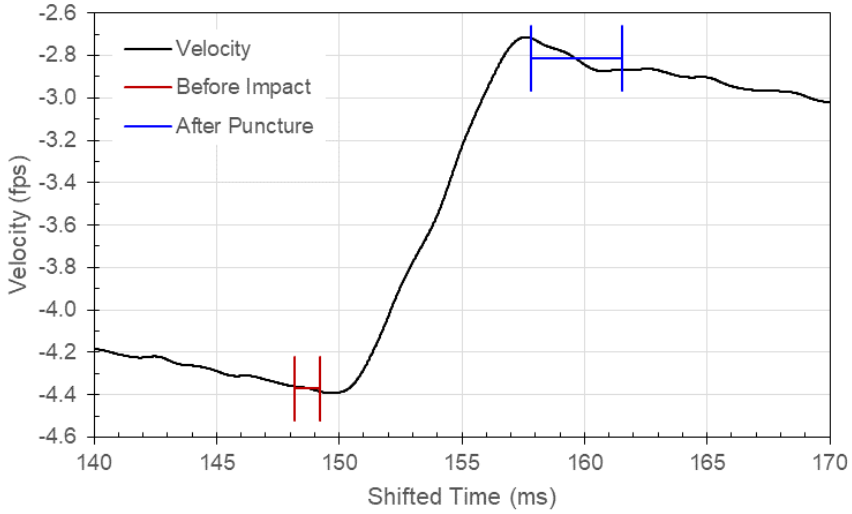

Figure 328: Carriage Velocity, Test 83, Specimen T114-28, 1.000-Inch Semi-spherical Probe

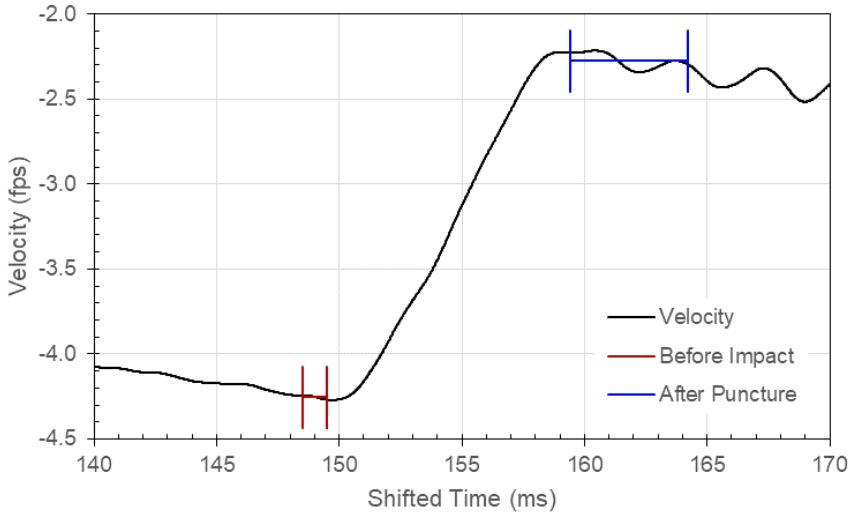

Figure 329: Carriage Velocity, Test 84, Specimen T114-31, 1.000-Inch Semi-spherical Probe

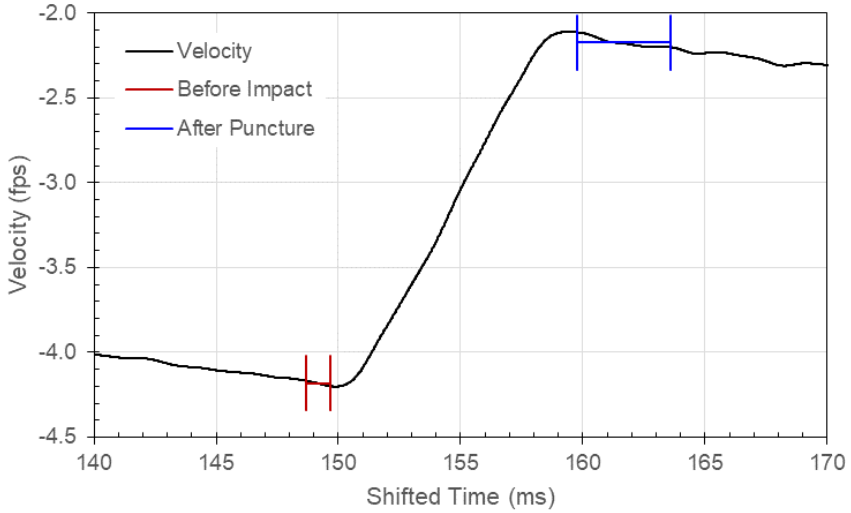

Figure 330: Carriage Velocity, Test 85, Specimen T114-32, 1.000-Inch Semi-spherical Probe

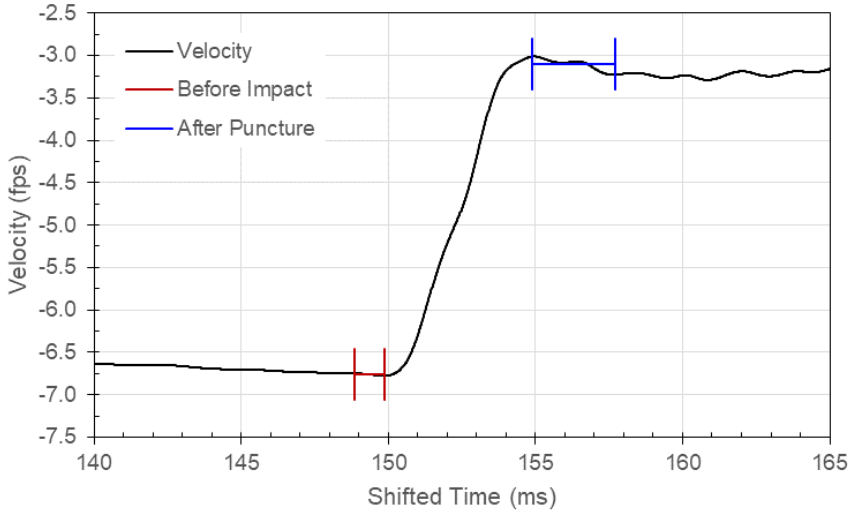

Figure 331: Carriage Velocity, Test 71, Specimen T250-05, 0.500-Inch Semi-spherical Probe

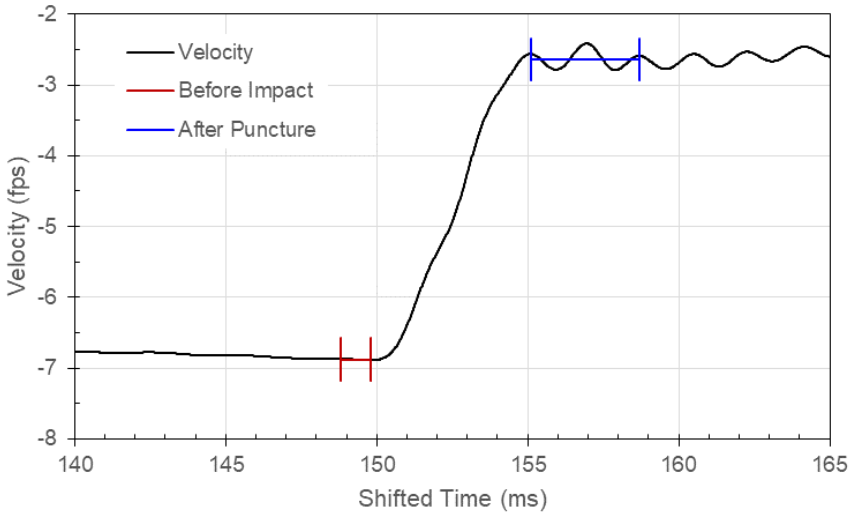

Figure 332: Carriage Velocity, Test 72, Specimen T250-14, 0.500-Inch Semi-spherical Probe

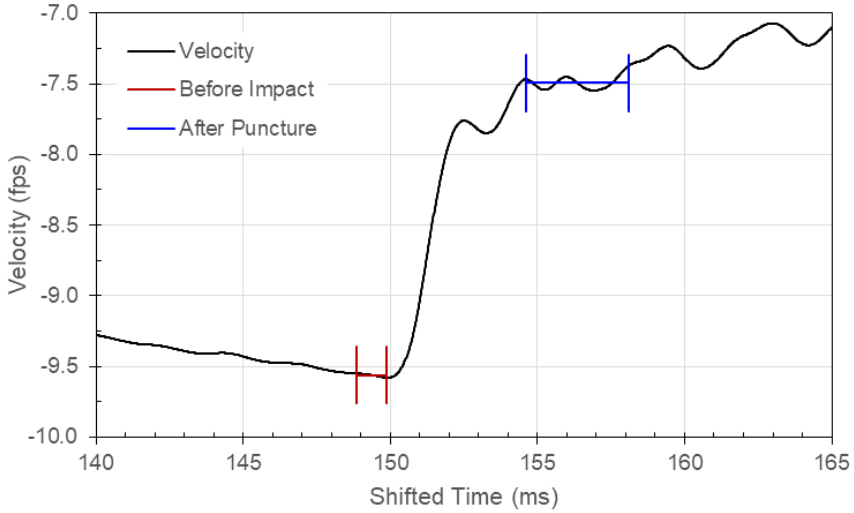

Figure 333: Carriage Velocity, Test 73, Specimen T250-22, 0.500-Inch Semi-spherical Probe

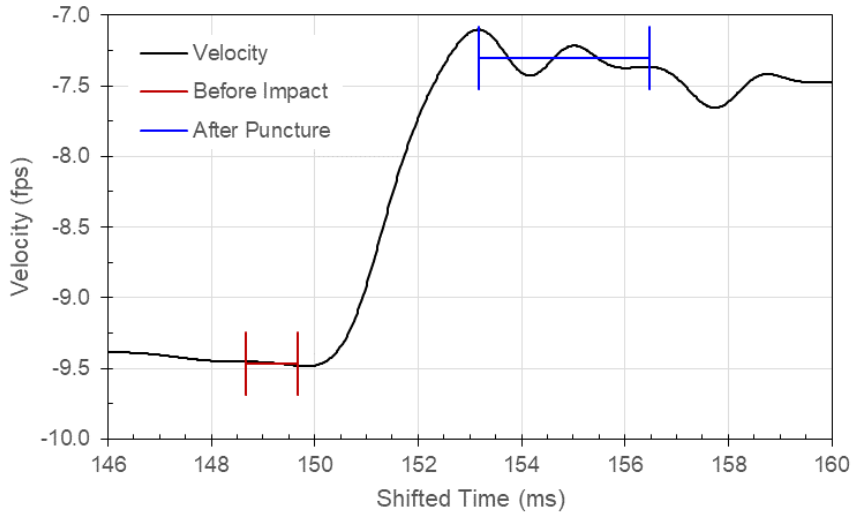

Figure 334: Carriage Velocity, Test 74, Specimen T250-32, 0.500-Inch Semi-spherical Probe

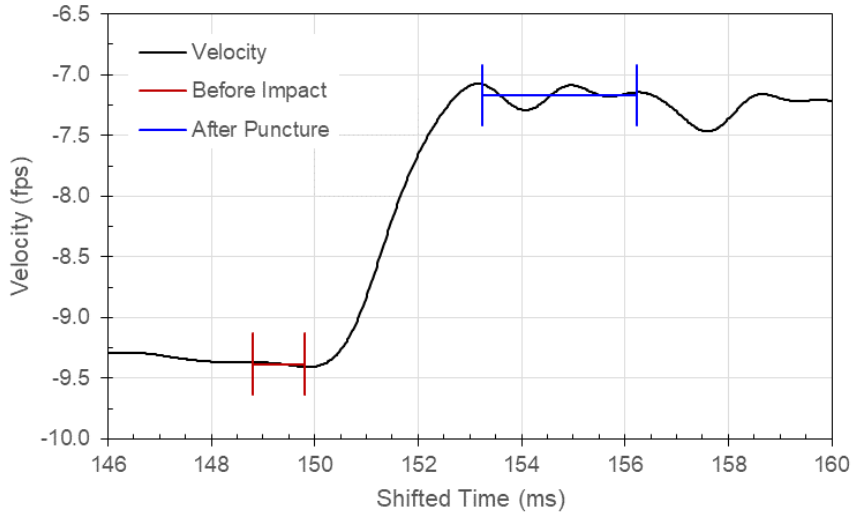

Figure 335: Carriage Velocity, Test 75, Specimen T250-33, 0.500-Inch Semi-spherical Probe

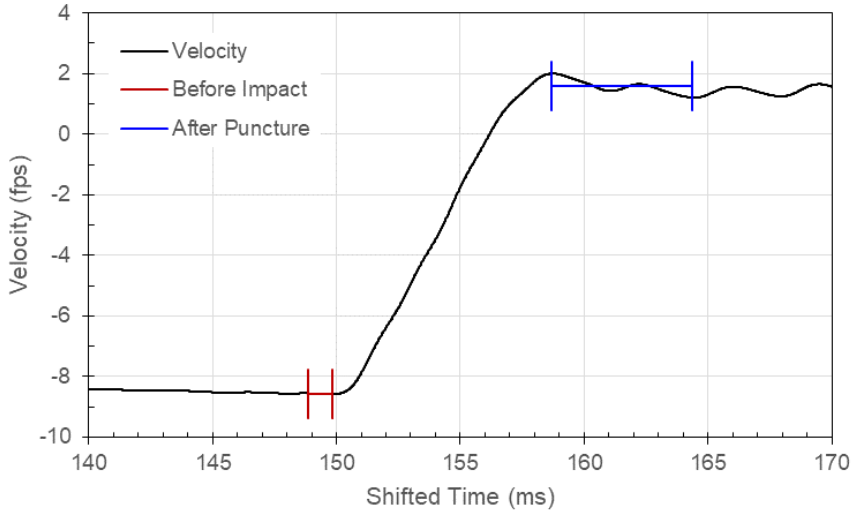

Figure 336: Carriage Velocity, Test 87, Specimen T250-13, 1.000-Inch Semi-spherical Probe

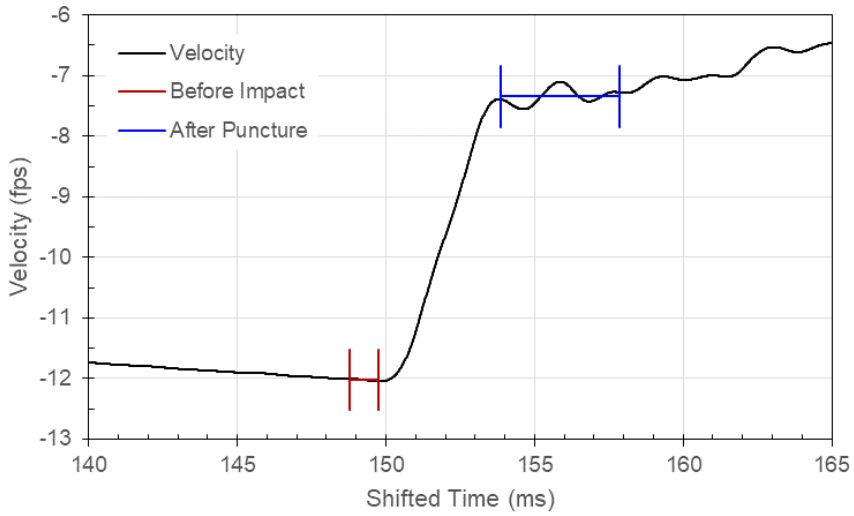

Figure 337: Carriage Velocity, Test 89, Specimen T250-20, 1.000-Inch Semi-spherical Probe

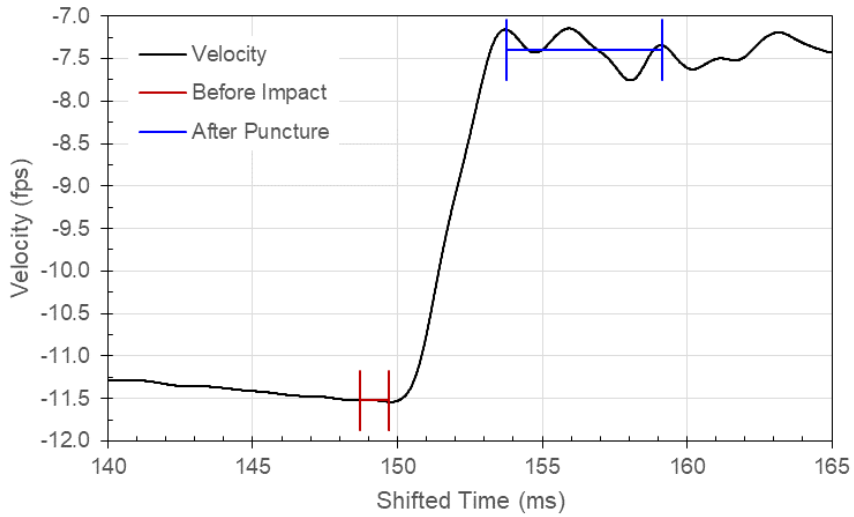

Figure 338: Carriage Velocity, Test 90, Specimen T250-21, 1.000-Inch Semi-spherical Probe

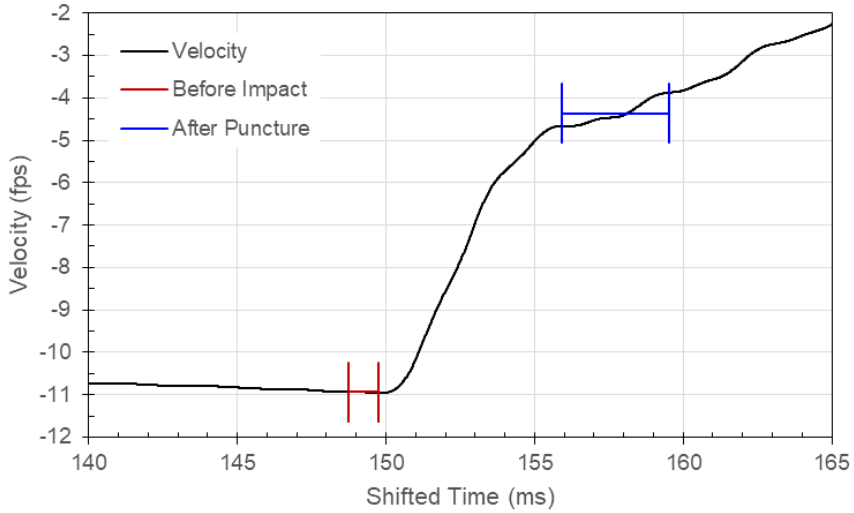

Figure 339: Carriage Velocity, Test 91, Specimen T250-27, 1.000-Inch Semi-spherical Probe

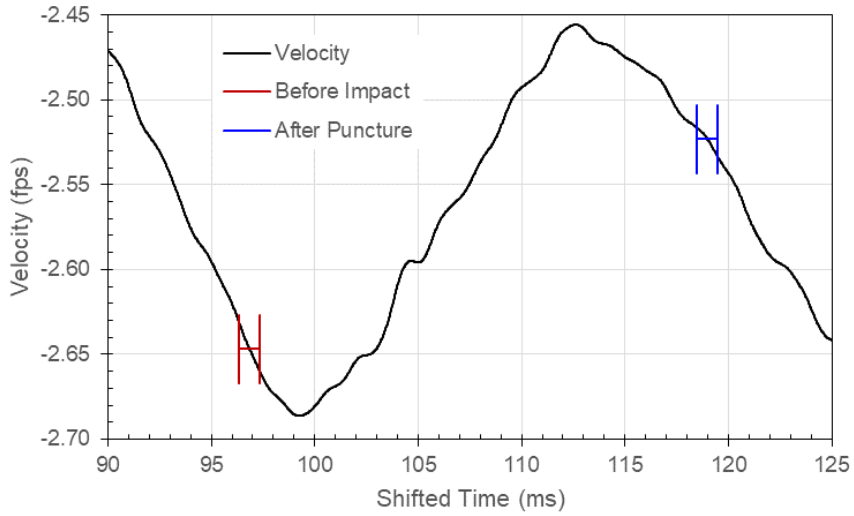

Figure 340: Carriage Velocity, Test 103, Specimen T051-01, 0.500-Inch Tri-corner Probe

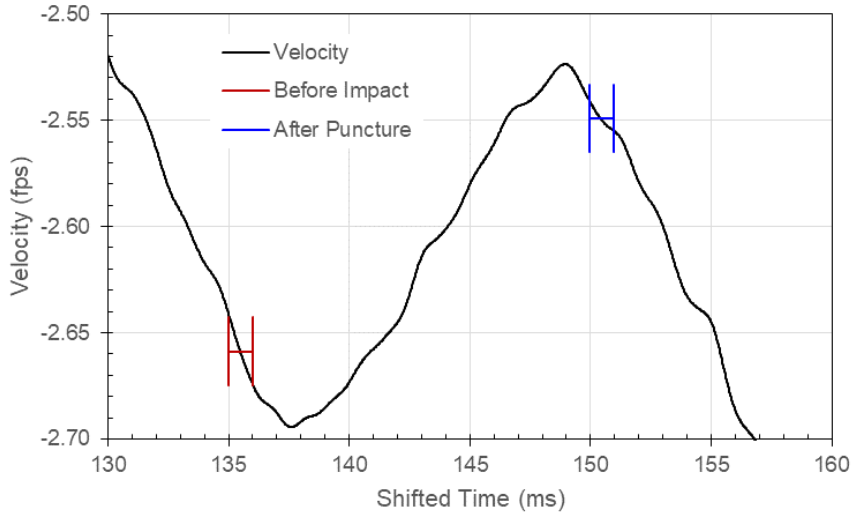

Figure 341: Carriage Velocity, Test 104, Specimen T051-02, 0.500-Inch Tri-corner Probe

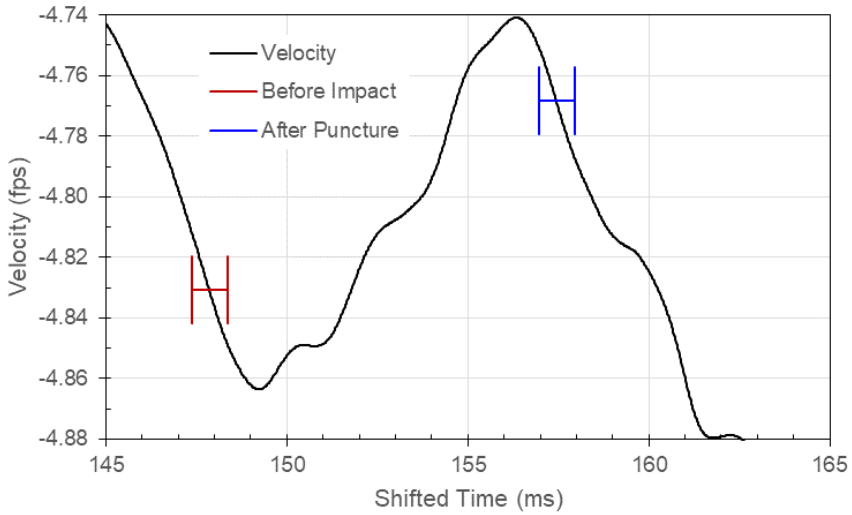

Figure 342: Carriage Velocity, Test 4, Specimen T051-31, 0.500-Inch Tri-corner Probe

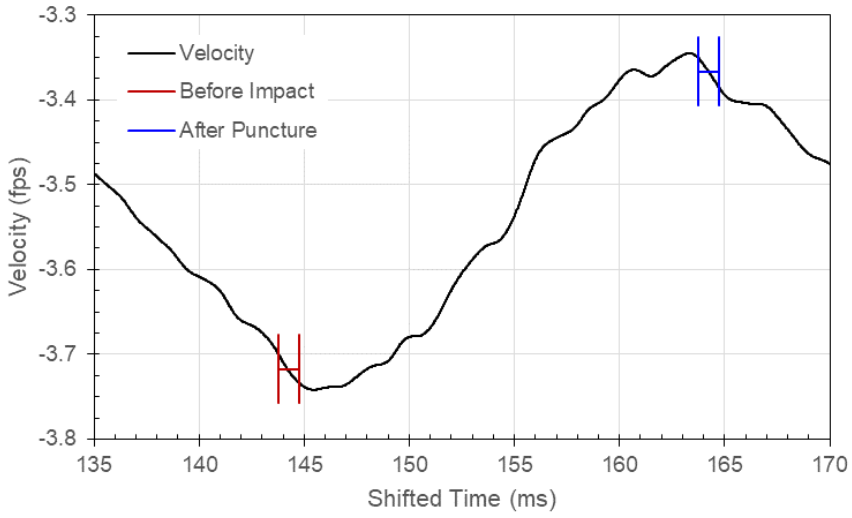

Figure 343: Carriage Velocity, Test 105, Specimen T051-05, 1.000-Inch Tri-corner Probe

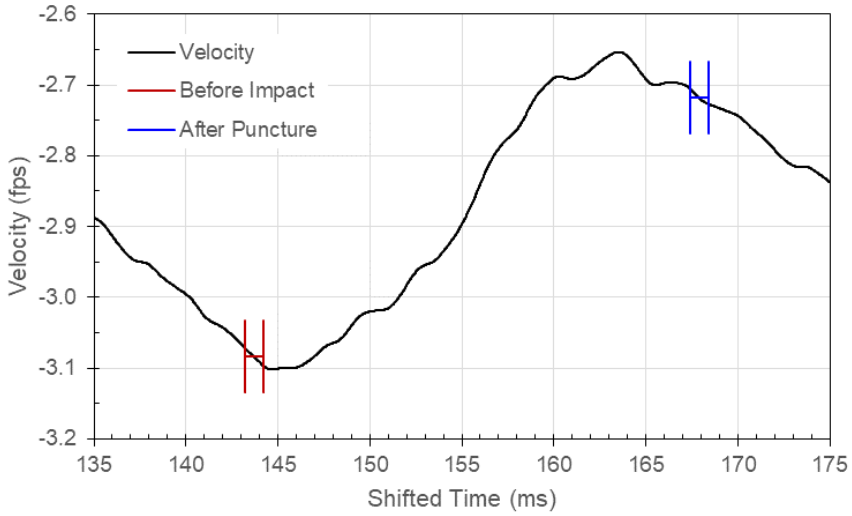

Figure 344: Carriage Velocity, Test 106, Specimen T051-25, 1.000-Inch Tri-corner Probe

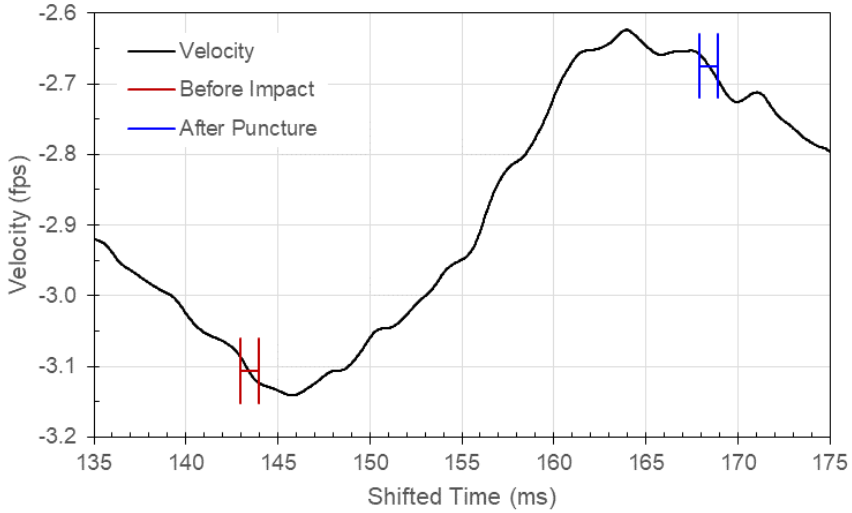

Figure 345: Carriage Velocity, Test 107, Specimen T051-33, 1.000-Inch Tri-corner Probe

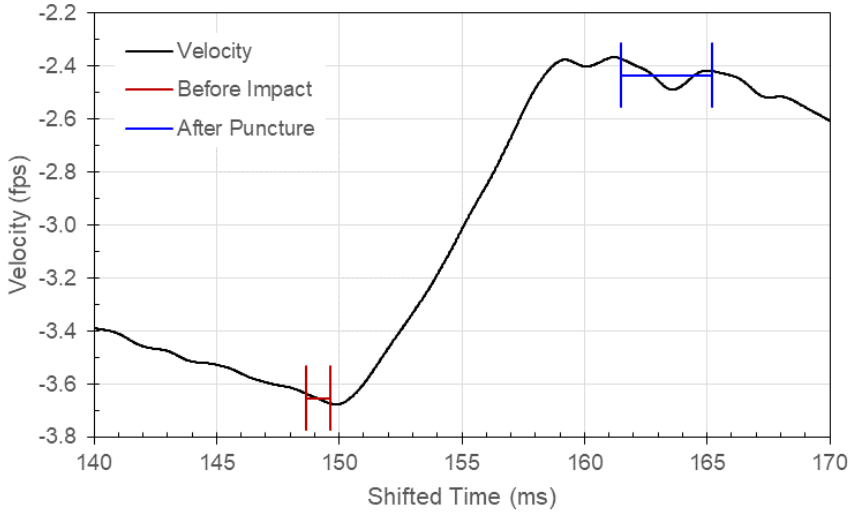

Figure 346: Carriage Velocity, Test 92, Specimen T114-03, 0.500-Inch Tri-corner Probe

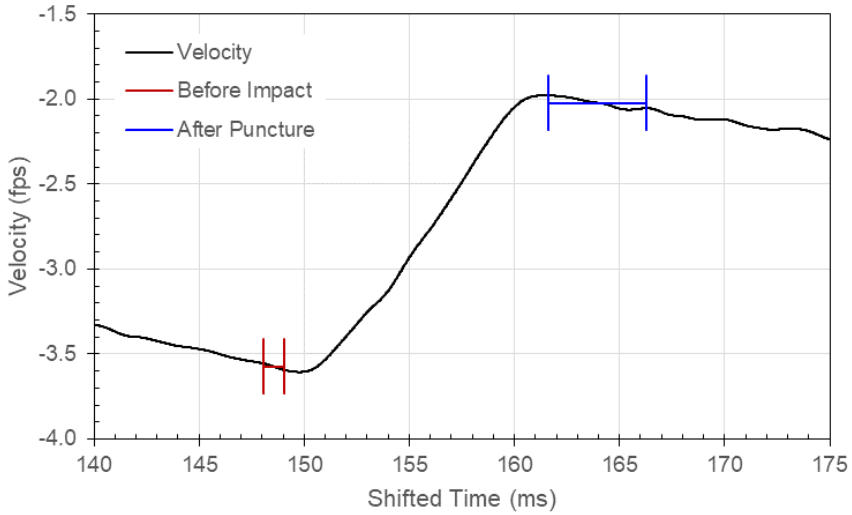

Figure 347: Carriage Velocity, Test 93, Specimen T114-12, 0.500-Inch Tri-corner Probe

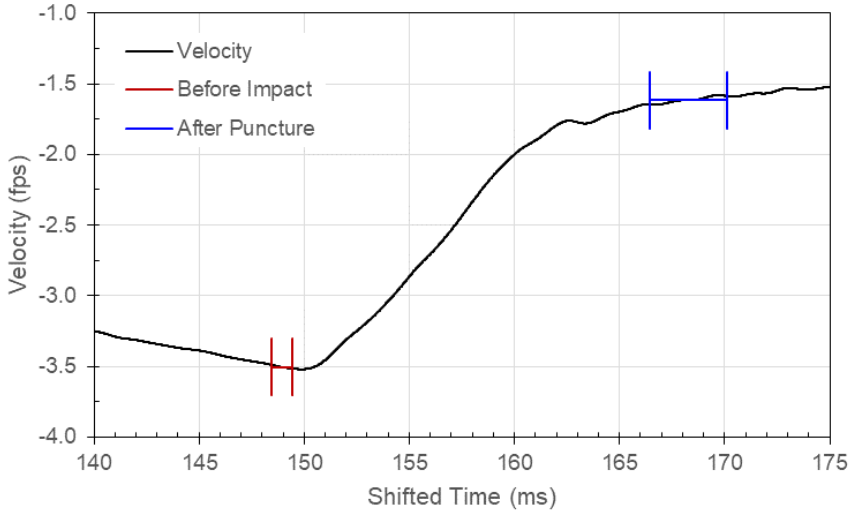

Figure 348: Carriage Velocity, Test 94, Specimen T114-19, 0.500-Inch Tri-corner Probe

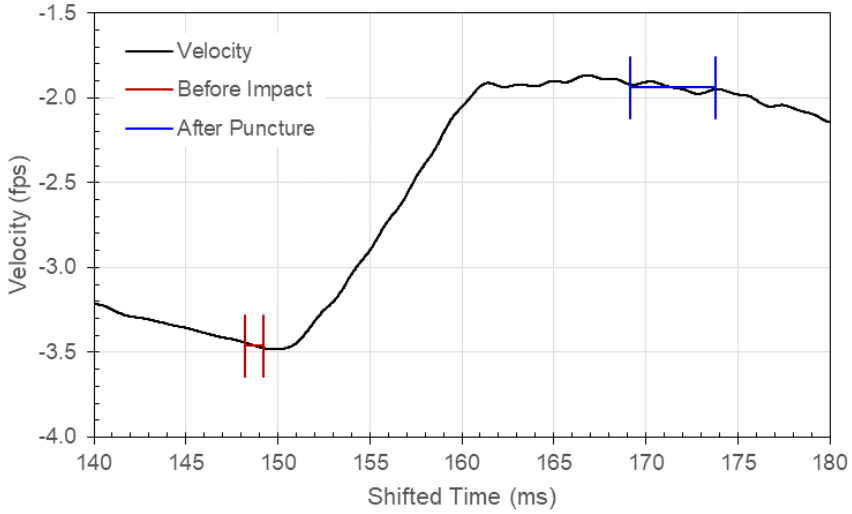

Figure 349: Carriage Velocity, Test 95, Specimen T114-20, 0.500-Inch Tri-corner Probe

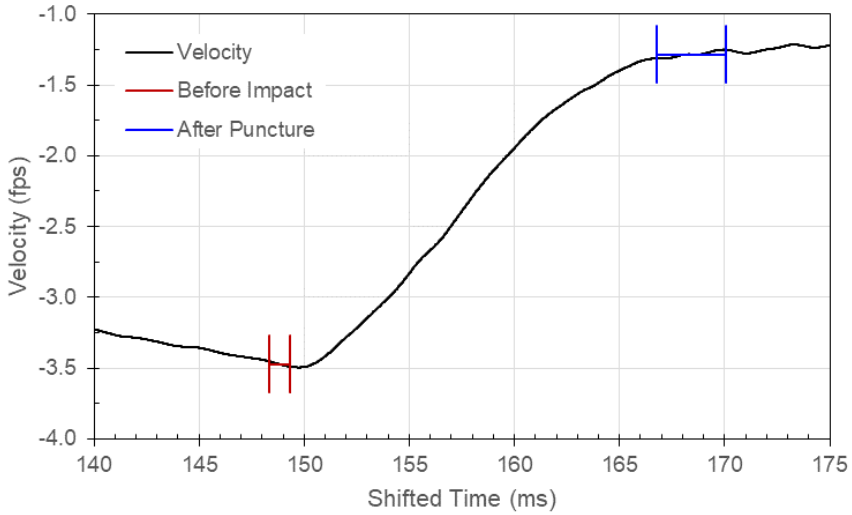

Figure 350: Carriage Velocity, Test 96, Specimen T114-34, 0.500-Inch Tri-corner Probe

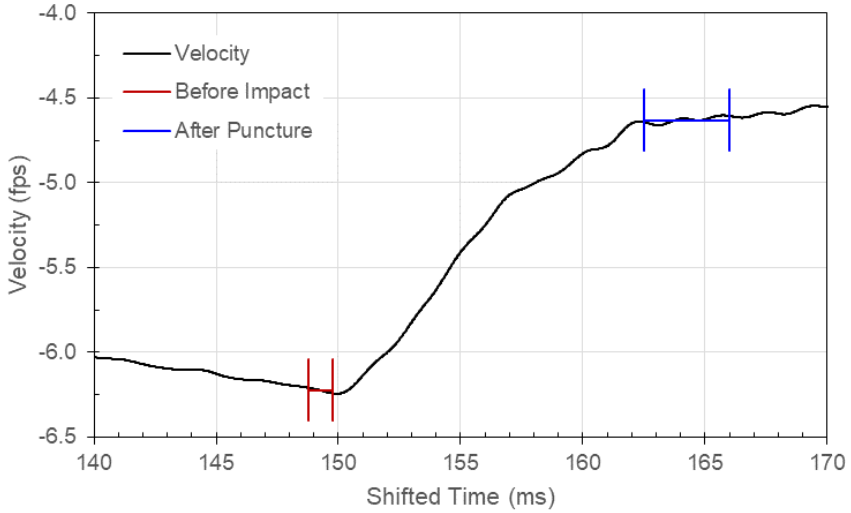

Figure 351: Carriage Velocity, Test 108, Specimen T114-01, 1.000-Inch Tri-corner Probe

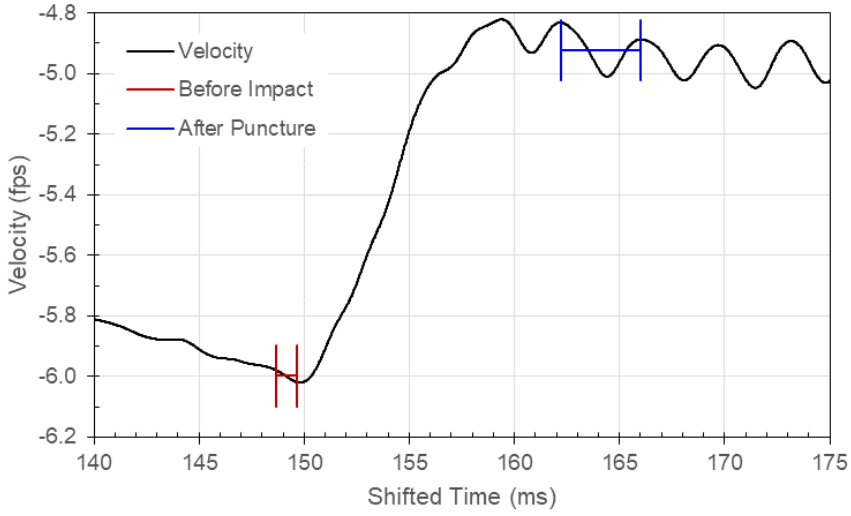

Figure 352: Carriage Velocity, Test 109, Specimen T114-02, 1.000-Inch Tri-corner Probe

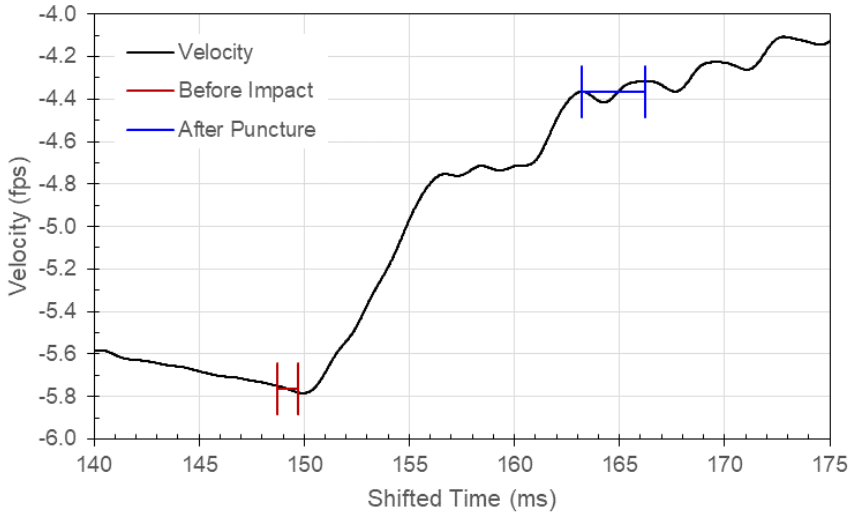

Figure 353: Carriage Velocity, Test 110, Specimen T114-10, 1.000-Inch Tri-corner Probe

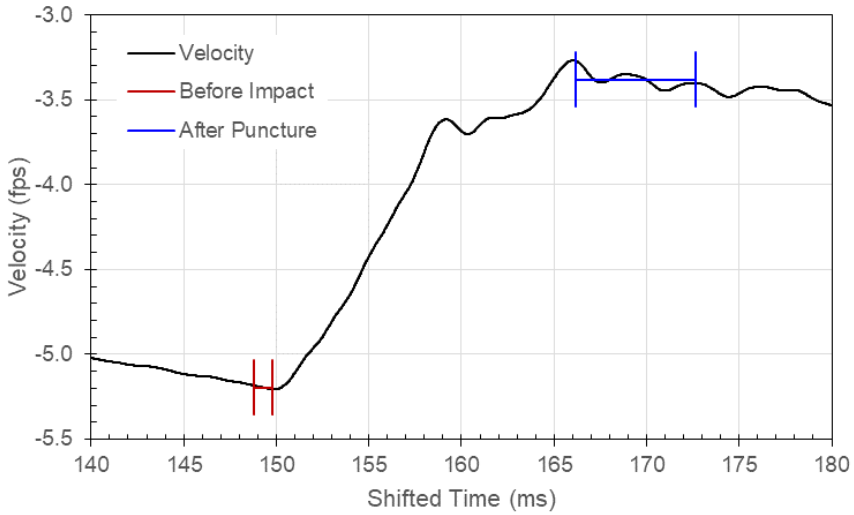

Figure 354: Carriage Velocity, Test 111, Specimen T114-11, 1.000-Inch Tri-corner Probe

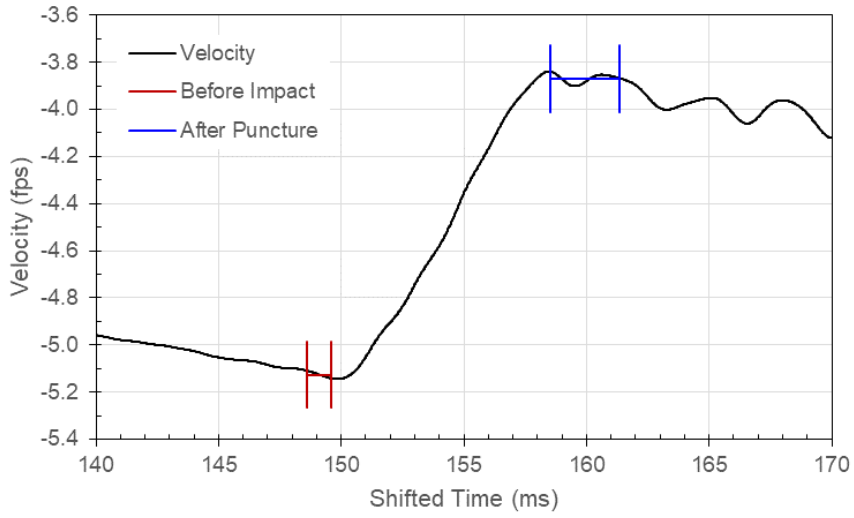

Figure 355: Carriage Velocity, Test 112, Specimen T114-26, 1.000-Inch Tri-corner Probe

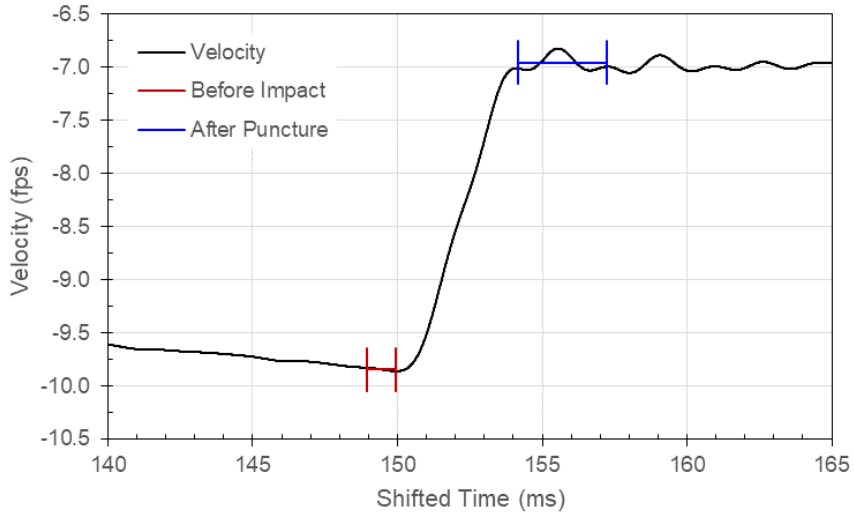

Figure 356: Carriage Velocity, Test 98, Specimen T250-01, 0.500-Inch Tri-corner Probe

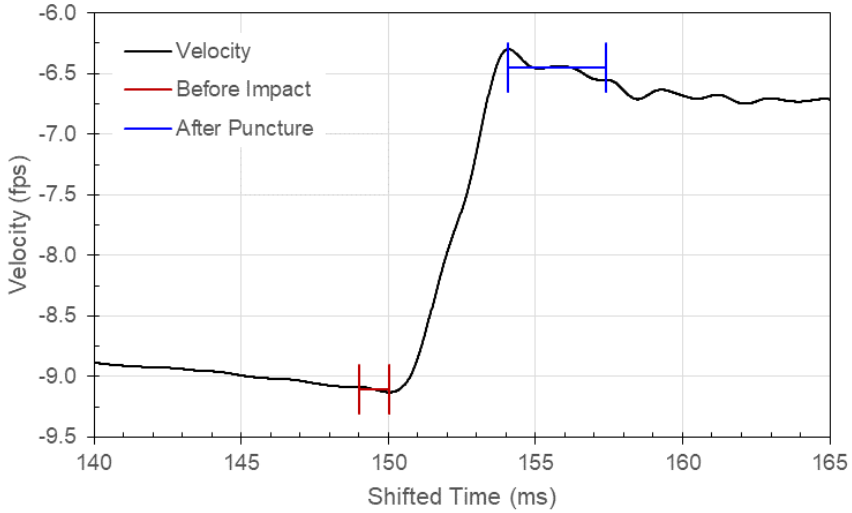

Figure 357: Carriage Velocity, Test 99, Specimen T250-10, 0.500-Inch Tri-corner Probe

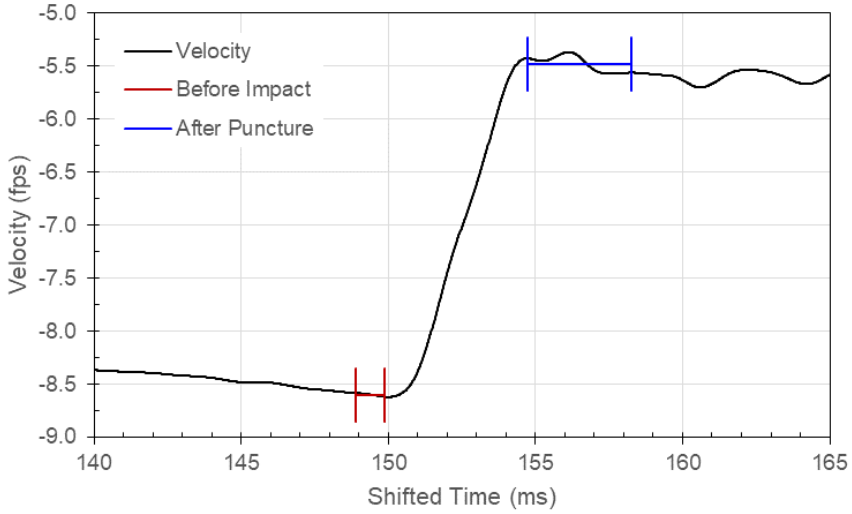

Figure 358: Carriage Velocity, Test 100, Specimen T250-19, 0.500-Inch Tri-corner Probe

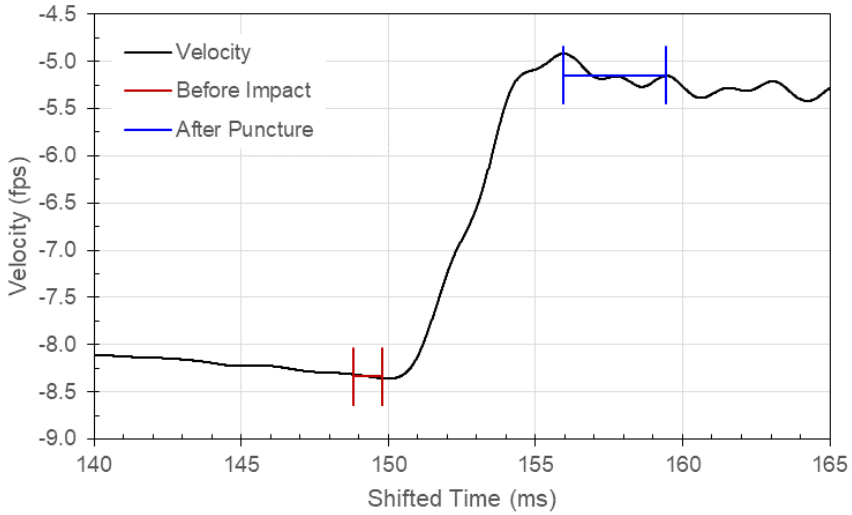

Figure 359: Carriage Velocity, Test 101, Specimen T250-25, 0.500-Inch Tri-corner Probe

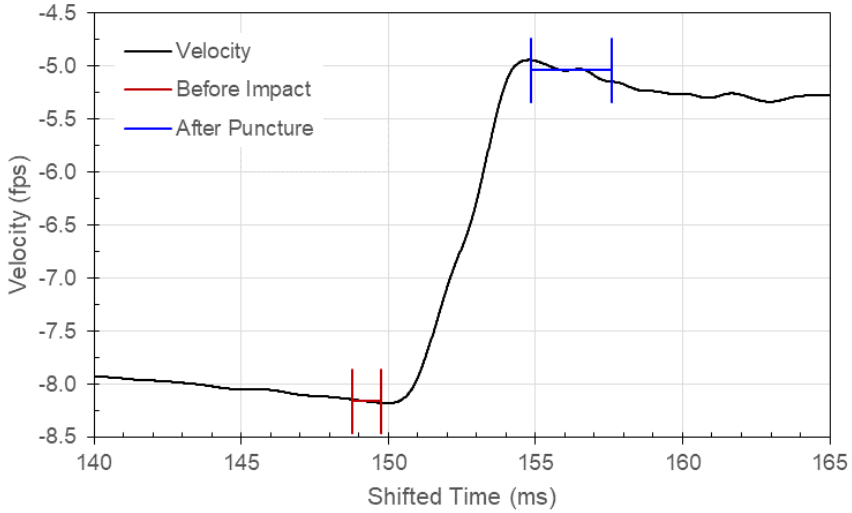

Figure 360: Carriage Velocity, Test 102, Specimen T250-31, 0.500-Inch Tri-corner Probe

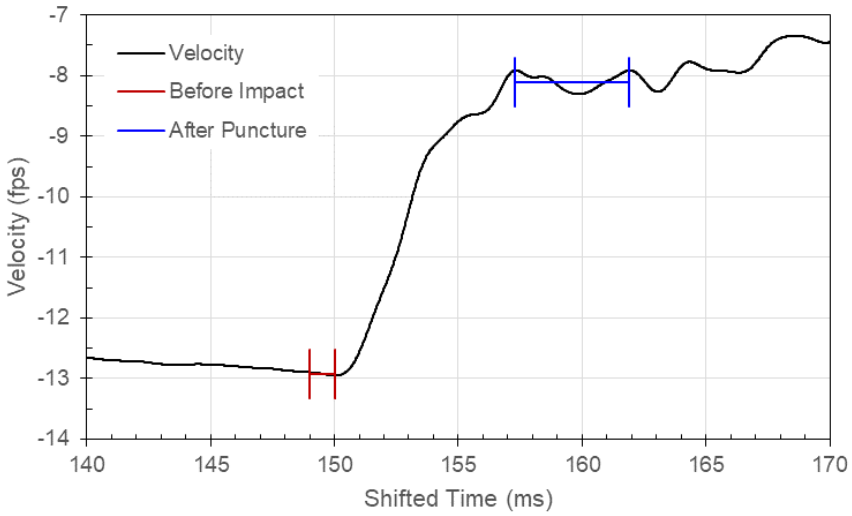

Figure 361: Carriage Velocity, Test 113, Specimen T250-02, 1.000-Inch Tri-corner Probe

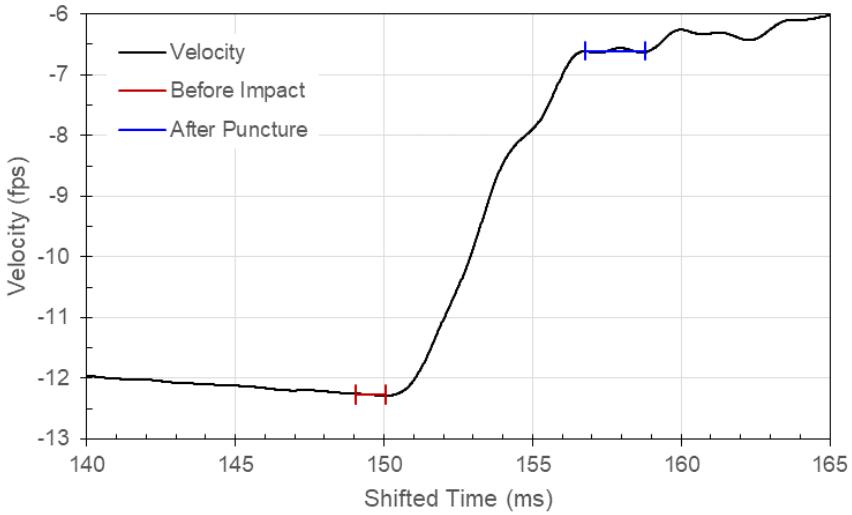

Figure 362: Carriage Velocity, Test 114, Specimen T250-03, 1.000-Inch Tri-corner Probe

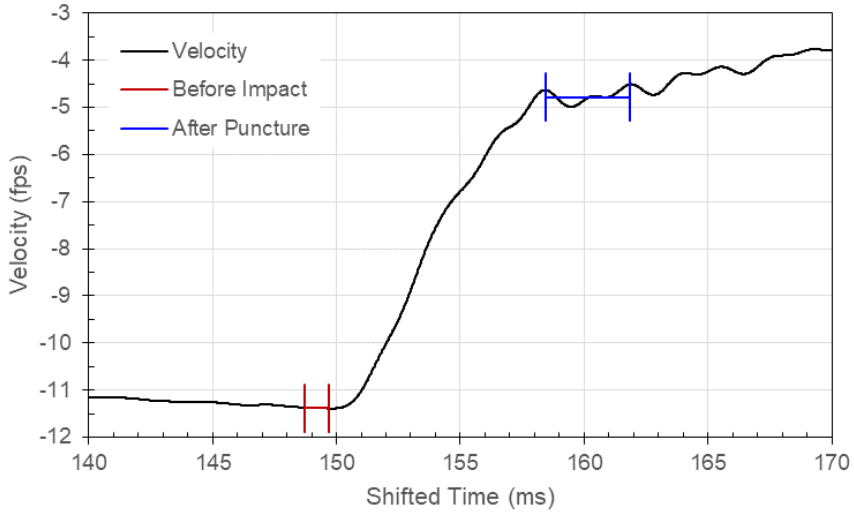

Figure 363: Carriage Velocity, Test 115, Specimen T250-11, 1.000-Inch Tri-corner Probe

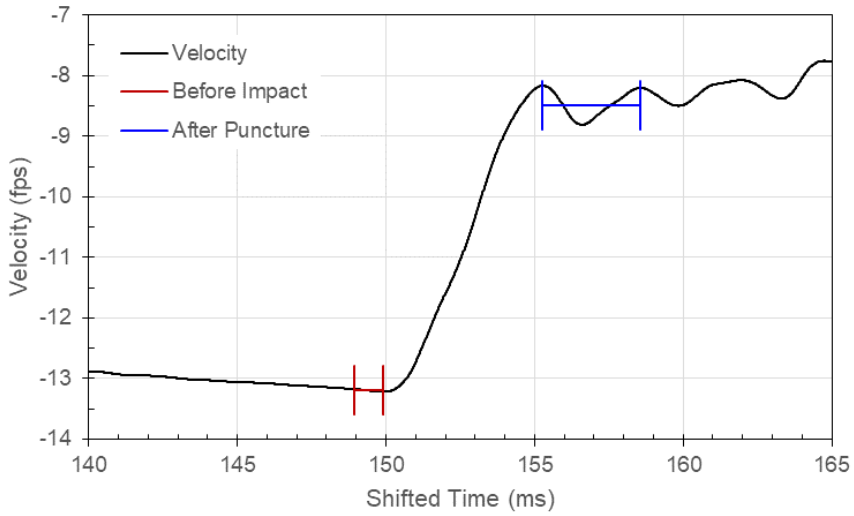

Figure 364: Carriage Velocity, Test 116, Specimen T250-12, 1.000-Inch Tri-corner Probe

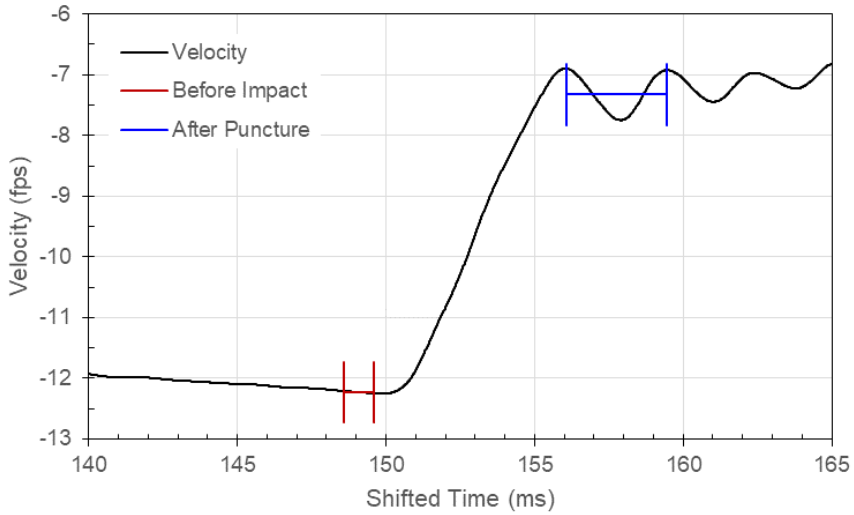

Figure 365: Carriage Velocity, Test 117, Specimen T250-26, 1.000-Inch Tri-corner Probe

Sandia National Laboratories is a multimission laboratory managed and operated by National Technology and Engineering Solutions of Sandia, LLC, a wholly owned subsidiary of Honeywell International, Inc., for the U.S. Department of Energy's National Nuclear Security Administration under contract DE-NA0003525.